Proceedings of the

FOURTH SDIO/ONR PULSE POWER MEETING 1991

June 20–21, 1991

University of Southern California
Los Angeles, CA 90089-0484

TABLE OF CONTENTS

FOREWORD

Three years ago when the first SDIO/ONR Pulse Power Meeting was held we met as a small group. Thanks to the interest and enthusiasm of the scientific community, the meeting has shown continued growth, and now serves as a forum for the promotion of pulsed power technology and its applications, reporting results of significance, and delineating issues. In addition, panel sessions have served to identify and focus attention on key issues and areas. The meeting has demonstrated that it is not just an instrument for competition, but has a team spirit–working together, to further this significant research. The meeting has also led to the formation of a University-Industry-Government Consortium on high power switching, about which we will communicate to colleagues in the near future. The calibre of research demonstrated in the programs and the substantial transitions that are taking place are exciting, and encourage continuing this pulsed power switching meeting as an annual event to foster research and development of high power switches. It is a pleasure to express my appreciation to Prof. Martin Gundersen and Ms. Shirin Mistry for the organization of the meeting, and to the pulsed power scientific community for their cooperation and participation. I am looking forward to seeing you again at future meetings.

Gabriel D. Roy

Biography

Gabriel D. Roy Received his Ph.D in Engineering Science from the University of Tennessee. He served as a faculty member for 12 years and as a researcher and research manager in university and industry for 15 years. At the Office of Naval Research Dr. Roy manages the propulsion and pulse power physics programs. He has over 30 publications and two patents, and his research interests include plasma dynamics, MHD, pulse power and propulsion. He is a recipient of the Roll of Honor award from TRW Inc. Dr. Roy is a member of ASME and Sigma Xi Honor Society, and an associate fellow of AIAA. He is also an associate editor of the AIAA Journal of Propulsion and Power.

FOURTH SDIO/ONR PULSE POWER MEETING 1991

Organizing Committee:

Dr. M. Gundersen
Dept. of Electrical Engineering-Electrophysics
University of Southern California
Los Angeles, CA 90089-0484

Dr. G. Roy
ONR - Code 1132P
800 N. Quincy Street
Arlington, VA 22217-5000

Lt. Col. P. Rustan
SDIO/T/IS
The Pentagon
Washington, DC 20301-7100

4th SDIO/ONR MEETING
June 20-21, 1991

AGENDA

THURSDAY, JUNE 20, 1991

Morning Session - 8:30 a.m.- 12:30 p.m.:

8:15 - Registration

8:30 - Introduction - G. Roy, M. Gundersen

Solid State Switches:

8:50 - F. Zutavern (Sandia National Labs.)
High gain GaAs photoconductive semiconductor switches for compact linear induction accelerators

9:15 - W. Nunnally (U. Texas, Arlington)
Photoconductive switching

9:40 - M. Levinson (GTE)
Progress in the development of semiconductor-metal eutectic transistors for high power switching

10:05 - C. H. Lee (U. Maryland)
Power gain in a photoconductive semiconductor switch controlled inductive pulsed power system

10:30 - Coffee Break

10:45 - K. Schönbach (Old Dominion University)
An optically activated opening semiconductor switch

11:10 - W. Donaldson (U. Rochester)
An optically triggered, superconducting, opening switch

11:40 - J. Hur (USC)
Solid state pulsed power device research at the University of Southern California

12:05 - Lunch - Gerontology Patio

Afternoon Session - 1:00 p.m. :

Gas Phase:

1:00 - C. Braun (ETDL, Ft. Monmouth)
Review of Ft. Monmouth Switch Research

1:25 - G. Kirkman (Integrated Applied Physics)
High power modulator development based on the back lighted thyratron switch

1:50 - M. Kristiansen (Texas Tech)
Texas Tech Research

2:15 - Coffee Break

2:30 - K. Schönbach (Old Dominion University)
Magnetic control of hollow cathode discharge switches

2:55 - M. Kushner (U. of Illinois)
Breakdown characteristics in nonplanar geometries

3:20 - M. Gundersen (USC)
Super-emissive cathode devices

3:45	-	Panel Discussion: A. Guenther (Moderator) Topic: Progress to date and future research goals
6:30	-	Dinner (USC Town and Gown)

FRIDAY, JUNE 21, 1991

Morning Session - 8:30 a.m. - 12:15 p.m.:

8:30	-	C. Johnson (Auburn Univ.) *Interactive space technologies consortium research*
8:55	-	B. Druce (LLNL) *High average power switching*
9:20	-	W. J. Sarjeant (SUNY, Buffalo)
9:45	-	Y. Maron (Weizmann Inst.) *Investigations of pulsed-power systems using high-resolution spectroscopic methods*
10:10	-	Break
10:25	-	T. Naff (Physics Intl.) *Development of high action sparkgaps for large capacitive energy stores*
10:50	-	C. Maxwell (STD Research Corp.)
11:15	-	D. Giorgi (ECR) *Experimental verification of a novel opening switch concept*
11:45	-	Lunch - Gerontology Patio

Afternoon Session - 12:45 p.m.

12:45	-	T. S. Sudarshan (U. South Carolina) *Investigation of pulsed surface flashover behavior of insulators and semiconductors*
1:10	-	P. F. Williams (U. Nebraska)
1:35	-	M. Mazzola (NSWC) *Solid state switching*
2:00	-	Break
2:15	-	Panel Discussion: A. Guenther (Moderator) Summary of accomplishments and impact Discussion of applications for pulsed power, Further Recommendations for continuing research Relationship to prime power Involvement of industry, universities in technology transfer
4:00	-	Administrative Session

HIGH GAIN GaAs PHOTOCONDUCTIVE SEMICONDUCTOR SWITCHES FOR COMPACT LINEAR INDUCTION ACCELERATORS*

F. J Zutavern, G. M. Loubriel, M. W. O'Malley,
W. D. Helgeson, and D. L. McLaughlin
Sandia National Laboratories
Albuquerque, NM 87185
(505) 845-9128

Abstract

This paper summarizes a series of experiments to develop high gain GaAs photoconductive semiconductor switches (PCSS) for compact linear induction accelerators (LIA). Three circuits have been built to initiate the PCSS in a high field switching mode called lock-on. Fast recovery is induced at low fields. The switching properties desired for accelerators and results achieved to date with PCSS are presented.

Introduction

The designs for compact linear induction accelerators, like those for transformers, get smaller and lighter at high frequencies. One design for a compact LIA demands many high power switches that will close and open (toggle) repetitively at 25 MHz for many microseconds. They must stand off 500 kV and interrupt 3 kA. To meet these requirements, large-scale PCSS are being developed.

PCSS with short carrier recombination times make very fast recovery switches.[1,2] Their ability to handle high powers and scale linearly in two dimensions to higher voltages and currents has been demonstrated with lateral geometry switches made from GaAs or silicon. Large lateral geometry PCSS, where the electric field and current are parallel to the surface of the switch, have switched several kiloamps at over 100 kV.[3,4] The main weakness of a linear (low field) PCSS as a simple closing switch is the excessive optical energy required for triggering that increases with the square of the length of the switch. For example, the energy required to trigger enough low field GaAs PCSS for an entire LIA was estimated to be in excess of 10 kJ per multi-microsecond burst.

Any PCSS designed for high power must be large enough to handle high voltage yet be as small as possible to minimize the optical trigger energy requirement. This implies high field operation which has led to surprises with some semiconductors, such as GaAs and InP.[5,6] High gain switching, presumably carrier generation at high fields, but empirically called lock-on until an explanation is confirmed, commences at average fields well below (less than 1/10th) the field required for avalanche bulk breakdown (100-200 kV/cm). Once triggered, switches in this mode stay on (at least for several microseconds) until the field across the switch disappears. Hence the term lock-on is used.

Although PCSS have potential advantages over conventional pulsed power closing switches (e.g. faster rise times, lower jitter, lower inductance, and higher reliability), their ability to operate as toggling (opening and closing) switches at high frequencies (above 10 MHz) really excels. Conventional pulsed power switches, such as gas spark gaps and thyratrons, can operate at best at a few kHz and typically run much slower. If fast recovery can be induced after switching in the lock-on mode, this low light level triggering mode can be applied to toggling applications. The behavior of these switches at high fields with emphasis on issues which affect switch recovery is the subject of this paper.

We have explored three categories of circuits to induce fast recovery after lock-on by temporarily reducing the field across the switch. Measurements of recovery times from 35-80 ns, multiple monopolar and bipolar bursts at 5-40 MHz, and hold-off fields ranging from 5-44 kV/cm (corresponding to 15-66 kV across individual switches), will be presented. A comparison will be made of the different circuits used to induce recovery from lock-on and the various factors that influence the recovery will be discussed.

Low Field Operation

At low fields (below 3.5-8 kV/cm, a material dependent threshold), carriers are generated in GaAs as the triggering light pulse is absorbed. These carriers recombine with a material dependent time constant (typically exponential) that leads to the recovery of the switch resistance after the light pulse ends. A quantitative analysis of the switch resistance as a function of time is given in reference 7. If the recombination time constant is small compared to the light pulse, the current through the switch simply follows the shape of the light pulse. On the other hand, if the recombination time constant is long compared to the laser pulse, the current through the switch shows a rise that is proportional to the integral of the light pulse shape and then a slower decay as the carriers recombine. An example of the current waveform for a relatively fast 3.4 cm long GaAs switch is shown in figure 1. This switch recovers its resistance in a few nanoseconds following a 250 ps wide light pulse from a frequency doubled, mode-locked Nd:YAG laser.

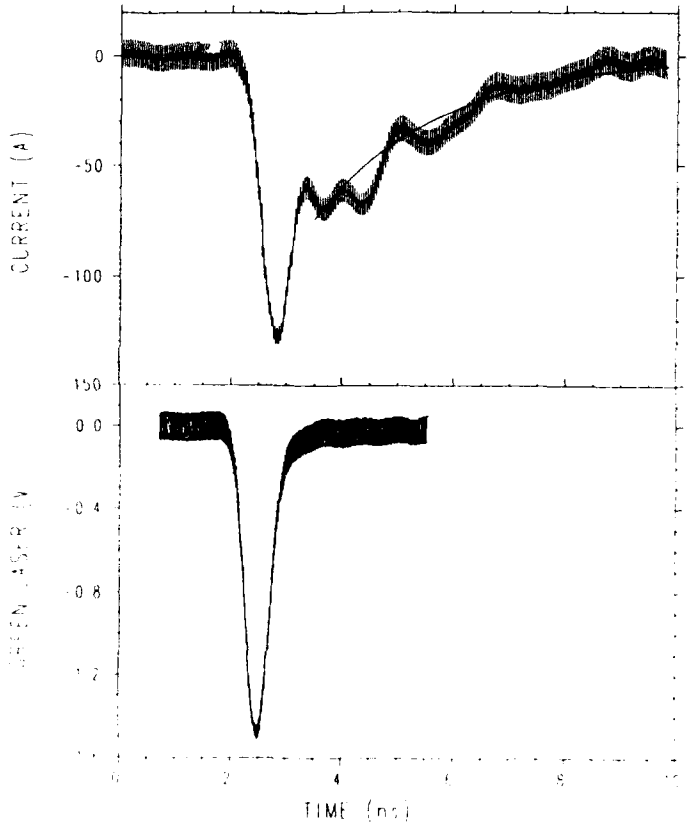

Fig. 1. The current (upper curve) produced by a GaAs PCSS when triggered by a 250 ps wide laser pulse (lower curve) at low fields. Initial switching is followed by carrier recombination which produces a 2 ns exponential decay. The current fall time and the laser pulse width were broadened by the 1 GHz bandwidth of the instrumentation.

*This work was supported by the U S Dept of Energy under Contract No DE-AC04-76DP00789 and SDIO under funding document No. N6092190WRW0036 through the Naval Surface Warfare Center

This type of switch can be used as a toggling switch at very ;h frequencies. Figure 2 shows the voltage delivered to a linear luction accelerator cavity by a 1.5 cm long Cr:GaAs PCSS. This itch was triggered by a burst of pulses from a frequency ubled (532 nm) RF-modulated Nd:YAG laser[8]. The switch may o be triggered with the 1064 nm output from the laser, but :overy is different as shown in figure 3. The initial rapid decay followed by a much longer (700 ns) exponential decay that is used by residual carriers which evidently have a longer :ombination time after being created with 1064 nm photons. ily the initial rapid decay was observed when the switch was ggered with 532 nm photons.

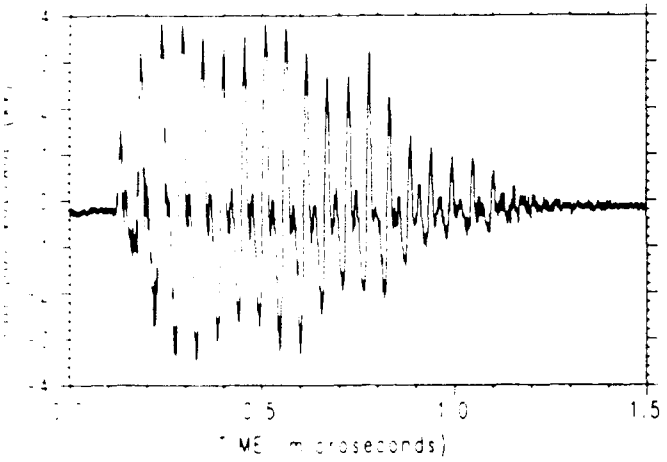

g. 2. This burst of pulses was produced using a Cr:GaAs PCSS low fields to drive an inverting transmission line and a small ear induction accelerator cavity. The phi-dot monitor measures e voltage produced by the cavity on a coil which surrounds the ignetic core. The switch was triggered with an RF-modulated ht source.

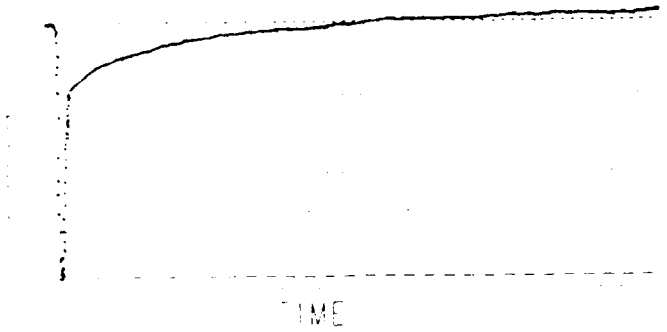

g. 3. Two distinct decay channels are indicated in this easurement of the current produced by a Cr:GaAs PCSS when ggered with 1064 nm (below bandgap) radiation. This current A division) shows a rapid decay (200 ns/division) followed by a ich slower 700 ns exponential decay. Only the fast decay is served when the switch is triggered with 532 nm (above ndgap) radiation.

High Field Operation

Above 3.5 - 8 kV cm (depending on the type of GaAs), ferent behavior is observed. Figure 4 shows the voltage across Cr:GaAs switch that was triggered after pulse charging to several ferent voltage levels. The optical trigger pulse was 8 ns wide m a frequency doubled, Q-switched Nd:YAG laser. At these gher fields, instead of following the light pulse shape, the switch ned on and stayed on (lock-on) until most of the energy in the cuit was discharged. While the switch was on, the voltage oss its contacts did not go to zero. Instead, it dropped to a constant value of about 1.2 kV, the lock-on voltage, which was independent of the initial charging voltage. The current appeared to be whatever the circuit could supply while maintaining the lock-on voltage drop across the switch.

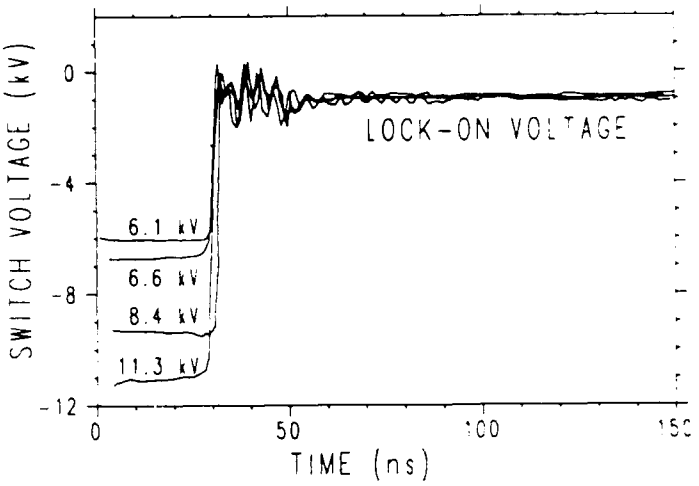

Fig. 4. High field switching of a 2 mm long GaAs switch. This plot shows a constant lock-on voltage for various initial charging voltages. The switch was triggered into this lock-on state with a 10 ns wide laser pulse at 26 ns. The switch continue to conduct until the energy is dumped from the circuit and a 5 kV cm lock-on field can no longer be maintained.

After many tests with different types of GaAs and also one type of InP, we have made the follow observations about this high field mode of switching that we empirically call lock-on:[2,3,6,8,9,10]

1. It occurs only when the voltage across the switch is greater than the lock-on voltage to which the switch settles upon switching.
2. The lock-on voltage of a given switch is given by a material dependent field times the length of the switch.
3. This lock-on field ranges from 3.5 kV m on our purest, lowest resistivity GaAs switches to 8 kV cm on our highest resistivity Cr:GaAs, and was 15 kV cm with InP at room temperature. This field can also be altered by varying temperature and by neutron irradiation.
4. The switch can be optically triggered. DC switches typically held 30 kV/cm without triggering for several minutes. At higher fields, the switches are pulse charged to prevent surface flashover. One 1.5 cm switch withstood 143 kV/cm (214 kV) for 2μs in the dark without switching. The triggering must be concurrent with high fields, as triggering on the rising edge of the pulse charging waveform below the lock-on voltage does not produce lock-on even when the voltage exceeds lock-on 200 ns later.
5. The switch can be triggered into lock-on with nearly three orders of magnitude less optical energy than is required to reach a comparable on-resistance with linear photoconductivity at low fields.

This last characteristic of lock-on indicates some type of gain mechanism and is dramatically apparent when triggering a PCSS with a semiconductor laser diode array[11]. Figure 5 shows the current switched in two different shots. The first shot, plotted against the left vertical axis, did not go into lock-on when charged to 25 kV and triggered with 850 W in 50 ns from a semiconductor laser diode array. The second shot, which is plotted against the right vertical axis, was triggered into lock-on with a similar optical pulse after being charged to 55 kV. Please notice the difference in the two current scales and fall times. In this second shot, an 8.5 MW electrical pulse was delivered to a 38 Ω load with a 1.5 cm long GaAs PCSS triggered by a semiconductor laser diode array.[12]

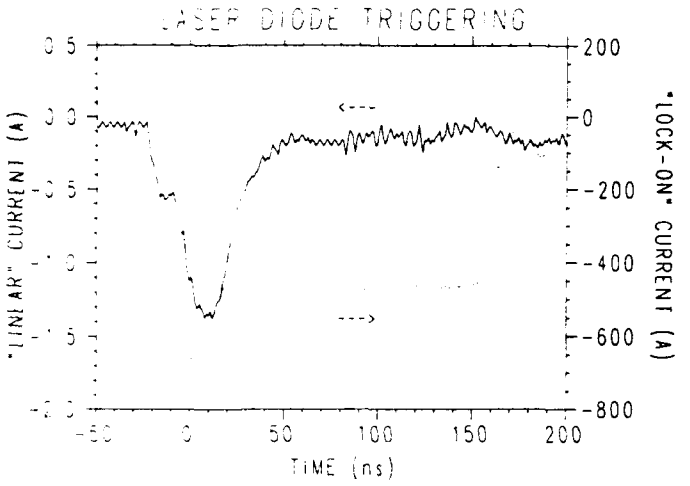

Fig. 5. A comparison of the currents produced by a GaAs PCSS with normal linear photoconductivity (solid, left axis) and with lock-on (dotted, right axis) when activated by a two dimensional semiconductor laser diode array. In the linear mode, the switch was charged to 25 kV, and the current waveform replicated the optical trigger pulse shape of the laser diode array with a 21 ns rise. In lock-on, the switch was charge to 50 kV and the current turned on in 4 ns (instrumentation limited), was 400 times larger, and stayed on until the energy was dumped from the circuit. In this test 850 W from the laser diode array delivered 8.5 MW to a 38 Ω load.

Since the level of the lock-on field is in a range just above the region of the Gunn effect, one explanation for this effect maintains that it is related to the negative differential resistivity exhibited by both GaAs and InP. Evidence of current filamentation[13,14] suggests a different type of negative differential resistivity that causes the Gunn effect. Other phenomena such as double injection, impact ionization of states within the gap, a change in capture cross sections at high fields, and/or a longer recombination time at high fields might explain lock-on, but to date a single explanation has not been confirmed.

Induced Recovery

If PCSS are to be developed as high power fast recovery switches which operate with reasonable optical trigger energies, then a way to induce fast recovery from lock-on must be found. Reducing the field across the switch temporarily after triggering it into lock-on might allow normal (low field) carrier recombination if the semiconductor has no "memory" of the lock-on effect. Three circuits have been explored to test this type of scheme for inducing fast recovery from lock-on.

The first circuit, described in figure 6, uses a transmission line in parallel with the load to reflect a pulse onto the switch and reduce its voltage drop for 20 ns. Recovery was observed when the switch current went to zero before the full voltage returned across the switch. A relatively long voltage pulse is produced at the load because it sees multiple reflections from the transmission line as the PCSS closes. Recovery was always observed provided the optical energy was above 1.5 mJ of 532 nm light. Lock-on could be triggered down to 0.5 mJ, but the switch did not recover when it was triggered with less than 1.5 mJ.[15] For these reasons another test circuit was proposed.

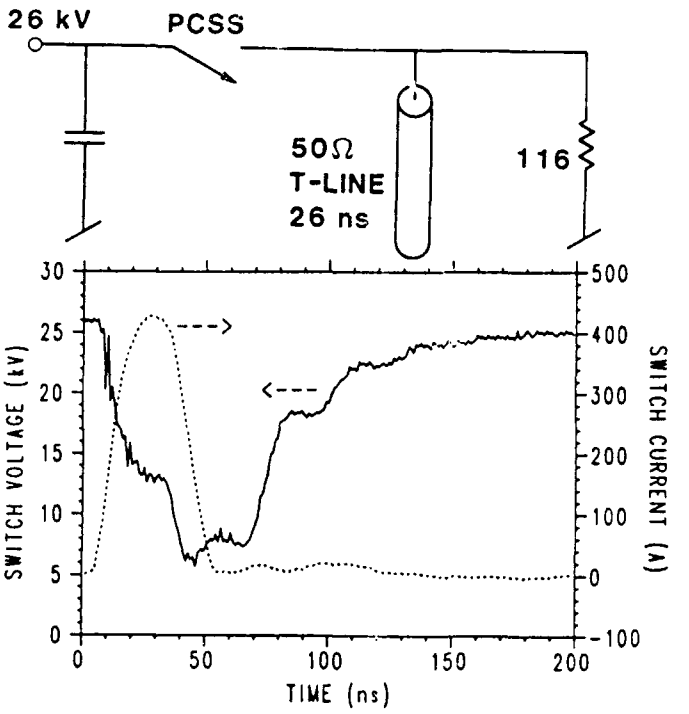

Fig. 6. Recovery from lock-on using a parallel transmission line circuit. The solid line is the voltage across the PCSS (left axis) and the dotted line is the current through the PCSS (right axis). After being triggered into lock-on at 10 ns, the switch sees a reflection from the transmission line at 35 ns which reduces its voltage below lock-on. Recovery of the switch is demonstrated as its current drops to zero by 50 ns. Late time plateaus in the voltage waveform are produced by the intentional miss-match between the load and the transmission line.

The second circuit, described in figure 7, uses a transmission line in series with the load to block the current after it is charged and force the voltage across the switch to drop. A second PCSS is used to discharge the transmission line and produce a pulse of the opposite polarity on the load. The fastest recovery observed was 30 ns after a 25 ns wide pulse was provided to the load (producing a 110 ns period for the complete bipolar waveform). Recovery in this time interval did not always occur, so tests were performed with delays out to 75 ns. Although somewhat more reliable operation was achieved at longer times, the improvement was not consistent with the model of exponential carrier recombination at low fields. Perhaps this circuit does not lower the field sufficiently to induce low field recovery, because the lock-on voltage drop still remains across the switch when the transmission line is charged. Alternatively, the lock-on effect may produce some longer lived carriers which recombine slowly even at low fields. The longest burst of pulses produced using this circuit is shown in figure 8. After the fourth pulse, the charging switch had not recovered when the discharging switch was triggered. When this happens, both switches form a path to ground which bypasses the load. All of the energy in the circuit is dissipated in the switches and at fields of interest they are destroyed.

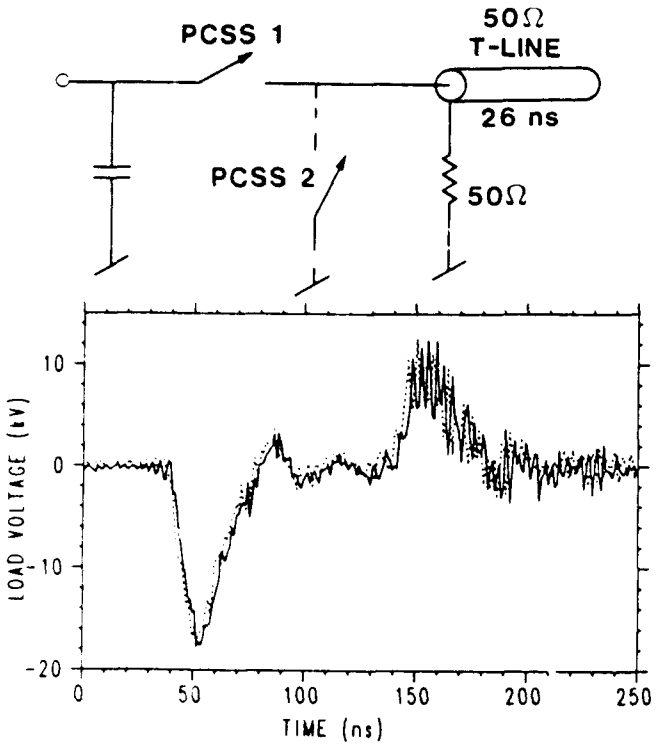

ig. 7. Recovery from lock-on using a series transmission line rcuit. Two waveforms show the reproducibility of this easurement. The first pulse occurs when PCSS 1 is closed and harges the transmission line (through the load). Once the line is harged, the voltage across PCSS 1 is reduced and it's resistance turns. The second pulse occurs when PCSS 2 discharges the ansmission line.

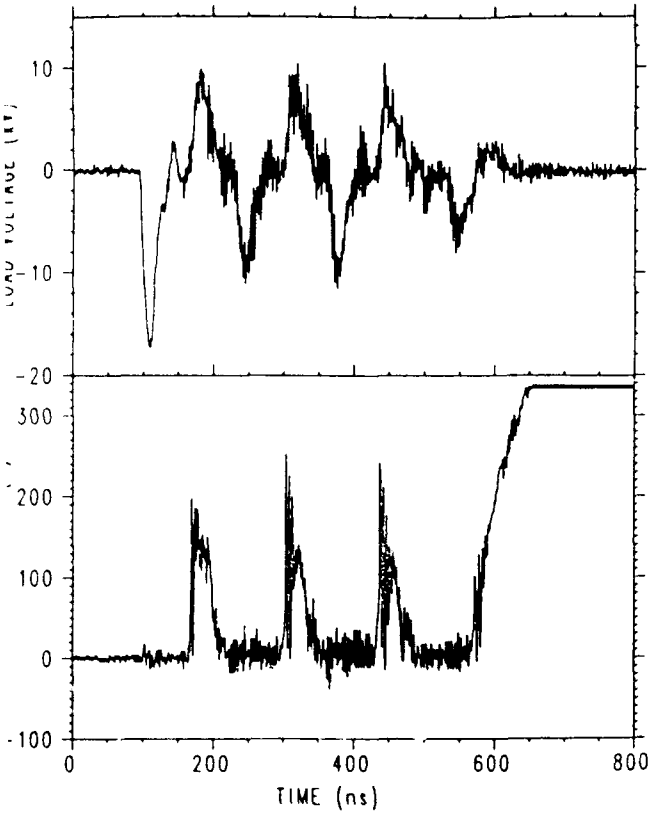

g. 8. A short burst of pulses produced by the circuit shown in e previous figure. Both switches are used to charge and scharge the transmission line repetitively at 5 MHz. The top gure shows the voltage produced across the load. The bottom ows the discharge current which is passed through PCSS 2. On e fourth repetition, PCSS 1 fails to recover it's resistance before SS 2 is triggered, dumping all the circuit energy to ground passing the load.

The third circuit, described in figure 9, is probably the simplest, but was not tested immediately because it appears to be the slowest method of inducing recovery. In this circuit, an inductor is used to limit the recharge current until the switch has recovered. If the transmission line is matched to the switch lock-on resistance (voltage dependent) plus the load resistance, all of the energy from the transmission line will be dissipated when the switch is triggered. A sufficiently large inductor will allow the PCSS to recover before the transmission line is recharged. Unfortunately, with a simple inductor, the recharge rate is fastest initially and approaches full voltage more gradually late in time. A saturable inductor might improve the circuit, but the fastest approach would be to use several of these circuits in parallel. Each switch could be fired successively after the previous switch has recovered, before the transmission line of the previous switch could be fully recharged. This circuit is under construction and will be tested in the near future. Figure 10 shows results from preliminary testing on one branch of the circuit without the PCSS. These "square" pulses are produced as the electrical energy rings back and forth through the saturable inductor. With faster, smaller ferrite cores, we hope to achieve a 200 ns period in each branch. The PCSS will be fired at the end of each charging pulse so that the cores are reset to recharge the line.

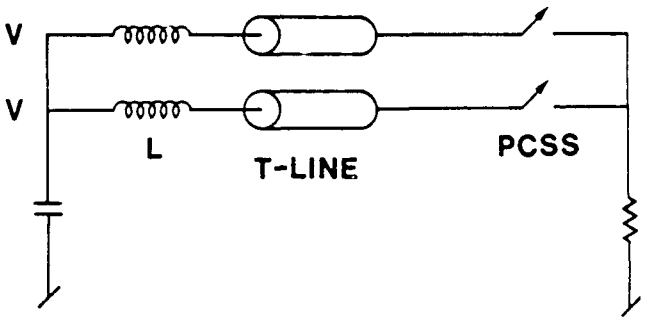

Fig. 9. This circuit uses inductively limited recharging current to give the switches some time to recover at low fields. Since inductive recharging slows as it approaches full voltage, the duty cycle of a single charge line and switch would be low. Saturable inductors and/or multiple charge lines and switches are used to achieve the fastest repetition rate possible.

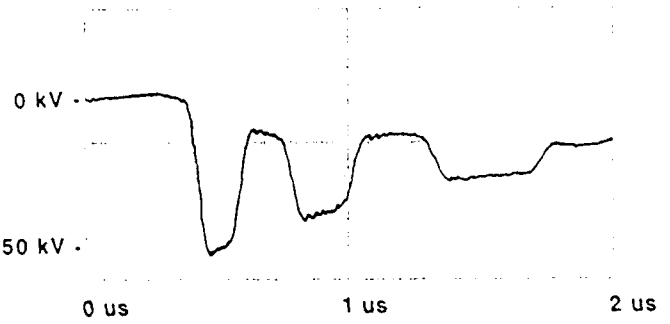

Fig. 10. This figure shows the charging voltage produced on the transmission line in one branch of the circuit shown in figure 9. Faster charging is being pursued.

Conclusion

This paper has discussed the recovery of GaAs PCSS after being triggered into a high gain switching mode called lock-on. The feasibility of inducing fast recovery (30-85 ns) was demonstrated with two circuits, but consistent recovery for many pulses is yet to be achieved. Initial results from a circuit which may produce more reliable conditions for recovery was presented. If reliable recovery is achieved, many high power, high repetition rate applications such as a compact LIA accelerator might be possible with the high gain switching mode called lock-on.

Acknowledgements

The authors would like to acknowledge a collaboration with Arye Rosen and Paul Stabile of David Sarnoff Research Center (DSRC), Princeton, NJ.[10] The (DSRC) laser diode array and one of our 1.5 cm long GaAs switches were used to produce the 8.5 MW results shown in figure 5.

References

[1] D. H. Auston, "Picosecond Photoconductors: Physical Properties and Applications," in *Picosecond Optoelectronic Devices*, edited by Chi H. Lee (Academic Press, New York, 1984) pp 73-117.

[2] F. J Zutavern, G. M. Loubriel, and M. W. O'Malley, "Recent developments in opening photoconductive semiconductor switches," in *Proc. 6th IEEE Pulsed Power Conf.*, Arlington, VA, pp. 577-580, 1987.

[3] W. C. Nunnally and R. B. Hammond, "80-MW photoconductor power switch," *Appl. Phys. Lett.*, vol. 44, pp. 980-982, May 15, 1984.

[4] G. M. Loubriel, M. W. O'Malley, F. J Zutavern, B. B. McKenzie, W. R. Conley, H. P. Hjalmarson, "High Current Photoconductive Semiconductor Switches," in *Proc. 18th IEEE Power Modulator Symposium*, Hilton Head, SC, pp. 312-317, 1988.

[5] R. L. Druce, M. D. Pocha, K. L. Griffin, and W. W. Hofer, "Subnanosecond Linear GaAs Photoconductive Switching," in *Proc. 7th IEEE Pulsed Power Conf.*, Monterey, CA, pp. 882-886, 1989.

[6] G. M. Loubriel, M. W. O'Malley, and F. J. Zutavern, "Toward pulsed power uses for photoconductive semiconductor switches: closing switches," in *Proc. 6th IEEE Pulsed Power Conf.*, Arlington, VA, pp. 145-148, 1987.

[7] F. J Zutavern and M. W. O'Malley, "Engineering Limits of Photoconductive Semiconductor Switching in Pulsed Power Applications," in *Proc. 17th IEEE Power Modulator Symposium*, Seattle, WA, pp. 214-218, 1986.

[8] F. J Zutavern, B. B. Mckenzie, G. M. Loubriel, M. W. O'Malley, R. A. Hamil, L. P. Schanwald, "Multiple Pulse Photoconductive Semiconductor Switching," in *Proc. 18th IEEE Power Modulator Symposium*, Hilton Head, SC, pp. 307-311, 1988.

[9] G. M. Loubriel, F. J Zutavern, B. B. McKenzie, and M. W. O'Malley, "Closing photoconductive semiconductor switches," in *Proc. 7th IEEE Pulsed Power Conf.*, Monterey, CA, pp. 365-367, 1989.

[10] F. J. Zutavern, G. M. Loubriel, M. W. O'Malley, D. L. McLaughlin, and W. D. Helgeson, "Rise Rime and Recovery of GaAs PCSS", in *Proc. SPIE Symposium on Optically Activated Switching*. Boston, Nov. 1990, pp 271-279.

[11] A. Rosen, P. Stabile, W. Janton, J. C. McShea, A. Rosenberg, J. C. Petheram, H. G. Miller, J. W. Sprague, and J. M. Gilman, "1 kW Peak Power 808 nm 2-D Laser Diode Array, "*IEEE Photonic Tech. Lett.*, vol. 1, pp. 43-45, Feb., 1989.

[12] Arye Rosen, Paul Stabile, F. J Zutavern, G. M. Loubriel, W. E. Helgeson, M. W. O'Malley, D. L. McLaughlin, "8.5 MW Pulse Biased GaAs Switch Optically Controlled by 2-D Laser Diode Arrays," *Photonic Tech. Lett.*, July, 1990.

[13] F. J Zutavern, G. M. Loubriel, B. B. Mckenzie, and M. W. O'Malley, "Photoconductive Semiconductor Switch Recovery," in *Proc. 7th IEEE Pulsed Power Conf.*, Monterey, CA, pp. 412-417, 1989.

[14] F. J Zutavern, G. M. Loubriel, M. W. O'Malley, W. D. Helgeson, D. L. McLaughlin, "High Gain Photoconductive Semiconductor Switching," to be published in *Proc. 8th IEEE Pulsed Power Conference*. San Diego, CA, 1991.

[15] R. Aaron Falk, Jeff C. Adams, and Gail L. Bohnhoff-Hlavlacek, "Optical Probe Techniques for Avalanching Photoconductors" to be published in *Proc. 8th IEEE Pulsed Power Conference*. San Diego, CA, 1991.

*

Fred J Zutavern is a senior member of the technical staff at Sandia National Laboratories (SNL), Albuquerque, New Mexico. He graduated with a Ph.D. specializing in solid state physics from Princeton University in 1982. After working briefly in the Department of Physics at the University of Virginia, he joined the staff at SNL to work in pulsed power development. In his eight years at SNL, he has conducted experiments on electrical breakdown in water, designed and tested multi-megavolt liquid dielectric transmission lines, and initiated an extensive research program to develop photoconductive semiconductor switches for pulsed power applications. His work on a team in the nuclear weapons program was recognized with an Award of Excellence in 1986.

*

Guillermo M. Loubriel received his Ph.D. degree in solid state physics from the University of Pennsylvania in 1979. Since then he has been at Sandia National Laboratories, where he is now a Senior Member of Technical Staff. His areas of research include surface science, photoemission, stimulated desorption, defects and flashover alkali halides, ion sources for particle beam fusion accelerators, flashover in semiconductors, and photo-effects and transports in semiconductors. He is presently the Senior Scientist in the efforts to use photoconductive semiconductor switches in conventional munition firing sets, nuclear weapons firing sets, and impulse radars. He has published over 50 papers with 20 or more on his research in photoconductive semiconductor switches.

*

M. W. O'Malley's biography not available at the time of publication.

*

W. D. Helgeson's biography not available at the time of publication.

*

D. L. McLaughlin's biography not available at the time of publication.

PROGRESS IN THE DEVELOPMENT OF SEMICONDUCTOR-METAL EUTECTIC TRANSISTORS FOR HIGH POWER SWITCHING

M. Levinson, Q. V. Nguyen, P. G. Rossoni, and B. M. Ditchek

GTE Laboratories Incorporated
40 Sylvan Road, Waltham, MA 02254

Abstract — Semiconductor-metal eutectic composite transistors have the potential for very high hold-off voltages combined with low on-state resistance. We have performed computer simulations and experimental studies of the effects of composite microstructure on Si-$TaSi_2$ composite device performance. They show how microstructural control can lead to enhanced hold-off voltage and on-state conductance, and affect response speed. Improved composite microstructures were achieved by modifying crystal growth procedures.

I. INTRODUCTION

We have previously demonstrated a new class of high power transistors based on Si-$TaSi_2$ semiconductor-metal eutectic (SME) composite materials.[1-3] These devices are bulk field-effect transistors with the potential for very high voltage operation, due to the unique device physics afforded by the composite microstructure. The device geometry is shown in Fig. 1. Source-drain current flows between the cylindrical Schottky junctions formed by the metal fibers and the semiconductor. Application of a bias to the gate contact expands the depletion zones of the junctions accessed by the contact, pinching off the current channels and controlling the drain current.

The high voltage properties of these devices arise from the uncontacted junctions which lie between the gate and drain contacts. These junctions float in potential in a manner similar to guard rings and spread increasing drain potential over successively larger distances. With proper carrier concentration and interjunction spacing, avalanche breakdown is suppressed. Breakdown will eventually occur at the drain voltage where the gate depletion region reaches the drain contact. Therefore, the avalanche breakdown voltage is determined primarily by the gate-drain distance, rather than the carrier concentration as in conventional devices. It can, in principle, be made arbitrarily large, although in practice the maximum device hold-off voltage may be determined by external factors such as surface breakdown.

We have previously reported Si-$TaSi_2$ SME transistors with hold-off voltages of 1000 V, made with material of carrier concentration which would yield avalanche breakdown at a maximum of 300 V in conventional devices.[2,3] We have also demonstrated high quality Si epilayers grown on Si-$TaSi_2$ composite substrates, which should allow the integration of these devices with conventional

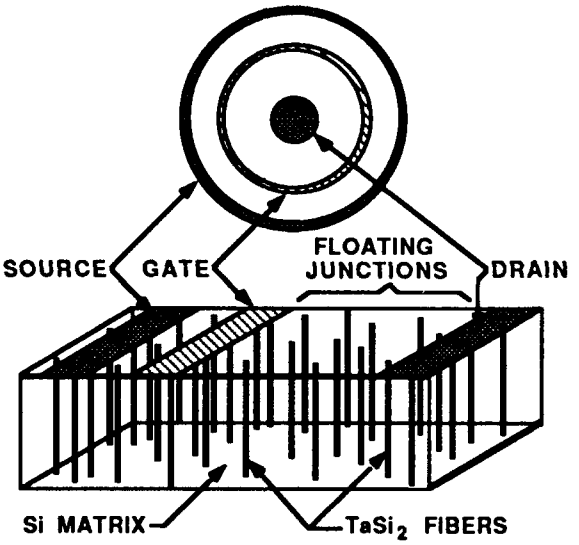

Fig. 1. SME transistor geometry.

Si circuitry.[4]

Here we describe computer simulations which show how composite microstructure could be optimized to simultaneously provide high hold-off voltage and low on-state resistance. A new electron microscopic technique was used to graphically observe the relationships between microstructure and electronic performance, including the effects of the floating junctions. We have also performed transient simulations and response speed measurements to identify factors affecting switching speed. Si-$TaSi_2$ material with improved microstructure was obtained by modifications of crystal growth procedures.

II. MICROSTRUCTURE OPTIMIZATION

In conventional high power semiconductor devices, maximum hold-off voltages are in general determined by avalanche breakdown. The breakdown voltage, V_B, is a greatest for planar junctions and is approximately inversely proportional to the carrier concentration. However, the on-state conductivity per unit junction area, σ_A, is also determined by the carrier concentration and the length of material needed to support the depletion zone at breakdown, with the result that $\sigma_A \propto 1/V_B^2$. Therefore, high voltage devices must have large cross-sectional area to achieve acceptably low on-state series resistance.

In SME devices, on the other hand, V_B is not directly determined by the carrier concentration, but rather is proportional to the gate drain distance. Increasing drain potential is spread over a continuously greater distance as the gate depletion zone expands towards the drain and "picks up" successive rows of floating junctions. This process may continue until the depletion zone reaches the drain contact where, with further voltage increases, avalanche will occur. In this case, $\sigma_A \propto 1/V_B$. Therefore, for a given microstructure, there exists a cross-over point in V_B above which the SME device can, in principle, have lower σ_A than any conventional transistor.[5]

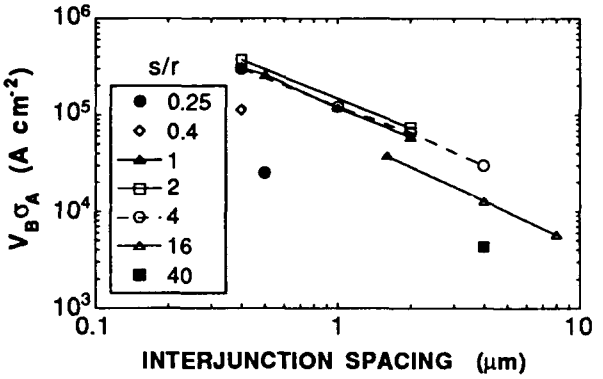

Fig. 2. Calculated $V_B\sigma_A$ vs. interjunction spacing, s, for various spacing/radius ratios.

In order to determine the effects of composite microstructural parameters on σ_A, simulations were performed using the PISCES-IIB code.[5,6] Cylindrical junctions of radius r were placed in a square array with interjunction spacing s. The primary criterion was to determine the maximum carrier concentration, N_D, that can be sustained without avalanche breakdown occurring. This condition corresponds to the N_D which yields a junction depletion zone width at avalanche just equal to s. In other words, as the drain bias, V_D, increases, the gate depletion zones expand, but just at the point where avalanche breakdown would occur, the depletion region intersects that of the next floating junction, which then floats in potential and takes on any succeeding increase in V_D.

Depletion widths at breakdown were calculated as a function of r and N_D using simulations of impact ionization in a cylindrical geometry. For a given r and s, N_D for a depletion width equal to s was used to simulate device I-V characteristics, from which σ_A was calculated. Because V_B is proportional to the gate-drain distance, and σ_A is inversely proportional, a useful figure of merit for comparing composite parameters which does not depend on distance is $V_B\sigma_A$. The results are shown in Fig. 2 as a function of s for a number of s/r ratios. For a constant r, performance improves with decreasing interjunction spacing, s, because higher N_D can be used without avalanche occurring, thus

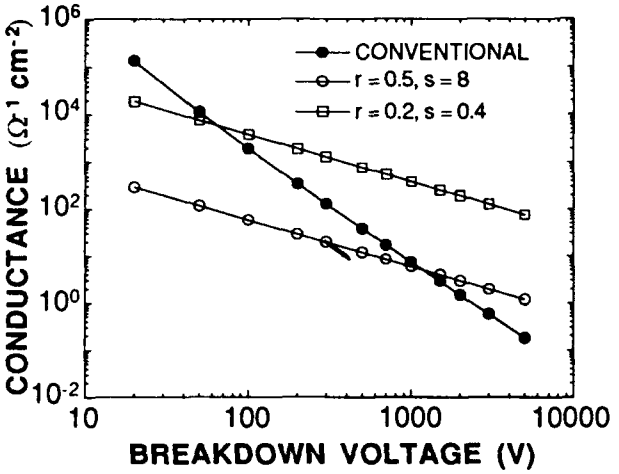

Fig. 3. Optimum areal conductance vs. breakdown voltage for conventional devices and SME devices with two combinations of junction radii and spacing.

lowering σ_A. The optimum s/r ratio is about 2:1. At lower values, σ_A is reduced by the smaller cross-sectional area of the current channels, while at higher values, a lower N_D is needed to prevent breakdown.

Fig. 3 compares the predicted optimum σ_A as a function of V_B for two sets of r and s values and for conventional semiconductor devices using planar junctions. For $r = 0.5$ μm and $s = 8$ μm, similar to existing Si-$TaSi_2$ composites, the optimum SME device will have higher conductivity than conventional devices for V_B in excess of ~1 kV. For example, σ_A should be greater by a factor of ~15 for V_B = 10 kV. However, devices made using a hypothetical denser composite with $r = 0.2$ μm and $s = 0.4$ μm could be superior to conventional ones for any V_B above ~ 50 V. In this case, σ_A could be up to ~50 times greater than in conventional devices for V_B = 1 kV and ~1000 times greater for V_B = 10 kV.

III. ELECTRONIC MICROCHARACTERIZATION

In addition to the effects of idealized SME microstructural parameters, real composites may have properties which vary on a microscopic scale because the active junctions are self-assembled during crystal growth and are not as uniform in size, shape, and spacing as those used in the simulation models. Previous studies showed that the spacing and arrangement of the $TaSi_2$ junctions in actual materials can have a large effect on current transport.[7,8] Therefore, the optimization of these devices will require a more detailed understanding of the relation between material microstructure and device electronic properties.

Recently, we devised a new three-terminal electron-beam-induced conductivity (TTEBIC) technique[9] which images the microscopic current characteristics of field-effect transistors during device operation and shows their relation to device structure. Image contrast is generated in the scanning electron microscope using variations of drain current which arise from electron-beam-induced perturbations of the electric fields within the device. In these images, darker contrast indicates areas where the drain current is constricted. The active areas of gate depletion zones are thus made visible and can be imaged at different points in the device I-V characteristic.

Fig. 4 shows a portion of the gate ring of an SME transistor. The electron beam is incident on the surface of the wafer opposite the contacts, and the drain is to the right of the image. Fig. 4(a) shows a conventional charge collection image of the ends of the $TaSi_2$ junctions which are accessed by the gate contact. The depletion zones appear as bright annuli around the fibers. In Fig. 4(b) at V_G = 0 V and V_D = 10 V, the dark areas of the TTEBIC image show those regions of the gate where the current is concentrated. It is seen that they are not uniformly distributed along the gate. They appear where the spacing between $TaSi_2$ junctions is greatest. These and other images show that non-uniformities of fiber distribution can result in delayed drain current saturation (the "knee" of the I-V curve occurring at higher V_D) and excess leakage current at pinch-off.[9]

Comparison of Figs. 4(a) and 4(b) also graphically shows the effect of the floating junctions. The right-hand dark regions are

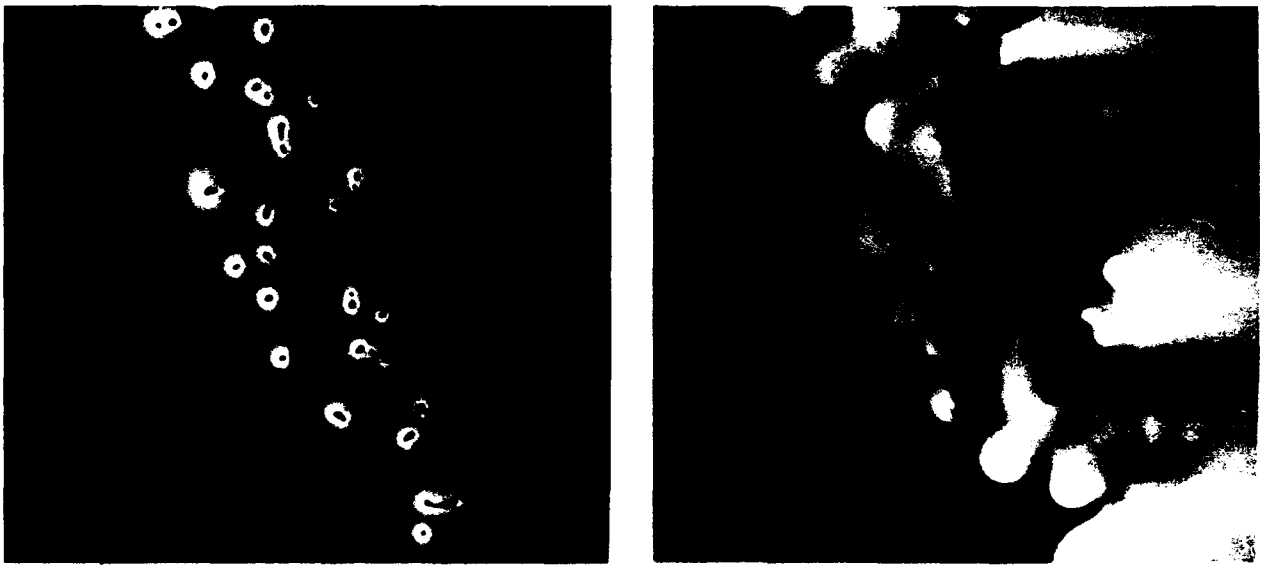

(a) (b)

Fig. 4. (a) Conventional EBIC image of a portion of an SME transistor gate. (b) TTEBIC image of the same region showing the principle current channels.

seen to lie to the right of the junctions accessed by the gate contact. These current-limiting areas are therefore created by junctions which are floating, and they are supporting a portion of the drain potential.

IV. CRYSTAL GROWTH

The crystal growth process is a crucial factor in the performance of SME devices because they rely on the operation and interaction of multiple junctions which are self-assembled during growth. Although the growth rate determines the average $TaSi_2$ fiber density, and thus the average interjunction distance, the work described above highlights the need for good microstructural uniformity on both a macroscopic and microscopic scale. Such uniformity can only come from a detailed understanding and control of composite crystal growth.

We have made progress in uniformity control by studying the effects of crucible and seed rotation rates in the Czochralski crystal growth used for these materials. Fiber densities were determined by automated counting of the number of fibers ends visible in a sequence of 85 μm square frames along a diameter of polished wafers.

It was found that by eliminating rotation of the seed, smaller variations in the fiber density were obtained. A wafer from a portion of a

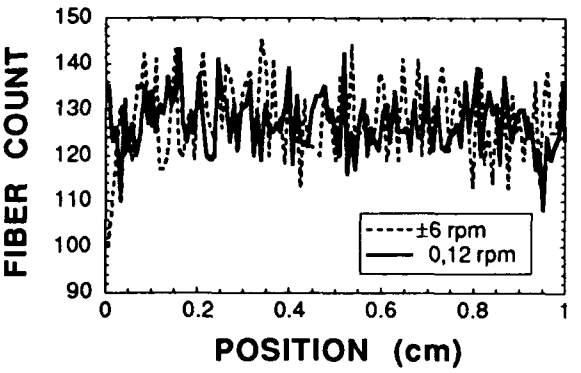

Fig. 5. Counts of $TaSi_2$ fibers in 85 μm square frames vs. position for two wafers grown with seed and crucible rotation of ±6 rpm and 0, 12 rpm.

a boule grown with no seed rotation and crucible rotation of 12 rpm exhibited a mean fiber count of 127.0 with a standard deviation of 6.85, compared to one grown with seed rotation of 6 rpm and crucible counterrotation of -6 rpm, which yielded a mean and standard deviation of 127.6 and 8.40, respectively. Fiber counts vs. position for the two wafers are shown in Fig. 5.

Although these measurements are on too large a scale to predict improvements in individual device performance by using material grown without seed rotation, they would at the least infer better device yield. Measurements of microscale uniformity in this material are in progress.

V. TRANSIENT RESPONSE

The response speed of SME transistors will be affected by transit time delay and parasitic capacitance and resistance in the same way as conventional FET's. But a major question is how, if at all, these properties will be affected by the floating junctions. The floating junctions in SME transistors create a depletion region whose length varies greatly between the on-state, where it is simply the length of the gate contact region, and the off-state, where it extends over a large portion of the gate-drain distance and depends on V_D. Therefore, it is expected that the transit time would differ between the turn-on (closing switch) and turn-off (opening switch) processes.

When the device is in the process of turning off, carriers which have passed through the gate contact depletion region will not contribute further to transit delays because their motion will be accompanied by current in the drain contact. Therefore, the turn-off process should not be greatly affected by the floating gates, but should be governed by parasitic capacitance and resistance as in conventional metal-semiconductor FET's.

During the turn-on process, on the other hand, the first carriers to transit the gate region must pass through the extended depletion zone before they can force current at the drain. The transit time will decrease significantly as the depletion region collapses back toward the gate contact. The rate of this collapse will be determined by the gate-source and gate-drain capacitances. Thus the turn-on transient may be slower than that of turn-off, with a time constant that would increase with increasing V_D.

There is an additional phenomenon that may affect the turn-on response of floating junction devices. It is commonly observed in devices using guard rings.[10] The floating junctions exchange charge with the bulk semiconductor as their potential shifts. During the turn-off process, they float towards the drain potential and lose charge by a majority carrier current to the drain. During turn-on, however, the opposite charging process must occur by minority carrier current or leakage and is relatively slow. During this time, the depletion zones of the floating junctions are larger than when they are neutral, thus constricting the current channel and producing a long time-constant tail to the drain current during turn-on.

PISCES simulations of SME transistor transient behavior illustrate this effect. Fig. 6 shows the calculated turn-on response of a model device for V_D = 50, 200, and 300 V. A constant value of load resistance was used, so that the on-state operating point is moving up the *I-V* curve with increasing V_D. At V_D = 50 V, the device is in the linear region in the on-state, so the gate depletion zones are not greatly

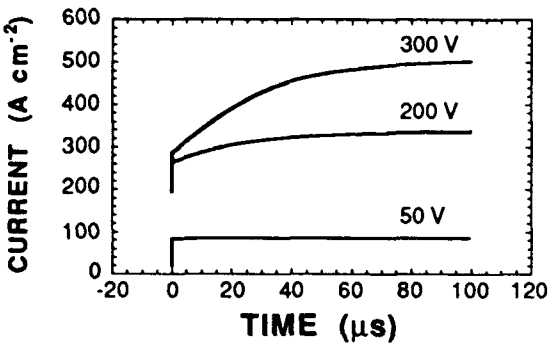

Fig. 6. Simulated SME transistor turn-on response for different V_D.

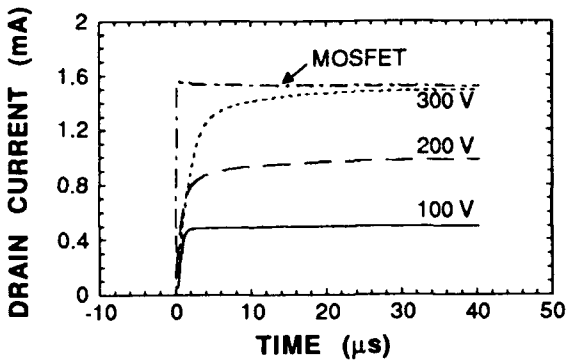

Fig. 7. Measured turn-on response of a Si-$TaSi_2$ transistor for different V_D. Conventional power MOSFET shown for comparison.

extended, and the floating junctions are neutral. However, at V_D = 200 and 300 V, the drain current is saturating and the floating junctions are active. Slow tails in these transients are seen whose magnitudes increase with V_D.

Experimental turn-on transients are shown in Fig. 7 for a Si-$TaSi_2$ device at V_D = 100, 200, and 300 V, again with a constant load resistor. A conventional power MOSFET is shown for comparison. The data show slow tails of increasing magnitude with increasing V_D, in agreement with model predictions. However, the time constants are faster than expected. This is likely due to larger than ideal reverse leakage current in the floating junctions of the actual device.

On the other hand, as expected, PISCES simulations showed much faster turn-off characteristics, on the order of a few hundred ps, although the very small simulation geometry leads to small capacitances. Measurements of the device shown in Fig. 7 revealed a turn-off transient of 20 ns, which is limited by the speed of the test circuit.

VI. CONCLUSIONS

The above work shows that SME transistors have the potential to simultaneously provide very high blocking voltages and low on-state resistance. As opening switches, they should be capable of very fast response speeds, although charging effects in the floating junctions which enable their high voltage performance can limit turn-on response in closing switch applications. We have also shown the importance of microstructural uniformity for the achievement of optimum device properties, and how higher junction density could lead to even lower on-state resistance while maintaining high blocking voltages. Improved composite microstructures will require better crystal growth methods, and we have made some progress by optimization of the seed and crucible rotation rates.

ACKNOWLEDGEMENTS

The assistance of J. Hefter and T. Middleton is gratefully acknowledged. This work was supported in part by the Strategic Defense Initiative Office/Innovative Science and Technology (SDIO/IST) and managed by the Office of Naval Research under contract N00014-86-C-0595.

REFERENCES

[1] B. M. Ditchek, T. R. Middleton, P. G. Rossoni, and B. G. Yacobi, "Novel high voltage transistor fabricated using the *in situ* junctions in a Si-$TaSi_2$ eutectic composite," Appl. Phys. Lett. **52**, 1147 (1988).

[2] M. Levinson, P. G. Rossoni, F. Rock, and B. M. Ditchek, "High voltage floating gate array transistors," Electron. Lett. **26**, 777 (1990).

[3] M. Levinson, P. G. Rossoni, W. Byszewski, and B. M. Ditchek, "High Voltage Bulk MESFET Using *In-Situ* Junctions," *Proc. 1990 Nineteenth Power Modulator Symposium, San Diego, CA*, (IEEE, New York, 1990), 347.

[4] M. Levinson, M. Tabasky, C. Sung, G. Hamill, D. H. Matthiesen, K. Ostreicher, and B. M. Ditchek, "Silicon Epitaxial Growth on Si-$TaSi_2$ Eutectic Composite Substrates," Appl. Phys. Lett., in press.

[5] P. G. Rossoni, M. Levinson, and B. M. Ditchek, "Floating junction effects in semiconductor-metal eutectic transistors," J. Appl. Phys., in press.
[6] PISCES-IIB, Stanford Electronics Laboratories, Stanford, CA
[7] B. M. Ditchek, B. G. Yacobi, and M. Levinson, "Depletion zone limited transport in Si-$TaSi_2$ eutectic composites," J. Appl. Phys. **63**, 1964 (1988).
[8] V. K. Samalam, " Si-$TaSi_2$ eutectic composites as an example of a percolation system," J. Appl. Phys. **67**, 2165 (1990).
[9] M. Levinson, P. G. Rossoni, and B. M. Ditchek, "Electrical microcharacterization of semiconductor-metal eutectic transistors by three-terminal electron-beam-induced-conductivity," J. Appl. Phys., in press
[10] M. K. Johnson, A. D. Annis, J. N. Sandoe, and D. Coe, "An analysis of the dynamic behavior of field-limiting ring-passivation systems," IEEE Trans. Electron Dev. **36**, 1203 (1989).

M. Levinson, photograph and biography not available at the time of publication.

Q. V. Nguyen, photograph and biography not available at the time of publication.

P. G. Rossoni, photograph and biography not available at the time of publication.

B. M. Ditchek, photograph and biography not available at the time of publication.

POWER GAIN IN A PHOTOCONDUCTIVE SEMICONDUCTOR SWITCH CONTROLLED INDUCTIVE PULSED POWER SYSTEM

E. E. Funk, E. A. Chauchard, Chi H. Lee, and M. J. Rhee

Department of Electrical Engineering
University of Maryland
College Park, MD 20742

ABSTRACT

An 80 kW, 2 kV pulse has been generated with a GaAs photoconductive semiconductor switch controlled inductive energy storage pulsed power system (IESPPS) with a current charged transmission line. The 2 kV pulse was generated from the energy stored in a capacitor initially charged to 300 V, yielding a voltage gain of 7, and a power gain of 49.

I. INTRODUCTION

Over the past two decades pulsed high power applications which require high performance switches have been developing at a rapid pace. Some of these applications include electrical-discharge lasers, electron beam pumped lasers, flash x-ray power supplies, and high power microwave generation. Switching voltage requirements can be up to a megavolt and often the timing must be very accurate[1].

The focus of this work is on the development of an optically controlled pulsed-power system which will be capable of delivering high-power pulsed energy for these applications. The key element in the system is the GaAs photoconductive semiconductor switch (PCSS). We discuss the advantages of using a GaAs PCSS as well as a scheme for employing the PCSS to produce the highest possible output voltage. A 2.1 kV, 80 kW output pulse was demonstrated with an initial charging voltage of 300 V, corresponding to a voltage gain of 7 and power gain of 49. The result is the first demonstration of voltage gain in an inductive energy storage pulsed power system (IESPPS). In order to obtain high voltage gain, it is necessary to match the switch design with the circuit design and laser pulse characteristics. This led to the development of a specially tailored Nd:Glass laser system which is used to activate the switch since no suitable commercial system was available. Details of this system and the PCSS design are given in the following sections.

II. INDUCTIVE ENERGY STORAGE PULSED POWER SYSTEMS

Capacitive energy storage pulsed power systems (CESPPS) are often used to produce pulsed power. In its most basic form, the CESPPS is merely a capacitor which is discharged through a closing switch into the desired load. A primary limitation in these systems is the maximum bias voltage of the capacitor, beyond which the capacitor may not be charged. The bulkiness of capcitors often makes them inconvenient for use in high-voltage pulsed power applications.

This has led to the development of the inductive energy storage pulsed power system (IESPPS), where energy is stored by the current in an inductive element such as a coil, rather than stored by charge on the plates of a capacitor. Voltage step-up is inherent in this scheme, rendering transformers and other voltage step-up devices unnecessary.

A typical IESPPS is shown in Figure 1. The switch is initially closed and the induc-

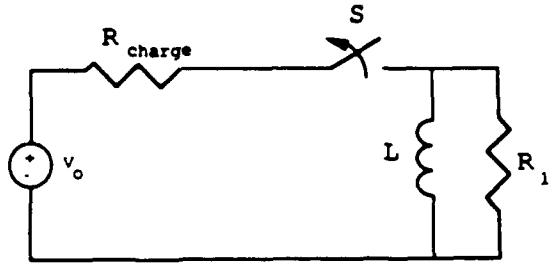

Figure 1:Basic inductive energy storage pulsed power system.

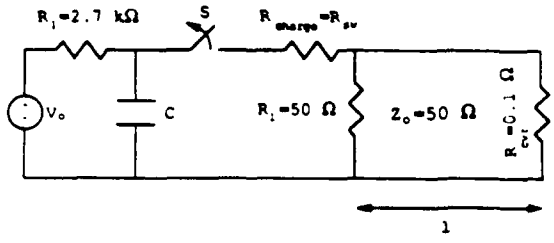

Figure 2:Experimental inductive energy storage pulsed power system.

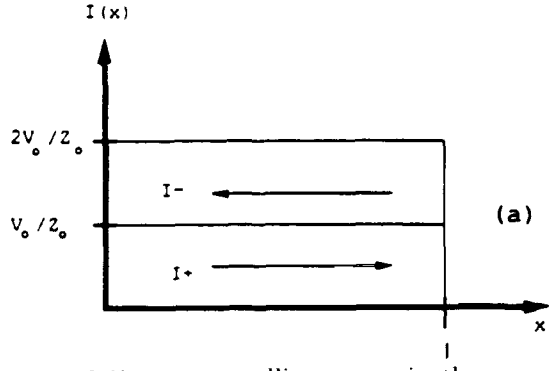

Figure 3:Current travelling waves in the current charged transmission line.

tor is charged to the current $I_o = V_o/R_{charge}$. When the switch is opened the stored current passes through the load, producing a voltage pulse of peak amplitude,

$$V_{out} = I_o R_l = V_o \frac{R_l}{R_{charge}} \qquad (1)$$

We see that if $R_l > R_{charge}$, there will be a voltage gain.

A variation of the IESPPS is achieved by adding a capacitor in parallel with the voltage source, replacing the inductor with a current charged transmission line (CCTL), and using a PCSS as the switch. A CCTL is used rather than an inductor because of it's fast response time. If the capacitance of the capacitor is large enough, the capacitor may be treated as a voltage source, and the charging resistance, R_{charge}, is then merely the PCSS on-resistance. The circuit is shown in Figure 2.

The CCTL is a transmission line of length l and characteristic impedance, $Z_o = 50\ \Omega$. A 0.1 Ω current viewing resistor (CVR) allows the current through the CCTL to be monitored.

The behavior of the CCTL is most easily understood by considering the ideal case where the capacitance, C, is large enough to be treated as a voltage source; that is, the voltage across the capacitor remains essentially constant, even after the switch is closed. The capacitor is initially charged to the voltage, V_o. When the switch is closed, the capacitor is the source of a current travelling wave of amplitude $I = V_o/Z_o$, where Z_o is the characteristic impedance of the CCTL, and V_o the voltage to which the capacitor is initially charged. This is shown in Figure 3. As the travelling wave meets either end of the CCTL, it is reflected in phase causing the current to increases by a step of $I = 2V_o/Z_o$ after each round trip in the CCTL. This is illustrated in Figure 4. When the switch is opened the travelling wave is terminated in the matched 50 Ω load resistor producing a voltage across the load. If the switch is closed for a period t_c

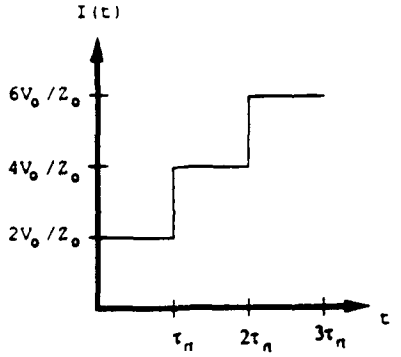

Figure 4:Theoretical staircase-like current charging in the current charged transmission line.

and then opened, the peak voltage delivered to the load exceeds the voltage to which the capacitor was initially charged. The factor of voltage gain, g, is:

$$g = t_c/\tau_{rt}, \qquad (2)$$

where τ_{rt} is the round trip transit time of the travelling wave. Figure 5 illustrates the current charging in steps as the result of reflections from the ends of the CCTL. The reflection coefficient for current from the shorted end and the end with the capacitor is taken as -100%. The voltage delivered to the load when the switch is opened is $V_l = I(t)Z_o/2 = V_o t_c/\tau_{rt}$.

The behavior of this circuit may also be analyzed from the point of view of a lumped circuit analysis. We treat the CCTL as a lumped inductance as shown in Figure 6. The equivalent inductance of the CCTL is $L = Z_o l/v$, where v is the travelling wave velocity in the CCTL. The theoretical current through the inductor, $I(t)$, may be found by using Kirchoff's Voltage Law and a Laplace transform. The result is:

$$I(t) = I_o(exp(s_1 t) - exp(s_2 t)), \qquad (3)$$

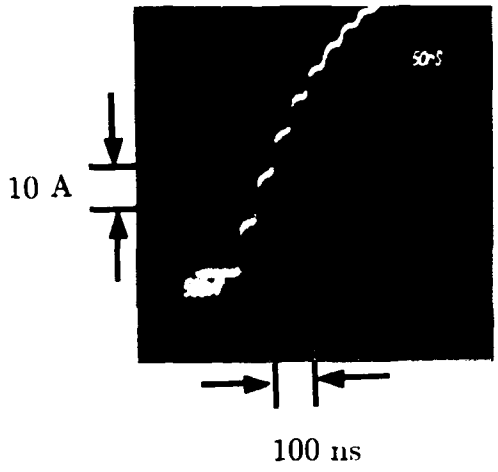

Figure 5:Experimental staircase-like current charging in the current charged transmission line.

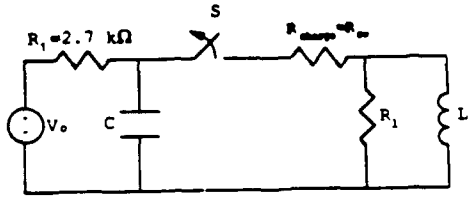

Figure 6:Current charged transmission line modeled as a lumped inductance.

where $s_{1,2} = \frac{-b \pm \sqrt{b^2-4ac}}{2a}$,
$I_o = \frac{V_o R_l}{2L(R_l+R_{sw})(s_1-s_2)}$,
$a = LC(R_{sw} + R_l)$,
$b = R_{sw}R_l C + L$, and $c = R_l$.

Depending on the values of a, b, and c, s will represent either an underdamped, overdamped, or critically damped oscillation of $I(t)$. The oscillation is underdamped if $4ac > b^2$, critically damped if $b^2 = 4ac$, and overdamped if $4ac < b^2$.

Equation (3) is essential for designing an IESPPS which provides voltage gain. The component values, R, C, and L are chosen along with an appropriate charging time to provide the highest possible charging current

at the time of the switch opening. When the switch is opened, the amplitude of the voltage pulse delivered into the load is given by $V_{out} = I(t_{open})R_l/2$, where t_{open} is the time at which the switch opens.

III. PHOTOCONDUCTIVE SEMICONDUCTOR SWITCH

The next component to consider in the IESPPS is the switch. So far, it has been assumed that the switch could be opened or closed at will. Furthermore, nothing has been said about how fast the switch must open or close, or by what means the switch is to be controlled. In this work, an optically controlled PCSS is used, and we will consider its performance in light of such considerations.

The ideal switch has the following charateristics[2]. (1) fast opening time compared to conduction time, (2) fast closing time compared to conduction time, (3) fast recovery, (4) controllable conduction time, (5) low switch on-resistance, (6) high switch off-resistance, (7) large stand-off voltage, (8) jitter free operation.

A fast closing switch significantly simplifies the analysis of the IESPPS performance. With a fast closing switch, we may invoke the relatively simple model based on equation (3) discussed above which predicts the charging current vs. time by assumming an infinitely fast closing switch.

Fast opening time, t_{op}, is essential in achieving high power gain with the CCTL. When the switch is opened, the current which is stored as a travelling wave in the CCTL is terminated in the matched load, producing the output pulse across the load. If the switch resistance does not immediately rise well above the load resistance, some of the energy stored as current in the CCTL will be dissipated in the switch rather than in the load. Therefore, the opening switch must reach its dark resistance value well before the end of the output pulse. The theoretical output pulse length is equal to the round-trip transit time, τ_{rt}, in the CCTL. Hence, the switch opening time imposes a design limit on the length of the CCTL. The CCTL must be kept long enough to ensure that $\tau_{rt} >> t_{op}$.

According to equation (2), the voltage gain, and hence the output voltage, is a function of the switch conduction time, t_c. Therefore, if we desire a stable output voltage, the conduction time must be well controlled. Equation (2) also indicates that, in order to achieve a voltage gain, t_c must be greater than the round-trip transit time, τ_{rt}. Since the CCTL length must be chosen such that $\tau_{rt} >> t_{op}$, it follows that a condition for voltage gain is that,

$$t_c > \tau_{rt} >> t_{op}. \qquad (3)$$

Fast recovery is necessary to operate at high repetition rates. The recovery time and jitter constraints are both goverened by the requirements of the application. Generally we want jitter free operation and high repetition rates.

The switch in Figure 2 is normally opened, and is required to hold off the charging voltage, V_o, until it is closed. Therefore, standoff voltage must be high. Also, if a PCSS is used, the switch off-resistance must be high enough to prevent thermal runaway.

The switch on-resistance must be as low as possible. If the on-resistance is high, much of the energy initially stored in the charged capacitor is lost as heat in the switch rather than stored as current in the CCTL. A reduction in stored current, I(t), subsequently reduces the output voltage and the voltage gain.

Most of these conditions for an ideal

switch are met in the GaAs PCSS. The PCSS is turned on by putting the GaAs semiconductor into a conducting state by illumination with a laser pulse. The laser pulse lowers the switch resistance by generation of carriers through the photoconductive effect. The switch is opened by extinguishing the laser pulse. The opening time of the PCSS is determined by the recombination time of the photo-generated carriers. Fast opening is achieved by choosing a semiconductor with a short recombination time, τ. If an optical pulse with a falltime faster than τ is used, the switch will then be opened in a time period on the order of τ. For this reason, GaAs is used in this work. With a carrier recombination time of $\tau \approx 1 - 10\ ns$[3], GaAs PCSS switch opening times on the order of nanoseconds may be acheived. GaAs also has a high dark resistivity of $10^8\ \Omega - cm$[4], therefore the switch off-resistance is high.

The switch conduction time, closing time, and jitter are controlled by the laser pulse length, risetime, and jitter respectively. The laser pulse must also have a falltime faster than the recombination time of the photo-induced carriers in the PCSS. A specially tailored laser pulse was produced which meets the criteria of fast rise and fall times, long conduction time, and absence of jitter.

IV. LASER SYSTEM SETUP

We now consider the charactersistics of the laser light necessary to controll the PCSS.

The wavelength of the light to be used is a primary concern. At first glance, it may seem most suitable to choose a wavelength with the photon energy greater than the bandgap, ensuring the greatest quantum efficiency. However, this does not provide the best results, since such wavelengths correspond to extremely shallow absorption depths. The electron-hole plasma which is created in the GaAs may be too shallow to significantly lower the switch resistance. This has been previously verified experimentally with $0.53\ \mu m$ wavelength pulses[5].

It is best to choose a wavelength with an energy less than the bandgap. Such a wavelength corresponds to a large absorption depth, allowing uniform generation of carriers throughout the semiconductor. In addition, the laser pulse must be long enough to provide a long charging time. The pulse must also be square yielding a switch with fast risetime, fast falltime, and constant on-resistance. There is no commercial laser system which will provide such a pulse, therefore a custom system has been implemented. The customized Nd:Glass laser system consists of a free running, flashlamp pumped, Nd:Glass oscillator coupled to a two-stage double-pass amplifier.

The oscillator pump energy is set just above the lasing threshold to ensure that a single long output pulse is produced. The oscillator output pulse is chopped into a nearly square 5-10 ns pulse using a Pockels cell and polarizers, and amplified to an energy of $\sim$ 10 mJ with a two-stage, double-pass amplifier. The laser and amplifier setup is shown in Figure 7. The square optical pulse is shown in Figure 8. The pulse has $\sim 7\ nS$ rise and fall times.

V. CURRENT CHARGED TRANMISSION LINE AND SWITCH SETUP

The PCSS was assembled from a GaAs p-i-n diode[6] provided by A. Rosen at the David Sarnoff Research Center. The p-i-n diode consisted of a 5 mm cube of bulk GaAs with a narrow layer of p^+ doping on one side and n^+ doping on the other. The doping and evaporated contacts provided a low re-

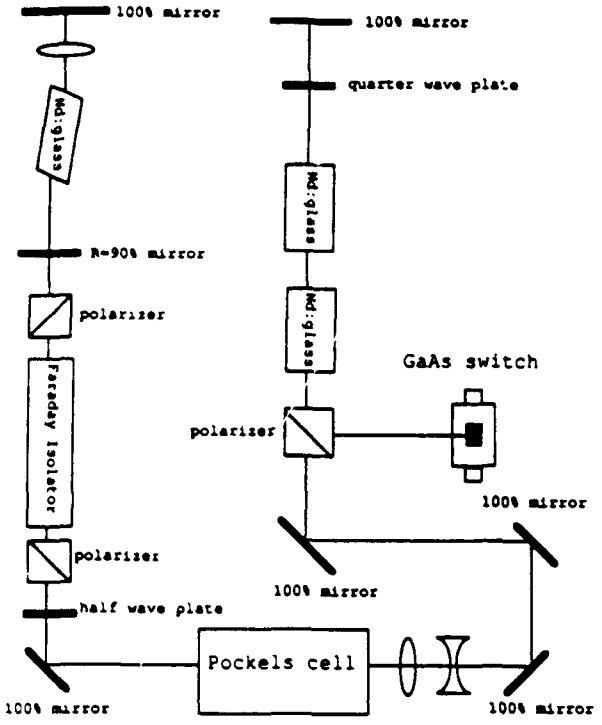

Figure 7:Nd:Glass laser system setup.

sistance ohmic contact to the semiconductor. The switch was placed on a rectangular aluminum mount between a panel mount BNC and an N connector as shown in Figure 9. Contacts to the GaAs samples were made by connecting a thin strip of copper foil to each of the side surfaces with silver paint, and these leads were connected in order to operate the p-i-n diode reverse biased.

Connections to the switch were then made in accordance to the schematic of Figure 2. The CCTL consisted of a 4.0 m length of RG-213U, 50 Ω cable. A 0.1 Ω CVR provided the nearly short circuit necessary at one end. The 50 Ω load resisance was provided by the 50 Ω input impedance of the oscilloscope, connected to the circuit through two 10 × attenuators.

The switch was illuminated with the laser pulse and the CCTL length was then optimized to achieve the highest voltage gain.

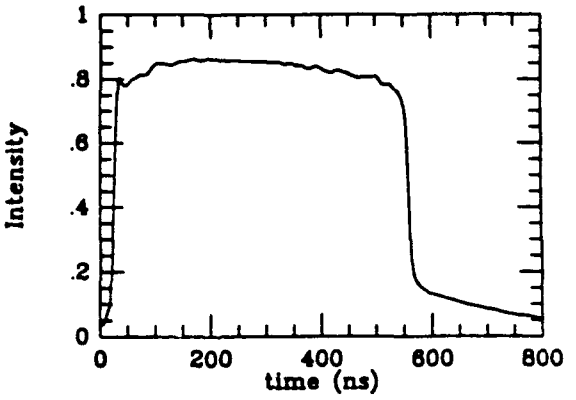

Figure 8:540 nS, ~ 10 mJ laser pulse.

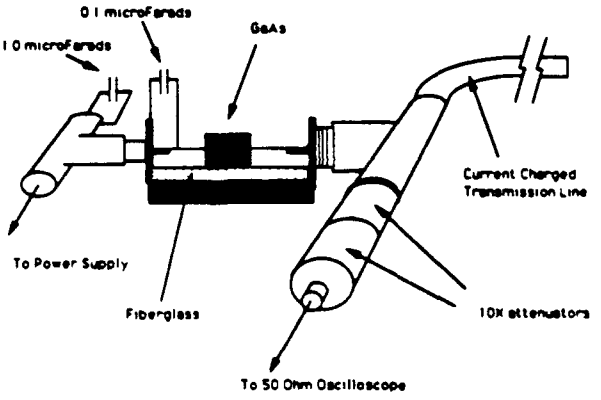

Figure 9:Experimental setup of the switch and current charged transmission line.

VII. RESULTS

The oscilloscope trace of the output voltage pulse produced across the load is shown in Figure 10. The voltage across the load is positive when the switch is closed. This voltage is equal to the voltage across the capacitor minus the voltage drop across the switch. When the switch is opened by the extinguishing of the optical pulse, a large negative pulse

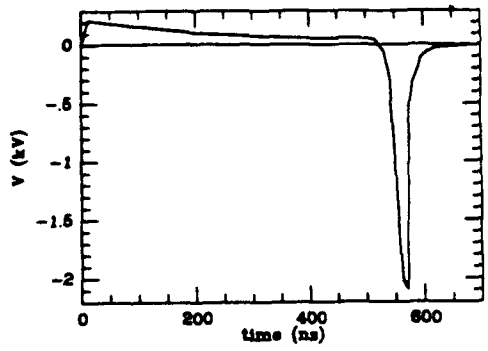

Figure 10:Voltage across the load resistor showing $-2.1\ kV$ output pulse.

appears in the load. This pulse is produced by the stored current in the CCTL passing through the load when the switch is opened.

The capacitor, in this case, was initially charged to 300 V. The amplitude of the peak output voltage is 2.1 kV. That corresponds to a voltage gain of 7.0 or a power gain of 49. The power gain is defined as the ratio of the peak power delivered to the load with the CCTL configuration to the peak power which would be delivered directly to the load with the CCTL removed,

$$G_{pow} = (V_l(max)/V_o)^2, \qquad (4)$$

where $V_l(max)$ is the maximum value of $|V_l|$. The power gain of 49 was obtained with the p-i-n GaAs switch. Other materials s:ch as Cr:GaAs and *non* p-i-n GaAs yielded much lower gains.

A trace of the current through the CVR is shown in Figure 11 as well as the theoretical prediction of equation (3) for this trace. This trace was taken simultaneously with the trace of Figure 10. The best fit of the experiment to the theory was obtained by taking the switch on-resistance as $R_{sw} = 1.2\ \Omega$ in the theoretical model.

Additionally, the dynamic switch on-resistance may be calculated by computer,

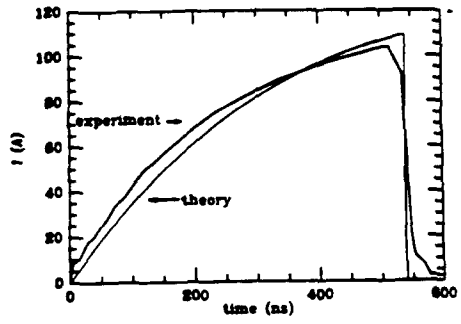

Figure 11:Current through the current viewing resistor, and theoretical prediction with the switch on resistance set to $R_{sw} = 1.2\ \Omega$.

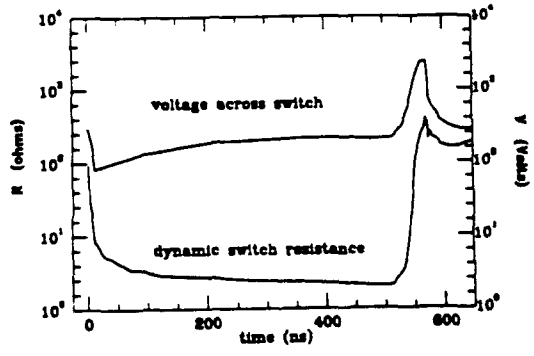

Figure 12:Dynamic switch resistance, $R_{sw}(t)$, and voltage across the switch,$V_{sw}(t)$. The drop in switch resistance after the extinction of the optical pulse is evidence of lockon.

since both the load voltage and CVR current are known at all times of interest. The dynamic switch resistance is computed with the following equation:

$$R_{sw}(t) = \frac{V_o - \frac{1}{C}\int I(t)\ dt - V_{out}}{I(t)}. \qquad (5)$$

The resulting dynamic switch resistance curve is plotted in Figure 12 as well as a plot of the voltage dropped across the switch, V_{sw}. One of the prominent features of this curve is the nearly constant $\sim 2.0\ \Omega$ on-state switch resistance, $R_{sw}(t)$, while the switch is closed.

The constant on-resistance is a result of using the specially tailored square optical pulse to activate the switch.

Another prominent feature of the $R_{sw}(t)$ curve in Figure 12 is the behavior of $R_{sw}(t)$ after the switch is opened. The extinguishing of the optical pulse causes an immediate rise in the switch resistance. The resistance increases rapidly until it reaches 400 Ω at which point the resistance begins to fall. This effect was found to limit the output voltage to 2.1 kV regardless of the charging voltage.

The switch resistance begins to fall at the point where the voltage across the switch reaches 2.4 kV correspondsing to an electric field of 4.8 kV/cm across the switch. Notice that this value is just above the reported range of threshold fields for the onset of lockon[7]

VIII. LIMITATIONS ON PERFORMANCE

Obtaining low switch on-resistance is an important factor in achieving a high power gain. It is essential that the switch resistance be kept low so that nearly all of the charging voltage appears across the CCTL. We have seen that a $\sim$ 2 Ω switch resistance gives a high power gain. Now let us consider the effect of a much higher on-resistance.

Using the simplest model where the capacitance C is taken to be infinitely large, a theoretical prediction of the closing switch performance can be made based on a calculation of reflection coefficients at each end of the CCTL. The voltage reflection coefficient, $\mathcal{R}$, from the end with the switch is:

$$\mathcal{R} = \frac{R_{sw}R_l/(R_{sw}+R_l) - Z_o}{R_{sw}R_l/(R_{sw}+R_l) + Z_o} \qquad (6),$$

while the reflection coefficient from the shorted end is -1. Thus, after each round trip in the CCTL the voltage will drop by a fraction of $1 - |\mathcal{R}|$.

As an example, consider the voltage waveform produced by a 5mm cube Cr:GaAS

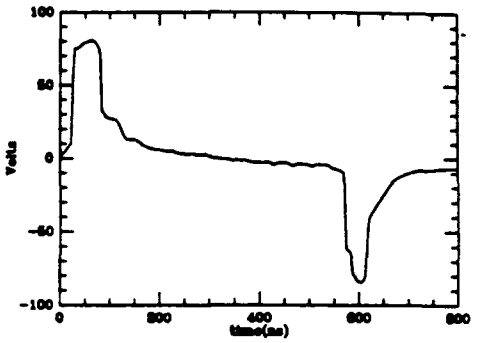

Figure 13:Voltage across the load with high switch on-resistance.

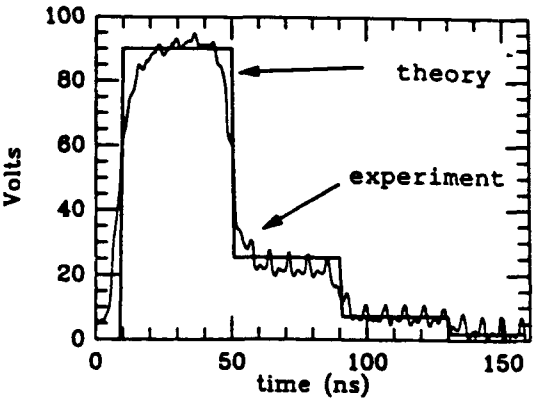

Figure 14:Voltage across the load with high switch on-resistance and theoretical prediction of equation (6).

PCSS under insufficient illumination as shown in Figure 13. A resistance of R_{sw} = 58.3 Ω is calculated from the amplitude of the voltage across the load, at t = 0. This yields a reflection coefficient of $\mathcal{R}$ = 28%. The theoretical result for the 28% reflection coefficient is in close agreement with the experimental results. The experimental results and theoretical prediction are both shown in Figure 14 with an expanded time scale. The high switch on-resistance causes significant resistive loss and the voltage across the capacitor falls quickly toward zero in a staircase like manner as the energy stored in consecutive travelling waves of current is partially dissipated in the switch on-resistance. Due to this source of loss, the output voltage pulse is only

$-80\ V$ which is less in magnitude than the intial charging voltage of $V_o = 300\ V$.

We can see from this result that it is essential that the switch on-resistance be kept well below the load resistance of 50 Ω. Maintainig low on-resistance is especially difficult when using a fast semiconductor such as Cr:GaAs. The recombination lifetime in Cr:GaAs may be more than an order of magnitude less than the GaAs recombination lifetime. Therefore, much higher optical energy is required to maintain the same on-resistance that can be achieved in GaAs. The best experimental result from a Cr:GaAs switch of similar dimensions ($5.2\ mm \times 4.5\ mm \times 4.5\ mm$) yielded a power gain of only 9.55 and the resistance could only be lowered to 9.89 Ω with the 10 mJ laser pulse.

IX. CONCLUSION

In this work, it has been shown that the GaAs photoconductive semiconductor switch (PCSS) is an effective closing and opening switch in an inductive energy storage pulsed power system (IESPPS) with a current charged transmission line (CCTL). Analysis has shown that switch on-resistance as low as 2 Ω was achieved, providing a power gain of 49. This is the first time that voltage gain and power gain were seen in such a system. To achieve gain, it is important that the laser pulse be designed to specifically meet certain criteria. The laser wavelength must have a corresponding photon energy which is less than the bandgap of the PCSS. Nd:Glass, with a 1.054 μm wavelength was chosen. An emphasis was then placed on obtaining a laser pulse which is long (540 nS) and which has a sufficiently fast risetime to produce high charging currents. The fast falltime of the laser pulse ensures that the switch opens quickly enough to deliver the stored current to the load. The transmission line length is then chosen to optimize the power gain.

The photoconductive switch design is equally important. The length of the gap must match the material and available laser energy. Contact resistance was minimized by doping the GaAs under the contacts before contact fabrication.

It is possible to obtain even higher output voltage pulses by scaling up the length of the PCSS in order to keep the critical lockon field from being induced across the switch. More optical energy is then required to produce the same switch on-resistance.

We are also considering the use of Cr:GaAs since the critical lockon field in Cr:GaAs is 8.5 kV/cm[7] which is higher than the 3.2 kV/cm critical field in GaAs. Since the recombination time in Cr:GaAs is less than in GaAs, a shorter CCTL may be used. The power gain scales with the reciprocal of the CCTL length; therefore the power gain should increase if the CCTL is shorter and the conduction time, t_c, is unchanged. However, Cr:GaAs requires more optical energy than GaAs to obtain the same on-resistance for the same PCSS dimensions, therefore a more powerful laser system is required.

The subject of lockon is also an interesting area of future investigation. We are currently seeking to understand the fundamentals of this mechanism. The observation and analysis of lockon in the CCTL configuration as opposed to the CESPPS configuration may provide some new insights.

ACKNOWLEDGMENTS

The authors wish to thank A. Rosen, of the David Sarnoff Research Center for providing the GaAs p-i-n diode switches. This work was supported by the Strategic Defense Initiative/Innovative Science and Technology

managed by the Office of Naval Research.

REFERENCES

[1]C. H. Lee (ed.), *Picosecond Optoelectronic Devices.* Academic Press Inc., New York, 1984.

[2]Karl H. Schoenbach, M. Kristiansen, Gerhard Schafer, "A review of opening switch technology for inductive energy storage," *Proceedings of the IEEE*, vol. 72, no. 8, pp. 1019-1040, 1984.

[3]Oved S. F. Zucker, David M. Giorgi, Adam Griffin, David E. Hargis, James Long, Iain A. McIntyre, Kevin J. Page, Paul J. Solone, and Deborah S. Wein,"Considerations of the limits and capabilities of light activated switches,"*SPIE Vol. 1378 Optically Activated Switching*, pp. 22-33, 1990.

[4]M. D. Pocha and W. W. Hofer, "Photoconductive switching for high power microwave generation," *SPIE Vol. 1378 Optically Activated Switching*, pp. 2-9, 1990.

[5]E. A. Chauchard, C. C. Kung, C. H. Lee, M. J. Rhee, V. Diadiuk, " A new method to generate square pulses: optoelectronic switching in a current charged transmission line," *IEEE Transactions on Plasma Science*, Vol. PS-15, pp. 70-72, 1987.

[6]A. Rosen, P. J. Stabile,A. M. Gombar, W. M. Janton, A. Bahasadri, and P. Herzfeld, "100 kW DC-biased, all semiconductor switch using Si p-i-n diodes and AlGaAs 2-D laser arrays," *Photonics Tech. Lett.*, vol.1, pp. 132-134, 1989.

[7]F. J. Zutavern, G. M. Lobriel, B. B. McKenzie, W. M. O' Malley, R. A. Hamil, L. P. Schanwald, H. P. Hjalmarson, "Photoconductive semiconductor switch (PCSS) recovery," *Digest of Technical Papers, Seventh IEEE Pulsed Power Conference*, pp. 412-417, 1989.

Eric E. Funk received his B.S. degree in Physics from Rensselaer Polytechnic Institute, Troy, NY in 1988. He received his M.S. degree in Electrical Engineering from the University of Maryland, College Park, MD in 1991. He is currently a PhD student at the University of Maryland conducting research on photoconductive semiconductor switches.

E. A. Chauchard, photograph and biography not available at the time of publication.

Chi H. Lee is a Professor of Electrical Engineering at the University of Maryland. His research interest includes ultrafast lasers and optoelectronic devices, optical control and characterization of microwave and millimeter-wave devices and circuits, optically-controlled closing and opening switches for pulsed power applications. Dr. Lee is a Fellow of IEEE and the Optical Society of America. He has served as the chairman of the technical committee on lightwave technology in the IEEE Microwave Theory and Technique (MTT) Society. He also served as the co-chair Or the OSA topical meetings on Picosecond Electronics and Optoelectronics.

M. J. Rhee, photograph and biography not available at the time of publication.

OPTICAL NONLINEARITIES IN POLYCRYSTALLINE ZnSe PHOTOCONDUCTIVE SWITCHES

P. Cho, P.-T. Ho, J. Goldhar, and Chi H. Lee

Department of Electrical Engineering
University of Maryland
College Park, MD 20742

ABSTRACT

Experimental investigation of polycrystalline ZnSe switches at bias field up to 100 kV/cm has been performed. Voltage dependent absorption of light become important in this regime. Under probably chosen operating conditions, negative resistance regions and bistability are expected. These effects can be used to improve performance of closing and opening photoconductive switches.

I. INTRODUCTION

Recent investigation[1] showed that polycrystalline ZnSe performed very well as a photoconductive material. Its properties are comparable to that of Cr:GaAs, but with much higher dark resistivity due to the large bandgap which is about 2.67 eV at room temperature. As expected from higher bandgap materials, ZnSe works well under very high fields and high current densities. Therefore we are continuing the investigation for the potential applications of this material to closing and opening photoconductive electrical switches.

Working with ZnSe switches in a longitudinal geometry (which will be described below in greater detail) we found that under high electric fields, at which the switches are typically operated, the bandgap shift in ZnSe is sufficiently large to seriously affect the switch performance. This effect may be used to improve the performance of pulsers based on photoconductive switching by relaxing the requirements on the rise and fall times of the laser pulses.

II. EXPERIMENT

Figure 1 shows a simple dye laser which was used for this experiment. Coumarine 480 dye was transversely pumped by a XeCl laser. An intracavity grating was used to tune the dye laser wavelength over the range of interest, 465 - 485 nm.

Electrical characterization of the switch was performed using the circuit shown in Figure 2. A variable DC voltage V_b was connected to one electrode of the switch via a 75Ω coaxial cable; the other electrode was connected to a similar 75Ω cable which was terminated with a matched load and connected through an electrical attenuator to an oscilloscope where the voltage across the load (V_{out}) was measured.

Two very different electrode structures were tested. One was a transparent liquid electrolyte electrode shown in Figure 3. A saturated solution of NaCl worked well as the electrolyte. For relatively low voltages (below 5 kV) we saw no problems with operating this switch with DC bias.

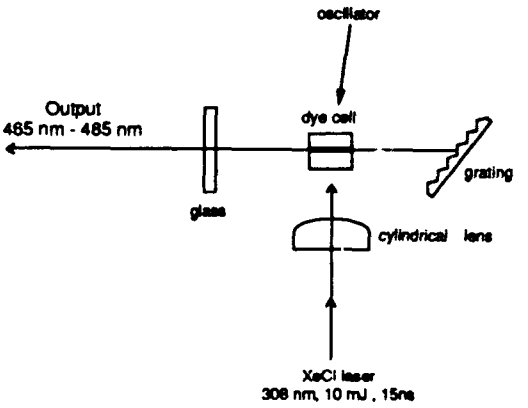

Figure 1: Laser system setup.

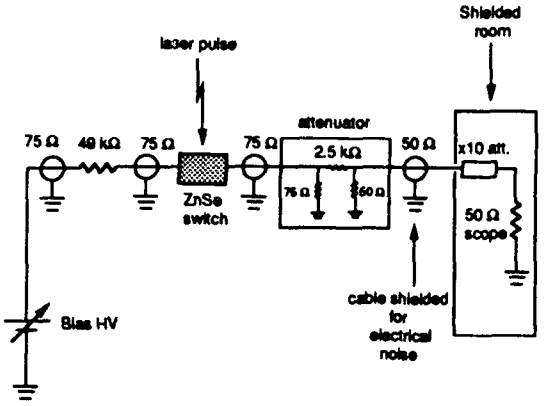

Figure 2: Electrical circuit for testing ZnSe switches.

Figure 4 shows a plot of the output voltage from the charged line pulser as a function of the incident laser energy. It is evident from the graph that only a few micro-Joules are sufficient to reduce the switch resistance below 75Ω. Liquid electrodes allow grading of the fringe fields on the crystal surface, and therefore permit operation at higher voltages. The switch was used with bias up to 10 kV without electrical breakdown. Unfortunately, a new problem was encountered at high biases. Electrolytic processes caused rapid deterioration (on tens of seconds time scale) of the crystal surface. This means that operating with this switch at higher fields will have to be done with pulsed bias. Also it may be possible to find a more agreeable (chemically inert) electrolyte solution.

One experiment which was easy to perform with a liquid electrode switch is variation of the conductive cross section. The size of laser spot on the switch was varied using a focus lens. Changing the spot size of illumination from 1 cm to below 100 μm showed no observable change in the electrical properties of the switch. This means that switch operation at current densities in excess of 100 kA/cm^2 presents no problems.

The other switch design, shown in Figure 5, uses a metal grid pattern as the electrode. The polycrystalline ZnSe is in a shape of a circular disc of 1 inch diameter and 1 mm thick. Electrodes of 0.5 inch were deposited on both sides of the crystal; the metals used were 50 Å thick layer of chrome underneath a layer of gold with 0.2 μm thickness. The electrodes had 0.1 mm slit openings through

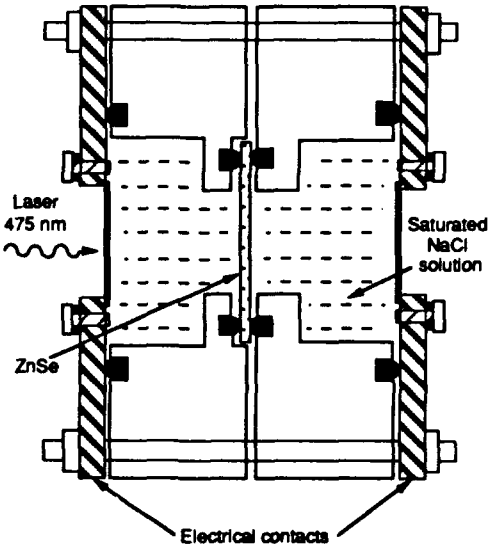

Figure 3: ZnSe switch with liquid electrodes.

which the laser pulse could propagate. Both the liquid-electrode and metal-electrode switches were biased in such a way that the applied field was in the same direction of the incident laser pulse. The two types of switches had comparable performance. In order to gain better understanding of processes taking place at high fields we conducted various measurements on the electrical and optical properties of the switch using the metal grid switch. The following is a discussion of our results.

III. Results and Discussion

We note that our switch geometry, with a light transmitting electrodes, has certain advantages. It is well known that the laser power required to lower the switch resistance to a given value depends quadratically on d, the separation between electrodes. Thus our switch,in longitudinal geometry, can minimize d without decreasing the flashover distance. Another features of this switch, however, is its strong dependence on laser wavelength near the bandgap: below the bandgap there is little absorption; near or above the bandgap all the light is absorbed on the surface. In either case the switch operation is very inefficient. When the photon energy is just below the bandgap so that the absorption depth is approximately the same

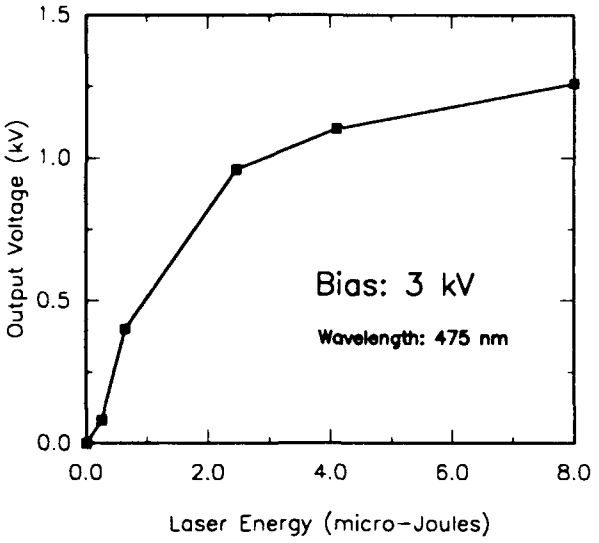

Figure 4: Performance of ZnSe switch as a function of laser energy.

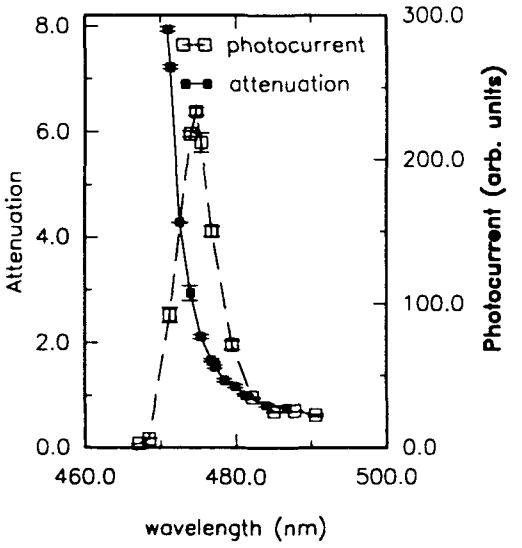

Figure 6: Response curve of 1 mm thick ZnSe switch (attenuation = absorption coefficient integrated in the longitudinal direction).

as the electrode separation, the efficiency should be maximum. This is indeed what we observed. The switch conductance, normalized to the laser energy, is plotted in Figure 6 as a function of laser wavelength. It peaks at $\sim$ 473 nm corresponding to photon energy of $\sim$ 2.63 eV. The absorption of our ZnSe crystal under no bias is plotted in the same figure.

A careful study of the performance of the ZnSe photoconductor under high bias fields showed some interesting effects. Figure 7 shows the plot of electrical output from a charged line pulser as a function of voltage for two different wavelengths. In this experiment the laser power was reduced so that the switch was not fully saturated. The curve corresponding to the longer wavelength shows super-linear behavior while the shorter wavelength shows sub-linear behavior. This is consistent with what we expected. Since the absorption edge of ZnSe is rather steep in the range of our operating wavelength, a small decrease of the input wavelength will cause a tremendous increase of absorption at high fields so that almost all the light is absorbed near the surface of the crystal. Thus, above certain applied field the conducting channel in the switch will disappear, i.e. the switch is pinched-off which explain the sub-linear profile in Figure 7 at short wavelength. In addition, other nonlinear effects become important at high fields. Velocity saturation due to inelastic collisions and carrier multiplication could also be playing a role. However, we believe that most likely the shift of the bandgap and therefore the change in the absorption coefficient of ZnSe due to strong applied field is a dominant factor for the effects observed.

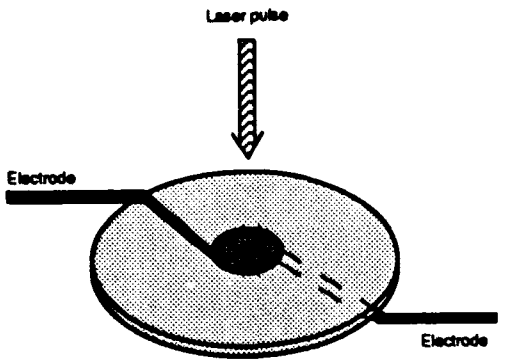

Figure 5: ZnSe switch with metal grid electrodes.

In order to observe the voltage induced change

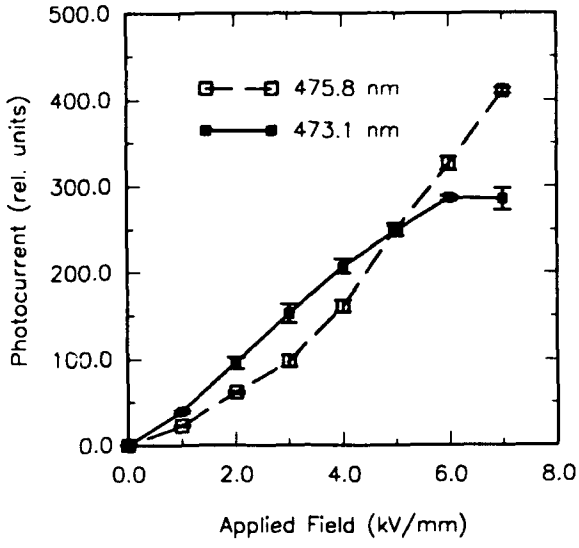

Figure 7: Voltage dependence of ZnSe switch response for different wavelengths.

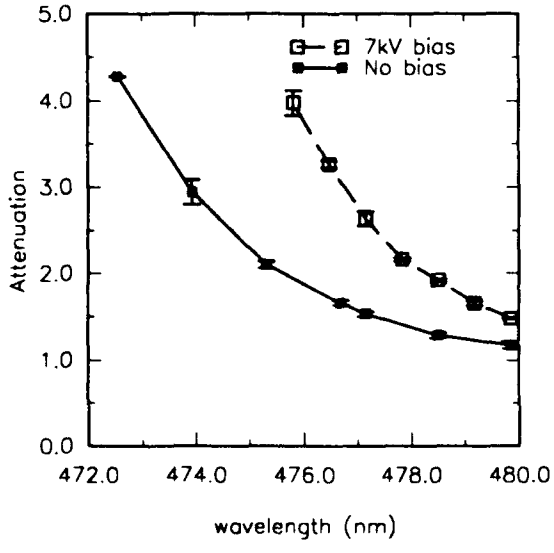

Figure 8: Attenuation of ZnSe with and without applied electric field.

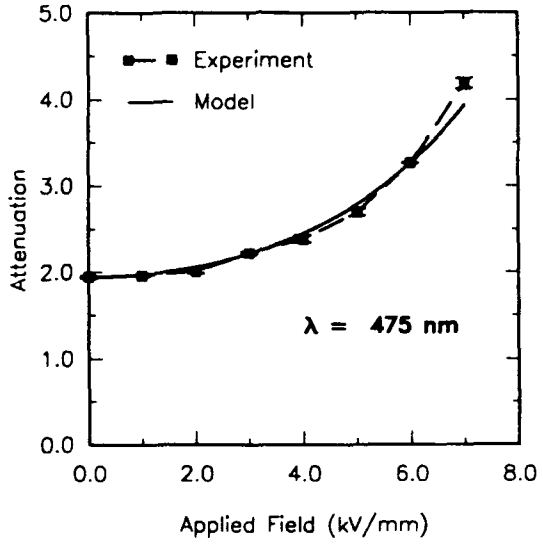

Figure 9: Voltage dependence of absorption coefficient in ZnSe, and comparison with an empirical model.

in absorption we monitored the transmitted laser pulse after the switch. Indeed the transmission was a strong function of the applied field. Figure 8 shows a plot of the absorption coefficient as a function of wavelength without bias and with 7 kV/mm across the switch. The shift of the bandgap to longer wavelength is expected due to Franz-Keldysh effect[2] and it has been observed in polycrystalline ZnSe in a transverse geometry[3]

The Franz-Keldysh effect can be stated as follow:

$$\Delta E_g \propto \frac{E^2}{E_c^2}$$

where ΔE_g is the amount of shift in bandgap, E is the applied field and E_c is a critical field which characterizes a given material and is about 8 kV/mm for the ZnSe we use. Voltage dependence of the induced absorption is shown in Figure 9 and it is consistent with a simple empirical model.

The change in absorption could be due to fast electronic processes, such as Franz-Keldysh effect, or could result from elastic deformation of crystal due to the stress created by the applied field. The latter effect would not be very interesting since it

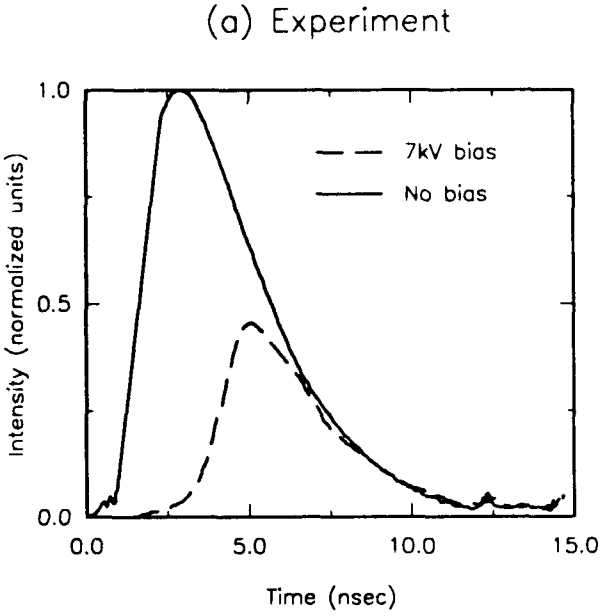

Figure 10a: Transmitted laser pulse shape – experiment.

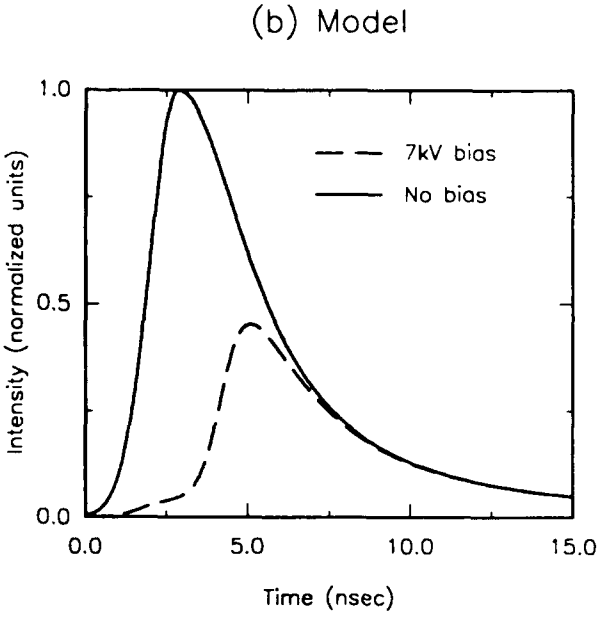

Figure 10b: Transmitted laser pulse shape – model.

would have a response time on microsecond time scale. In order to test if the absorption can change on the nanosecond time scale we performed the following experiment. The charged line was eliminated from the electrical circuit. Thus voltage across the switch could be reduced quickly by the laser pulse discharging the switch capacitance of several picofarads. Typical data are shown in Figure 10a. It is evident that the strong-field-induced absorption is eliminated when the switch discharges.

We can use the empirical model for field induced absorption to predict the performance of our switch. Numerical simulation of dielectric relaxation inside the switch gives results which agree quite well with experiment as can be seen from Figure 10b.

IV. Conclusions

We have observed a strong nonlinear behavior of ZnSe photoconductive switch which can be explained by field induced bandgap shifting. This type of nonlinear behavior of the switch can have many important applications. It is similar to the effects utilized in the quantum well SEED devices[4] and ZnSe waveguide modulators[5]. Regions of negative resistance and bistability are expected. It should be possible to obtain fast closing and opening photoconductive switches without the need for special laser pulse shape when operating in such a regimes. We are presently investigating such possibilities.

Acknowledgments

This work was supported in part by DARPA and the Strategic Defense Initiative Organization/Innovative Science and Technology managed by the Office of Naval Research.

References

[1]P.T. Ho, F. Peng, J. Goldhar, "Photoconductive Switching Using Polycrystalline ZnSe," *IEEE Trans. Electron Devices* **37**, 2517 (1990).

[2]W. Franz, *Z. Naturforsch.* **13a**, 484 (1958).

[3]G. Motosugi, "Absorption-Modulation of Light in ZnSe Crystals and Its Application to a Page Composer," *Jap. J. Appl. Phys.* **16**, 591 (1977).

[4]D. Miller, D. Chemla, T. Damen, T. Wood, C. Burrus, A. Gossard, W. Wiegmann, "The Quantum Well Self-Electrooptic Effect Device: Optoelectronic Bistability and Oscillation, and Self-Linearized Modulation," *IEEE J. Quantum Electron.* **21**, 1462 (1985).

[5]M. H. Jupina, E. M. Ga.....e, N. Shibata, S. Zembutsu, "ZnSe/$ZnSe_{0.92}S_{0.08}$/GaAs single-crystal waveguides as visible modulators," *Appl. Phys. Lett.* **57** , 2894 (1990).

P. Cho received the B.S. degree in electrical engineering from the University of Pittsburgh, Pittsburgh, Pennsylvania. He is currently a Master candidate at the University of Maryland in the Department of Electrical Engineering. At present he is conducting research on high-power photoconductive semiconductor switches.

P.-T. Ho, photograph and biography not available at the time of publication.

Julius Goldhar was born in Tbilisi, U.S.S.R., in 1948. He received the B.S. and Ph..D. degrees from the Massachusetts Institute of Technology, Cambridge, in 1971 and 1976, respectively. From 1976 to 1985 he was at the Lawrence Livermore National Laboratory, Livermore, CA, conducting research on the development of advanced drivers for laser fusion. In 1985 he joined the Electrical Engineering Department at the University of Maryland in College Park. At present he is conducting research on ultrafast phenomena and high-power lasers.

Chi H. Lee is a Professor of Electrical Engineering at the University of Maryland. His research interest includes ultrafast lasers and optoelectronic devices, optical control and characterization of microwave and millimeter-wave devices and circuits, optically-controlled closing and opening switches for pulsed power applications. Dr. Lee is a Fellow of IEEE and the Optical Society of America. He has served as the chairman of the technical committee on lightwave technology in the IEEE Microwave Theory and Technique (MTT) Society. He also served as the co-chair of the OSA topical meetings on Picosecond Electronics and Optoelectronics.

AN OPTICALLY ACTIVATED OPENING SEMICONDUCTOR SWITCH

K.H. Schoenbach and V.K. Lakdawala

Physical Electronics Research Institute
Old Dominion University
Norfolk, VA 23529

ABSTRACT

The bulk optically controlled switch (BOSS) is a new type of photoconductive switch which can be jitterfree closed and opened on command. It turns into a metal-like conductor when illuminated with near infrared radiation, and switches back into a semi-insulating state when subsequently irradiated with light of longer wavelength. With silicon doped, copper compensated, gallium arsenide (GaAs:Si:Cu) as switch material, turn-on and turn-off of the photocurrent has been demonstrated on a nanosecond time scale. Picosecond switching seems to be possible with picosecond lasers and by adding recombination centers to the base material. The BOSS was shown to operate in the linear range as well as in the lock-on state where temporary interruption of the photocurrent was achieved. Besides gallium arsenide as base material, other wide band gap semiconductors, such as cadmium sulfide, were also shown to have the potential to be used as optically controlled opening switches. A time dependent, one dimensional code was used to describe the temporal response of the switch to laser radiation. This model allowed to calculate the dark current characteristics of GaAs:Si:Cu, which exhibits a region of negative differential resistance. The model includes the lock-on effect as a trapfilling effect in a semiconductor switch with injecting contacts.

INTRODUCTION

Photonic control of electronic circuitry has proceeded rapidly during the past few years. The primary advantages of optically controlled semiconductor switches compared to other high power switches, such as triggered gas discharges, is their jitter free, ultrafast ($< 10^{-12}$ s) response to laser pulses. Pulses with power levels up to 10 MW and subnanosecond risetime have been generated with GaAs switches using a 850 W GaAs laser diode array as light source.[1] The repetition rate was 1 kHz for a total of 10^5 shots.

Photoconductive switches are mainly used as closing switches in capacitive discharge circuits. Closing is obtained by generating electrons and/or holes using the internal photo effect. The photoconductivity is established during the laser pulse duration and then decays with a time constant determined by recombination, trapping and carrier sweep out. Decay time constants vary from hundreds of femtoseconds in radiation damaged silicon-on-sapphire[2] to more than seconds in wide band gap semiconductors. By sustaining the photoconductance with a well defined laser pulse, which can be terminated on command, it is possible to use the photoconductive switch as an opening as well as a closing switch. However, since the efficiency or gain of a photoconductor is linearly dependent on the decay time, fast decay, which means fast switch opening, and high gain seems to exclude each other.

CONCEPT

A switching concept which is based on photoinduced quenching of photoconductivity in high gain photoconductors[3] allows to overcome this dilemma. The BOSS (Bulk Optically controlled Semiconductor Switch) concept utilizes the wavelength sensitive optical

ionization of electrons and holes, respectively, from impurity centers in wide band gap semiconductors. The material which was studied sofar is silicon doped, copper compensated, gallium arsenide (GaAs:Si:Cu), fabricated by diffusing Cu into commercially available GaAs:Si. Silicon-doped GaAs is an n-type material. Copper introduces deep acceptor levels, and therefore allows to compensate Si and to create a highly resistive switch material. One of the Cu-levels, Cu_B, is located at 0.44 eV above the valence band (VB), a second one, Cu_A, is 0.14 eV above VB. Both are hole traps with extremely small electron capture cross-sections ($8*10^{-21}$ cm^2). Recent studies on fabrication techniques for GaAs:Si:Cu have shown that it is possible to influence the ratio of the Cu-concentration in the two energy states, and therefore to make Cu_B the dominant center.

The switching cycle is discussed for the case that Cu_B is so dominant that the influence of other deep centers on electron and hole ionization can be neglected. Generation of free electrons - closing of the switch - is obtained through photoexcitation of Cu^-_B-centers (the negative sign indicates a center with an excess electron) with photons of a quantum energy, which exceeds the energy between conduction band and Cu^-_B-level ($h\nu > 1$ eV). Simultaneously holes are generated through photoionization of Cu^0_B where the superscript 0 indicates an empty trap. The holes are quickly trapped by Cu^-_B-centers, whereas the free electrons remain for a much longer time in the conduction band (Fig. 1a). In other words the photoconductor has a high gain. The depletion of the free electron concentration - opening of the switch - is induced by hole ionization of the Cu^-_B-traps with photons of quantum energy greater than the energy of the deep centers relative to the valence band, but less than the energy of these centers relative to the conduction band (0.44 eV < $h\nu$ < 1 eV). This transition stimulates the recombination of free electron with free holes (Fig. 1b) and leads to nanosecond opening of the switch. Even subnanosecond opening can be achieved if the recombination time is reduced by means of recombination centers, such as Cr in GaAs.

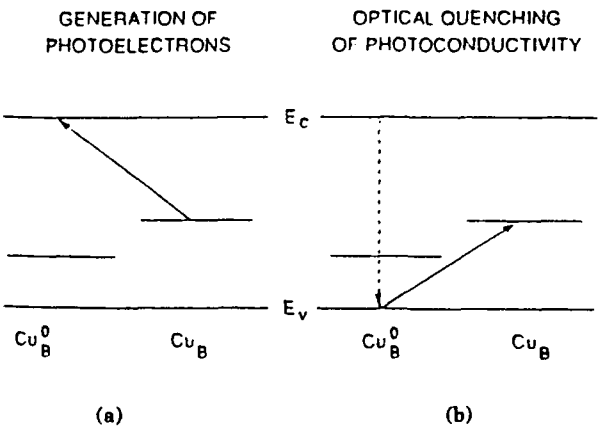

FIG. 1. Switch closing due to electron excitation and switch opening caused by hole excitation and subsequent electron-hole recombination.

MATERIAL PREPARATION AND CHARACTERIZATION

Silicon doped gallium arsenide, with a Si-density of about $5*10^{+16}$ cm^{-3}, was used as base material. A 1 µm thick layer of copper was evaporated onto one of the faces of GaAs:Si wafer. The sample was then placed in a diffusion furnace and annealed in a low pressure arsenic environment for several hours at temperatures around 575 K. Variable parameters are time and temperature for the diffusion process, and the arsenic pressure in the diffusion chamber. After removing the remaining copper from the sample and after polishing it, gold germanium contacts were placed in either a coplanar or a sandwich-type configuration. Current-voltage measurements in the voltage range up to 100 V were performed to determine the dark resistivity of the sample after the diffusion and also to test the contacts with respect to their conductance. Resistivities of up to 10^{+6} Ohmcm were

measured for compensated samples. Earlier experiments on similar material indicate that resistivities of up to 10^{+8} Ohmcm can be obtained with this method.[4]

The performance of the optically controlled GaAs:Si:Cu switch, gain and speed, is strongly dependent on the Cu-concentration and on the distribution of the Cu-centers in the various energy states. In order to optimize the switch it is necessary to characterize the material with respect to the impurity properties. Measurements of the dark current-voltage characteristics[5], Hall measurements, optical spectroscopy[6], and transient capacitance[7] and transient photocurrent[8] measurements have been used to study the material properties. Except for photo induced transient current spectroscopy (PICTS) the standard procedures for recording and evaluating of data in these various diagnostic techniques have been used.[9] In PICTS a novel evaluation technique has been developed, which by curve fitting of the deep level emission current transients, instead of using the conventional window method, yields a considerable improvement in the accuracy of the deep level data.[10]

The dark current measurements revealed that the switch material GaAs:Si:Cu has a pronounced negative differential resistance region (Fig. 2). For the higher doped sample (Cu) the current increases linearly up to a voltage of 2.3 kV, corresponding to an average field of 46 kV/cm, and then jumps from ten's of mA to almost 100 A at a much reduced voltage of 600 V. The current at this point corresponds to a current density of about 1.5 kA/cm^2. The hold off voltage (highest applied voltage at low currents) was found to be smaller for lower Cu-concentrations in GaAs:Si:Cu and so was the current at the low voltage point in the range of Cu-densities around $5*10^{+16}$ cm^{-3}. When a step voltage is applied at the GaAs:Si:Cu sample in series with a load resistor, such that the loadline intersects the high and the low current branch of the current voltage characteristics, the transition from the low current to high current shows a breakdown like behavior. The delay times for this transition depend on the applied overvoltage as shown in Fig. 3. The current rise was measured to exceed 10^{11} A/s for a voltage of 3 kV, corresponding to an average applied field of 60 kV/cm.

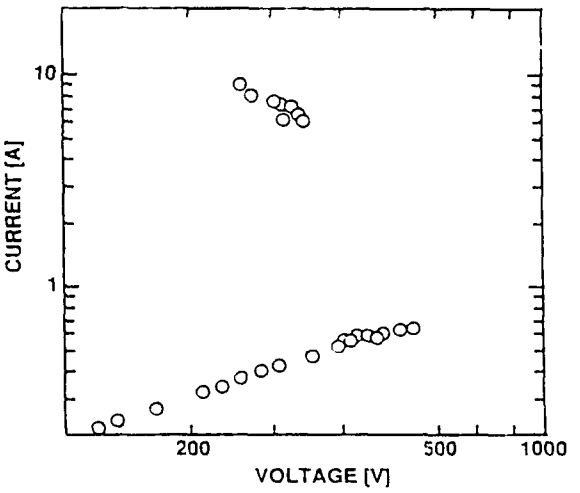

FIG. 2. The experimentally obtained dark current curve for GaAs:Si:Cu.

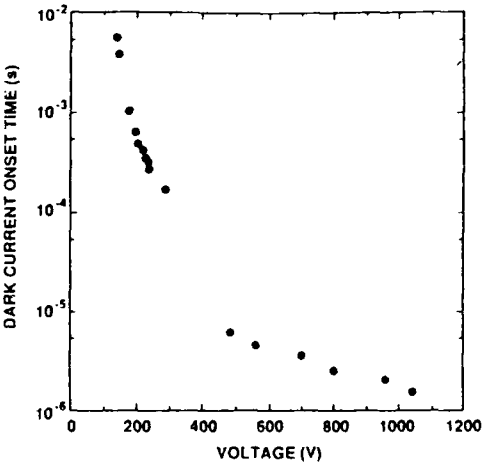

FIG. 3. Dark current "onset" time versus applied voltage.

The dark current characteristics of semiconductors and insulators is strongly dependent on the deep centers in the semiconductor. First efforts to determine the deep level structure of the switch material were made using DLTS (Deep Level Transient Spectroscopy) as diagnostic technique. However, because this technique relies on the electrical injection of carriers through contacts, it is only usable for n- and p-type semiconductors which allow the fabrication of diodes. n-type GaAs:Si which serves as the base material for the BOSS-switch, could be explored with DLTS, and such dominant traps as EL2 and EL5 were identified and their density was determined.[7] In order to get information on the deep centers in semi-insulating GaAs:Si:Cu a related deep level spectroscopic method was developed: PICTS (Photo Induced Current Transient Spectroscopy). This method, like DLTS, is based on the measurement of temperature dependent changes in the density of trapped charges following free carrier injection. Unlike DLTS, PICTS uses optical injection of carriers to fill the deep traps and therefore allows to study the deep level structure in compensated material where injection through the contacts would only be possible at very high applied fields.

A typical PICTS spectrum for compensated GaAs:Si:Cu is shown in Fig. 4. The peaks at various temperatures indicate the presence of distinct deep energy levels in the semiconductor. The evaluation of these spectra allows to find the energetic position of the levels with respect to a band edge and also gives information on the concentration of traps in these energy states. Peak #4 in the GaAs:Si:Cu spectrum (activation energy: 0.75 eV) was assumed to correspond to transitions from $EL2^0$. The presence of Cu_B, which is quoted in reference 11 as a deep acceptor with an activation energy of 0.14 eV, is indicated by the rising slope of the PICTS curve at temperatures below 130 K. Peak #2 corresponds to a deep level which is about 0.3 eV above the valence band or below the conduction band (PICTS does not allow to discriminate between electron and hole excitation). Several other peaks around peak #3, which could not be spectrally resolved indicate the presence of Cu_B traps. Cu_B has an activation energy of 0.44 eV.

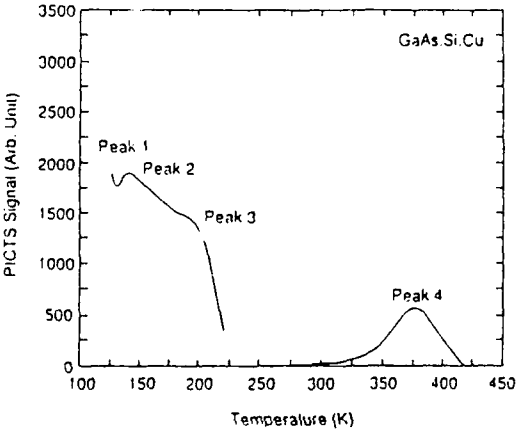

FIG. 4. PICTS spectrum of silicon doped, copper compensated GaAs.

Cathodoluminescent measurements on GaAs, GaAs:Cu and GaAs:Si:Cu at a temperature of 10 K revealed information on the optical transitions in these materials. The cathodoluminescent spectrum of GaAs:Si:Cu is shown in Fig. 5. The peak with maximum at 8000 cm^{-1} ($h\nu$ = 0.99 eV) indicates a strong transition to the levels at about 0.4 eV to 0.5 eV. Although there is a possibility that this peak is related to a transition from the conduction band to Cu_B, one would not expect such a strong signal, taking the small electron capture cross-section for Cu_B into account. A more likely transition is electron capture by ionized EL2 centers which are created by Cu-doping. The peak near 11000 cm^{-1} is clearly related to Cu (electron capture by Cu_A).

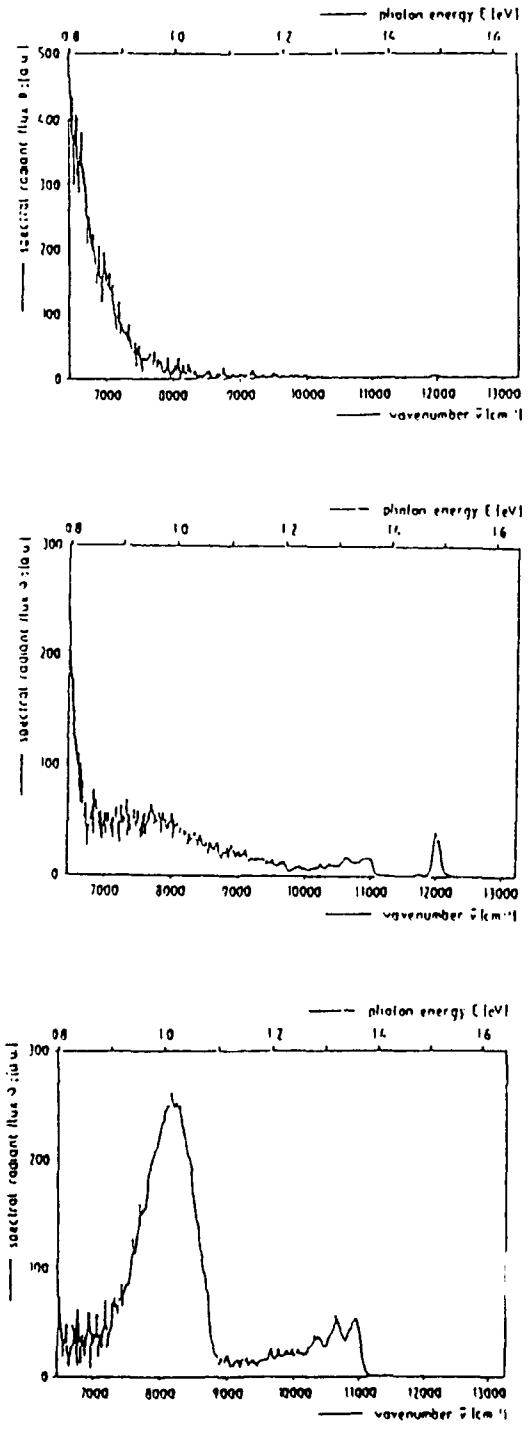

FIG. 5. Cathodoluminescence spectra of a) undoped GaAs, b) copper doped GaAs, and c) doped, copper compensated GaAs.

The energy level diagram consistent with the data obtained by means of DLTS, PICTS and cathodoluminescence, and also including results from reference 11 is shown in Fig. 6. The unidentified level X, with an activation energy of 0.3 eV, does not seem to play an important role in the switch kinetics according to our cathodoluminescent results. The concentration of the various deep centers, particularly the Cu-related centers, can be influenced by the fabrication technique. By varying the ambient As-pressure during the Cu-diffusion process, it is possible to change the ratio of Cu_A and Cu_B. Fig. 7 shows the PICTS spectrum for GaAs:Si:Cu at two ambient As-pressures, Fig. 8 shows the Arrhenius plot with three lines corresponding to Cu-related levels at 0.14 eV, 0.41 eV, and 0.44 eV. The results indicate the possibility to modify and therefore optimize the Cu-concentration in the switch material with respect to closing and opening applications by enhancing the rate for certain ionization and trapping processes which determine the efficiency and speed of closing and opening switch processes.

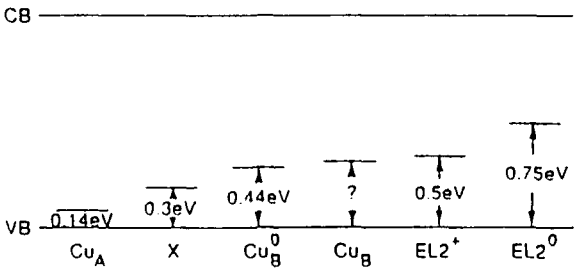

FIG. 6. Energy level diagram of GaAs:Si:Cu.

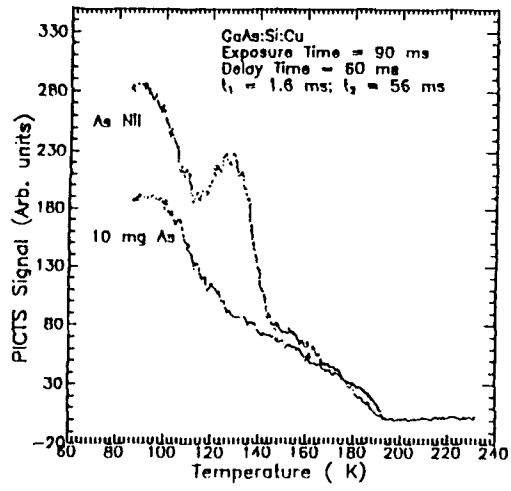

FIG. 7. PICTS spectrum for GaAs:Si:Cu showing the effect of As overpressure on the deep traps.[28]

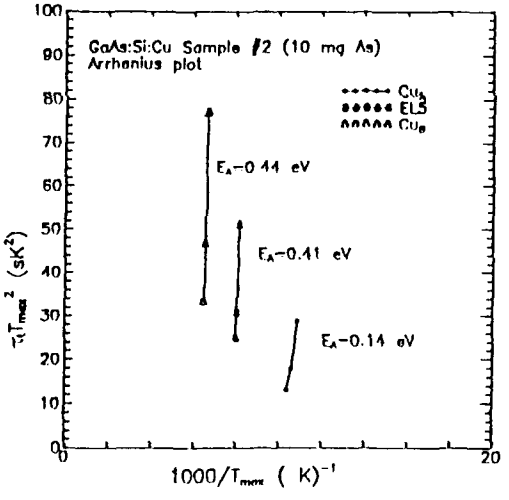

FIG. 8. Arrhenius plots for the PICTS spectrum of Fig. 7.[28]

MODELING OF THE SWITCH

Numerical calculations of the transient behavior of the GaAs:Si:Cu switch when irradiated at first with a 1.06 μm laser pulse and subsequently with a 1.6 μm laser pulse were performed using a rate equation method.[7] The code includes the rate equations for free electrons and holes, and for bound electrons in Cu_A, Cu_B, EL2, EL5, and an effective recombination center in the middle of the bandgap. The results of this model which assumes homogeneity of charge distributions in the switch is shown in Fig. 9. This diagram shows clearly the bistable behavior of the switch: after illumination with the 1.06 μm laser, the photocurrent stays almost constant. This is quite different from the photoconductive decay in undoped GaAs which has a nanosecond or even subnanosecond time constant. The photocurrent can be quenched, according to these calculations, on a timescale which is determined by the pulse duration of the second IR laser pulse.

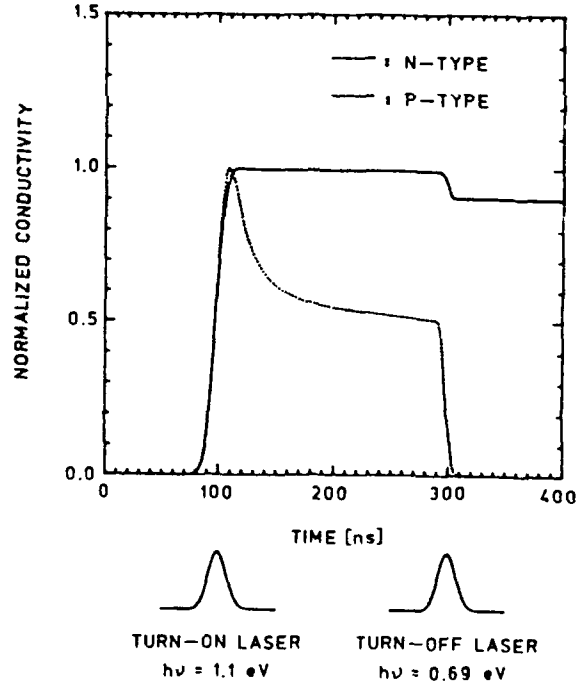

FIG. 9. Simulated photoconductivity of the two samples during the switching operation.

The rate equation method has also been used to determine the parameter range (laser wavelength and intensity, Cu-doping density with respect to Si concentration, and influence of recombination centers) for which successful operation of the BOSS system can be expected. Whereas this rate equation model describes the switch operation at low voltages rather well, it is not suitable for switches operating at higher voltages. These are voltages which correspond to electric fields where trap filling becomes important. According to the dark current measurements this level is reached for GaAs:Si:Cu at average fields of several kV/cm. At these field strengths the contributions of the space charge in the deep traps to the overall field distribution cannot be neglected anymore. A one-dimensional, time dependent model which takes this space charge effect into account was developed, which allows to model the switch as part of an electrical circuit.[12] The model includes the generation of free charge carriers through radiative, thermal or impact ionization, their field dependent transport and their recombination or trapping. Calculations were performed for a GaAs:Si:Cu switch with the assumption that the charge carrier generation can be described by a homogeneous source function for electron-hole pairs. The contacts were assumed to be injecting.

The steady-state current-voltage characteristics for various source functions S from zero to 10^{26} $cm^{-3}s^{-1}$ are plotted in Fig. 10. The curve with S = 0 is the dark current curve for the 0.5 mm thick GaAs:Si:Cu sample. For low voltages, V < 100 V, it exhibits a linear (ohmic) behavior; the conductivity in this range is determined by the thermal carrier concentration. For higher voltages, 100 V < V < 5 kV, deviations from the ohmic behavior arise due to the nonlinear dependence of the drift velocities on the electric field in GaAs, but the voltage curve is still monotonic. At about 5 kV, however, the current begins to rise steeply and the current curve eventually bends back to lower voltages.

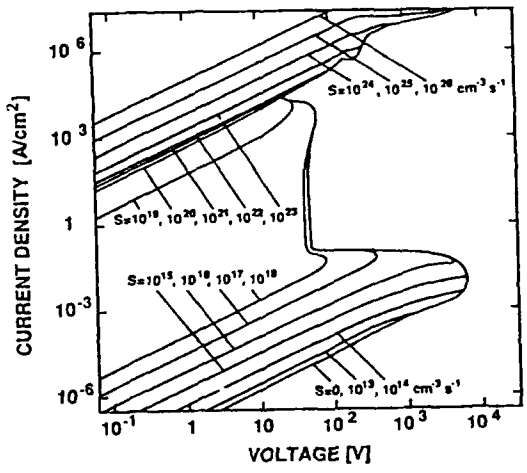

FIG. 10. The steady state *I-V* curves with and without electron-beam irradiation, and the load line of the voltage source.

The occurrence of such a current controlled negative differential conductivity has first been predicted by Lampert for semiconductors with deep acceptors, such as Cu_B, and double injection.[13] The effect can be understood by considering trap filling of Cu_B. At low voltages (and low current densities) the holes injected through the negative electrode are quickly trapped in the vicinity of this contact and create a considerable space charge in the anode region. The current is mainly carried by electrons. At higher current densities, however, in our case at about 10 mA/cm^2, the deep hole traps are essentially filled, the hole lifetime increases, such that the injected electrons and holes can form a plasma which allows to carry high currents at reduced forward voltages. The observed steep rise of the current following this transition to low voltages can be explained by double injection, the (in theory) unlimited injection of both electrons and holes through cathode and anode contacts. At current densities above several kA/cm^2 a transition into the "post-breakdown" range with moderately increasing current densities is found. This increase in differential resistance is due to direct recombination, a loss

mechanism which becomes important at large electron-hole concentrations. This dark current characteristic, obtained from the one-dimensional model shows a good qualitative agreement with the experimental results shown in Fig. 2.

The photocurrent (current at $S \neq 0$) shows like the dark current a linear behavior at low voltages, corresponding to a homogeneous field distribution. This is the range where a rate equation model such as the one discussed earlier is adequately describing the switch behavior. At higher voltages, however, deviations from the linear slope become significant because the carrier injection through the contacts cannot be neglected anymore against the photo generation of charge carriers in the bulk of the switch. This carrier injection through the contacts becomes more and more dominant at higher voltages until, eventually, the photocurrent curves merge with the dark current curve.

The time to establish a current which corresponds to the dark current is the filling time for the deep traps, $T = N/S$, where N is the trap density and S the source function. A more quantitative description of the temporal development of the current is obtained with a time dependent, one-dimensional model of the BOSS system.[12] The modeled discharge system consists of a step voltage generator with constant voltage V_0 and a load resistor of 50 Ohm in series with a BOSS. Results of the transient simulation of a GaAs:Si:Cu switch irradiated with a laser, which is turned on 30 ns after the application of the voltage V_0, has a pulse duration of 750 ps and generates a homogeneous source function $S = 10^{25}\ cm^{-3}s^{-1}$ in the bulk of the switch, are shown in Fig. 11. The voltage across the switch drops from 5 kV to about 50 V in about 300 ps and reaches a value of 1 V at the end of the laser pulse at 750 ps. After the source function is switched off the voltage increases very slowly, the typical behavior of the "bistable" BOSS. Eventually, at about 200 µs after turn-off it reaches the "lock-on" voltage where a constant dark current, the "lock-on" current is established. Because of the small resistance of the switch (small compared to the load resistance) during the laser sustained photoconductive phase, the bistable BOSS-phase and the lock-on phase, the current does not change in time.

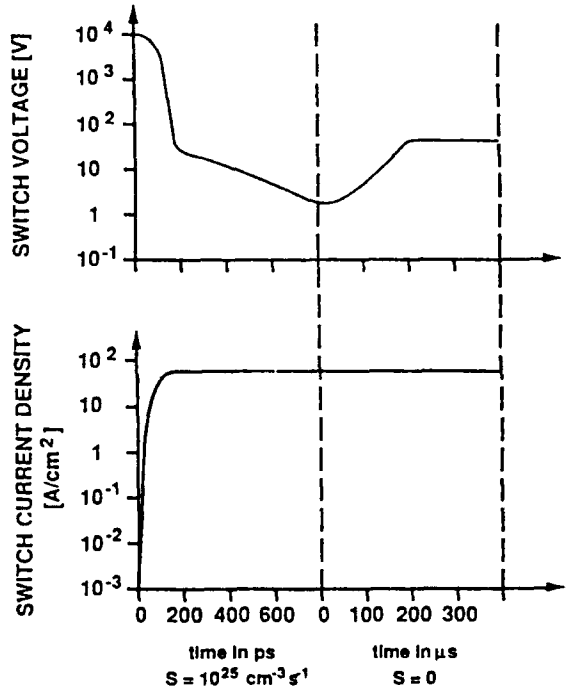

FIG. 11. Computed temporal development of switch voltage and switch current.

The results of the one-dimensional model show that the BOSS can be used in two modes. If delay times of µs or even ms are tolerable switching with large current rise can be achieved with relatively small laser power. A source function of $10^{19}cm^{-3}s^{1}$ corresponding to laser power of 10 W/cm^2 is sufficient to switch the BOSS into a highly conductive state in ns time, however with a delay which could be several hundred µs. An example for such a

process, where switching into "lock-on" occurs long after the laser pulse is shown in Fig. 12.[26] With source functions of > $10^{25}cm^{-3}s^{-1}$, on the other hand, switching can be obtained on a subpicosecond timescale. Although the corresponding laser power seems to be high, 100 MW/cm^2, the required laser energy is only 10 mJ for an area of 1 cm^2.

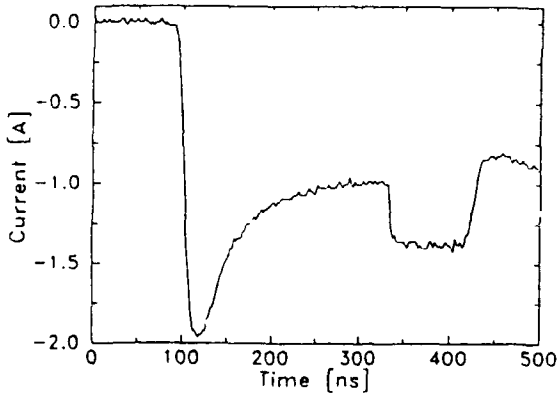

FIG. 12. A current pulse showing the transition at 330 ns to the gain mode of operation. The applied voltage was 258 V (4 kV/cm).[26]

The transition from the low current to the high current regime through a range of current controlled negative differential conductivity is generally leading to the current filament formation.[15] Such occurrence of filaments has been reported for photoconductive switches operating in the lock-on mode.[16] The one-dimensional model is certainly not able to describe this filament formation, it needs to be extended into a two-dimensional model. However, this described model is still able to predict filaments through a stability analysis[17] and to describe the conditions which lead to filament formation.

SWITCHING EXPERIMENTS

As discussed in the section "Concept", the compensation of n-type GaAs with copper leads to long photoconductivity decay time constants if the generation of photoelectrons occurs dominantly through ionization of the deep Cu-centers. This slow decay, which can be on the order of ms for cooled GaAs:Si:Cu, allows to use this material in jitterfree closing switches, similarly to silicon[18], without having to use the so-called lock-on effect. The advantage over silicon as switch material is the lower dark current and higher mobility which allows improved power handling.[18]

Experiments were performed to get quantitative results on the design of GaAs:Si:Cu switches as optically controlled closing switches.[19] The rectangular switch samples with dimensions of 0.4 cm*0.6 cm and a thickness of 0.022 cm had a resistivity of $3*10^4$ Ohmcm. The coplanar contacts were separated by a 0.25 cm gap. The electrical system used to test the switch consisted of a 50 Ohm Pulse Forming Network which generated voltage pulses of 160 ns duration in a matched load with voltages of up to 5 kV. The switch was illuminated with a Nd:YAG laser (wavelength: 1064 nm) having a pulse energy of about 120 mJ and a 10 ns pulsewidth. Figure 13 demonstrates a typical switching event for peak fields less than 10 kV/cm. Upon application of the laser pulse, the current rises to 55 A and than decays to an almost constant "tail current" which after 160 ns has settled to 25 A. This value corresponds to a current density of 3.7 kA/cm^2. As the peak field increases to values above 10 kV/cm, the typical lock-on effect is observed. In the lock-on state the current is locked-on to a constant voltage, similar to the breakdown behavior of a Zener-diode.

The closing switch experiments showed that in GaAs:Si:Cu current densities in excess of kA/cm's can be switched with moderate laser energies. Average fields of up to 20 kV/cm could be applied in an atmospheric pressure air environment without reaching the breakdown level. It could be shown that this material has a conductivity time constant comparable to

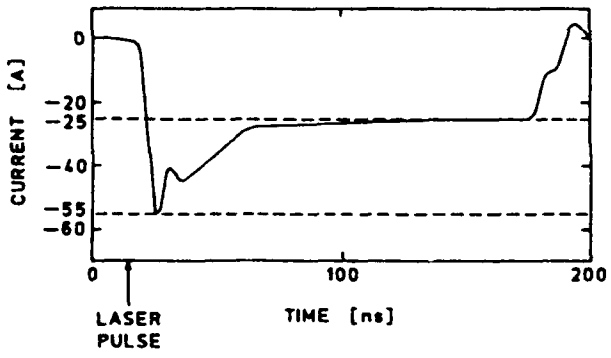

FIG. 13. Sample current vs time (note that the collapse of the current after 160 ns is due to the end of the transmission line voltage pulse).

that of bulk Si-switches, but with the advantage of higher dark resistance and better electron mobility than Si. The decay time in GaAs:Si:Cu can actually be adjusted to a desired value by varying the Cu concentration in the semiconductor with respect to the Si-concentration. Highly compensated material, where the Cu^--concentration equals the Si^+-concentration, has a much longer electron lifetime than material where the Cu^--concentration exceeds that of Si^+ (p-type GaAs:Si:Cu). This effect is demonstrated in Fig. 14 where the temporal response of compensated GaAs:Si:Cu is compared to slightly p-type material.[14]

Combined closing and opening switch experiments with GaAs:Si:Cu as switch material were conducted with a Nd:YAG laser for closing operation and an IR laser operating at wavelengths around 1800 nm as a light source for switch opening. The 26 ns FWHM Nd:YAG laser had a typical photon flux of $5*10^{23}$ $cm^{-2}s^{-1}$ (90 kW/cm^2). The photoquenching laser pulse was generated by a tunable laser system (Spectra Physics). The pulse duration was 7 ns at a maximum photonflux of $5*10^{25}cm^{-2}s^{-1}$ (6 MW/cm^2). The electrical circuit which provided the voltage pulse to the sample was a PFN (50 Ohm cable) with 300 ns pulse duration into a matched load. The applied voltages were in the range of up to 100 V, much less than in the previously described closing switch experiments.

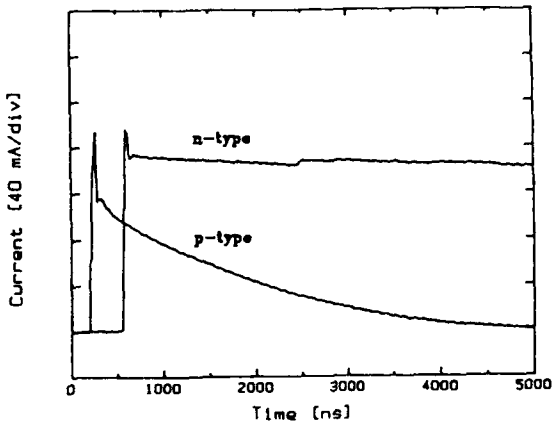

FIG. 14. Comparative turn-on current responses for the p- and n-type samples under similar conditions of voltage and light intensity.

The response of the GaAs:Si:Cu photoconductive switch (with coplanar contacts) to excitation by the two, subsequent laser pulses is shown in Fig. 15.[20] The photoconductance is turned on by the Nd:YAG laser at 30 ns. The laser irradiation causes a current overshoot to a peak of more than 0.5 A. Then the current decays to about 0.3 A. Two hundred nanoseconds after turn-on the 1800 nm laser pulse is incident. The photocurrent is immediately quenched by this radiation. The intensity of this quenching laser was varied from $5*10^{25}cm^{-2}s^{-1}$ to $5*10^{22}$ $cm^{-2}s^{-1}$ with neutral density filters. Figure 16 shows the intensity dependence of the quenching factor Q which is defined as the ratio of the difference in the conductivities before and after quenching to that before quenching. The maximum value of Q which could be resolved was 0.98, a value which is reached with a photon flux above $3*10^{24}cm^{-2}s^{-1}$.

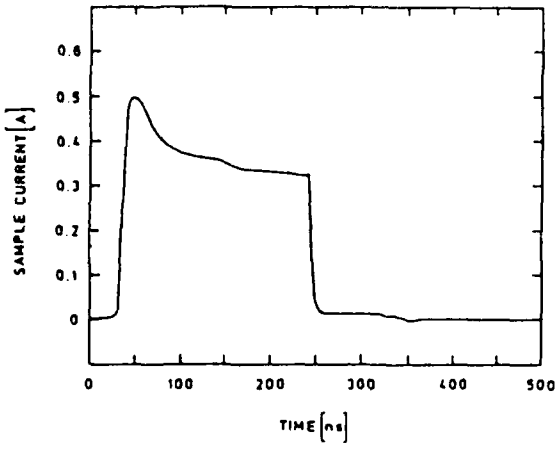

FIG. 15. Measured current flowing through the *p*-type crystal. Sample conductivity is induced initially by the 1.06 μm laser pulse. The sample conductivity is quenched 200 ns later by the 1.8 μm laser pulse. The initial bias voltage is 55 V.

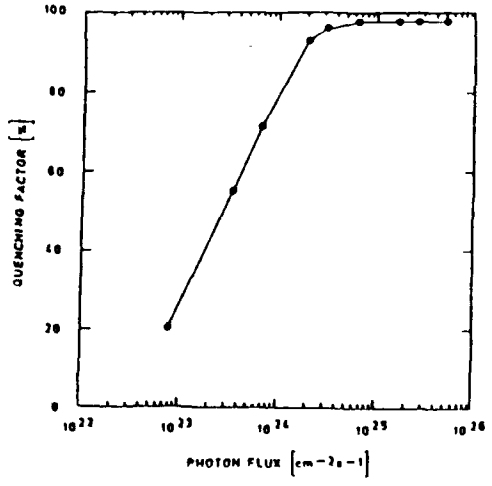

FIG. 16. Quenching factor as a function of the 1.62 μm laser pulse peak intensity. The maximum quenching factor that could be resolved was 98%.

In order to extent the power range of the switch which for coplanar contacts is limited by the thickness of the photoconductor (0.022 cm) and the surface flashover strength, the switch was redesigned such that the contacts were on the two faces of the GaAs:Si:Cu sample (sandwich configuration). This contact configuration reduced the probability for surface flashover because of the lengthened path between the contacts along the surface and it allowed to enlarge the cross-section of the photoconductor considerably. However, because the illumination of the active part of the switch needs to be side-on and therefore optical energy is lost through absorption in the inactive part (outside the contact area) of the switch, a higher photonflux is requ' d to obtain the same quenching effect as in sw. es with coplanar contacts.

The experimental setup for the high power BOSS experiment is shown in Fig. 17.[21] The small gap distance of less than 0.05 cm allowed to operate at field strengths exceeding the lock-on field for GaAs:Si:Cu (about 10 kV/cm for this particular sample) with moderate applied voltages in the range of several hundred volts. Figure 18 demonstrates the typical temporal development of the photo-induced and photo-quenched current for peak fields of less than the lock-on field. In this case the optical energy of the turn-off laser pulse at 250 ns was not sufficient to quench the photocurrent completely. After partial quenching the photocurrent resumes a persistent conductance on a reduced level. This indicates that the BOSS cannot just be used as a closing and opening switch but also as current valve which is controlled by two light sources, one for current increase and the second one for current reduction.

When the switch is operated at applied electric fields exceeding the lock-on field it is still possible to quench the photocurrent with IR light. However, as shown in Fig. 19, the photocurrent, after a 25 ns delay, rises again. A permanent photocurrent is then re-established albeit with a magnitude below the initial photocurrent level. It is therefore possible to interrupt lock-on currents, at least temporarily, in a controlled way. This is to our knowledge the only controlled quenching of

lock-on current in against an applied electric field. Sofar the only other quenching of lock-on currents was achieved by temporarily reducing the applied voltage below the lock-on level.[22]

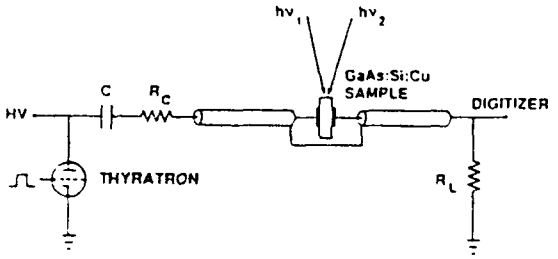

FIG. 17. Experimental Set-up (6).

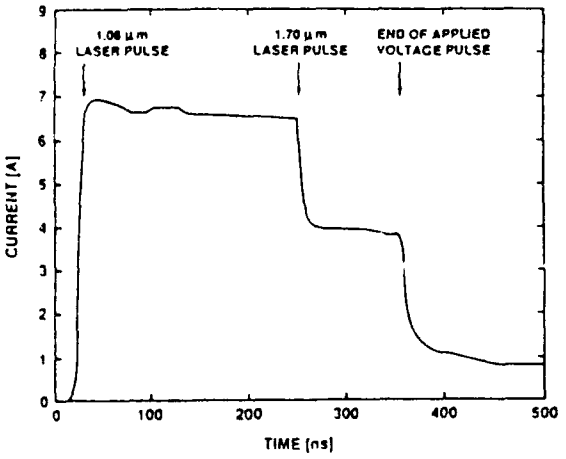

FIG. 18. Optical quenching of the photocurrent in GaAs:Si:Cu for a bias electric field of 875 V/cm (6).

Since the switch concept is not only applicable to GaAs:Si:Cu but to any semiconductor with deep acceptors where the electron capture cross-section is very small compared to the hole capture cross-section, other wide band gap semiconductors with similar deep level configuration should also be considered as BOSS systems. That cadmium

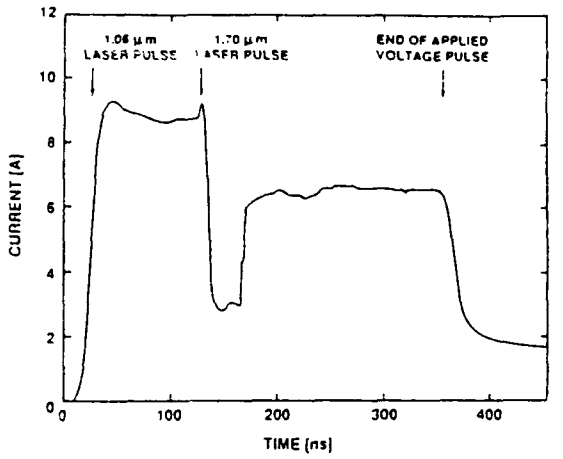

FIG. 19. Optical quenching of the photocurrent in GaAs:Si:Cu for a bias electric field of 20 kv/cm (6).

sulfide (CdS:Cu) shows a similar temporal response to light of different wavelengths as GaAs:Si:Cu does, has been demonstrated experimentally.[23,24] A CdS:Cu crystal has first been illuminated with light of a flashlamp in order to generate photoconductivity, and then was irradiated with a Nd:YAG laser. The energy differences between the Cu-levels and the valence band in CdS are such, that near-IR radiation should cause a photoquenching effect. Figure 20 shows the temporal development of the CdS-switch: the current increases due to the increasing intensity of the flashlamp over the entire time-range if there is no second light source; if, however, the Nd:YAG laser is turned on during this illumination process, the photocurrent is quenched. The time constant for quenching seems to be determined by internal trap-emptying and trap-filling processes rather than by electron-hole recombination as the case of GaAs as base material. Similar experiments as with CdS have been performed with ZnS:Cu, ZnO:Cu, and ZnSe:Cu.

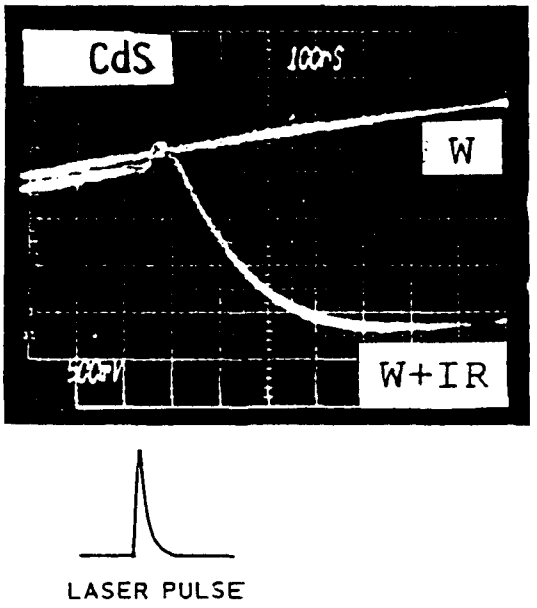

FIG. 20. Turn-on (upper trace and turn-off (lower trace) response of a CdS sample.

SUMMARY

A new, highly resistive material (> 10^6 Ohmcm), silicon doped, copper compensated, gallium arsenide, was fabricated and characterized by using various deep level spectroscopic methods. The deep level configuration of GaAs:Si:Cu is such that the photo-ionization of Cu-centers by means of Nd:YAG laser radiation creates a conductor with long lifetime, free electrons and bound holes. The subsequent ionization of these holes by longer wavelength radiation stimulates direct electron-hole recombination and consequently quenching of the conductance. The efficiency of these processes and the lifetime of the photo-electrons is determined by the absolute and relative (with respect to silicon) concentration of copper in the base material. Copper doping of GaAs:Si therefore allows to tailor the material with respect to its application as a closing and/or opening switch.

The performance of GaAs:Si:Cu as material for optically controlled switches was studied by means of a rate equation model and a one-dimensional, time dependent drift-diffusion model. The rate equation model allowed to find the optimum density of the impurities in GaAs for various switching processes. The more advanced drift diffusion model which includes contact effects was able to predict the dark current characteristics of GaAs, which has a pronounced range of negative differential resistivity, and to model the so-called lock-on effect in this material. The lock-on effect, which is characterized by a permanent conductance at constant voltage, was found, with the assumptions made in this model, to be caused by trap filling due to double injection. The plasma-like charge distribution in the bulk of the semiconductor, which at a certain voltage is sustained by carrier injection through the contacts, allows a continuous high current flow, the lock-on current.

Experimental studies on the closing and opening switch performance of the BOSS were performed with a Nd:YAG laser as lightsource for photo conduction and an IR-laser operating above 1600 nm for photo quenching. Nanosecond closing and opening was demonstrated. The required power levels for closing and opening were found to be about 100 kW/cm^2 for closing and 300 kW/cm^2 for opening. The penetration depth of the light was measured to be about 0.3 cm (for impurity densities around $5*10^{16}$ cm^{-3}) which makes the construction of relatively large (cm) size switches possible if the Cu-concentration is lowered to about 10^{16} cm^{-3}. On the other hand, if the switch size can be reduced from cm's to ten's of micrometers, laser diodes could be utilized as control elements.

The photoconductance depends linearly on the photonflux (for the closing switch operation) if the applied electric field is less than a critical field, which for GaAs:Si:Cu is around 3 kV/cm. Above this critical field the

current locks on at constant voltage. According to our model this represents a state where a free electron - bound hole plasma, sustained by carrier injection through the contacts, is able to carry almost any current as long as the voltage is high enough to replenish the free carriers lost through recombination and trapping. As in the case of photogenerated conductivity, the excitation of holes from the Cu-center causes quenching of the conductance, however, only as long as the photoquenching effect prevails over the double injection effect. Quenching of the lock-on current was demonstrated using the 1800 nm laser. After about 25 ns the current recovered to the lock-on current as expected from our model of the lock-on effect.

The BOSS performance has sofar been tested on a power level of kW, in the temporal range of nanoseconds. Theoretical results indicate that extension into the MW range is possible with commercially available lasers. They also indicate that the temporal range can be extended in the picosecond range. Repetition rates in the multi MHz range can be obtained with lasers operating at these reprates. Switching the BOSS out of the lock-on state, repetitively, requires just one laser operating in a burst mode. The switch, after opening, will automatically return into lock-on, as demonstrated experimentally. Another interesting development using the BOSS concept could be the miniaturization of the switches, which would allow to utilize laser diodes or even LED's as control elements.

ACKNOWLEDGEMENTS

This work was supported by SDIO/IST and managed by ONR under contract number N00-14-86-K-560. The program monitor is Gabriel Roy.

REFERENCES

1. G.M. Loubriel, M.T. Buttram, W.D. Helgeson, D.L. McLaughlin, M.W. O'Malley, F.J. Zutavern, A. Rosen, P.J. Stabile, "Triggering GaAs lock-on switches with laser diode arrays," Proc. SPIE Conf. on Optically Activated Switching, Boston, MA, Vol. 1378, 179 (1990).

2. P.R. Smith, D.H. Auston, and M.C. Nuss, "Subpicosecond photoconducting dipole antennas," IEEE J. Quantum Electronics, 24, 255 (1988).

3. K.H. Schoenbach, V.K. Lakdawala, R. Germer, and S.T. Ko, "An optically controlled closing and opening semiconductor switch," J. Appl. Phys. 63, 2460 (1988).

4. J. Blanc, R.H. Bube, and H.E. MacDonald, "Properties of high-resistivity gallium arsenide compensated with diffused copper," J. Appl. Phys., 32, 1666 (1961).

5. R.A. Roush, R.P. Brinkmann, and K.H. Schoenbach, "The temporal development of the dark current in highly resistive gallium arsenide compensated with diffused copper," submitted to J. Appl. Phys.

6. K.H. Schoenbach, H.J. Schulz, V.K. Lakdawala, B. Kimpel, R.P. Brinkmann, R.K.F. Germer, and G. Barevadia, "The deep-level configuration of GaAs:Si:Cu - a material for a new type of optoelectronic switch," Proc. SPIE Intern. Conf. on Physical Concepts of Materials for Novel Optoelectronic Device Applications, Aachen, Germany, Vol.1362, 428 (1990).

7. S.T. Ko, V.K. Lakdawala, K.H. Schoenbach, and M.S. Mazzola,"Optimization studies of materials for optically controlled semiconductor switches," Proc. 7th Pulsed Power Conf., Monterey, CA, 1989, p. 861.

8. V.K. Lakdawala, K.H. Schoenbach, R.A. Roush, G.R. Barevadia, and M.S. Mazzola, "Photoquenching and characterization studies in a bulk optically controlled GaAs semiconductor switch," Proc. SPIE Conf. on Optically Activated Switching, Boston, MA, Vol. 1378, 259 (1990).

9. D.K. Schroder, "Semiconductor material and device characterization," Chapter 7, John Wiley & Sons, Inc. New York, 1990.

10. R.P. Brinkmann, to be published.

11. N. Kullendorf and L. Jansson, "Copper-related deep level defects in III-V semiconductors," J. Appl. Phys. 54, 3203 (1983).

12. R.P. Brinkmann, K.H. Schoenbach, R.A. Roush, D.C. Stoudt, V.K. Lakdawala, and G.A. Gerdin, "High power switching with electron-beam controlled semiconductors," Proc. SPIE Conf. on Opticallly Activated Switching, Boston, Ma, Vol. 1378, 203 (1990).

13. M.A. Lampert and P. Mark, "Current injection in solids," Chapter 14, Academic Press, New York and London, 1970.

14. M.S. Mazzola, K.H. Schoenbach, V.K. Lakdawala, and S.T. Ko, "Investigation of a photoconductive closing and opening bulk GaAs semiconductor switch," Proc. 7th IEEE Pulsed Power Conf., Monterey, CA, 1989, p. 418.

15. B.K. Ridley, "Specific negative resistance in solids," Proc. Phys. Soc. 82, 954 (1963).

16. W.R. Donaldson, L.E. Kingsley, "Optical probing of field dependent effects in GaAs photoconductive switches," Proc. SPIE Conf. on Optically Activated Switching, Boston, MA, Vol 1378, 226 (1990).

17. R.P. Brinkmann, K.H. Schoenbach, D.C. Stoudt, V.K. Lakdawala, G.A. Gerdin, and M.K. Kennedy, "The lock-on effect in electron-beam controlled gallium arsenide switches," IEEE Trans. Electron Devices, 38, 701 (1991).

18. W.C. Nunnally and R.B. Hammond, "Optoelectronic switch for pulsed power, in picosecond optoelectonic devices," Chi H. Lee, ed., Academic Press, Inc. 1984.

19. M.S. Mazzola, K.H. Schoenbach, V.K. Lakdawala, R. Germer, G.M. Loubriel, and F.J. Zutaversn, "GaAs photoconductive closing switches with high dark resistance and microsecond conductivity decay," Appl. Phys. Lett. 54, 742 (1989).

20. M.S. Mazzola, K.H. Schoenbach, V.K. Lakdawala, and S.T. Ko, "Nanosecond optical quenching of photoconductivity in an bulk GaAs switch," Appl. Phys. Lett. 55, 2102 (1989).

21. M.S. Mazzola, K.H. Schoenbach, V.K. Lakdawala, and R.A. Roush, "Infrared quenching of conductivity at high electric fields in bulk copper compensated optically activated GaAs switches," IEEE Trans. Electron Devices, 37, 2499 (1990).

22. F.J. Zutavern, G.M. Loubriel, B.B. McKenzie, W.M. O'Malley, R.A. Hamil, L.P. Schanwald, H.P. Hjalmarson, "Photoconductive semiconductor switch (PCSS) recovery," Proc. 7th IEEE Pulsed Power Conf., Monterey, CA, 1989, p.412.

23. R.K.F. Germer, K.H. Schoenbach, and S.G.E. Pronko, "A bulk optically controlled semiconductor switch," J. Appl. Phys. 64, 913 (1988).

24. R.K.F. Germer and K.H. Schoenbach, "Stimulated switch-off and repetitive switching of a bistable optically controlled semiconductor switch," J. Phys., Appl. Phys., 22 398 (1989).

25. V.K. Lakdawala et.al., to be published.

26. D.C. Stoudt, M.S. Mazzola, and S. F. Griffiths, "Characterization and switching study of an optically controlled GaAs switch," Proc. Conf. on Optically Activated Switching, Boston, MA, 1990, SPIE Volume 1378, p.280.

K. H. Schoenbach, photograph and biography not available at the time of publication.

V. K. Lakdawala, photograph and biography not available at the time of publication.

INVESTIGATION OF PULSED SURFACE FLASHOVER BEHAVIOR OF INSULATORS AND SEMICONDUCTORS

T. S. Sudarshan and T. Asokan
Department of Electrical and Computer Engineering
University of South Carolina
Columbia, SC 29208

ABSTRACT

Pulsed surface breakdown (flashover) characteristics of polycrystalline alumina, single crystal quartz (x-cut and z-cut) and photoconducting silicon were investigated. A new electrode system was designed and validated which greatly facilitates time-coordinated electrical and optical measurements of surface discharges along insulators. The surface flashover characteristics obtained using the new electrode system are discussed and compared with those obtained using the conventional parallel plane electrode system. The single crystal quartz specimens exhibit superior hold-off strength compared to polycrystalline alumina. For quartz, the highest conditioned breakdown strength, obtained using the new electrode system, is ~350 kV/cm, which is approximately equal to the strength of a plain vacuum gap. This value is the highest reported in the literature. The surface breakdown characteristics of photoconducting silicon were investigated by modifying the surface by mechanical, chemical, and thermal treatments. The investigation was performed both in vacuum and air. The surface treatments play an important role on the breakdown characteristics in vacuum, whereas they do not influence significantly the surface breakdown behavior of silicon in air. The influence of gold contacts on the breakdown characteristics was also investigated. The pulsed breakdown strength of Si with gold contacts is higher in air compared to that in vacuum by a factor greater than 3.0. The results are discussed in terms of space charge limited conduction and carrier injection phenomena. The report is divided into two major headings: I, validation of a novel electrode system to study the surface flashover behavior of insulators, and II, influence of the test environment on the surface breakdown characteristics of photoconducting silicon.

I. VALIDATION OF A NOVEL ELECTRODE SYSTEM TO STUDY THE SURFACE FLASHOVER BEHAVIOR OF INSULATORS

1. Introduction

It is well known that a solid insulating spacer in vacuum is the weakest link in any insulating system [1]. When a sufficiently high voltage is applied across a solid insulator in a vacuum environment, a flashover which is an indication of surface breakdown occurs on or near the insulator surface. The ability of the insulator to sustain high voltages is limited due to the surface flashover behavior. The surface flashover characteristics of solid insulators have therefore received considerable attention in the past.

Extensive investigations have been made with a view to understanding the mechanism of surface flashover and to increasing the surface flashover voltage by means of modifying a) the shape of the specimens, b) surface properties, and c) bulk properties through doping [2-5]. Presently, there is general agreement on the processes involved with the initiation and the final breakdown stages of surface flashover. But there is considerable disagreement concerning the mechanism and details of the intermediate growth stage, primarily because the role of the surface physical and chemical properties of the insulators is not understood clearly. Besides, the well-established uniform field parallel plane electrode system is not suitable for time-coordinated optical and x-ray diagnostics. For instance, when the diagnostic tools are focused towards a particular

face of the specimen, we miss the details of the flashovers that occur on the opposite side. It is, therefore, imperative to modify the electrode system, making it suitable for optical and x-ray diagnostics so that time-coordinated measurements of the various electrical and optical signals can be made.

In the present investigation, a new electrode system is designed and validated for its suitability to study the surface flashover characteristics. The results obtained by using the new electrode system are discussed and compared with those of the conventional electrode system.

2. Experimental Procedure

a) Electrode Configuration: The new electrode system used to perform the surface flashover investigation is shown in Fig. 1. The electrical field distribution in this system is non-uniform. The electrical stress at the tip of the electrode-insulator interface is higher than that in the uniform field electrode system. An analysis of the field distribution in the new electrode system has been performed by a computer simulation technique and is discussed in the next section.

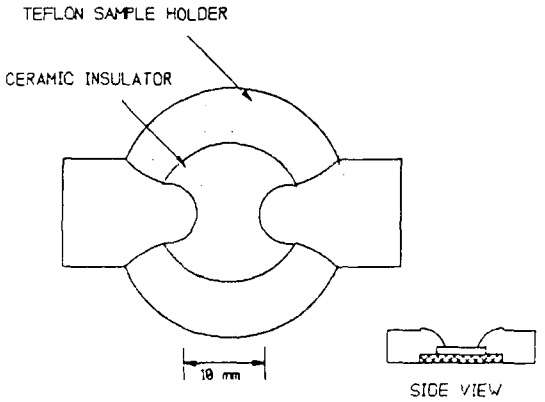

Fig. 1 New electrode assembly

b) Electrode and Sample Preparation: The electrodes in both the electrode systems (parallel plane and non-uniform field) are made of stainless steel. The parallel plane electrodes are approximately 10 cm in diameter with well-rounded edges. The electrode surfaces in both systems were polished successively with the final polish using 0.5 μm alumina to attain a mirror finish. After polishing, the electrodes were cleaned ultrasonically for one hour and dried.

Cylindrical insulators (25.4 mm dia and 10 mm thickness), of single crystal quartz and polycrystalline alumina, were used in the present study. Two quartz samples, with the piezoelectric axis parallel (x-cut) and perpendicular (z-cut) to the axis of the right circular cylindrical specimen, were studied [6]. The high purity alumina sample (99.9% Al_2O_3) was polished (both the flat ends and the cylindrical surface) to 1 μm finish. It is important to note that the flashover in the parallel plane electrode system occurs on the cylindrical side, whereas the flashover in the new planar electrode system occurs on the flat side. Hence the breakdown characteristics were obtained corresponding to the two flat sides of the cylindrical specimen. The gap between anode and cathode is the same (10 mm) in both electrode systems. In the new electrode system, since the electrodes make contact on the planar surface of the cylindrical specimen, for the x-cut quartz (piezoelectric axis parallel to the cylinder axis) the planar surface on which electrode contacts are made refers to the x-plane. The samples were cleaned ultrasonically in deionized water for one hour and dried.

c) Experimental Set Up: The experimental set up used in the present study is discussed elsewhere [7]. For the investigation, a 0.5/15 μs impulse waveform was chosen. The voltage was measured using a self-integrating, coaxial, capacitive divider in line with the test gap. The linear sensitivity of this divider was measured to be 3.87 mV/kV. The breakdown current was measured using a 15 mΩ, current-viewing resistor (CVR) in series with the test gap on the ground side. The signals (voltage and current) were acquired by using two dual-channel digitizing oscilloscopes (Hewlett Packard 54111D). The acquired signals were then transferred to a computer (Hewlett Packard 9000 series) for detailed analysis.

d) Test Procedures: The test chamber was pumped down to a pressure of about 2×10^{-5} torr and allowed to remain so overnight before commencing the test. The insulator was subjected to voltage pulses (0.5/15 μs) beginning at 10 kV. The voltage was increased in steps of 1.0 kV. The time interval between successive voltage applications was about five minutes. The sequence of the voltage applications followed in the present study is illustrated in Fig. 2. The voltage at which the first breakdown occurred is called "breakdown voltage" (V_{bd}).

Once the breakdown occurred, the sample was subjected to two more voltage applications at the V_{bd} level. In most of the cases the subsequent voltage applications at this level did not result in breakdown. If

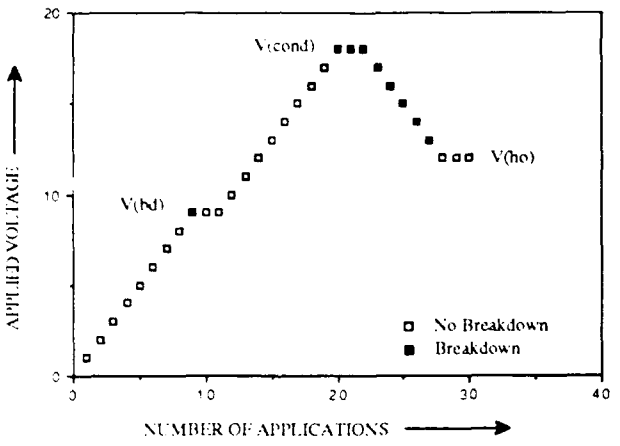

Fig. 2 Sequence of voltage applications followed in the present work

the material underwent breakdown at the subsequent applications at V_{bd}, the same voltage level is also considered as the "conditioned voltage" (V_c). Otherwise, the voltage was increased again in steps of 1.0 kV. The voltage at which three out of three voltage applications resulted in breakdown is termed conditioned voltage.

After determining the conditioned voltage level, the voltage is decreased in steps of 1.0 kV. The voltage level at which three consecutive applications do not result in breakdown is termed "hold-off voltage" (V_{ho}). After the initial test, the sample was left in the vacuum chamber overnight without any voltage applications (rest period). The next day the sample was again subjected to voltage applications, as described above, to determine V_{bd}, V_c, and V_{ho}. The test cycle was extended, after similar rest periods, to three or more days, depending upon the performance of the sample. In the new electrode system, the sample was reversed, after the test cycles, and subjected to similar test cycles.

3. Results and Discussion

The electric field distribution corresponding to the new test geometry (planar) is simulated on a computer by numerical analysis using a 3-d finite difference program. Because of the symmetry along the mid-plane, between the two electrodes, it is sufficient to analyze only one half of the test-gap arrangement as shown in Fig. 3. The electrode was assumed to be at a potential "V," and the mid-plane between the electrodes and the bounding surfaces are assumed to be at ground potential. Fig. 4 shows the potential distribution in the region surrounding the electrode at potential V. The electric stress can be seen to be a maximum at the triple junction near the tip of the electrode-insulator interface. Fig. 5 shows the variation in the electric stress with position along the axis of the test gap. The maximum field which occurs at the tip of the electrode is 4.77V/cm/applied volt between the electrodes. Hence the maximum field intensification factor for this geometry is 4.77 compared to a uniform field system.

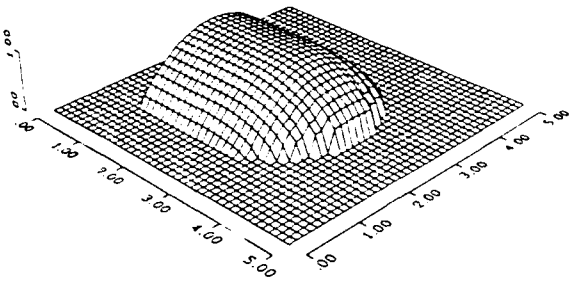

Fig. 3 Computer simulated electrode geometry

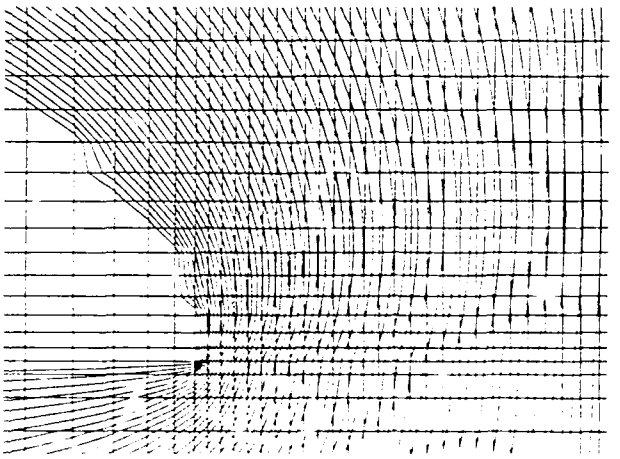

Fig. 4 Potential distribution near the electrode

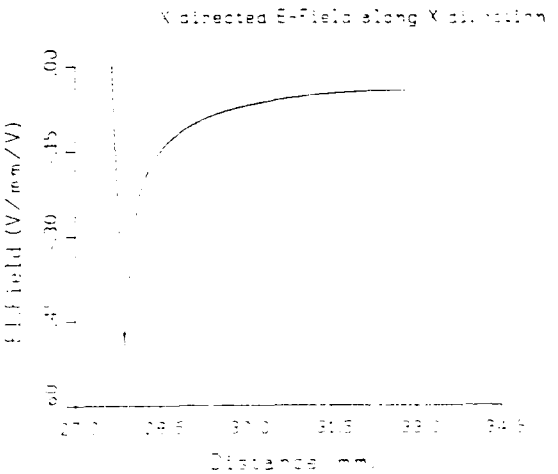

Fig. 5 Electric stress distribution near the electrode

The surface flashover characteristics of quartz (x-cut and z-cut) and alumina samples obtained by using the new electrode system are given in Table 1. The breakdown values given within the brackets correspond to those obtained on the reverse side of the same cylindrical specimen. It is interesting to note that, in all the cases, the first breakdown voltage (V_{bd}), conditioned voltage (V_c), and hold-off voltage (V_{ho}) levels increased significantly after being left overnight (rest period) following the initial test. However, these voltage levels decreased during the subsequent tests.

TABLE : 1 BREAKDOWN CHARACTERISTICS OF VARIOUS INSULATORS OBTAINED BY USING NEW ELECTRODE SYSTEM

SAMPLE TYPE	TEST NO AND DETAILS	FIRST B.D VOLT(KV)	CONDITIONED VOLT (KV)	HOLD OFF VOLT (KV)
QUARTZ (X CUT)	1 (1st day)	36.23 (46.83)	44.19 (46.83)	40.10 (42.59)
	2 (2nd day)	73.85 (57.13)	73.85 (57.13)	43.71 (42.59)
	3 (3rd day)	65.74 (64.96)	65.74 (64.96)	24.66 (50.81)
	4 (4th day)	38.70 (54.79)	38.70 (54.79)	29.64 (49.69)
	5 (5th day)	--- (45.84)	--- (56.00)	--- (41.47)
QUARTZ (Z-CUT)	1 (1st day)	48.94 (60.29)	48.94 (60.29)	34.49 (47.57)
	2 (2nd day)	56.51(72.40)	56.51 (72.40)	24.03 (44.83)
	3 (3rd day)	29.53 (60.49)	29.53 (60.49)	16.67 (23.54)
ALUMINA (1um Finish)	1 (1st day)	39.42 (36.11)	41.86 (36.11)	37.86 (31.76)
	2 (2nd day)	49.06 (48.08)	49.06 (48.08)	24.28 (12.26)
	3 (3rd day)	40.23 (16.09)	40.23 (29.28)	17.68 (12.05)
	4 (4th day)	31.95 (23.11)	31.95 (23.11)	21.27 (13.24)
	5 (5th day)	--- (16.31)	--- (16.31)	--- (14.57)

* Values within parentheses correspond to the results of the same sample obtained on the reverse side

The surface flashover characteristics of the same samples using the conventional parallel plane electrode system are shown in Table 2. As the breakdown voltages of the samples were limited by the bushing at the Marx generator, the test was not performed above 170 kV [6]. Therefore, the actual breakdown voltages, after the first rest period, were not obtained. However, it may be observed that, in all the cases, the voltage levels corresponding to V_{bd}, V_c, and V_{ho} increased significantly after the first rest period, similar to the new electrode system.

TABLE : 2 BREAKDOWN CHARACTERISTICS OF INSULATORS OBSERVED USING THE PARALLEL PLANE ELECTRODE SYSTEM

SAMPLE TYPE	TEST NO AND DETAILS	FIRST B.D VOLTAGE (KV)	CONDITIONED VOLTAGE (KV)	HOLDOFF VOLTAGE (KV)
QUARTZ (X-CUT)	1 (1st day)	93	124	122
	2 (2nd day)	>170	>170	>170
QUARTZ (Z-CUT)	1 (1st day)	95	>170	>170
	2 (2nd day)	>170	>170	>170
ALUMINA POLISHED	1 (1st day)	120	130	128
	2 (2nd day)	>170	>170	>170

A direct comparison of the breakdown strengths of insulators corresponding to the two electrode systems cannot be made because of the different electric field configurations in the two cases. Since the stress enhancement factor in the new test configuration (planar) is ~4.77, the values given in Table 1 will have to be multiplied by 4.77 to get a fair comparison with those corresponding to the parallel plane geometry (Table 2). Hence the new electrode system has the advantage that breakdown studies can be performed at considerably lower voltages. However, the primary advantage of the new system is that it affords unambiguous measurement of optical activity associated with the dielectric surface under stress.

From Table 1 it can be seen that the difference in the breakdown strengths of the x-cut and z-cut specimens of quartz cannot be discerned clearly due to the scatter in the results. However, in general, the voltage hold-off performance of quartz is distinctly superior to that of polycrystalline alumina, especially after the initial rest period. The conditioned breakdown strength of quartz after the initial rest period reached a value as high as 352.3 kV/cm (i.e, at 73.85 kV, assuming an enhancement factor of 4.77). This value, if correct, is nearly equal to the strength of a plain vacuum gap. On the negative side, all the samples exhibit a low voltage hold-off after reaching a high conditioned voltage subsequent to the initial rest period. The mechanisms responsible for the improved behavior following the initial rest period, and the subsequent degradation in the hold-off voltage, are the subject of our present investigations. It would also be interesting to study if relatively high voltage hold-off levels could be maintained (for, e.g., 50 kV) by not subjecting the dielectrics to breakdown at high stresses which are reached during the conditioning process (e.g., 73.85 kV).

Table 3 shows the comparison between the breakdown strengths of the as-received alumina specimens which were not subject to any mechanical polishing. Note the large scatter in the breakdown data. Hence it is difficult to study and compare the material characteristics with such a large scatter in the data from sample to sample. It is to be noted that the scatter in data is considerably reduced when the as-received alumina sample is carefully polished, using successively finer grades of diamond paste , with the final polish being with 1 μm paste (Table 1). In addition to the reduced scatter, the polished samples exhibit significantly higher breakdown strengths over the as-received samples.

TABLE : 3 BREAKDOWN CHARACTERISTICS OF AS RECEIVED ALUMINA SAMPLES OBSERVED IN THE NEW ELECTRODE SYSTEM

SAMPLE NO	TEST NO AND DETAILS.	V(b.d) (KV)	V(cond) (KV)	V(ho) (KV)
1	1 (1st day)	21.~ (25.4)	27.4 (25.4)	21.9 (<18.0)
	2 (2nd day)	23.2 (31.9)	23.2 (31.9)	17.6 (<25.0)
2	1 (1st day)	23.5	35.9	31.8
	2 (2nd day)	39.1	39.1	28.6
3	1 (1st day)	28.9 (17.9)	28.9 (17.9)	16.1 (15.9)
	2 (2nd day)	26.2 (<15.9)	26.2 (<15.9)	17.9 (15.9)

* Values within parenthses corresponds to the results of the sample obtained on the reverse side.

Pre-breakdown x-ray activity was observed for all the specimens (quartz and 1 μm finish Al_2O_3) for which the breakdown values are given in Table 1. Since the first breakdown voltage is high for quartz specimens after the initial rest period, the prebreakdown x-ray activity was obtained, above a threshold applied voltage, at various levels up to breakdown. Typical variation in prebreakdown x-ray magnitude (arbitrary units) vs. applied voltage is shown in Fig. 6. The x-ray intensity increases with applied voltage for both the x-cut and z-cut quartz. The figure shows only two data points for Al_2O_3.

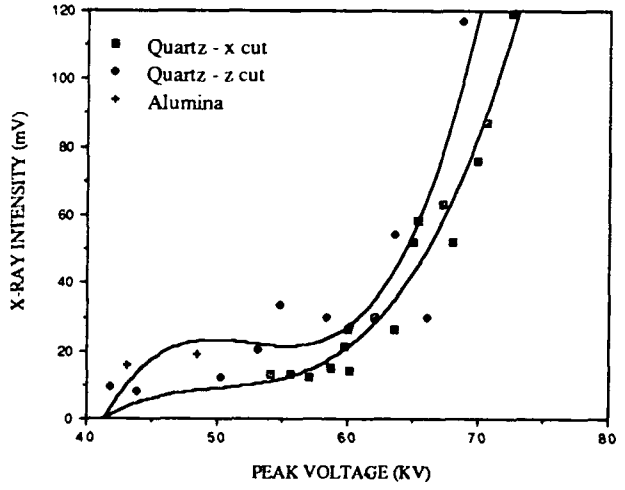

Fig. 6 Variation of pre-breakdown x-ray intensity as a function of applied voltage

Figure 7 shows (for x-cut quartz) a typical variation of x-ray and luminosity amplitudes as the peak applied voltage at breakdown is decreased from the conditioned value to the hold-off level. It is interesting to note that for all the samples studied, the x-ray intensity increases initially and then decreases as the breakdown voltage decreases. But the intensity of the luminosity decreases gradually in all the cases as the breakdown voltage decreases.

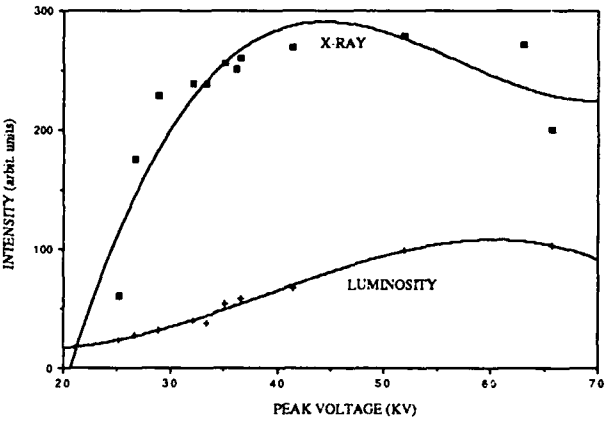

Fig. 7 Variation of x-ray and luminosity magnitudes (during breakdown) of quartz (x-cut) with peak applied voltage

In-depth studies of these processes are presently underway. In the new electrode system there is no ambiguity as to the detection of the x-ray and luminosity signals whenever they are present, a major advantage over the previous plane parallel electrode system.

II. SURFACE BREAKDOWN CHARACTERISTICS OF PHOTOCONDUCTING SILICON

1. Introduction

Photoconductive semiconductor switches have gained considerable attention recently in several fields, including the pulsed power, high power microwave, and millimeter wave communities. This recognition is primarily due to their unique characteristics, such as jitter-free response, high-power handling capability, and fast response time [8]. However, the major problem associated with these materials is surface breakdown (or flashover) characteristics. The surface breakdown occurs at applied fields lower than that of the bulk breakdown. The development of the photoconducting devices is therefore hindered by the poor surface flashover properties.

Several mechanisms based on various processes such as avalanche, thermal runaway, quantum-mechanical tunneling, band bending, and absorp-

tion of impurity atoms have been proposed [9-12]. Despite these various theses, the process involved in the surface flashover event is unclear. As the surface flashover characteristics of semiconductors are believed to be associated with many parameters, it is essential to understand the role of such factors as contact type/potential, bulk properties, surface condition, and the test environment on the conduction phenomena. In the present investigation an attempt has been made to understand the influence of surface treatments by means of mechanical, chemical, and thermal processes on the surface flashover characteristics of P-type silicon samples. The role of gold contacts on the charge injection characteristics has also been investigated. The above studies were carried out in vacuum and in air.

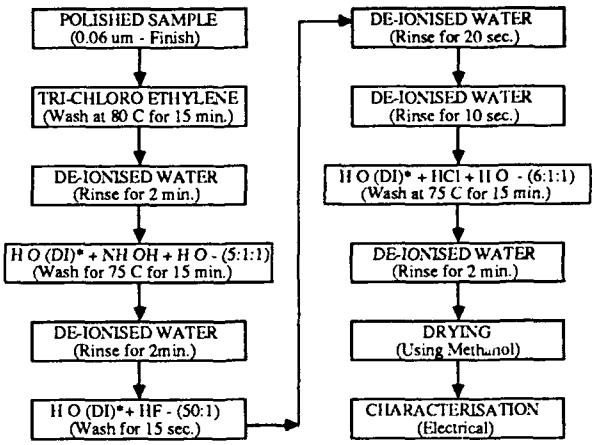

FIG: 8 MODIFIED RCA CLEANING PROCEDURE ADOPTED FOR SILICON
(* de-ionised water)

2. Experimental Procedure

a) Sample Preparation: Single crystal extrinsic semiconductors (P-type silicon), doped with boron, possessing resistivity greater than 30 kΩ cm at 25° C, were used in the present investigation. The samples were cylinders 10 mm in thickness and 25.4 mm in diameter. The crystallographic orientation of all the samples (along the cylindrical axis) was <111>.

The surface of the samples were modified in a controlled manner by one or more treatments - mechanical, chemical and thermal - as discussed below.

i) **Mechanical Treatment**: The samples were polished (all the faces) down to 1 μm finish using abrasive alumina slurry, starting from 10 μm particle size. After polishing, the samples were cleaned ultrasonically and subjected again to polishing using colloidal SiO_2 (average particle size 0.06 μm) for about one hour. The latter polishing was believed to decrease the concentrations of the surface defects. Finally, the polished samples were cleaned ultrasonically in deionized water, dried by methanol, and used for the electrical characterization.

ii) **Chemical Treatment:** Selected polished samples, prepared as above, were subjected to surface cleaning by a modified RCA procedure [13] involving major steps such as organic wash, ammonium hydroxide cleaning, and acid wash, as shown in Fig. 8. The samples were transferred immediately (after cleaning) to the vacuum chamber for testing. The flat ends of a few samples were coated with gold.

iii) **Thermal Treatment:** Some of the samples cleaned by the RCA procedure were subjected to surface oxidation by heating at 1100° C for two hours in oxygen atmosphere. After cooling the sample slowly to room temperature, the flat ends of the specimens were polished by 0.06 μm colloidal silica to remove the oxide layer. The polished specimens were cleaned again by the RCA procedure as above. In this case, the cleaning in HF solution was skipped to avoid the dissolution of the oxide layer on the cylindrical side.

b) Electrical Characterization: The experimental set up used for the electrical characterization of the samples is shown elsewhere [14]. The samples, prepared under different conditions, were placed between the uniform field-stainless steel electrodes with well-rounded edges. Prior to testing, the electrodes were polished down to a 0.5 μm finish using alumina slurry and cleaned thoroughly in deionized water by employing an ultrasonic stirrer. The tests in vacuum were performed at a pressure of about 8×10^{-6} torr.

A single-stage Marx pulse generator was used to generate 0.39/10 μs pulses. The voltage applied across the specimens was monitored by a voltage probe consisting of an E-dot sensor and a passive integrator. The E-dot sensor was placed in line with the high voltage cable at the entry point of the test cell, via the high voltage bushing. The prebreakdown and breakdown currents were monitored by using a 50 Ω current viewing resistor (CVR) and a Rogowski coil (RC) respectively. The luminosity was monitored by using a photomultiplier tube possessing sensitivity in the range of visible and infra red (IR). The voltage and the corresponding current (CVR and RC) and luminosity signals were acquired by employing a four-channel digitizing oscilloscope (Hewlett Packard 54112 D).

The samples were subjected to voltage pulses in steps of 1 kV, starting from 2.0 kV. The voltage, current, and luminosity waveforms were recorded at each voltage level. The application of voltages was stopped once the material underwent surface flashover. In most cases, the voltage applications were stopped at levels below the surface flashover voltage to avoid catastrophic failure at the surface.

3. Results and Discussion

Three distinct current phases have been observed in P-type silicon during the application of voltage pulses and reported earlier [14]. These phases are classified on the basis of voltage signals as a) the process involving prebreakdown conduction (Phase I), b) the process involving a partial collapse of voltage (Phase II), and c) the process leading to surface breakdown or complete collapse of voltage (Phase III). The current obtained in Phase I region is characterized by displacement, ohmic, charge injection or space charge limited (SCL) current, depending upon the condition of the sample and the voltage level. In the present work, the voltage levels (inception voltages) at which these phases were observed were recorded for all the specimens. Table 4 summarizes the inception voltages of different phases obtained for various types of samples. The Phase I inception voltage is defined as the voltage at which the space charge dominated current (not displacement or ohmic current) exceeds 5 mA. It may be observed that the uncoated sample cleaned by the RCA procedure (#A1) exhibits higher inception voltages than that of the sample (#6A) cleaned by an ultrasonic stirrer, though both samples were polished under identical conditions. A typical voltage, current, and luminosity waveforms obtained for the sample cleaned by the RCA procedure (#A1) is shown in Fig. 9. It may be observed that the displacement and space charge limited current peaks are separated by about 5 μs duration. In order to understand the process involved during conduction, the space charge limited current is plotted against the peak applied voltage as shown in Fig. 10. The non-linearity factor (x) estimated from the plot is 7.347, indicating that the sample does not obey the square law ($I \alpha V^2$). The deviation from the square law may be attributed to the trap density and temperature effect. It is to be noted that the Phase I inception voltage of 20.4 kV, for sample No. A1, is the highest observed so far. Also, the prebreakdown (Phase I) current values for this sample are considerably lower than those reported previously by our group [14]. It is not clear if the observed improvements are either a result of improved surface preparation techniques or due to the intrinsic properties of the specimen. Further, it may be seen that the oxidized sample (#5A) displays higher inception voltage levels after etching the oxide layer in 20% HF solution. The results indicate that the thermally grown oxide layer on the surface is undesirable, as the inception voltage levels are lower than that of a specimen without an oxide layer (sample A1).

TABLE : 4 VARIATION OF INCEPTION VOLTAGES AS A FUNCTION OF SAMPLE CONDITION

SAMPLE NO.	SAMPLE PREPARATION	VACUUM			AIR		
		V1	V2	V3	V1	V2	V3
6A	Polished and ultrasonically cleaned	16.15	16.84	---	---	---	---
A1	Polished and cleaned by RCA procedure	20.40	30.30	---	---	---	---
5B	a) Polished, oxidised, flat ends polished and cleaned by RCA procedure	5.99	10.33	12.50	---	---	---
	b) Oxide layer etched in 10% HF solution	9.81	13.37	22.31	---	---	---
18	Polished, gold deposition on flat ends and ultrasonically cleaned	5.99	---	8.68	8.16	>30	>30
19	Polished, gold deposition on flat ends and cleaned by modified RCA method	6.51	7.55	---	9.20	>30	>30
17	Polished (only flat ends), gold deposition on flat ends and ultrasonically cleaned	8.16	10.07	---	10.33	>30	>30

* V1 - Voltage corresponding to the onset of SCL dominated current
V2 - Voltage level at which a partial collapse observed in voltage waveform
V3 - Complete collapse in voltage (Surface breakdown)

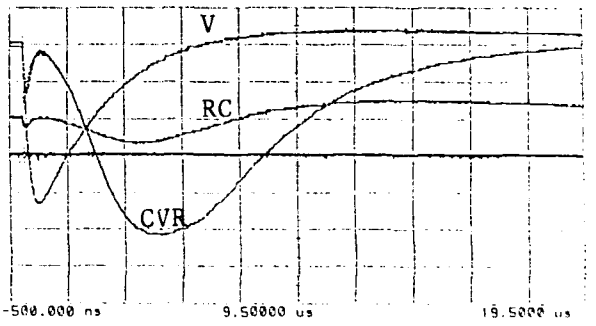

Fig. 9 Typical voltage, current and luminosity waveforms obtained for silicon sample - A1 (Voltage-4.34 KV/div, Current(CVR) -396mA/div, Current(RC)-2.48Amp/div, Luminosity- 5mv/div)

In the case of gold-coated samples (Nos. 18, 19, and 17), the Phase I and III processes (in vacuum) appear at lower voltages compared to those of the samples without gold contacts. Further, the same samples (gold coated) exhibit significantly higher Phase II inception voltages in air compared to those in vacuum. It may also be observed that the cleaning procedure and the polishing on the cylindrical surface did not influence significantly the inception voltages of the samples both in air and vacuum. However, a marginal increase in the inception voltages was observed when the sample was cleaned by the RCA procedure . Besides, it is interesting to note that the sample (#17) which was not polished on the cylindrical side exhibits better characteristics than those of the samples (#18 and 19) polished on the cylindrical side.

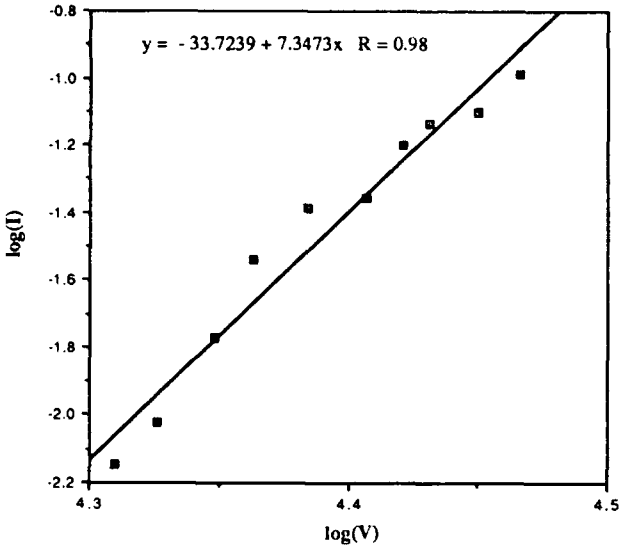

Fig.10 Variation of phase 1 current with voltage for silicon without gold contacts in vacuum

This behavior was observed both in air and in vacuum. Fig. 11 compares the variation of SCL current (Phase I), observed in air, as a function of peak voltage for the three gold-coated samples. It may be seen that the variation is not significant with respect to the sample preparation. The power factor (x) indicating the non-linearity, defined as $I \alpha v^x$, was calculated for these samples from the respective log I vs. log V plots. The power factors estimated from the plots of the samples No. 18, 19 and 17 are 2.2965, 2.7528, and 3.3038, respectively. The variation in the power factor observed above is consistent with the variations of the inception voltage levels.

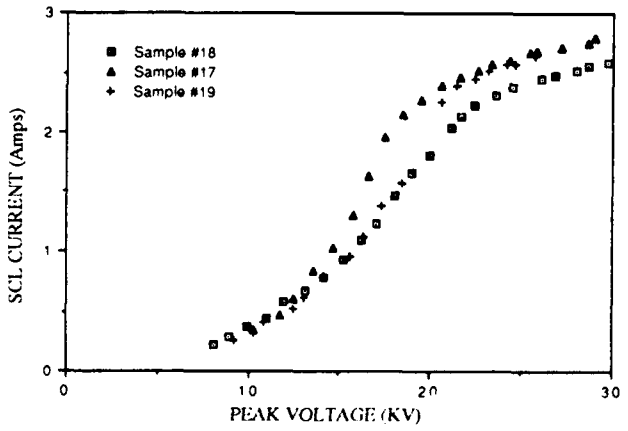

Fig.11 Variation of phase 1 current with voltage for silicon with gold contacts in air

In order to understand the charge injection characteristics, the gold-coated sample, No. 19, was subjected to further investigation. The gold contact at one end of the sample was removed by etching in aqua-reqia solution (HCl + HNO_3, 3:1). The sample with gold contact at one end and plain butt contact with the stainless-steel electrode at the other end was subjected to the voltage pulses as above. The tests were conducted with the above sample in two configurations - the gold contact being the anode and the gold contact being the cathode - in air and vacuum. In Table 5, the inception voltages of the sample observed in the two configurations are compared with those with gold contact at both sides. It is interesting to note that the sample exhibits better properties with the gold contact at the cathode than that with the contact at the anode. Further, the samples in air exhibit characteristics superior to those in vacuum. Fig. 12 shows the variation of the SCL dominant current as a function of applied voltage for all the above cases. It may be seen from the figure that the SCL current is higher in magnitude when the gold contact is the cathode, compared to when the contact is the anode, with the current corresponding to gold contacts on both ends falling between the above two values. These results clearly indicate that both the majority carriers (holes) and the minority carriers (electrons) participate in the conduction as discussed below. It is to be noted that both the currents and the inception voltage levels observed for specimens with gold contacts were highly repeatable from test to test.

TABLE : 5 VARIATION OF INCEPTION VOLTAGES AS A FUNCTION GOLD CONTACT POSITION

TEST CONDITION	VACUUM			AIR		
	V1	V2	V3	V1	V2	V3
Gold contact at both ends	6.51	7.55	---	9.20	>30	>30
Gold contact at cathode only	4.34	---	---	5.03	>25	>25
Gold contact at anode only	5.99	6.83	---	8.13	---	12.33

* V1,V2 and V3 corresponds to the inception voltages of phases 1,2 and 3 are defined above (Table 1)

It has been reported that the contact potential of the gold-silicon (P-type) system varies from positive to negative value, with respect to the dopant concentration. Based on the dopant (boron) concentration of 10^{12} cm^{-3}, the sample (P-type) studied in the present

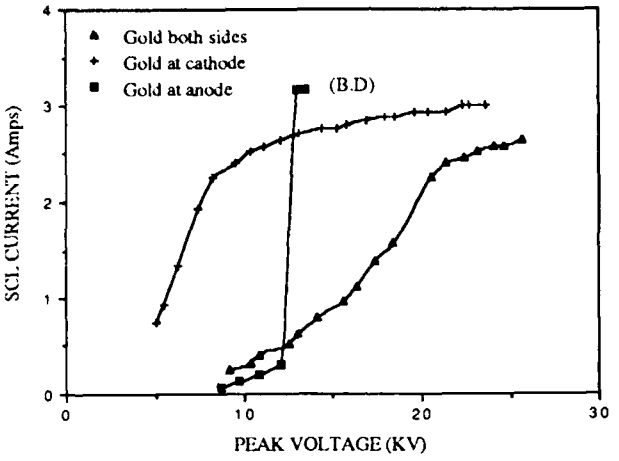

Fig. 12 Variation of phase 1 current with voltage for silicon with one end gold contact in air

investigation is believed to exhibit an ohmic contact with gold at the anode. Therefore, the contact at the cathode side is a blocking contact for electrons. The barrier height at the cathode side is believed to be around the band gap energy level (i.e., 1.1 eV). At low voltages the holes are injected (or thermally generated) from the anode contact. When the injected carrier density exceeds the thermally generated carriers, space charge controlled conduction dominates. As the conduction process transforms from ohmic to charge injection, the electric field builds up at the cathode contact due to space charge build up. At a critical field the electrons from the cathode are injected by tunneling or by an avalanche process, neutralizing some of the space charge field produced by the holes. Thus a much higher voltage has to be applied to cause surface breakdown.

The results obtained for the single end contact system may be explained as follows. When the gold contact is on the anode side only, the injection of holes predominates, as the contact is ohmic. When the field builds up at the cathode due to the injection of holes, the electron injection into the bulk is limited due to the presence of surface states introduced during sample preparation (polishing) at the flat end (cathode) which is not covered by a layer of gold. Hence when the gold contact is not available at the cathode, the electrons injected from the cathode are trapped in the surface states available at the contact. These accumulated charges will prevent injection of electrons into the bulk. Therefore the neutralization of the space charge field due to the holes is limited or absent. We propose that the enhanced field at the cathode contact leads to surface breakdown. However, when a gold layer is present at the cathode, it is proposed that electrons are injected from the cathode contact (due to the absence of charge trapping in the surface states at the contact) into the bulk by a phenomenon described earlier (space charge enhanced field). The injected electrons will neutralize some of the positive space charges within the bulk and alleviate the stress at the cathode contact, a process similar to that of samples with gold at both the contacts. Hence a higher breakdown strength is achieved.

The mechanism responsible for the significantly enhanced breakdown strength in air over that in vacuum is not fully understood. A speculative process is proposed. The electrons injected at the cathode contact partially neutralize the space charge field near that contact due to the accumulation of holes. Some of the electrons injected at the cathode triple junction can gain sufficient energy, when in vacuum, due to the large mean-free paths, resulting in a rapidly building avalanche process. However, the electrons from the triple junction, when emitted in air, are rapidly absorbed by atmospheric molecules due to the low mean-free path in air; hence the avalanche process does not develop until larger voltages are applied. In fact, in atmospheric air, breakdown was not achieved ever at ~31 kV/cm. Higher voltages were not applied since breakdown will occur in air at ~30 kV/cm. The breakdown in samples with gold contacts was thus limited by the breakdown in the ambient medium. Studies will be conducted in SF_6 to determine the ultimate breakdown strength of gold-coated Si samples. These results are highly encouraging.

ACKNOWLEDGMENTS

We wish to thank Dr. C. Le Gressus of the French Atomic Energy Commission for providing us with the single crystal quartz samples. We also wish to thank Profs. George Cokkinides and Benjamin Beker of the University of South Carolina for their assistance with the electric field numerical computations.

The work presented in this paper is supported by SDIO/IST and managed by ONR.

REFERENCES

1. T. S. Sudarshan, J. D. Cross and K. D. Srivastava, "Breakdown processes associated with surface flashover of solid dielectrics in vacuum," *IEEE Trans. Elec. Insul.*, 12, 200 (1977).

2. A. S. Pillai and R. Hackam, "Surface flashover of conical insulators in vacuum," *J. Appl. Phys.*, 56, 1374 (1984).

3. J. D. Cross and T. S. Sudarshan, "The effect of cuprous oxide coating on surface flashover of dielectric spacers in vacuum," *IEEE Trans. Elec. Insul.*, 9, 146 (1974).

4. P. H. Gleichauf, "Electrical breakdown over insulators in high vacuum," *J. Appl. Phys.*, 12, 766 (1951).

5. H. Craig Miller, "Surface flashover of insulators," *IEEE Trans. Elec. Insul.*, 24, 765 (1989).

6. R. G. Bommakanti and T. S. Sudarshan, "Pulsed surface flashover of monocrystalline SiO_2 bridged vacuum gaps," XIth Int. Symp. on Discharges and Electr. Insul. in Vacuum, 337 (1990).

7. R. G. Bommakanti and T. S. Sudarshan, "Trap dominated breakdown processes in an insulator bridged vacuum gap," *J. Appl. Phys.*, 66(5), 2091 (1989).

8. M. D. Pocha, P. L. Druce, M. J. Wilson and W. W. Hofer, "Avalanche photoconductive switching," presented at the 7th IEEE Pulsed Power Conference, held at Monterey, California (1989).

9. R. Feverstein and B. Senitzky, "Contact effects on silicon surface flashover studies," presented at the 7th IEEE Pulsed Power Conference, Monterey, California (1989).

10. B. L. Thomas and W. C. Nunnally, "Recent developments in the investigation of surface flashover on silicon protoconductive power switches," ," presented at the 7th IEEE Pulsed Power Conference, Monterey, California (1989).

11. P. F. Williams and F. E. Peterkin, "A mechanism for surface flashover of semiconductors," presented at the 7th IEEE Pulsed Power Conference, Monterey, California (1989).

12. S. H. Nam and T. S. Sudarshan, "Initiation mechanism of pulsed surface flashover along silicon in vacuum by prebreakdown conduction and photon emission," presented at the 7th IEEE Pulsed Power Conference, Monterey, California (1989).

13. W. Kern, "Hydrogen peroxide solutions for silicon wafer cleaning," *RCA Engineer*, 28 (1983).

14. S. H. Nam and T. S. Sudarshan, "New findings of pulsed surface breakdown along silicon in vacuum," *IEEE Trans. Elec. Devices*, 37, 2466 (1990).

15. H. F. Wolf, "Semiconductors," John Wiley and Sons, NY (1971).

Tangall S. Sudarshan (MS '73 - M '74 - SM '84) received the B.Sc. degree in 1968 from the University of Bangalore, India, and the M.Sc. degree in 1970 from the University of Mysore, India. He received the M.A.Sc. degree in 1972 and the Ph.D. degree in 1974 in electrical engineering from the University of Waterloo, Waterloo, ONT, Canada. He was with the National Research Council of Canada from 1974 to 1979 as a research officer in the Power Engineering Section, where he worked on the degradation and aging of polymeric materials at room and cryogenic temperatures.

He joined the faculty of the University of South Carolina at Columbia in 1979, where he is currently a professor of Electrical and Computer Engineering and a Carolina Research Professor. His research interests include the study of the basic surface conduction and failure mechanisms along dielectric and photoconducting materials. He is currently studying the role of surface microstructural properties on the electrical prebreakdown and breakdown processes using fast electrical and optical diagnostics.

T. Asokan received the B.Sc. and M.Sc. degrees from the University of Madras, India, in 1980 and 1982 respectively. He received the Ph.D. in ceramic engineering in 1986 from the Indian Institute of Science (IISc), Bangalore, India. From 1986 to 1988, he was a scientific officer at IISc, India. From 1988 to 1989, he was a research associate at the University of Manchester Institute of Science and Technology. From 1989 to 1990, he was a technical manager at Carborundum University Ltd., India. Since December 1990 he has been working as a research associate at the University of South Carolina, Columbia. His area of interest is in electronic ceramic materials - microstructural and electrical characterization, relationship between the mechanical and electrical properties, etc.

AN OPTICALLY-TRIGGERED, SUPERCONDUCTING, OPENING SWITCH

W. R. Donaldson
Laboratory for Laser Energetics
University of Rochester
Rochester, NY

A. M. Kadin, P. Ballentine, K. Kortkamp
Department of Electrical Engineering
University of Rochester
Rochester, NY

ABSTRACT

The availability of high-temperature superconductors (HTS) introduced the possibility of a new class of opening switches.[1] The switches exploit the dramatic change in conductivity at the critical temperature, T_c, in the HTS materials. These types of switches are well suited to HTS materials.[2] HTS materials have normal state resistivities indicative of semiconductors or very poor metals, depending on the method of fabrication. The transition to the normal state can form the basis of an opening switch. Since this phase transition is fully reversible, the switch can be operated repetitively. Such a device could switch currents in the range of a few kA with switching time of the order of nanoseconds.

INTRODUCTION

A high-power opening switch can be constructed from high-temperature superconductors. The switch exploits the fact that HTS materials have normal state resistivities from several hundred to several thousand times the normal state resistivity of low-temperature superconducting metals. Thus, when a superconductor is raised above its transition temperature, T_c, its resistance can be raised high enough that it may effectively be considered an open circuit.

One objection to the use of HTS materials for power applications has been their inability to handle large currents. If the density current in a superconductor exceeds some critical value, J_c, the material will go normal. This value is dependent on a number of factors including sample geometry and is typically about 10^3 A/cm^2 for bulk HTS materials. However, our thin films are approaching 10^7 A/cm^2 at 77 K. A 1-μm-thick film that is 1 cm wide can then carry 1 kA. Even when the reduction of the volumetric packing fraction due to the substrate is considered, thin films exceed the bulk material in current carrying capability by at least an order of magnitude.

To fabricate an opening switch with HTS material, it is necessary to have some method of triggering the switch into the normal state. The transition should be as rapid as possible because the heating of the switch due to the non-zero current-voltage product, IV, can be very large during the transition. Before the transition, the current is large but the voltage is zero and after the transition the current is approximately zero. The method of excitation should also allow for thermal isolation of the switch before it is triggered. In the pre-trigger

state, the device will be at cryogenic temperatures. Good thermal isolation reduces the load on the cryogenic cooling system. A method of triggering that is compatible with both of the above points is excitation with short optical pulses. HTS materials are highly absorbing at visible and near infrared frequencies and have very low reflectivities. Thus, most of the optical energy is coupled into the material. We have constructed and tested low power versions of these devices. The transient electrical response of superconducting films irradiated with 170-ps optical pulses from a Nd:YAG laser have been investigated. A number of parametric studies of the voltage transient that was switched to the load were carried out.

EXPERIMENTAL STUDIES

The switches were fabricated from thin films of $YBa_2Cu_3O_{7-\delta}$. The films ranged in thickness from 0.2 to 1.3 μm. A variety of substrates were used including MgO, zirconia, $SrTiO_3$ and $LaAlGaO_3$. A focused laser beam was used to ablate parts of the film and thereby pattern device structures. The fabricated structure consisted of an "H" with a central bridge region 200-mm wide and 2-mm long.[3] Low resistance contacts (about 1 Ω) were obtained by evaporating 0.2 μm of Ag on top of the YBCO films. The pads were wire-bonded to the external circuit. The dc-resistive transition of the bridge region of one such patterned film, 0.7 μm thick, is shown in Fig. 1. For the pulse excitation measurements (see Fig. 2), the sample was mounted in a vacuum chamber on a cold finger whose temperature could be controlled from 20 K to 100 K. The switch was provided with a dc bias current (typically 0.1–100 mA) across two of its legs, and a 50-Ω load resistor across the other two. The device was mounted in a transmission line geometry and the input and output cables were long enough that no reflections occurred in the temporal window of interest. The voltage across the load was measured with either a fast analog or a digital sampling oscilloscope, both with temporal resolution of about 1 ns. The switch was illuminated through a quartz window with 170-ps pulses from a Nd:YAG infrared laser with an energy per pulse of up to 300 mJ and a repetition rate that could be varied from 1 Hz to 1 kHz. Typically the switches were operated at about 50 Hz. The optical pulse was cylindrically focused to overfill the switch. We typically achieved 20% uniformity of the illumination over the active area of the switch.

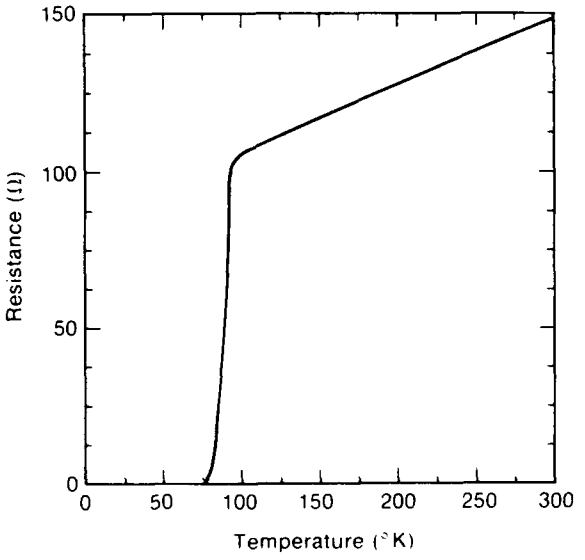

Fig. 1 The resistance versus temperature for a 0.7-μm thick film. The strip was 2 mm long by 0.25 wide.

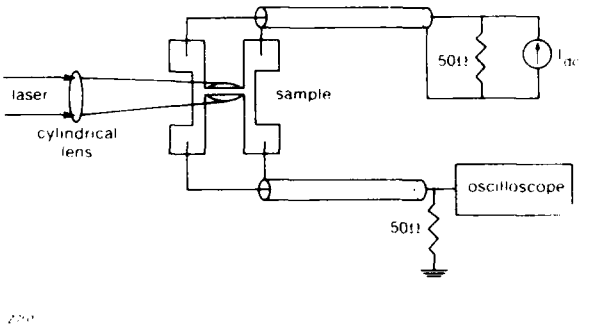

Fig. 2 The experimental schematic showing the laser illuminating the bridge.

The signal at the load varied with temperature, current, and optical energy. Typically there is an immediate fast rise time (1–10 ns) followed by a slower to the peak of the pulse (10–50 ns). Finally the signal decayed with a recovery time that went from 100 ns to several microseconds. The fast initial rise time was not present at the lowest light intensities. Fast rise times occur in samples at low temperature (10–30 K) and with depressed T_c, i.e., $T_c < 60$ K. Figure 3 shows a switch operating under these conditions. It is difficult to switch samples whose T_c is greater than 70 K with the optical energy available in our laser system. The fast component of the rise time disappears at temperatures in an intermediate region that extends from 10 to 30 K below T_c. Figure 4 shows a switch with a 40 ns rise time operating at a temperature of 70 K, which was 9 K below the critical temperature for this sample. Finally, the rise time becomes very fast for temperatures just below T_c. Figure 5 shows the same sample as Fig. 4 with the operating temperature at 75 K. Notice the dramatic increase in the fast component of the rise time.

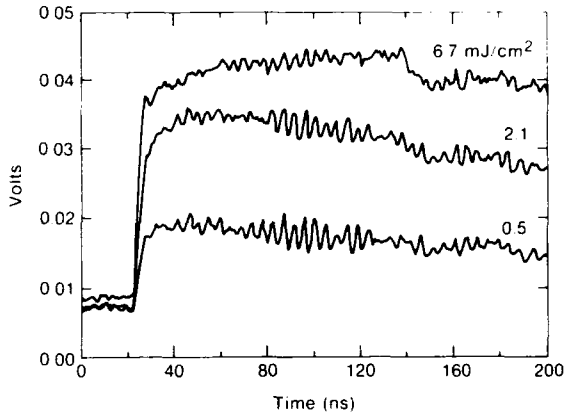

Z699

Fig. 3 The fast response of a switch operating at low temperature at three different light intensities.

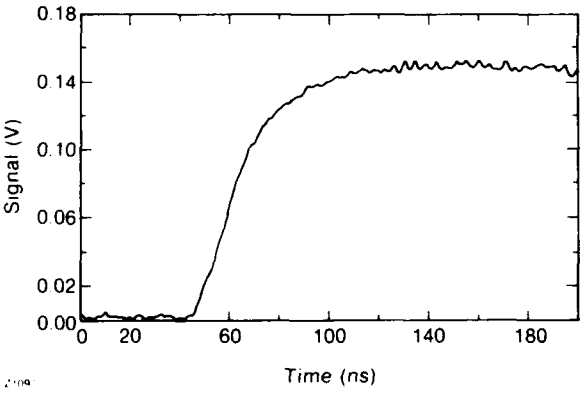

Fig. 4 At intermediate temperature (70 K) the switching speed is limited to about 50 ns. The current was 30 mA and the intensity was 8.7 mJ/cm^2.

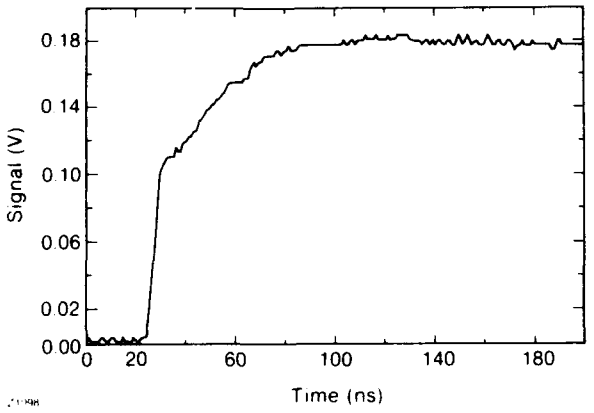

Fig. 5 The same conditions as Fig. 4, but the temperature was now 75°K, that is 4°K less than T_c. The fast component of the rise time becomes dominant.

The fast rise times are somewhat unexpected for samples thicker than 0.5 μm. YBCO has a measured absorption depth (1/e) of 0.17 μm. For thick films, most of the optical energy is deposited in the front surface of the film. The material has a very poor thermal conductivity. Figure 6 shows a simulation where the deposited optical energy decreases exponentially with distance from the surface. Using published values for the thermal conductivity and heat capacity of YBCO, heat equation is solved using finite differences in one dimension.[4] It takes at least 50 ns for the back of the sample to rise above T_c. The sample current density was well below J_c. Thus, the signal at the load should have taken at least 50 ns after the light pulse to reach its peak. All of the current should have diverted to the superconducting regions and no current would have appeared at the load at times less than 50 ns. Experimentally, the signal was seen to rise in 1 ns.

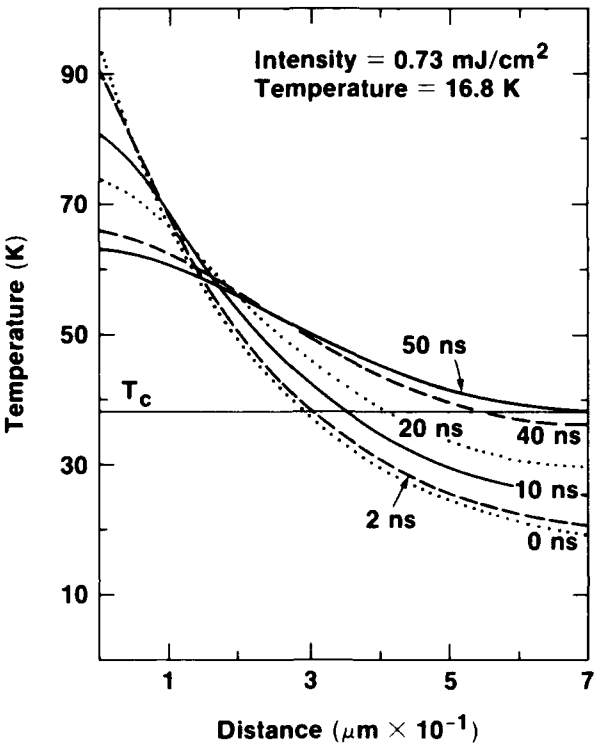

Z769

Fig. 6 Simulation showing that the heat pulse takes 50 ns to raise the entire film above T_c.

The most likely explanation is that the light pulse created a large number of hot electrons at the surface of the sample. At low temperatures, the phonons in the sample are frozen out. The mean free path of the electrons is about 1 μm and they will traverse this distance in about 1 ps. These hot electrons will then thermalize with the lattice a few picoseconds (1–30) later. This gives a mechanism for the transport of the optical energy throughout the bulk of the film on a

time scale much faster than the thermal diffusion time. As the temperature rises, this mechanism will become less important. The mean free path will become smaller as the temperature rises due to increased phonon scattering. The deposited energy will be confined closer to the surface. Thus, the rise time should increase as the temperature increases as is seen experimentally. At higher temperatures, the simulations show thermal transport taking about twice as long as the experimental rise times. Uncertainties in the thermal properties which will vary with the degree of crystal orientation and may change from sample to sample could easily account for these differences. It is not possible to say if hot electron transport plays any role at temperatures above 60 K. At temperatures very close to T_c, even the small amount of optical energy that is directly absorbed at the rear of the switch should be sufficient to uniformly drive the switch normal. In these cases, as with the case of very thin samples, the rise time will be limited by the optical pulse duration or the electrical circuit parameters, whichever is slower.

Regardless of the energy transport mechanism, the amplitude of the signal corresponds to thermal heating. The resistance verses temperature curve is measured for each switch. We can calculate the expected temperature rise for a given amount of optical energy and use that to determine the resistance of the switch. From a simple circuit model, the signal voltage can be predicted. As the operating temperature of the switch is decreased, more optical energy is needed to heat the switch above T_c. There should be a threshold energy will be needed to drive the switch normal if the mechanism of excitation is heating. A nonbolometric mechanism may not have a threshold. Figure 7 shows the measured signal amplitude plotted against the optical intensity at various temperatures. There is clearly a threshold that increases with decreasing temperature. The slow decay time is also indicative of heating. If the thermal coupling between the cold finger and the switch is reduced, the decay time will become longer.

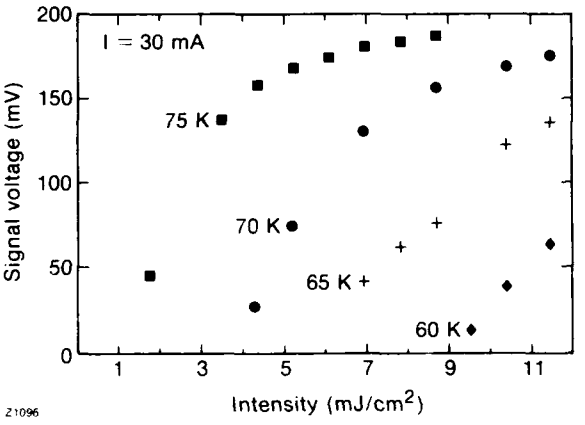

Fig. 7 The peak signal shows saturation at high intensity. There is a threshold intensity that increases with decreasing temperature.

Currently, the effect of sample preparation on switch performance is under investigation. The material used in this investigation is grown using a system developed at the University of Rochester in collaboration with CVC, Inc. This sputtering system permits large-area uniform deposition of YBCO films onto heated substrates, to produce highly oriented films that are superconducting at 87 K without a high-temperature anneal. This system has been used to study various aspects of the growth process on switch performance. For example, Fig. 8 shows a switch similar to

that shown in Fig. 5. Each sample was grown from the same target material, they were processed in the same manner, they were the same thickness and had the same substrate material. The only difference was the substrate preparation. The sample shown in Fig. 8 was on a cleaved substrate and that in Fig. 5 was on a polished substrate. Figure 8 still shows a fast response but its magnitude is greatly reduced. Most of the voltage rise occurs during the slow secondary rise. The reason for the difference is still under investigation.

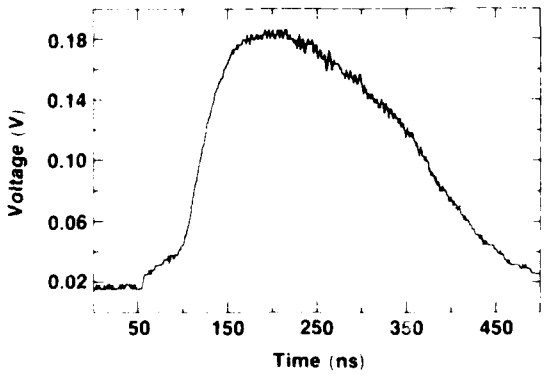

I 30 mA; switch dimension: 2 mm · 0.2 mm · 0.0007 mm

Fig. 8 The transient response pulse shape is a function of surface preparation. The initial fast rise was suppressed on cleaved MgO surfaces.

APPLICATIONS AND FUTURE WORK

The work done so far has enabled us to address the problems associated with finding applications for these switches. First, it must be demonstrated that these switches can carry currents of 10^2–10^3 amperes. The film deposition system is capable of producing centimeter- size films that are necessary to carry these large currents. There are two possible obstacles to implementing higher currents. The switches do not switch to infinite impedance, so some current will continue to flow through the switch after it has been triggered. So self-heating in the switches must be explored. If self-heating is determined to be a problem, there are adjustable parameters available to lessen its impact. The most likely candidate would be the oxygen deficiency parameter, δ, where $YBa_2Cu_3O_{7-\delta}$ is the chemical formula. As δ goes from 0 to 1 the transition temperature decreases, the critical current density decreases and the normal state resistivity increases. The ideal switch would have each one of these quantities increase in unison. Since this is impossible, some compromises may have to be made to achieve a working switch. There is also a possible heating mechanism that will effect the switch before the switch is triggered. This involves the contacts to the switch. Significant progress has been made in producing low resistance contacts to YBCO with Ag and Au metal films.[5] However, it is unknown at this time if the heating of these contacts in response to a kA current will induce thermal runaway in the switch. Further efforts will require some trial and error in the fabrication process. Related to these efforts will be the need to accurately determine the thermal coupling to the substrate so that heat extraction may be modeled.

The issues raised in the previous paragraph as well as others such as the true nature of the fast rise time component must be addressed in the context of how the switch will be used. In general terms these switches will be most useful when used to extract energy stored in a superconducting coil. Because the switch is itself superconducting,

it will not degrade the efficiency of the superconducting coil. This immediately raises the problem of contacts again since it is impossible to fabricate a coil out of HTS material at the present time. So a superconducting contact must be fabricated between HTS material and a low-temperature superconductor.

There are two ways the energy can be extracted from the coil. The pulse power mode would cause the switch to open and all the energy stored in the coil would be extracted in a single pulse. Alternatively, the switch could be made to recover back to the superconducting state soon after it was triggered. Thus only a small fraction of the energy stored in the switch will be released during any single trigger event. The combination of the coil and switch would then act as a high-energy-density battery. Different thermal management techniques must be used for these two types of operation.

The concept of an optically-activated, HTS, opening switch has been demonstrated at low power. It appears that the concept can be scaled up to devices that can carry 1 kA with switching speeds of the order of nanoseconds and repetition rates as high as 1 kHz. Such switches can have significant impact on the pulse power community.

ACKNOWLEDGMENT

This work was supported by the Sponsors of the Laser Fusion Feasibility Project at the Laboratory for Laser Energetics, as well as by the NSF grant DMR-8913524.

REFERENCES

1. W. R. Donaldson, A. M. Kadin, P. H. Ballentine, and R. Sobolewski, "Interaction of Picosecond Optical Pulses with High T_c Superconducting Films," Appl. Phys. Lett. **54**, 2470 (1989).

2. Y. Tzeng, C. Cutshaw, T. Roppel, C. W. Tanger, M. Belser, R. Williams, L. Czekala, M. Fernandez, and R. Askew, "High-Temperature Superconductor Opening Switch," Appl. Phys. Lett. **54**, 949 (1989).

3. P. H. Ballentine, A. M. Kadin, M. A. Fisher, D. S. Mallory, and W. R. Donaldson, "Microlithography of High-Temperature Superconducting Films: Laser Ablation vs Wet Etching," IEEE Trans. Magn. **MAG-25**, 950 (1989).

4. H. Fischer, S. K. Watson, and D. G. Cahill, "Specific Heat, Thermal Conductivity, and Electrical Resistivity of High-Temperature Superconductors," Comments on Condensed Matter Physics **14**, 65 (1988).

5. J. Talvacchio, "Electrical Contact to Superconductors," IEEE Trans. Compon. Hybrids Manuf. Technol. **21**, 21 (1990).

BIOGRAPHIES

Dr. William D. Donaldson is a Scientist in Ultrafast Science and Technology at the Laboratory for Laser Energetics (LLE) and presently serves as the Acting Director of this program.

Dr. Donaldson holds a B.S. degree in Physics and Mathematics from the Carnegie-Mellon University and a Ph.D. degree in Electrical Engineering from Cornell University in 1983. He joined LLE in 1984 as a Research Associate. He is currently working in the area of ultrahigh-speed high-voltage switching, covering such topics as device physics, high T_c superconductor switches, and applications to compact linacs.

Dr. Donaldson has also worked in nonlinear optics. He developed an organic crystal optical parametric oscillator capable of being tuned over the entire visible spectrum. He is a member of the American Physical Society and the Institute of Electrical and Electronics Engineers.

Dr. Alan M. Kadin (Member, IEEE) was born in Brooklyn, New York in 1952. He received the A.B. degree from Princeton University in 1974 and the Ph.D. degree from Harvard University in 1979, both in Physics. Since 1987, Dr. Kadin has held the position of Associate Professor of Electrical Engineering at the University of Rochester. His research has concentrated on fabrication and device applications of superconducting films. Dr. Kadin is also a member of the American Physical Society and the American Vacuum Society.

Ms. Krista L. Kortkamp received the M.S. degree in Electrical Engineering from the University of Rochester in May 1991. For the past year, she has been working as a research assistant at the Laboratory for Laser Energetics. She also holds the B.S. degree in Physics from the State University of New York at Binghamton.

OPTICAL PROBING OF FIELD DEPENDENT EFFECTS IN GaAs PHOTOCONDUCTIVE SWITCHES

W. R. Donaldson

LABORATORY FOR LASER ENERGETICS
University of Rochester
250 East River Road
Rochester, NY 14623-1299

ABSTRACT

An electro-optic probe is used to study the physics of semiconductors subjected to high fields with 100-ps time resolution. A variety of phenomena have been seen in GaAs in photoconductive switches. There appears to be evidence of current channeling in switches operating in lock-on mode. In addition, the affects of contact preparation on switch operation have been investigated.

INTRODUCTION

Photoconductive switches can switch tens of kilovolts with picosecond rise times. They have been used for microwave generation, in Pockels cell drivers, and in innovative accelerator designs.[1,2] The need to improve switch reliability and the desire to explain certain physical phenomena associated with high-voltage switching have motivated the investigation of the dynamics of photoconductivity. For switching speeds of the order of a picosecond, conventional electronics do not have sufficient bandwidth to temporally resolve the switching dynamics. An ultrafast, 2-D, electro-optic imaging system was developed that can monitor rapid variations of the electric field over an extended region. This system can produce maps of the surface electric field between contacts on photoconductive switches. The surface electric field is related to the internal field in the semiconductor because the tangential component of the electric field is continuous across a dielectric interface. The internal field is modified by the presence of carriers in the contact gap. Thus, surface field imaging can be used to investigate the behavior of charge carriers within the semiconductor. Switch performance parameters, such as switching efficiency, carrier transport, and switching speed, can be measured by this optical technique.

2-D ELECTRO-OPTIC SAMPLING

A large area sampling beam interrogates the electric field over a wide surface. The polarization of the sampling beam interacts with the surface electric field through an electro-optic crystal that sits on the semiconductor surface. The crystal changes its birefringence in response to the electric field. This in turn rotates the polarization of the probe beam. The probe beam is then imprinted with an optical analog of the spatial electric field distribution. The electric field in the crystal is sampled only when the probe pulse is present so a snapshot of the instantaneous electric field is taken. The pump pulse was the optical trigger for the

the photoconductive switch. The pump and probe were of different frequencies derived by frequency doubling a Nd:YAG laser. Two different probe geometries were used and the pump/probe roles of the fundamental and second harmonic of Nd:YAG could be reversed. Figure 1 shows the set up to measure the field of a surface device type. Figure 2 shows the probe set up to measure the field of a bulk photoconductive switch, which has contacts on opposite faces of a rectangular slab of a semiconductor. The geometry shown in Fig. 2 had the advantage of a much simpler (i.e., spatially uniform) field distribution. For either type of switch, probe operation was the same, only the pump geometry was different.

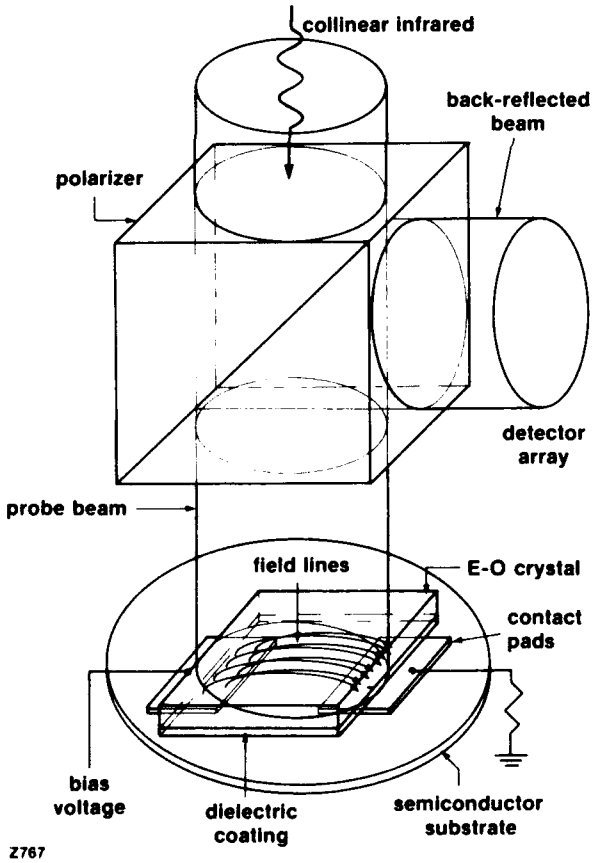

Fig. 1 Surface switch configuration.

The laser source is a Nd:YAG regenerative amplifier seeded by a Nd:YAG mode-locked oscillator with a wavelength of 1064, a pulse width of 160 ps, an energy of 300 μJ, and a prepulse to main pulse contrast ratio of at least 4000:1.[3] The infrared beam from the amplifier was split, 90% for switching use and 10% for second-harmonic generation. This green beam is upcollimated and serves as the probe beam. The modulated probe beam pulses are imaged onto a 512 × 512 element CID camera. The CID camera goes to a video frame grabber, supplying a digital image of the modulated probe beam. By sweeping the 113-ps sampling windowthrough the photoconductively induced event, the switch surface field is

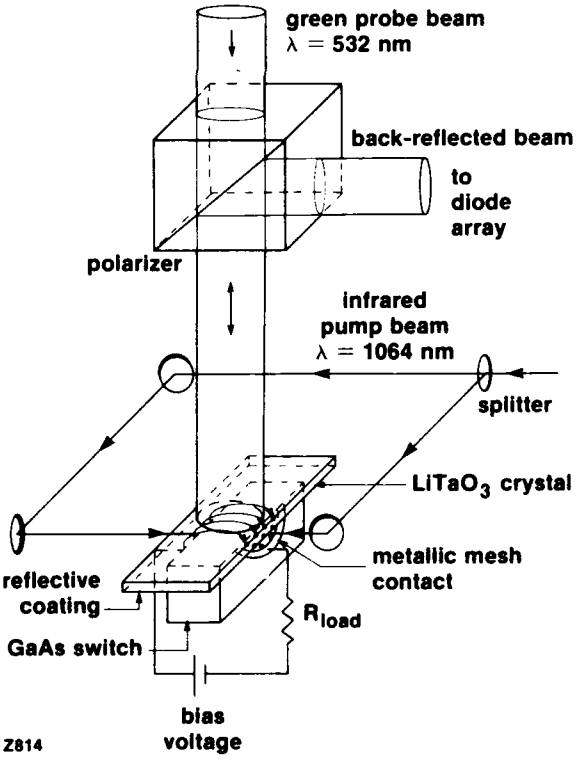

Fig. 2 Bulk switch configuration.

monitored as it evolves in time. The sampling window is moved in time by changing the length of an optical delay line in the pump beamline.

When a bias voltage is applied to the metallic contacts, an electric field is established and a fringing field extends above the surface of the semiconductor. The probe beam diameter is greater than the contact gap so that the entire contact gap is illuminated. The beam traverses the crystal and is reflected back onto itself by the dielectric mirror on the semiconductor side of the crystal. Any component of the back-reflected beam with polarization different from the incoming beam will be rejected by the polarizer. Each point in the rejected beam has sampled the local birefringence of the corresponding point in the crystal. Thus, the intensity of the rejected beam is an optical replica of the electrically induced birefringence pattern in the crystal. The transmission to a detector element (i,j) can be written:

$$T_{i,j}(V) = I_{ij}(V)/I'_{ij}$$

$$= \sin^2 [(\alpha_{ij}E_{ij} + \beta_{ij})] \qquad (1)$$

where $I_{ij}(V)$ is the light intensity measured at camera pixel (i,j) when a voltage V is applied to the electrodes; I'_{ij} is the intensity that appears at the camera if 100% of the light is imaged onto the camera without bias voltage applied; E_{ij} is the magnitude of the local electric field; α_{ij} is a constant for a given point (i,j) which relates the electro-optic coefficient[4] to the local electric field and whose value depends on material parameters, optical path length in the crystal, electrode geometry, and frequency of applied optical field; and β_{ij} is a constant optical rotation due to static birefringence in the crystal and $\lambda/4$ wave plate. The $\lambda/4$ plate chooses where the probe beam sits on the sine-squared transmission curve with no voltage applied. By comparing the intensity at the camera with and without voltage applied, the rotation due to the electric field can be determined. The complete probe system is shown in Fig. 3.

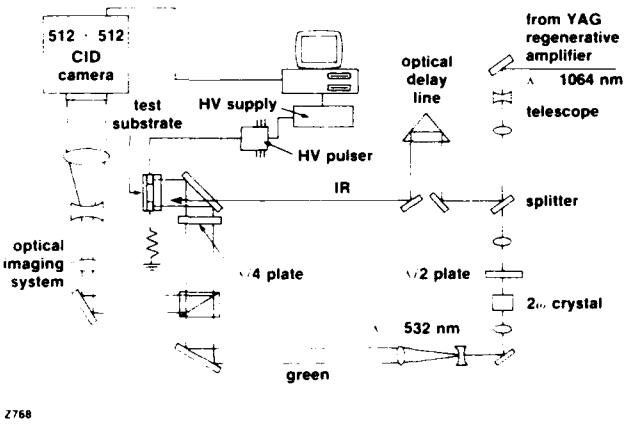

Fig. 3 Complete experimental setup.

CHARACTERIZATION OF PHOTOCONDUCTIVE SWITCHING

The primary physical system investigated was the collapse of the electric field in a GaAs photoconductive switches both bulk and planar. GaAs has a band gap of 1.42 eV. Photoexcitation of an electron into the conduction band with the IR pump (λ = 1064 nm, 1.17 eV) is due to the mid-gap donor EL2. At 532 nm, the excitation is direct band-to-band electron-hole generation.[5] The bulk switches were fabricated by the U.S. Army Electronic Technology and Device Laboratory by depositing circular contacts of NiAu:Ge on opposite faces of a blocks of intrinsic GaAs 0.6 to 1-cm thick.

The GaAs was high resistivity material ($\rho \sim 10^7$ cm) supplied by MA-COM. The absorption coefficient was measured to be 1.39 cm^{-1} at 1.06 μm. The center region of the contact was perforated with holes to allow light to pass through into the bulk of the GaAs. The contact preparation was also varied. Initially, the switches were fabricated with an ion implantation under the metalization to make ohmic contacts or had contacts deposited on bare GaAs. Later designs had the ion implantation under both the metalization and the perforated areas. In addition, the later switches were fabricated with either donor or acceptor impurities under the contacts. Thus intrinsic, NIN and PIN structures were tested. This switch design is of interest for its applicability to the coaxial geometry.[7] This design is also useful because the parallel contact geometry allows for uniform fields which facilitate extraction of absolute field values. The coplanar geometry, by contrast, has a much more complicated field pattern. To access the fields between the contacts, this design has been modified by cutting the GaAs in a plane passing through the center of the contacts. Connection to the external circuit was made by pressure contacting copper electrodes coated with indium along the outside circumference of the NiAu:Ge electrodes. The Cu electrodes were bored out so that IR light could reach the switch contacts. By placing a dielectric beam splitter in the IR pump beam, approximately 50% of the IR light could be directed onto each electrode.

The initial switches suffered from a buildup of extremely high fields at both contacts. In particular, the cathode showed very significant enhancements. This lead to arcing and deterioration at the electrodes. These fields were not present before the illumination was applied. The field buildup occurred a few hundred picosecond after the trigger pulse. The enhancement is associated with the optical switching processes and is not an intrinsic property of the contacts. With NIN structures, the enhancement at the cathode virtually disappeared as shown in Fig. 4. This figure shows the average field between the contacts averaged over the length of the switch. There is a very high peak at the positive electrode that extends a significant distance into the switch. The peak only arises after the switch has been illuminated. This improved behavior was attributed to the

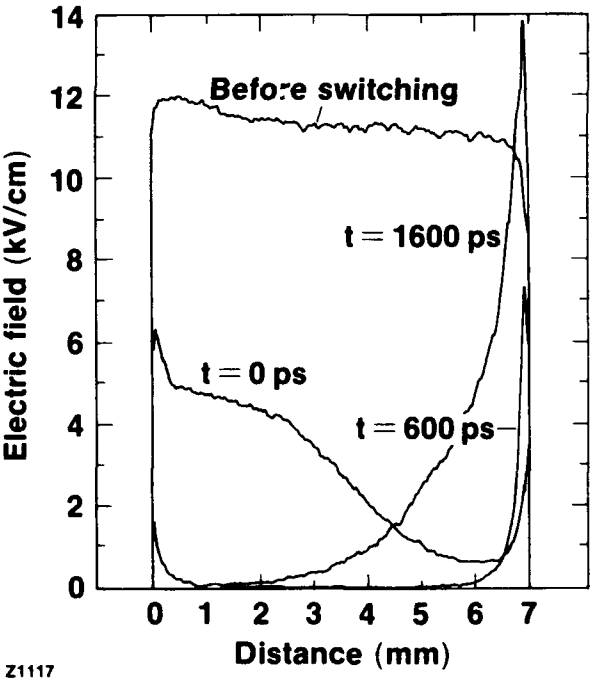

Fig. 4 Lineouts showing the average electric field across the contacts. The NIN structure eliminated the field enhancements at the cathode.

forward biased contact at the cathode. Next a PIN structure was tried. In this case, the n-type contact was the cathode and the p-type was the anode. The suppression of the field enhancement at the n-type contact was still observed. However, the p-type contact only showed a slight improvement. The enhancement was slightly reduced and it did not extend as far into the bulk of the switch. This behavior is shown in Fig. 5. The study of the bulk switching behavior extended to only 1600 ps after switching pulse. The temporal behavior beyond that time was studied on surface switches described below.

PHOTOCONDUCTIVE SWITCHING: LOCK-ON

GaAs switches were also investigated using the surface geometry, primarily to look at lock-on behavior in GaAs. In GaAs the photogenerated electron hole pairs should recombine in about 1 ns. This should limit the duration of electrical pulse delivered with GaAs switches. Lock-on is the phenomenon where GaAs switches remain in the conducting state for a long time (hundreds of nanoseconds) after the optical excitation. The bias field has to be greater than a threshold value of 3 to 8 kV/cm, depending on the material preparation. Typically, there will be a voltage drop across the switch in this state equal to the gap length times the threshold field. Lock-on behavior has several interesting features. Lock-on can be triggered with very low light levels and it has the potential for producing long duration pulses from GaAs switches. Lock-on is not well understood and the electro-optic imaging system can explore its physical dynamics.

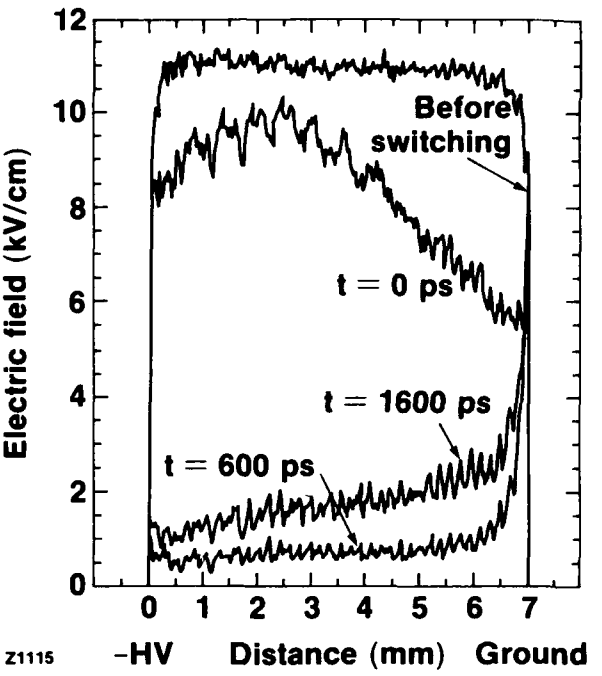

Fig. 5 A PIN structure did not suppress the enhancement at the anode

The switches used in this study were supplied by Sandia National Laboratory. They were 2.5 mm wide and had a gap of 2.5 mm. The switches had an electron mobility of 7000 $cm^2/V\text{-}sec$, an impurity concentration of 10^7 cm^{-3}, and a lock-on threshold of 4 kV/cm. To eliminate any complicating effects due to impurity concentrations, the photoconductive switching was done with 532-nm light, which has an energy greater than band gap. This necessitated converting the optics to interchange the pump and probe. Because lock-on is a phenomenon that occurs several nanoseconds after optical trigger pulse, the measurements were taken out to 6 ns after the trigger. The measurements reveal a very complicated behavior. Below the threshold

for lock-on, the field collapses uniformly in roughly the full width half maximum (FWHM) of the laser pulse. The rapid collapse is followed by a rapid recovery of the order of a few hundred picoseconds, followed by a slower recovery to the initial bias field in about 5 ns. This trend is illustrated in Fig. 6, which shows the average electric field along a line parallel to contacts and through the center of the switch. Above the threshold for lock-on the behavior is much more complicated. The field collapses and starts to recover as in below threshold case. However, at about 1 ns after peak illumination the collapse begins again as shown in Fig. 7. The second collapse of the electric field across the switch is much slower than first optically induced collapse. It is also not monotonic. An oscillatory structure is superimposed on the decay of the electric field. This second decrease in the electric field is apparently associated with the lock-on state. A current probe at the output of the switch indicated that conduction through the switch continued longer than would be expected from that determined by the recombination of the electron-hole pairs.

Lineouts reveals only a small portion of the complex behavior of these devices. Figure 8 shows three different electro-optic images at different times after illumination. The images have been manipulated such that a dark region in the active switch area indicates the absence of an electric field greater than 2 kV/cm. A white region indicates the presence of an electric field greater than 2 kV/cm. The first image shows the electric field at the peak of the photoinduced conductivity. The active area of the switch is uniformly black, indicating complete switching, and the edges of the contacts are clearly delineated. At time beginning about 1 ns after complete switching has occurred, the electric field develops an 2-D structure. In some places the

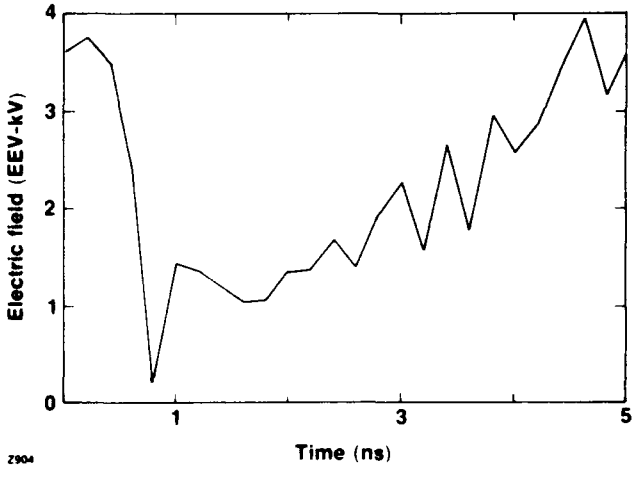

Fig. 6 Average E-field on a surface switch below lock-on.

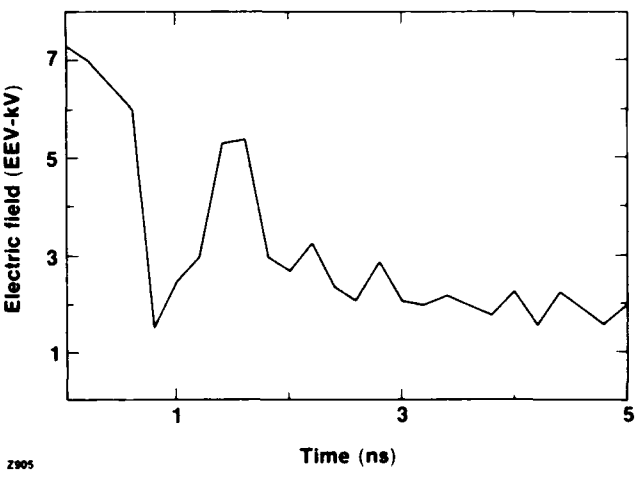

Fig. 7 Average E-field above lock-on showing secondary conduction.

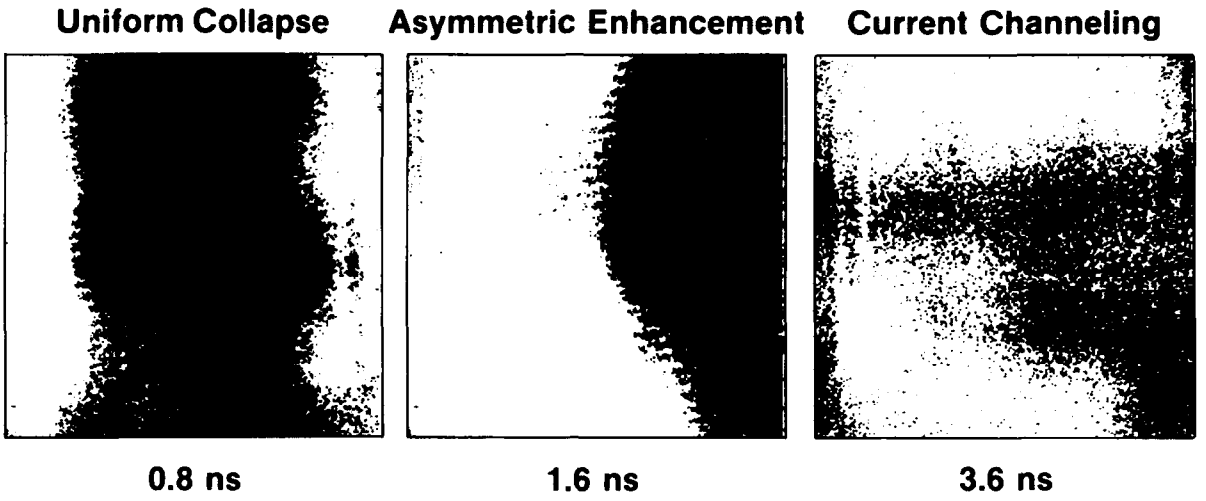

Fig. 8 The time evolution of the electric field in a photoconductive switch showing the development of low field channels within the switch.

field has collapsed and in other places it has increased to values that may even be greater than the original applied field. At 0.8 ns after peak conductivity, the electric field is concentrated near the high voltage contact. This then evolves into a state shown in the last picture. A region of low field, which could indicate the presence of carriers in the underlying semiconductor, extends out from the low voltage contact. A region of low field or high conductivity extends from the low voltage contact to the high voltage contact. This region is only about 25% of the active area of the switch. This may indicate that the current is being carried in channels through the switch in the lock-on regime. This could seriously degrade switch performance in the long term.

CONCLUSION

The electro-optic imaging system has been used to observe the dynamics of photoconductive switching in GaAs. Both overhead and through the contact illuminated switches have been studied. GaAs has two distinct regions of operation. At biases below about 3–6 kV/cm (depending on material preparation), the switches behave in a simple fashion. The field collapses with the integral of the absorbed light and then recovers as the carriers recombine. Above 6 kV/cm, the electric field across the switches exhibit transient anomalies. Specifically, in both geometries, there are field enhancements at the contacts. These enhancements may be implicated by the failure mechanism of these switches, which usually result in electrical

breakdown. Some success has been achieved by placing n-type contacts on the cathode. However, there is still an enhancement at the anode that does not seem to go away with doping the material directly under the contact.

ACKNOWLEDGMENT

This work was supported by SDIO/IST under the Office of Naval Research, Contract #N00014-86-K-0583 and by the Sponsors of the Laser Fusion Feasibility Project at the Laboratory for Laser Energetics. The samples were provided by G. Loubriel at Sandia National Laboratory and M. Weiner at U.S. Army ETDL.

REFERENCES

1. G. Mourou, W. H. Knox, and S. Williamson, Picosecond Optoelectronic Devices, (Academic Press, New York, NY, 1984), ch. 7, pp. 219–248.
2. C. Bamber, W. Donaldson, T. Juhasz, L. Kingsley, and A. C. Melissinos, "Radial Compression of Picosecond Electrical Pulses," Part. Accel. **23**, pp. 255–263, 1988.
3. I. N. Duling III, T. Norris, T. Sizer II, P. Bado, and G. A. Mourou, "Kilohertz Synchronous Amplification of 85-Femtosecond Optical Pulses," J. Opt. Soc. Am. B **2**, 616–618, 1985.
4. A. Yariv, Quantum Electronics, 2nd Ed, (John Wiley & Sons, New York, 1975), p. 340.
5. T. Burke, M. Weiner, L. Bovino, and R. Youmans, "The Role of Deep Level Traps in the Optically Controlled Semi-Insulating GaAs Switch," in Digest of Technical Papers, 6th IEEE Pulse Power Conference, edited by B. Bernstein and P. Turchi, (IEEE, New York, 1987), p. 283.
6. L. Bovino, T. Burke, R. Youmans, M. Weiner, and J. Carter, "Recent Advances in Optically Controlled Bulk Semiconductor Switches," in Digest of Technical Papers, 5th IEEE Pulse Power Conference, edited by P. Turchi and M. F. Rose, (IEEE, New York, 1985), p. 242.

BIOGRAPHIES

Dr. William D. Donaldson is a Scientist in Ultrafast Science and Technology at the Laboratory for Laser Energetics (LLE) and presently serves as the Acting Director of this program.

Dr. Donaldson holds a B.S. degree in Physics and Mathematics from the Carnegie-Mellon University and a Ph.D. degree in Electrical Engineering from Cornell University in 1983. He joined LLE in 1984 as a Research Associate. He is currently working in the area of ultrahigh-speed high-voltage switching, covering such topics as device physics, high T_c superconductor switches, and applications to compact linacs.

Dr. Donaldson has also worked in nonlinear optics. He developed an organic crystal optical parametric oscillator capable of being tuned over the entire visible spectrum. He is a member of the American Physical Society and the Institute of Electrical and Electronics Engineers.

SOLID STATE PULSED POWER DEVICE RESEARCH AT THE UNIVERSITY OF SOUTHERN CALIFORNIA

J.H. Hur, P. Hadizad, H. Zhao, S.G. Hummel, J.S. Osinski, P.D. Dapkus, H.R. Fetterman,* C.W. Myles,** and M.A. Gundersen

Department of Electrical Engineering-Electrophysics
University of Southern California
Los Angeles, CA 90089-0484

*University of California, Los Angeles
**Texas Tech University

Abstract—Solid state pulsed power device research activities at the University of Southern California (USC) are discussed. III-V compounds, particularly GaAs and AlGaAs, are being studied as potential materials for junction pulsed power devices, namely opto-thyristors and static induction transistors. A model for lock-on effect observed in certain pulsed power switches is being developed.

INTRODUCTION

The main thrust of the solid state pulsed power research at USC is to study III-V compound-based junction devices, specifically for pulsed power applications. Most of the III-V compounds have optoelectronic property which is unique to these materials and may play an important role in the device operation. Along with the advanced state of III-V compound heterojunctions, the optoelectronic property of III-V compounds allows a greater flexibility in pulsed power device design.

GaAs is presently being studied in device structures of opto-thyristor and static induction transistor (SIT). In addition, a model for the lock-on effect is being developed to gain a better understanding of the effect so that the effect can be used advantageously in a device design. Understanding of the lock-on effect is also very important in defining the future direction of the solid state pulsed power device research.

OPTO-THYRISTORS

A junction device that is attractive for pulsed power applications is opto-thyristor. For our research, an opto-thyristor with semi-insulating (SI) GaAs base layer was studied [1]. The device structure is shown in Fig. 1. A Cr-doped, Bridgman grown semi-insulating (100) GaAs was used as the starting material, and the epitaxial layers were formed on both sides of the wafer by metal organic chemical vapor deposition (MOCVD). The thickness of the SI base was obtained by mechanical lapping and chemomechanical polishing.

The opto-thyristor was optically triggered at the edge of the device with an AlGaAs laser diode with pulse energy of ~2 μJ. The switching characteristics of the device were measured with a capacitive discharge circuit. A typical current pulse switched with the GaAs opto-thyristor is shown in Fig. 2. The

blocking voltage of the thyristor was ~800 volts, and the peak current was ~300 A. The switching pulse indicates a *di/dt* of >1.5x10^{10} A/sec which is limited by the test circuit inductance.

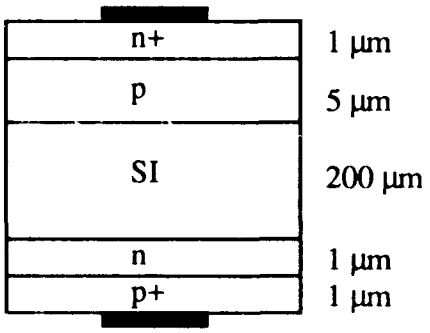

Fig. 1. Opto-thyristor structure with semi-insulating GaAs base layer.

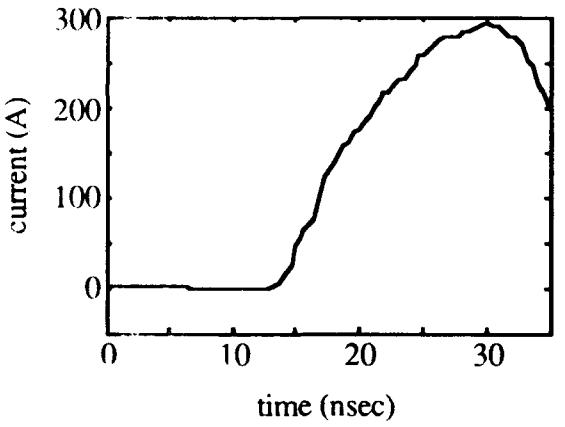

Fig. 2. A typical profile of a current pulse switched with the GaAs opto-thyristor.

To measure the forward drop of the device, a pulse forming line comprised of 50-Ω cable with 260-nsec delay was used. The forward drop of the device was measured to be ~100 volts which corresponds to an electric field of ~5 kV/cm in the base layer. This field is very similar to the lock-on field observed in SI GaAs photoconductive switches. We thus conclude that the mechanism responsible for the lock-on is also occurring in the base layer of the device. The modeling effort to understand the lock-on effect is discussed in a later section.

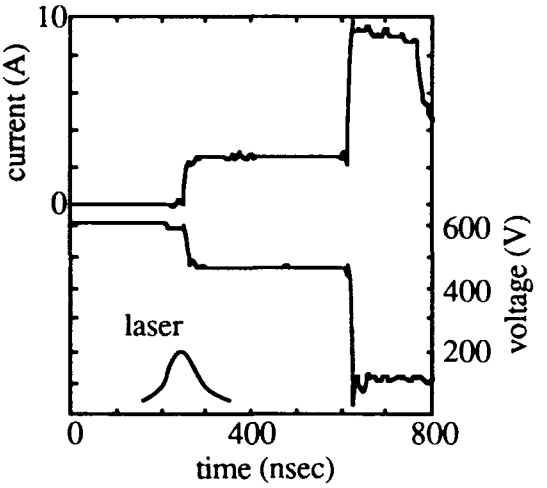

Fig. 3. Forward drop measurement result.

For further work, a heterostructure opto-thyristor (HOT) with AlGaAs *n*-emitter and *p*-base layers is being fabricated. This structure allows an efficient coupling of surface gated photons to the n-base region where most of the electric field is distributed. The surface gating is highly desirable since the edges of the device are susceptible to permanent damage when edge gated. Thus, the limitations due to the edge quality can be reduced. The *n*-base layer of HOT will be comprised of a GaAs substrate with an electron concentration of ~10^{13} cm^{-3}. The breakdown characteristic of the reverse biased *p-n* heterojunctions formed with MOCVD will be critical for HOT operation.

AVALANCHE BREAKDOWN OF HETEROJUNCTIONS

The avalanche breakdown characteristic of reversed biased *p-n* AlGaAs-GaAs

heterojunctions was studied theoretically [2]. It was found that a *p-n* heterojunction with 10^{14} cm^{-3} *n*-GaAs and 10^{14} cm^{-3} *p*-AlGaAs with ~45% Al content has a larger avalanche breakdown voltage (by ~400 volts) than a homojunction with same doping densities. The result of the calculation is shown in Fig. 4.

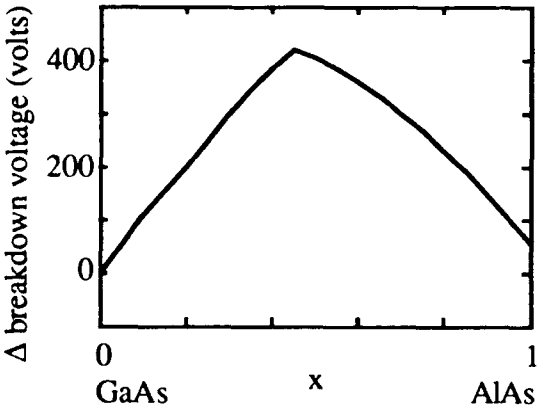

Fig. 4. Avalanche breakdown voltage of a reverse biased *p-n* heterojunction with respect to that of a *p-n* homojunction.

This result indicates that the use of heterojunctions not only allows bandgap engineering in the design of the pulsed power devices, but also improves the blocking capability of the device.

STATIC INDUCTION TRANSISTORS

A GaAs static induction transistor (SIT) is another promising device for pulsed power switching applications. It is a field-controlled, majority carrier device which can provide fast switching, low forward drop, and both the closing and opening capabilities. An *n*+ GaAs substrate was used as the starting material, and liquid phase epitaxy (LPE) was used to grow *n*- and *n*+ layers. The cross-sectional area of the source region for a single device is 16x100 μm^2. The SIT Schottky gate contacts are formed with aluminum. Both the recessed gate and planar gate structures are being fabricated. The recessed gate structure for a single device is shown in Fig. 5. The measured forward drop voltage is ~1.8 volts at an estimated current density of ~100 A/cm^2 per device.

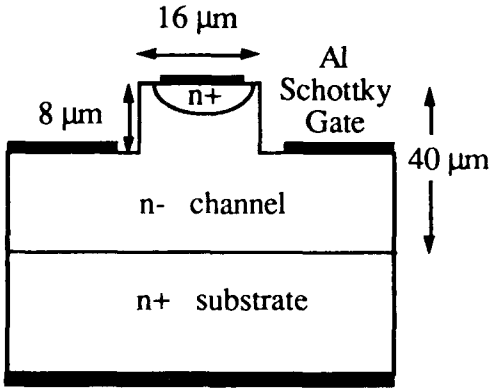

Fig. 5. Static induction transistor structure

Optimum device design for better blocking gain and switching speed will be explored by varying the channel width and the recessed gate depth, and by forming *p-n* junctions for the gate structure. Optical controlling of the device will also be studied for fast switching applications.

LIQUID PHASE EPITAXY SYSTEM

An LPE system is being tested and characterized for the various growth requirements of pulsed power devices. One of the major needs is the growth of thick, homogeneously and lowly doped epitaxial layer to serve as the base region for pulsed power devices.

Before the growth, the system is purged with hydrogen and baked out at high temperatures (800-900° C). A desirable purge

and bake-out time is several days. The two-phase growth technique was used at a growth temperature of ~800° C with a cooling rate of 0.5° C/min. The preliminary growth showed a highly uniform layer of *n*-type GaAs with a carrier density of $2x10^{16}$ cm^{-3}. Effort to lower the carrier concentration and to maintain the uniformity over a large thickness and cross-sectional area is continuing.

LOCK-ON MODELING

A phenomenon commonly called "lock-on" effect is observed in various pulsed power switches, and came to the attention of pulsed power community through the studies of SI GaAs photoconductive switches [3]. Stationary, high field domain due to transferred-electron effect is proposed as a model to explain this effect [4]. This high-field layer enhances injection from the contact and/or generates more carriers through impact ionization.

This effect may be similar to the breakdown effect of the Gunn diodes [5] and the burn-out effect in MESFETs (metal-semiconductor field effect transistors) [6]. Recently, GHz and THz signals were observed in an optically triggered M-S-M (metal-semiconductor-metal) device in which the semiconductor is SI GaAs [7,8]. Their experimental and theoretical works indicate a high electric field layer near a contact from which high frequency signal is produced.

An electro-optics measurement of the electric field distribution in photoconductive switches also indicates a stationary, high field domain near a contact [9]. This work also shows a pinching effect, similar to the filament effect known to occur in devices that exhibit negative differential resistance.

This model thus far may explain the device condition of lock-on state. In regards to the turn-on dynamics of the lock-on devices, the optical triggering of the device may initially create a moving domain or domains which become quenched in the steady state, and the device redistributes the potential as described above.

The role of the deep levels in lock-on devices is uncertain. An experiment in conjunction with computational effort is under way to confirm the aforementioned model. Specifically, M-S-M structures with either semi-insulating or lowly doped semiconductor, and various combinations of *p*- and *n*-type metal contacts will be studied.

SUMMARY AND FUTURE DIRECTION

In summary, the opto-thyristor with SI GaAs base layer showed switching characteristics that are desirable for pulsed power applications. The SIT with Al-Schottky gate demonstrated very low forward drop voltage in the on-state. These results indicate that III-V compound-based junction devices have significant potential as pulsed power devices. In a continuing effort, heterostructure opto-thyristors and optimized SITs are being fabricated for further study of III-V compound-based junction pulsed power devices.

The future direction for III-V compound-based junction pulsed power devices may require novel device structures to take advantage of the optoelectronic property (which is unique in these materials) and the highly advanced state of heterojunctions and thin-film technology. It is known that much of the effort in the areas of III-V compound technology is directed toward the low-power, microelectronic devices. Especially in the area of thin-film,

epitaxial growth, the MBE and MOCVD techniques can grow highly controllable, thin layers with high purity, precise thickness and high quality surface and uniformity. Pulsed power devices should take advantage of this rapidly advancing technology.

ACKNOWLEDGMENT

This work is supported by SDIO through ONR.

REFERENCES

[1] J.H. Hur, P. Hadizad, S.G. Hummel, K.M. Dzurko, P.D. Dapkus, H.R. Fetterman, and M.A. Gundersen, "GaAs-Based Opto-Thyristor for Pulsed Power Applications," *IEEE Trans. Electron Devices* vol. 37, p. 2520, 1990.

[2] J.H. Hur, C.W. Myles, and M.A. Gundersen, "Avalanche breakdown in *p-n* AlGaAs/GaAs heterojunctions," *J. Appl. Phys.* vol. 67, p. 6917, 1990.

[3] M.A. Gundersen, J.H. Hur, and H. Zhao, "Lock-on effect in pulsed power semiconductor switches" (submitted for publication).

[4] F.J. Zutavern, G.M. Loubriel, and M.W. O'Malley, "Recent developments in opening photoconductive semiconductor switches," in *Proc. 6th IEEE Pulsed Power Conf.* (Arlington, VA, 1987), p. 577.

[5] H.W. Thim and S. Knight, "Carrier generation and switching phenomena in *n*-GaAs device," *Appl. Phys. Lett.* vol. 11, p. 83, 1967.

[6] R. Yamamoto, A. Higashisaka, and F. Hasegawa, "Light Emission and Burnout Characteristics of GaAs Power MESFET's," *IEEE Trans. Electron Devices* vol. 25, p. 567 (1978).

[7] C.J. Clark, E.A. Chauchard, K.J. Webb, K. Zaki, C.H. Lee, P. Polak-Dingels, H.A. Hung, and H.C. Huang, "A New Optoelectronic CW Microwave Source," in *Picosecond Optoelectronic Devices* (C.H. Lee, ed., Academic Press, 1984), p. 269.

[8] S.E. Ralph and D. Grischkowsky, "Extremely High Fields at Semi-insulator/Metal Interfaces: Enhanced Generation of Ultrafast THz Radiation," in *Conf. Lasers and Electro-Optics, 1991* (Washington, DC, 1991), p.604.

[9] W. Donaldson and L. Kingsley, "Optical probing of the field dependent effect in GaAs photoconductive switches," in *SPIE Proc. Conf. Optically Activated Switching* (Boston, MA, 1990), vol. 1378, p. 226.

Jung H. Hur was born in Korea on June 11, 1963. He received the B.S. degree (with Highest Honor) in electrical engineering from the University of Texas, Austin, in 1986, and the M.S. degree in electrical engineering from the University of Southern California, Los Angeles, in 1987. Presently, he is working towards the Ph.D. degree in electrical engineering at USC. His current research interests include the physics of high field effects in III-V compound semiconductors and its applications to the semiconductor power devices.

Peyman Hadizad received the M.Eng. degree in electrical engineering and the M.S. degree in engineering science from Rensselaer Polytechnic Institute in 1986 and 1987 respectively. He is currently working towards the Ph.D. degree in electrical engineering at the University of Southern California. His research interests are in the areas of III-V based power semiconductor devices, liquid-phase epitaxial growth of III-V compounds and the study of defects at the metal-semiconductor interfaces.

Hanmin Zhao was born in China on January 26, 1965. He received both B.S. and M.S. Degrees in physics from Peking University, China, in 1985 and 1988. he is currently working toward the Ph.D. degree in electrophysics at the University of Southern California. His current research interests are in the areas of III-V material based power semiconductor devices, high purity LPE growth, high speed photoconductive switches and photodetectors. Mr. Zhao is a member of the American Physical Society.

Steven G. Hummel was born in Tarrytown, N.Y., on January 23, 1958. He received the B.A. degree in chemistry from Rutgers College of Rutgers University, New Brunswick, N.J., in 1980, and the M. S. degree in electrical engineering from Rutgers University in 1986. He is currently working towards the Ph.D. degree in electrical engineering-electrophysics at the University of Southern California, where he is a Center for Photonic Technology Fellow and a GTE Fellow. From 1980 through 1983 he was at AT&T Bell Laboratories, Murray Hill, N.J., where he worked on the growth and characterization of III-V semi-conductors by a novel epitaxial growth technique which he co-developed called Vapor Levitation Epitaxy (VLE). At its inception in 1984, he joined Bell Communications Research, Red Bank, N.J., where he continued to work on VLE growth mechanisms and materials. Since 1987 he has been at USC, where his research interests include the MOCVD growth of III-V materials and devices, growth mechanisms, and the structural and physical characterization of materials. Mr. Hummel is a member of the American Physical Society and the American Association for Crystal Growth.

J. S. Osinski, photograph and biography not available at the time of publication.

P. Daniel Dapkus was born in Chicago, IL, on January 26, 1944. He received the B.S. degree in engineering physics and the M.S. and Ph.D. degrees in physics from the University of Illinois, Urbana, in 1966, 1967, and 1970, respectively. He was a Member of the Technical Staff at Bell Laboratories, Murray Hill, NJ, from 1970 to 1976 where he worked on GaP and AlGaAs light-emitting diodes and displays. In 1976 he joined Rockwell International, Anaheim, CA, where he led the effort to develop the metalorganic chemical vapor deposition (MOCVD) process for electronic and optoelectronic devices. He was later the Manager of the group responsible for optoelectronic devices at the Microelectronic Research and Development Center, Thousand Oaks, CA. This group was involved in the development of long wavelength fiber optic devices and integrated optoelectronic components. Since 1982 he has been a Professor of Electrical Engineering and Materials Science at the University of Southern California, Los Angeles. His research interests include MOCVD and atomic layer epitaxy growth mechanisms, nonlinear optical properties of artificially structured materials, heterojunction bipolar transistors and ultra low-threshold semiconductor lasers.

Harold R. Fetterman received the Ph.D. degree from Cornell University in 1967. He is currently a Professor in the Department of Electrical Engineering at the University of California, Los Angeles. He

joined UCLA after 14 years at the MIT Lincoln Laboratory, where he was active in submillimeter/millimeter-wave detector and source programs. He successfully developed heterodyne receivers and solid-state sources with applications in plasma diagnostics, remote sensing, and imaging radars. Since coming to UCLA, he has concentrated on millimeter-wave GaAs devices and the optical control and testing of high-frequency systems.

C. W. Myles, photograph and biography not available at the time of publication.

Martin A. Gundersen received the Ph.D. degree in physics from the University of Southern California, Los Angeles. From 1973 to 1980 he was with the Department of Electrical Engineering, Texas Tech University, and in 1980 he joined the Department of Electrical Engineering at the University of Southern California, where he is currently Professor of Electrical Engineering. He has been Visiting Professor at the University of California, Los Angeles (1986-1987), Visiting Scientist at the Massachusetts Institute of Technology (MIT) (1986-1987), CERN (1987), and MIT (1989). His research activities are in applied physics in the areas of high-power electronics, high-power physics, quantum electronics, lasers, and semiconductor devices and physics. Work in quantum electronics has included laser research and development in the areas of optically pumped and discharge lasers, and the development of powerful single-mode IR lasers. Semiconductor research includes the investigation of the physical processes occurring during recombination in semiconductors, optoelectronic devices, and GaAs-based pulsed-power devices. Pulsed-power activities also include the invention and development of the back-lighted thyratron switch for laser and particle accelerator applications, research into the basic cathode-emission mechanisms leading to the superdense glow operation of high-current plasma devices, studies of fundamental problems in pulsed-power physics, and applications of high-density plasma-based devices to accelerator problems. Dr. Gundersen is a Fellow of the Optical Society of America. He has served as Chairman of the Power Conditioning Workshop (Dec. 1985), co-Chairman, SPIE Pulsed-Power for Lasers (Jan. 1987), Symposium Chair, Pulse-Power for Lasers, 1989 OSA Meeting. He is Technical Program Chairman, IEEE Power Modulator Symposium, 1990, and was Director of the 1989 NATO Advanced Research Workshop on High Power Glow Switches.

EXPERIMENTAL VERIFICATION OF A NOVEL OPENING SWITCH CONCEPT[1]

A.H. Griffin, D.M. Giorgi, O.S.F. Zucker

Energy Compression Research Corporation
990 Highland Dr Suite 101
Solana Beach, CA 92075

ABSTRACT

Experimental verification of a high current compound opening switch capable of mega-amperes of current commutation is described. The switch is based on a large current carrying foil stretched across a pressurized tube. The foil is weakened at one end and the ensuing crack propagates lengthwise down the foil perpendicular to the current flow causing a resistance excursion large enough to transfer the current to a fast acting fuse which then generates the required voltage. The switch is augmented with a Metal Oxide Varistor (MOV) which prevents the fuse from restriking and dissipates the switch energy in a controlled manner. By removing the dissipation away from the foil and fuse, they can be made substantially less massive allowing for faster replacement. Initial experiments aimed at demonstrating the principle of operation have shown crack velocities of over 200 m/sec and the opening of 15 kA while generating 680 volts without the formation of an arc.

INTRODUCTION

Switches required for the SDI Electromagnetic Gun (EM) program must be capable of conducting mega-amperes for periods in excess of one millisecond, dissipating commutation energies in the mega joule range, developing commutation voltages in excess of 1kV, and withstanding transient voltages of approximately 10 kV developed by the gun. The ability to carry and commutate large currents requires massive mechanical systems or explosive systems, both of which are limited in either repetitive operation or life. To develop a high energy repetitive switch, it is necessary to separate the dissipation of the commutation energy from the opening switch. This allows the use of relatively lightweight opening switches which can be replaced at a meaningful reprate.

A concept developed by ECR Corporation

[1] Work sponsored in part by DNA/SDIO contract number DNA001-90-C-0045 and ONR/SDIO contract number N00014-88-C-0650.

Table I: Properties of commercially available MOVs

Properties of Commercial MOVs	
Parameter	Typical Value
E field (kV/cm)	1-10
Current Density (A/cm^2)	2500
Adiabatic energy absorption (J/cm^3)	80
Leakage Resistivity (Ω-cm)	10^9
Specific Heat ($J/g\,^\circ K$)	0.8
Operational Temp ($^\circ K$)	220-350

which removes the commutation energy from the opening switch is to place a Metal Oxide Varistor (MOV) in parallel with the switch. An MOV has current/voltage characteristics similar to back-to-back zener diodes but with much higher current and energy capability. Table I gives the relevant characteristics of commercially available MOVs. Work by isolated groups has demonstrated electric fields[1] between 10-100 kV/cm and current densities[2] in excess of 4.2 kA/cm^2. However, to date, MOVs have not been engineered for pulsed power systems.

The MOV, beyond its ideal electrical characteristics for current commutation to inductive loads, is a bulk device with excellent thermal properties. It has a large heat capacity and can be engineered for water or other fluid cooling.

An MOV in parallel with an opening switch initially assumes a high resistance until the switch has developed a voltage larger than the "knee" voltage of the MOV. Then it exhibits a very low resistance and current is shunted to the MOV. In the case of a fuse this allows the fuse to open while carrying very little current. This minimizes arcing and collateral damage caused by the explosive nature of an ordinary fuse. By conducting the current and developing the commutation voltage for the entire transfer time the MOV dissipates a majority of the energy associated with the opening in a controlled manner. The MOV also keeps the voltage across the switch constant, which delivers the required volt-seconds at the lowest peak voltage. ECR has used MOVs to augment the switching performance of MOSFETS, Transistors, SCRs and fuses. A fuse/MOV combination has been operated at 250 kA for the opening switch of an EM gun[3].

A single fuse and MOV combination is still insufficient for EM gun applications because of the limited time compression. The time compression is given by the ratio of the conduction to commutation time ($T_{conduct}/T_{commute}$). The ideal candidate

would be a variable geometry fuse which starts initially with a large mass (low resistance), with the means to subsequently shed most of its mass in a controlled manner in order to affect a rapid opening. Work at Los Alamos National Lab has demonstrated a variable geometry fuse with the use of explosives[4]. The concept described here is to take advantage of the well known failure mechanism in pressurized pipes. A large current carrying foil is placed across a slit in a pressurized pipe. The foil is weakened at one end causing a pressure induced crack to propagate in the axial direction. The ensuing crack redirects the current flow which excludes the current from the majority of the foil. This non-violent change in geometry allows the foil to essentially shed its mass. The foil is designed to generate sufficient voltage to either transfer the current to a much smaller fuse which then transfers the current to the MOV or transfer directly to the MOV. The latter approach requires a more precise construction of the last foil section to act as a fuse. This is desirable in a final system but provides less experimental freedom and was not attempted in the work reported here. However, the external fuse is closely coupled to the foil and can be envisioned as an integral part of the foil. The foil/fuse combination is also designed to transfer the current to the MOV without reaching explosion temperatures. This is typical of a fuse/MOV combination as we have demonstrated previously.[3]

Figure 1 shows a schematic view of the crack propagation down a pressurized pipe. Notice how the crack excludes the current from a majority of the foil. The crack velocity is dependent on the gas and magnetic pressure. Since the magnetic pressure is dependent on the current per unit length, the magnetic pressure dominates towards the end of the rip. With large magnetic pressures, velocities approaching the speed of sound in the material (3000 m/sec) can be achieved and the use of gas pressure may not be required.

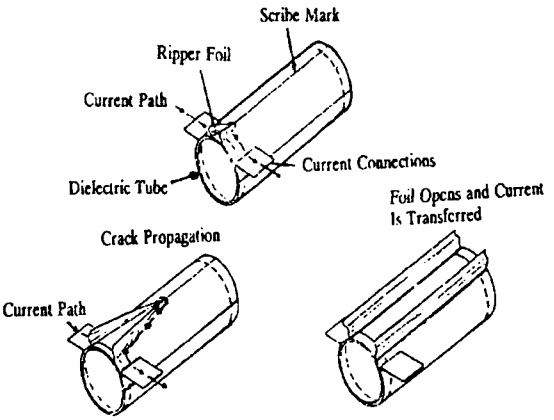

Figure 1: Schematic of the ripping process in the current carrying foil. The crack excludes the current from a majority of the foil causing a resistance excursion.

Unlike mechanical switches, single fuses and explosive switches, the compound switch is well suited for repetitive applications due to the following reasons; 1) The section which suffers damage (foil) is replaced every shot. Thus the

performance of the switch is not degraded due to wear. 2) The MOV is a solid state device and like any solid state system the lifetime is very long when the device is operated within its current density and electric field limits. 3) By having the majority of the energy dissipated in the MOV collateral damage is minimized thus reducing the need for large confinement vessels. 4) Since the replaceable section is in the form of a tube (see Figure 1) it can be fed in machine gun style. Thus reprates from 1-10 Hz should be achievable.

EXPERIMENTAL RESULTS

The purpose of the experimental program was to investigate the nature of the crack propagation and to demonstrate arc free commutation. Since the area of the foil which has the most potential for arcing problems is at the end of the crack, short foils were used and the end of the ripping process was closely investigated. For this concept to be viable the foil must generate sufficient voltage to commute the current to the fuse before the foil opens. If the foil opens while carrying meaningful current an arc may form.

Foils were fabricated on a copper-clad Kapton substrate and patterned to the desired dimensions. Typical dimensions were 4-6 cm long and 2 cm wide. The foils were electroplated to the required thickness, typical values ranging from 3-5 mils. The Kapton was etched from under the tips of the foil to reduce the chance of surface flashover across the kapton when the foil opened. The kapton at the rip initiation end was required in order to form an adequate pressure seal. Figure 2 shows the various foil geometries attempted throughout the program. The foils shown in Figure 2a and Figure 2b on average exhibited a smaller resistance excursion than the foil shown in Figure 2c. The low resistance excursion manifested itself in a lower commutation voltage. The foil shown in Figure 2d was inferior to that shown in Figure 2c because insufficient mass towards the tip caused the critical current density to be exceeded. This was partially remedied by electroplating the tip of the foil. However, due to the narrow tip the crack did not always propagate down the center.

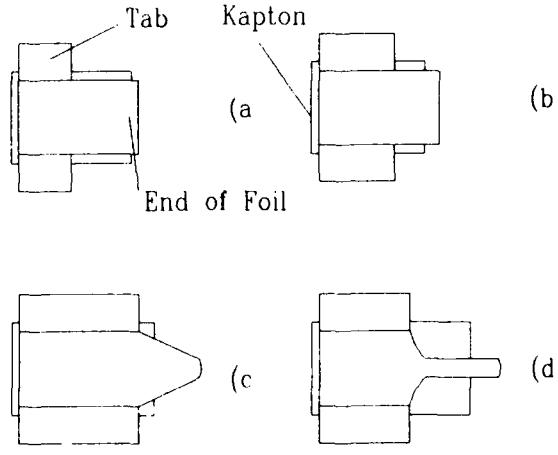

Figure 2: Various foil geometries that were used throughout the program.

The foils were housed in a pressure mounted fixture (see Figure 3). The tip of

the foil was located over a section of the PVC pipe that was isolated from the pressurized chamber. Since this section of pipe was not pressurized, a 2 cm x 2 cm section was removed directly under the foil tip. This eliminated flashover across the surface of the PVC pipe when the foil opened. Since the last section of the foil is not over the pressurized opening we relied solely on magnetic pressure to rip the last section. The tube was transiently pressurized by a fast valve to approximately 150 psi.

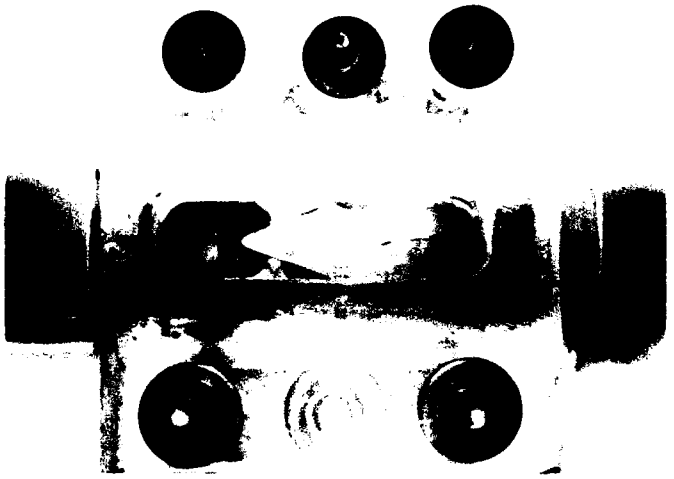

Figure 3: Foil housing used to contain the foils. This clamping arrangement allowed for easy removal of foils.

The switch was tested in the inductive circuit shown in Figure 4. Crack initiation was performed by discharging a capacitor through a needle placed on the foil. The discharge sufficiently weakened the foil to initiate the crack.

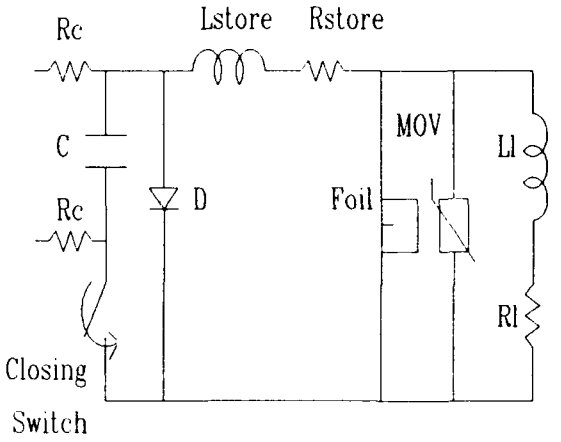

Figure 4: Schematic of the inductive storage and transfer circuit used for opening switch experiments.

The foil design shown Figure 2b was used to transfer 9.1 kA to a 3.2 μH load without the formation of an arc. Figure 5 shows the load current and load voltage. A peak current of 9.1 kA was established in the load with a peak voltage of 75 volts. The next series of experiments examined the maximum commutation voltage achievable with the present foil and housing configuration. To demonstrate a larger commutation voltage the load inductor was removed and the switch was operated into an open circuit. This is a much more demanding task on an opening switch because all of the energy in the storage inductor needs to be dissipated by the switch.

Figure 6 shows foil current and fuse voltage and Figure 7 shows the fuse

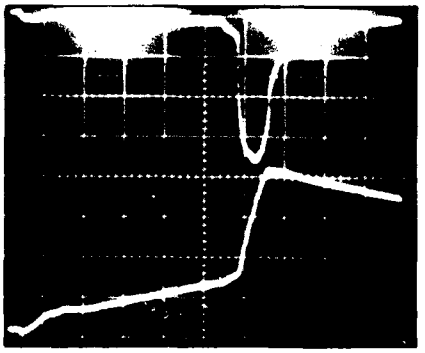

Figure 5: Establishment of 9.1 kA into a 3.2μH load. The peak load voltage was 75 volts. (2160 amps/div bottom trace, 20 v/div top trace and 200 μs/div)

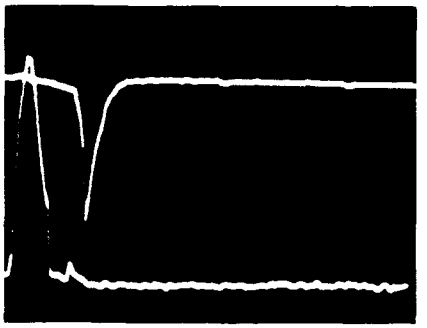

Figure 6: Foil current (bottom trace 2000 amps/div) and voltage (top trace 200 v/div) showing the foil completely opening without arc formation and the subsequent voltage generation by the fuse. (500 μs/div)

current and storage current for a 15 kA, 680 volt shot using the foil geometry shown in Figure 2c. Figure 6 is interesting because it shows that the foil completely opened and was allowed time to clear before the fuse generated any voltage. The rise time to peak voltage is approximately 150 μs. In Figure 7 one can see that after 400 μsec the fuse is carrying the full current and dwells at this current for approximately 350 μs before generating any voltage. The total volt-seconds generated by the switch was 0.17. The action of this fuse agrees with the expected value of approximately 10^9 amp^2-sec/cm^4. In this experiment the total crack time is 300 μsec which corresponds to an average velocity of 200 m/sec for a 6 cm foil. Figure 8 shows the foil after carrying 15 kA and its subsequent opening. Notice that there is no damage at the tip of the foil. This is because the resistance excursion was large enough to commute a majority of the current out of the foil before it opened.

These results demonstrate that utilizing a crack propagating down a current-carrying

foil will cause a resistance excursion large enough to commute the current to a faster fuse without the formation of an arc. Thus the foil/fuse combination makes for an opening switch with large compression ratios which can be scaled to higher currents.

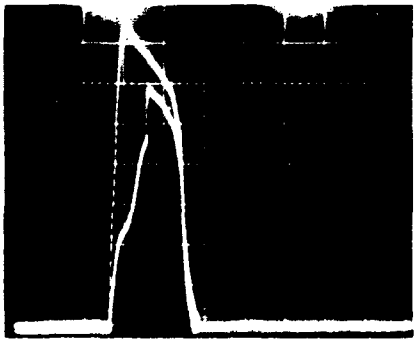

Figure 7: Storage current (upper trace 2000 amps/div) and fuse current (lower trace 2190 amps/div) showing the current transfer to the fuse, and the subsequent opening. A load was not used in this experiment. (500 μs/div)

AREAS FOR FUTURE WORK

Current Scaling

The scaling to higher currents requires the use of a substantially more massive foil. ECR corporation has designed foils for peak currents of over 1 MA. The switch was designed to work in an inductive storage and transfer circuit. The design

Figure 8: Picture of the foil after carrying 15 kA and its subsequent opening transferring the current to the fuse. Notice very little foil damage indicating an arc free commutation.

was to conduct 1 MA of current for 50 ms and then open in 200 μs to transfer to an EM gun type load. This corresponds to a compression ratio of 250. Figure 9 shows the circuit currents along with the current in the foil and MOV. In this model the last section of the foil generated enough voltage to simulate the fuse like characteristics.

The foil dimensions are given in Table II. The tab is used to connect to the external circuit and the tab width and thickness determine the temperature rise during the

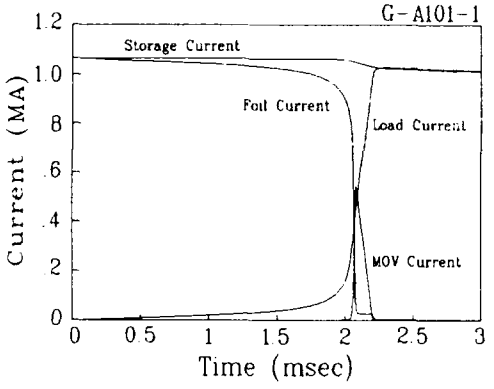

Figure 9: Circuit currents, showing the transfer of 1 MA in 200 μs using the compound switch.

Table II: Foil dimensions for a 1 MA foil.

Length	80 cm
Width	10 cm
Thickness	0.25 cm
Tab Width	40 cm

charge phase. Due to the high current capability of the foil its overall dimensions are substantially larger than the ones used in the experimental program.

For the mega-ampere system, the foil housing, crack initiation circuit and all interconnects will be redesigned to handle the larger foil and current. However, at the mega ampere current level the use of gas pressure may not be required due to the high magnetic pressure.

Voltage Scaling

The generated voltage of 680 volts is sufficiently close to that required by most EM guns, thus further extrapolation is not required. However, since large crack velocities can be achieved with higher currents this switch is useful for fast opening (non EM gun applications) applications where commutation voltages of approximately 10 kV are typical. Presently these voltage levels have not been achieved. However, due to the nature and speed of the crack propagation, voltages of approximately 10 kV should be achieved. The commutation voltage must be held across the fuse and the tips of the foil as it separates. A voltage of 10 kV should be easily held across the fuse because the fuse is designed to transfer the current to the MOV before it reaches the burst phase. Experiments conducted by Maxwell Labs[5] have demonstrated electric fields during burst and clearing of 7 kV/cm and 20 kV/cm respectively with fuses in water. Thus the last section of foil will easily hold the required voltage of 10 kV with moderate length.

The maximum voltage holding across the tips of the foil is dependent on the delay

between commutation of the current out of the foil and subsequent voltage generation by the fuse. With a maximum electric field across the tips of 30 kV/cm the foil tips must separate at least 0.3 cm to hold 10 kV. Computer calculations have shown that at mega-amperes of current the velocity at which the tips of the foil separate can reach 3000 m/sec. Thus the foils will have separated a distance of 0.3 cm in 1.1 μs. This is the minimum delay time between current shunting to the last section (fuse) and the subsequent voltage generation.

Larger Time Compression

Achieving a larger time compression simply requires a more massive foil. This will allow the build up of current over a longer time. Large time compressions are usually required in discharge systems in which the driving voltage is low.

CONCLUSIONS

The opening switch concept based on crack propagation along pressurized foils has been demonstrated. The switch opened 15 kA and generated 680 volts in 150 μs without the formation of an arc. The total volt-seconds was 0.17 and the average crack velocity exceeded 200 m/sec. Computer modeling has shown the feasibility of scaling to mega-amperes of current with larger foils. Future experiments will be aimed at demonstrating the higher current capability of this unique compound switch.

ACKNOWLEDGEMENTS

The authors would like to thank Greg Listvinsky for his original analysis of crack propagation down pressurized tubes.

REFERENCES

1) T. J. Gardner, and S. J. Lockwood, "Sintering schedule and sample geometry effects on the electrical and physical properties of high field varistor material," Sandia Report SAND88-2449 UC-25, (1989).

2) Tapan Gupta, Private Communication

3) K. Lindner, et. al. "Fuse opening switch performance enhancement", Proceedings of the 6th IEEE Pulsed Power Conference, Arlington VA (1987).

4) J. H. Goforth, et. al "Experiments with explosively formed fuse opening switches in higher efficiency circuits", Proceedings of the 7th IEEE Pulsed Power Conference, Monterey, CA, (1989).

5) G. M. Wilkinson and A. R. Miller, "Generation of sub-μsec current rise times into inductive loads, using fuses as switching elements," Proceedings of the 5th IEEE Pulsed Power Conference Arlington, VA (1985).

Adam Griffin received the B.S.E.E degree from University of California, San Diego in 1988. He is currently a Research Engineer with ECR Corporation. His current research includes, sequentially switched inductive circuits, high current opening switches, high power electronics and silicon device processing.

David Giorgi received the B.S.E.E and M.S.E.E. degree from the University of California, San Diego in 1984 and 1986. He is currently the Experimental Programs Manager at ECR Corporation. His current research includes, light activated switches, high current opening and closing switches, and pulsed power.

Oved Zucker received the B.S.E.E. degree from City College, N.Y. in 1965. In 1965 he join Lawrence Livermore National Laboratory where he conducted research with lasers, inductive storage, exploding wires and plasma diagnostics. From 1978 to 1981 he was a Staff Scientist at Physics International Company where he developed novel pulse compression schemes and induction accelerator concepts. In 1981 he join the staff at the International Nuclear Energy Systems Company where he was involved in the Riggatron program. Presently he is President of ECR Corporation and is actively involved with light activated switching for pulsed power applications.

REVIEW OF SDIO-SPONSORED WORK AT THE U.S. ARMY PULSE POWER CENTER

C. Braun
Pulse Power Technology Branch
Electronics Technology and Devices Laboratory
ATTN: SLCET-ML
Fort Monmouth, New Jersey 07753
(908) 532-0271

ABSTRACT

The U. S. Army Pulse Power Center as a government research center for high average power components has strong ties to the research and development of the Strategic Defense Initiative Office. Historically, a large share of the internal and contractual work at the Pulse Power Center has been funded by SDIO. The SDIO sponsored programs include evaluation and test of high average power plasma switching devices (F266, CX 1536, CX 1700 series thyratrons, orientation independent ignitron) as well as development and evaluation of high-voltage MOS Controlled Thyristor power semiconductor switches. A summary of the significant technical results of these programs is presented.

INTRODUCTION

The Pulse Power Center at the Electronics Technology and Devices Laboratory is the U. S. Army's center for high power component development, prototyping of power systems, and body of expertise for dealing with high power electronics. We have had a long and fruitful relationship with the Strategic Defense Office in advancing the technology in high power switching. This paper will present a brief overview of the programs and technical results.

There are two main and complimentary SDIO sponsored research efforts: one dealing with the evaluation of high power plasma switching devices such as thyratrons and ignitrons, the other has developed a high voltage/high power version of the MOS Controlled Thyristor (MCT).

As part of the process of sharing development costs and ensuring acceptance of new technology, we have been very active in pursuing joint programs with manufacturers, other government organizations, and industry. Some examples of our partners include the Electrical Research Power Institute (EPRI), Harris Semiconductor, and English Electric Value. These collaborations have given strength to our development programs which can often find a means to continue research in spite of funding variations.

GAS PHASE SWITCHING PROGRAMS

Thyratrons, ignitrons, spark gaps and other plasma switching devices are important for handling high voltages and high powers. Typical applications are in grid pulsers for microwave tubes in accelerators and high power microwave generation, electric gun closing switches, and discharge lasers. A key limitation for these devices is operation at high repetition rate and at high average (≥1MW)

In a non-SDIO funded effort, an improved sealed orientation independent ignitron is under development as a high current, high coulomb switch for electrothermal chemical guns. There is also some interest in possible future applications of the OII as a crowbar switch.

MOS CONTROLLED THYRISTORS

Device Development Overview

The MOS Controlled Thyristor (MCT) is a power thyristor which is turned on and off by a highly interdigitated surface array of MOSFET gates. These switches require control energies equivalent to those required to charge the gate capacitance of a power MOSFET. Two types of MCTs have been investigated at ETDL. The first type being an epitaxially grown MCT which are rated for blocking voltages ranging from 500 V to 1000 V with peak controllable currents from 60 A to 120 A. This type of MCT is now in limited production at the Harris Corporation Mountaintop facility. The second type is a higher voltage 1 cm^2 active area diffusion-doped MCT developed under a two million dollar SDIO/ETDL contract. The prototype MCT devices have blocking voltages up to 3kV with a maximum controllable turn-off current density of 325 $A/cm.^2$

Epitaxial MCT Evaluation

Internal to ETDL during FY90-91 we continued device test and evaluation, and began examining device applications issues. For much of this in-house work we used epitaxial/low voltage MCT devices which were provided by Harris Semiconductor Corporation on an informal sharing of devices and test results. The recent achievements are:

- Developed SPICE model of MCT device using two-transistor concept
- Detailed device characterizations to establish the safe operating area
- Engaged in extensive parallel/series operation of MCTs - running up to 5 in series, three in parallel and a three by three array. Proved that mismatched devices can be compensated by a good snubber design.
- Operation of MCT at 20kHz square wave at high (2kW) average power; operation of MCT at 50kHz
- Preliminary examination of MCTs from 77 K (LN2) to 423 K

Diffusion-doped High-Voltage MCTs

As a the final deliverables from the SDIO/ETDL contract with Harris Semiconductor we have received 75 high-voltage MCT devices. Harris has performed characterization for low powers/single shot. The initial goal of this contract was not met (>2,500 V, >1,000 A modules), however the devices are a significant milestone in handling high voltages and good current densities. The general strategy is that the Phase II follow on work will be a collaborative program between Electric Power Research Institute (EPRI) and SDIO/ETDL. EPRI is currently in negotiations with Harris for the first part of the Phase II follow-on contract. We expect from a fully funded Phase II contract to have in four years N-type large area, multiple sub-element MCTs, symmetrical and asymmetrical, capable of switching off $\geq$1 kA at $\geq$4 kV in about 1 μs.

Internal to ETDL we have been very active in evaluating the deliverables of the Phase I contract. These MCT switches block up to 3 kV and can turn off up to 325 A/cm^2 in a 1 cm^2 area die. Devices from three different lots (PM069, PM081, PM091) were delivered. The progress from one production lot to the next in has been encouraging: the yield for blocking voltage went from 60% at 2.5 kV for PM069 to over 95% at 3 kV for PM091. The test results for these high-voltage diffusion-doped MCTs are as follows:

powers. The most recent generation of thyratrons has been under detailed evaluation to determine the actual operating limits.

High Average Power Testing of Thyratrons

In support of development of advanced directed energy weapons, the Pulse Power Center has evaluating the IT&T F266 and the English Electric Valve CX 1536 thyratrons for the past two years. Both thyratrons have been operated up to 8 kHz at 40 kV with an average power of 1.2 megawatts in a 100 second burst. These results demonstrate a significant advance in the technology of thyratron switching and represent a major milestone in the development of the next generation high average power/high frequency thyratron.

Orientation Independent Ignitron

The Hughes Orientation Independent Ignitron (OII) was evaluated in conjunction with the testing of high energy density pulsed discharge capacitors. The OII was operated at 10 Hz at 5-7 kV with a current up to 80 kA in a millisecond pulse at different orientations. Both the OII and the high energy capacitor were operated with a 500 pulse burst; over 200 bursts have been demonstrated for a lifetime of at least 10^4 shots.

Test Facility for EEV CX 1700 Series Megawatt Average Power Thyratrons

We have established test facilities to begin high average power testing of three English Electric Valve CX 1700 series thyratrons. All three tubes share the same large area dispenser cathode structure. The first device, the CX 1700HAH, will be tested at up to one megawatt continuous average power for several hour runs at 40 kV and 250 Hz. Performance so far has been limited to 500 kW operation for 15 minutes at 40 kV. The CX 1700HAH thyratron has a hollow anode structure which allows the tube to safely conduct in the reverse direction. During testing an inverse conduction re-ionized the gas in the tube and lead to holdoff failure upon immediate reapplication of voltage during recharge. The testbed is currently being rebuilt to include a command charge switch, to avoid the recovery problems associated with the hollow anode.

The second thyratron, the CX 1710, is designed with an extremely high gas pressure to conduct very high currents for millisecond pulse lengths and up to 500 amperes of average current. The voltage rating for this tube is only 12 kV because of this high gas pressure. Testing to date has proven operation at 5 kV (the voltage rating of an available capacitor bank) and up to 151 amperes of average current. Parameters of this circuit yielded a 1.2 millisecond pulse length with a 15 kA peak current, at a pulse repetition rate of 10 Hz for a 500 pulse burst. The inductors and load resistors are being changed and the power supply reconfigured to increase average current capability to 450 amperes.

Low power, high voltage tests are currently in progress with he CX 1776. Present testing has been done at up to 65 kV at low repetition rates. This tube will be tested up to 75 kV at one megawatt average power, and up to 45 kV at multi-megawatt average powers, both at pulse repetition rates of up to 6 kHz.

Future Work

We plan to continue plasma switching work in a number of areas. The IT&T F266 and EEV CX 1536 tubes will be evaluated at high repetition rate operation, up to 10 kHz, at a power level greater than one megawatt. The testbeds for the EEV CX 1700 series thyratrons will undergo modification to add a command charge circuit, increase the average current capability to 500 A, and to operate up to multi-megawatt level.

- All devices block ≥2,000 V with most devices falling 2,500 V.
- The maximum turn-off current densities range from 100-325 A/cm^2 depending upon design, edge termination, and processing.
- The forward voltage drops ranged from 1.6-4.2 V at 100 A.
- Reliable turn-off at 150 A at -1700 V at 100 Hz has been shown.
- Parallel operation of three devices with good current sharing to 300 A turn-off at -1700 V has been demonstrated.
- Series operation of three devices to 5 kV and 150 A turn-off has been proven.
- A single device has been operated at an average power to 160 kW turn-off (in a burst mode of a few cycles).
- A single device has been able to withstand a turn-on surge to 15.5 kA/26 MW (single shot).
- 50 kHz switching at 157 kW has been demonstrated.
- Switching efficiencies for operation from 5 to 50 kHz ranged from 98.9% to 92.1%, respectively.

Although this high-voltage diffusion-doped MCT is still in the development stage, experimental results from these devices indicate that they have good potential for pulse power and high voltage switching applications. However, our experience with these devices has also clearly shown a number of flaws and further highlights the need for continued device development. Specific areas to address in the near term are a better process control to produce MCTs with consistent specifications, adjust the buffer layer to better withstand avalanching, and improve the packaging to reduce electrical and thermal resistance.

A high-power, high-frequency 100+ kW inverter

As part of our goal to understand both device issues and system issues, we plan to construct a 100+ kW level power inverter operating from 400 Hz to 50 kHz using MCTs. Both a series stack of 3 epitaxial devices as well as a single high voltage MCTs will be used as a "hard" switch. This switch will transfer energy from a storage capacitor into an output step-up transformer to a load. From this work we will have the opportunity to conduct the first measurements for reliability and lifetime at high average power operation.

Significant progress has been made in operating the MCT devices at the power/frequency ranged desired, including operation of a high voltage MCT to 50 kHz and a single device at 160 kW average (burst) power. The next major steps are to assemble the testbed for continuous power and cooling to allow continuous high power operation.

SBIRs

In FY91 we were chosen as the contracting agent for three SDIO Phase I SBIR contracts. The funding, about $50K each, was received in March 1991 and the contracts awarded in May 1991. These SBIRs focus on innovative research of interest to SDIO as well as the Army:

- "Light Activated Switches for Megahertz Pulsed Induction Accelerators" by Energy Compression Research, D. Giorgi .
- "A Self-Restoring Fault Limiter Utilizing High Temperature Superconductor Components" by Illinois Superconductor Corporation, Dr. James Hodge.

- "Aggreate Suspended Particle Electric Charge Collector" by Hayes & Associates, Dr. Claude Hayes.

SUMMARY

The Pulse Power Center at the ETDL has the mission to develop and test high power electrical components, and prototype power systems. We have a strong relationship with the Strategic Defense Office and have been fortunate in working closely together in the development of high-power plasma and semiconductor switches to support future space and ground system needs. New levels of thyratron performance of up to 6 kHz and at megawatt average powers with both the IT&T and EEV tubes have been demonstrated. Operation of the orientation independent ignitron has been shown for 10^4 pulses. We are in the process of upgrading our thyratron testbed facilities to handle high average currents (500 A) and multi-megawatt average powers.

For solid-state devices, we have made good progress in understanding and applying epitaxial MCTs. The Phase I high-voltage MCT contract is complete. Recent measurement of these diffusion-doped MCTs have proven these devices are capable of turning off 325 A, blocking 3 kV, withstanding a surge current of over 15 kA, and operating up to 50 kHz. Three SDIO Phase SBIRs have been awarded for an optical switching development, a novel capacitor concept, and an HTc superconducting current limiter.

Christopher G. Braun received the B.S. degree in both electrical engineering and in physics from the Mass. Institute of Technology, Boston, in 1982, and the M.S. and Ph.D. degrees in electrical engineering from the University of Southern California, Los Angeles, in 1984, and 1987, respectively. He is currently a Captain in the U. S. Army and has been assigned to the Electronics Technology and Devices Laboratory at Fort Monmouth, New Jersey since 1989. Since arriving at ETDL he has been the project leader for the MOS Controlled Thyristor program there involving both in-house research as well as contractual oversight. His research interests include applications of power electronics, modeling and computational physics.

HIGH POWER MODULATOR DEVELOPMENT BASED ON THE BACK LIGHTED THYRATRON SWITCH

G. Kirkman-Amemiya, N. Reinhardt, M. S. Choi
and M. A. Gundersen
Integrated Applied Physics Inc.
140 East Santa Clara Street #19
Arcadia, California 91006

Abstract- A project to develop improved high power high repetition rate modulators for accelerator and pulsed laser applications is described. The modulator development is based on the back lighted thyratron or BLT switch which has demonstrated improved performance in voltage holdoff >100kV, peak current >80kA, rate of current rise $>6x10^{11}$A/sec and ability to handle high reverse currents >40kA. A BLT switched Marx bank has been demonstrated and a transformer based high current, high voltage modulator designed.

I. INTRODUCTION

Many particle beam accelerator and pulsed laser systems are limited by the performance of the pulsed power modulator which in many cases is limited by the performance of the switch. In this project we are developing improved modulators based on a new development in high power switch technology. The new switch is the back lighted thyratron or BLT switch and is a thyratron switch that has shown improved performance in the areas of peak current , voltage holdoff, rate of current rise, triggering and construction.

The Back of the cathode Light activated Thyratron or BLT switch[1] is a low pressure gas discharge closing switch which operates with peak currents and current rates of rise comparable to high pressure spark gaps but with the repetition rates and low electrode erosion characteristic of hydrogen thyratrons. Unlike the hydrogen thyratron the switch requires no cathode heater power and has a much simpler gridless structure, also the symmetric structure of the BLT allows it to conduct reverse currents without electrode damage. The BLT can be triggered optically by a laser or flashlamp and electrically by several pulsed discharge methods[2].

II. KEY TECHNICAL RESULTS

During the period of funding by the Strategic Defense Initiative several important technical accomplishments have been made in the development of the BLT switch for high power modulators. These results include:

Development of three single gap versions of the BLT switch

Development of a two gap BLT switch

Two gap operation at 105kV, 26kA

Single gap operation at >70kV

High current operation at 82kA

Short risetime 18nsec operation

BLT optically triggered Marx bank operation

Design of high voltage and high current modulators

A. Development of Hermetically Sealed BLT Switches

1) Single Gap BLT Switches: Three ceramic-metal hermetically sealed versions of the single gap BLT have been developed. The single gap structure consists of an anode and cathode electrode separated by a ceramic insulator as shown in figure 1. All triggering electrodes an windows are below the mounting flange and therefore do not interfere with the implementation of very low inductance connections to the anode and cathode.

The BLT-250-T and BLT-250-W are 6.4cm diameter switches capable of operation at up to

40kV, 20kA, at a heating factor of several 10^{10}V·A·Hz. The former is the electrically triggered tetrode and the latter is optically triggered. Average power and current ratings have not yet been determined but are expected to be compatible with present modulator requirements.

The BLT-175-T is an electrically triggered 4.2cm diameter switch capable of operating at similar power levels as the 250 series switches. The high current density super emissive cathode[3] of the BLT switch allow the same current capability in this smaller diameter switch.

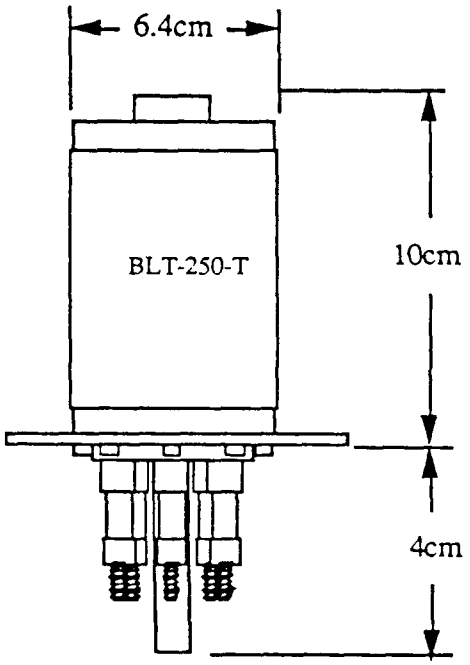

Figure 1. The BLT-250-T switch.

2) Multiple Gap BLT Switches: A two gap switch designated the BLT-250-2T has been fabricated and tested at >100kV. The switch is a two gap version of the BLT-250-T. The switch consists of anode cathode, intermediate electrode and biased field grading electrodes in the cathode and intermediate electrode. The switch shown in figure 2 is 24cm long and is electrically triggered.

B. Switch Performance

1) >100kV Operation: A two gap electrically triggered BLT switch has been operated at 104kV, 26kA and repetition rate up to 10Hz. Details of this result are presented in the figure 3. This is the first time a BLT or pseudospark switch has been demonstrated to operate repetitively at high voltage and high current simultaneously. The result presented here was limited by our circuit and not the switch. Our circuit was only designed for 80kV, therefore operation in excess of 80kV was limited to a few pulses only to demonstrate capability. Continuous operation (several hours) has been achieved at 78kV, 19kA and 10Hz.

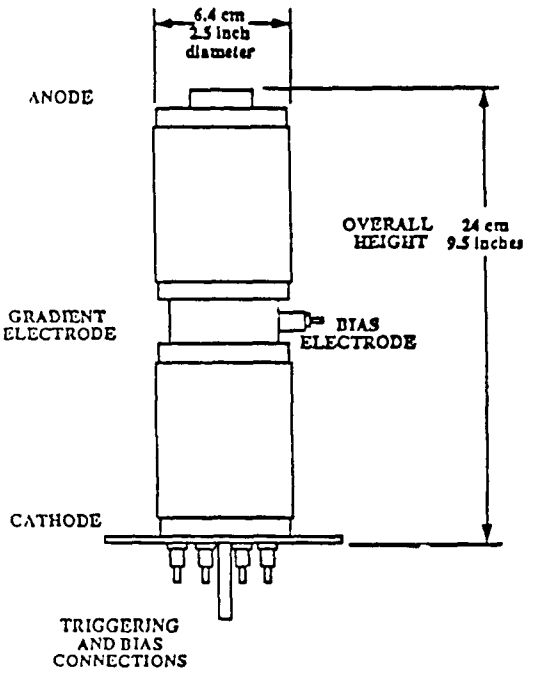

Figure 2. The two gap BLT-250-2T switch.

The circuit consisted of a 20nF capacitor and 1ohm load. The capacitors used were TDK UHV-9A rated at 40kV, 2nF each, these are stacked in series to give 80kV capability, 20 of these stacks in parallel give 20nF at 80kV. Most of the testing was therefore done at voltages below 80kV, however for low repetition rate testing the voltage rating has been exceeded by as much as 30% for a small number of shots($<10^4$) without difficulty. For testing at voltages >100kV more capacitors in series were used reducing the total capacitance, resulting in lower peak currents and shorter pulse length.

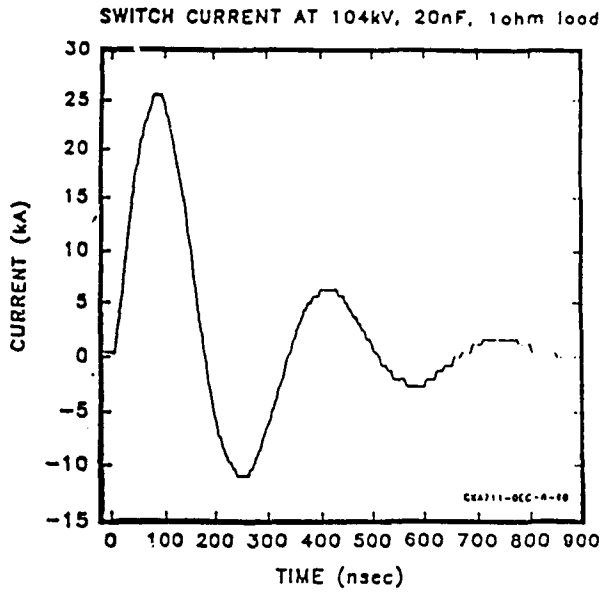

Figure 3. Performance of the two gap prototype switch at >100kV.

2) Single Gap High Voltage BLT Switch: The ultimate voltage holdoff capability of a single gap device is determined by several factors including the field emission limit due to macroscopic electrode features[4], field enhancement due to electrode microgeometry[5], surface flashover on the insulator surface[6], and ionization avalanche in the gas[7]. These factors limit single gap thyratron switches to about 40kV maximum holdoff voltage. The simple electrode structure and absence of the hot cathode in the BLT switch allow it to operate at higher voltages in a single gap structure.

Voltage holdoff capability in the BLT is improved by using very clean fabrication techniques, precision electrode and insulator shaping and fabrication, and biased trigger electrodes in the hollow electrode spaces. We have obtained >70kV holdoff in a single gap switch under pulse charged conditions. The breakdown voltage vs pressure for the single gap switch is shown in figure 4.

These preliminary results indicate that 100kV voltage holdoff may be obtainable with minor modifications to the electrode structure. The compact structure of the single gap BLT switch will be capable of higher repetition rate operation than is possible with a multiple gap switch. Previous high voltage switch development of both BLT switches and hydrogen thyratrons has used multiple gap structures to obtain high voltage holdoff. The resulting multiple gap structure has a long recovery time due to the large volumes of ionized plasma in the electrode structure that must recombine before voltage can be reapplied. The recovery voltage of multiple gap tubes is typically more than an order of magnitude greater than that of single gap tubes. The single gap BLT switch achieves high voltage holdoff capability while preserving the short recovery time of a single gap switch.

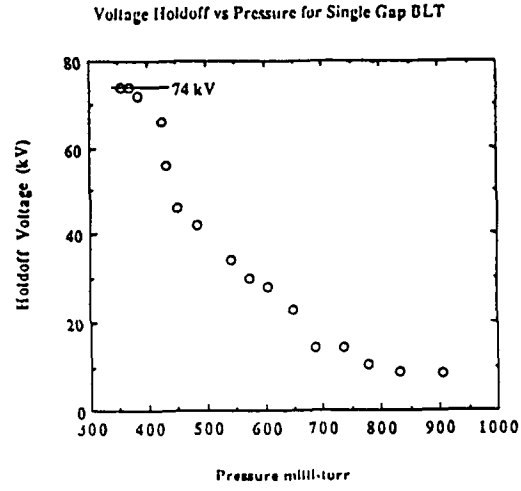

Figure 4. Voltage holdoff vs gas pressure in a pulse charged single gap BLT switch.

3) High Current BLT Operation: Single and multiple gap BLT switches have been tested at peak currents up to 82kA. The two gap BLT-250-2T switch has been operated at peak currents in the range 5-25kA at voltages up to 104kV, the peak currents at these voltages were limited by our circuit and charging supply. In a demountable three gap switch 76kA operation was demonstrated at 100kV on a single shot basis. To demonstrate high current operation in the range 5 to 100kA we have used a single gap switch operating at voltages up to 25kV. The peak current capability of the BLT is a characteristic of the superemissive cathode and is therefore relevant to both single and multiple gap switches.

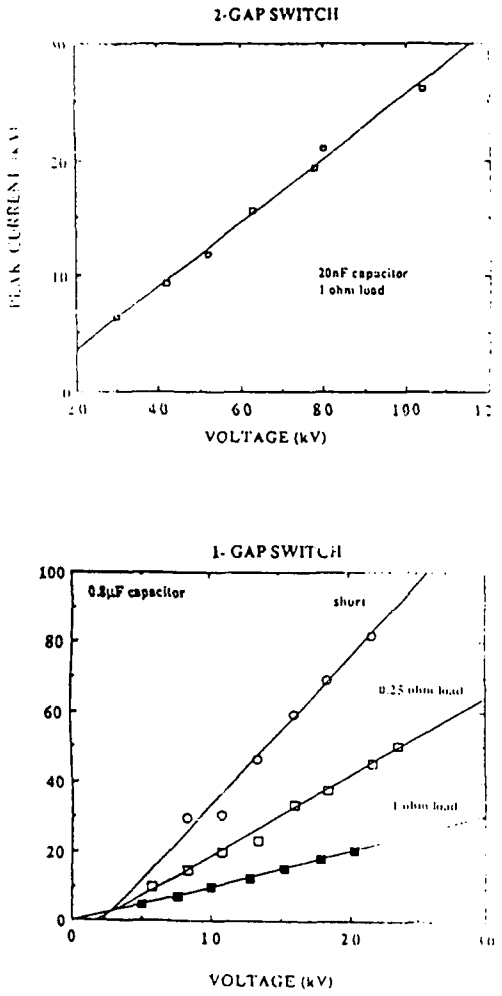

Figure 5. High current performance for 1-gap and 2-gap BLTs showing no current limit even >80kA.

The high current performance is described in figure 5. In all cases the peak current increases linearly with voltage showing pulse shapes determined by the circuit. In this range of currents 5-100kA the BLT shows no peak current limit.

Operation at very high forward and reverse currents has been demonstrated in a single gap flashlamp triggered switch specifically designed for high current operation. Modifications to the electrode structure have been made to improve high current performance. The modified electrode structure is shown in figure 6. This electrode structure positions the main discharge in a region that is completely surrounded by metal walls, this protects the insulator surface from the discharge plasma and allows for efficient removal of the energy deposited in the switch. This electrode structure could also be implemented in multiple gap designs. The discharge circuit for very high peak current testing consisted of two 0.4μF capacitors switched in parallel. Carbon block load resistors were used which could be changed to produce various levels of peak current and reverse current. The repetition rate in this circuit was limited by the power supply and resistive charging to about 5Hz.

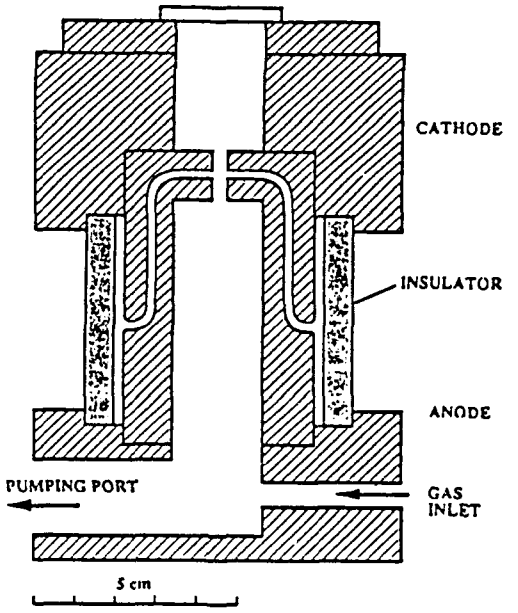

Figure 6. High current BLT switch tested at peak currents from 3.5kA to >80kA with pulse lengths of about 500nsec. In all cases no current interruption was observed and circuit limited pulse shapes were observed.

Under short circuit conditions the switch was operated at 17.5kV, 122.5J/pulse and 5Hz giving a peak current of 60kA followed by 40kA reverse current. The rise time was 140nsec, a dI/dt of 3.4×10^{11}A/sec. A circuit inductance of 40nH and resistance of 60mΩ were calculated from the current waveform (figure 7). Under these conditions the switch was run continuously for $>10^4$ pulses with no performance degradation observed.

After running the switch at various pulse conditions for about 10^6 pulses the switch was dismantled and no severe damage to the electrodes or insulators could be observed visually or by optical microscope. Through these observations the active cathode area can be determined and the deposition of evaporated electrode material on insulators and windows can be observed. The cathode shows a

uniformly etched area of 1.1cm^2 surrounding the cathode hole, there is very little plasma etching or arc damage to the outer areas of the electrodes or the parts of the electrodes near the insulator. This corresponds to the superemissive behavior previously reported. The anode shows a slightly larger etched area that has a much brighter appearance than the cathode. The insulator shows only a very light deposition of electrode material indicating that the electrode shape protects the insulator from the evaporated electrode material and most of this material is probably deposited on the electrode walls surrounding the high current discharge. The cathode window which was positioned 7.5cm behind the cathode show a dark coating directly on axis with the electrode apertures. This darkening is only about 1cm in diameter indicating that window lifetime can be greatly increased by positioning the window slightly off axis.

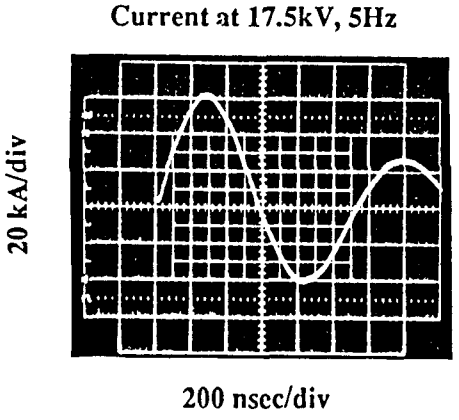

Figure 7. High current waveform obtained with the flashlamp triggered BLT at 5Hz.

The above observations show that high current performance of the BLT is not limited by switch diameter as in hot cathode thyratrons, currents >80kA can be conducted in a 2.5 inch diameter device without current quenching or damage to the switch. Previously a high current thyratron required a large diameter thyratron, sometimes eight to ten inches in diameter. Fabrication of large diameter thyratrons is very costly for several reasons, large amounts of expensive electrode materials (Mo and W) are required, large diameter ceramics are difficult to fabricate with the close tolerances required and most importantly ceramic to metal seals of large diameter are very difficult to produce reliably with a high production yield and low failure rate during operation. Furthermore larger switches require more processing and standby power during operation and are difficult to mount in very low inductance circuit configurations. The high current capability and small diameter package of the BLT switch is a significant improvement in switch technology and opens the possibility for modulator designs and performance not possible with previously available switches.

4) Fast Risetime BLT Switches: The BLT switch has been evaluated in several fast risetime test circuits. For this work pulse forming networks (PFN) producing fast rising square pulses were constructed. Two different implementations of a Type E pulse forming network were used to give an impedance at the one ohm and six ohm level. At the 1 ohm level two 2 ohm lines are used in parallel each made up of 4 parallel 1nF ceramic capacitors per section and parallel plate conductors to provide the low ~16nH inductance of each section, 40 sections are used to give a 400nsec pulse[8]. At the six ohm level two 12 ohm lines are used in parallel each made up of 2nF ceramic capacitors per section and a solenoid wound using 1/4 inch diameter copper tubing on a 6.5cm diameter air core with three turns per section giving ~300nH/section, 11 sections are used to produce a ~600nsec pulse. The main emphasis of our work was the performance of the switch therefore in both cases the PFNs were not optimized for pulse shape, overshoot compensation or impedance matching. The PFNs used were sufficient to demonstrate the risetime and peak current capabilities of the BLT switch. A schematic diagram of the BLT switch and test circuit are shown in figure 8.

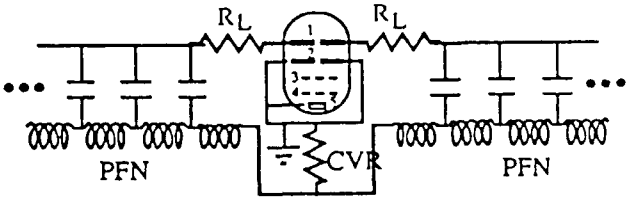

Figure 8. Schematic diagram of BLT switch and test circuit 1) anode, 2) cathode, 3) G2, 4)G1, 5) reservoir.

The BLT-250-T is triggered using two triggering electrodes, G1 and G2. A DC bias of +50 to 200 V is applied to G2 to enhance voltage holdoff capability, for triggering a pulse of 3-6kV is applied to both G1 and G2. G1 can be used as a preionization electrode by applying a positive pulse of 1-5μsec duration prior to triggering G2.

The BLT switch has been operated at up to 17kA at 30kV with <60nsec risetime in the ~1 ohm PFN and 1.5kA at 20kV with <18nsec risetime in the ~6.5 ohm PFN. In both of these circuits the switch was not limiting the risetime. In a 1.25 ohm, 100nsec PFN the BLT was operated at up to 240Hz at 20kV for short periods of time (minutes) and and continuously (several hours) at 20kV and 120Hz for a total of $>2X10^7$ shots with no degradation of performance.

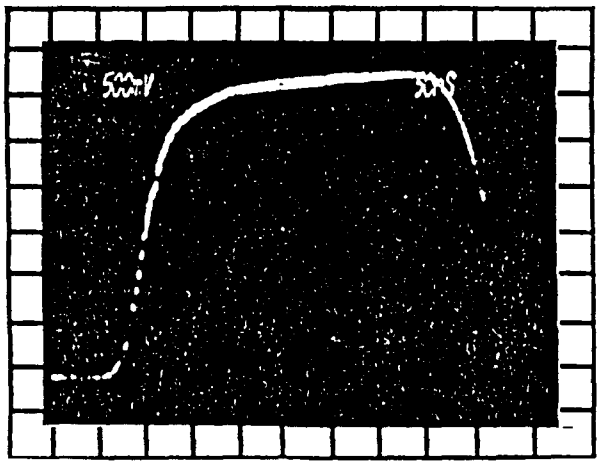

Figure 9. BLT switch current obtained in the ~1ohm PFN at 30kV, 50nsec/div horizontal, 2.5kA/div vertical.

The current waveform obtained with the 1 ohm PFN is shown in figure 9. This current trace was obtained at 30kV at 1Hz. A slight load mismatch resulted in a peak current of about 17kA, followed by current reversal, the rate of rise was $2.5x10^{11}$A/sec, the 40 section PFN results in a very flat pulse shape and the measured current pulse shows no ripple that can be attributed to the switch.

Most modulators are designed at higher impedance levels due to circuit size and component constraints, Results obtained with a 6.5 ohm PFN have demonstrated that the BLT also performs well at these impedance levels. Figure 10 a, shows the current obtained at 20kV, the PFN was not optimized for pulse shape and therefore shows overshoot and ripple. The current shape does not differ greatly from computer modeling results[9] for a similar PFN indicating that the BLT switch is not limiting the performance of this circuit. Figure 10 b, shows the current in this circuit with better time resolution to show the <18nsec risetime. The current shows a smooth rise with no prepulse. The rise from zero to top of overshoot is ~30nsec. The time from zero current to after the overshoot is still <50nsec indicating that with proper circuit compensation the risetime requirements of most modulator systems can be obtained with the BLT switch.

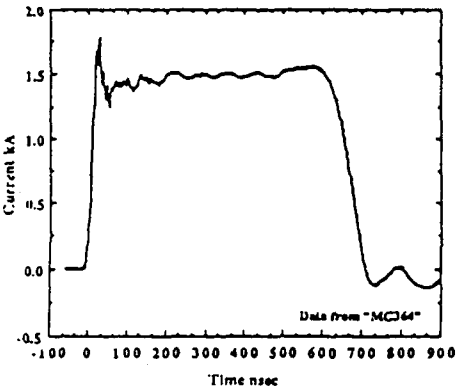

Figure 10 a. BLT current pulse obtained in 6.5 ohm PFN.

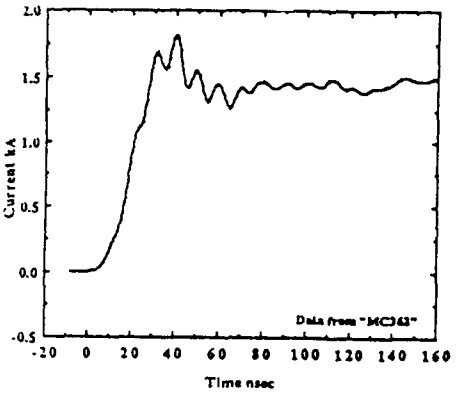

Figure 10 b. BLT current in 6.5 ohm PFN showing <18nsec risetime.

C. High Voltage, High Current BLT Based Modulators

1) Fiber optically triggered Marx bank: Preliminary proof of principle experiments have been used to establish the feasibility of using the BLT switch in optically triggered high power modulators. These experiments were directed at demonstrating the use of BLT switches in modulators requiring simultaneous triggering of many switches. For these experiments demountable switches with O-ring seals were used, therefore high average power and life testing was not possible.

An important advantage of the BLT switch is the optical triggering of the switch which allows many switches to be triggered simultaneously from a

single light source. In multiple switch modulator development this advantage is exploited by using a fiber optic delivery system to distribute light from one source to trigger many switches.

A Marx bank is typically switched by spark gaps operating at or very near self-breakdown. Many stage Marx banks can fail to fire because although the first gap closes, the overvoltage erected by each stage may not be sufficiently large to trigger the following spark gaps. It is therefore common practice in Marx bank technology to trigger more than one gap. However, as a result of the high voltages involved the triggering circuit is affected by feedback from the stage voltage when the individual gaps close. Isolation of individual switches can be very difficult with electrically triggered switches. Optical triggering provides a method to isolate circuits from each other, eliminating the feedback problem.

Figure 11 shows the electrical and vacuum arrangements for a three stage BLT Marx bank. Each BLT is connected from the cathode side to the vacuum and gas handling system through glass valves which provide electrical isolation among the BLTs. The valves also allowed independent variation of the pressure in each switch. The BLTs were triggered simultaneously by an excimer laser pulse through an optical fiber. The laser wavelength and pulse duration were 308nm and 10nsec respectively. The light energy incident at the cathode of each switch was about 3mJ.

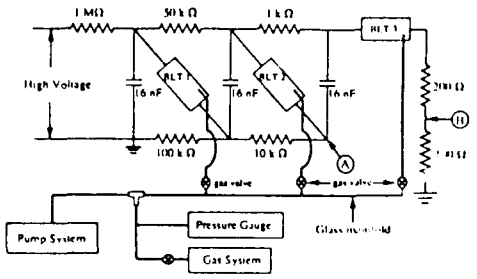

Figure 11. BLT switched Marx bank.

For this work, 16nF capacitors were charged to 35kV and were discharged by optically triggering the BLT1 and BLT2 simultaneously. BLT3 was operated in a self-breakdown fashion as the output switch of the Marx bank giving a maximum peak voltage of 105kV. The output pulseshape depended on the load resistor used and was measured at point B. Using a total load resistance of 300ohm an output pulsewidth of 1600nsec with a risetime of 50nsec was obtained. The Marx bank was operated a a repetition rate of 4Hz.

This experiment demonstrated a BLT based Marx bank designed to obtain medium high voltages, when optically triggered in low repetition rate operation. These results have demonstrated the feasibility of developing modulators that require simultaneous optical triggering of several BLT switches.

2) Design of High Current, High Voltage Transformer Based BLT modulator: The high current capability of the BLT switch make high voltage, high current transformer based modulators possible. A high voltage, high current square pulse to a matched resistive load can be produced by using a transformer in type A pulse forming network. The type A network has the advantage that the pulse shaping circuitry appears on the secondary side of the transformer. This allows the PFN to be designed at the higher impedance level of the secondary circuit resulting in a circuit that can be fabricated with realistic inductance values and readily available capacitors.

When operating at short pulse length, high voltages and low impedance the effects of non-ideal components have a significant effect on the pulse shape obtained. A computer aided PFN design procedure including effects of stray elements has been described by Cravey et al.[10] One result is that an ideal circuit designed for triangular pulse shape actually will give a flat top pulse due to the frequency response limit of the series inductance of the non-ideal capacitors used.

A pulse forming system based on this design procedure will be developed. An air core transformer will be used in the type A PFN. The absence of a magnetic core gives the air core transformer several advantages in this application. The lack of core saturation makes this transformer a friendly companion to the high current BLT switch which also shows no high current limit. The lack of high frequency limits also matches the fast pulse capabilities of the BLT switch. Finally, lightweight makes the air core transformer suitable for space based application.

The transformer uses a single turn primary surrounding several secondary turns with a spiral strip type construction. A preliminary design of the BLT switched air core transformer is shown in figure 12. This transformer design was adapted from previous work at Los Alamos National Laboratory. Utilizing the previous LANL work and other published data the design and fabrication of the pulse transformer should be straightforward and inexpensive. The pulse generator circuit using BLT switch and air core transformer and including inductance due to non ideal components is shown in figure 13.

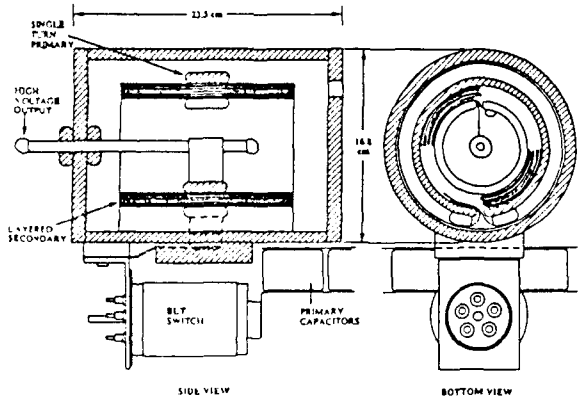

Figure 12. Air core transformer and BLT switch.

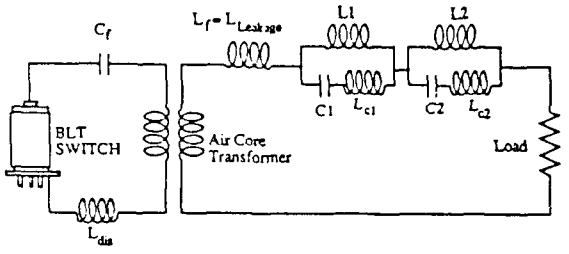

Figure 13. Circuit for the BLT based modulator system. The circuit incorporates the air core transformer in a type A network including inductance to account for non-ideal components.

III. CONCLUSIONS

This work has demonstrated that the BLT switch is capable of improving the performance of high voltage and high current modulators. The scaling of the BLT switch to voltages of 100kV and currents of >80kA has been demonstrated using single and multiple gap switches. Design and preliminary testing of BLT based modulators has been started. In the coming year of work we plan to implement a prototype type A modulator using the BLT switch to produce output pulses with parameters required by induction accelerators and high power microwave systems.

ACKNOWLEDGMENTS

This work was supported by the Strategic Defense Initiative, Office of Innovative Science and Technology, managed by the Office of Naval Research.

Some portions of this work were also supported by the Department of Energy.

M. A. Gundersen is with the University of Southern California, Department of Electrical Engineering, Los Angeles, California, 90089-0484.

REFERENCES

1. G. F. Kirkman and M. A. Gundersen, "Low pressure, light initiated glow discharge switch for high power applications," *Appl. Phys. Lett.*, vol. 49, p. 494, 1986.
2. K. Frank, E. Boggasch, J. Christiansen, A. Goertler, W. Hartmann, C. Kozlik, G. Kirkman, C. Braun, V. Dominic, M. A. Gundersen, H. Reige, and G. Mechtersheimer, "High power pseudospark and BLT switches," IEEE Trans. Plasma Sci., PS-16, 317, (1988).
3. W. Hartmann, G. Kirkman, V. Dominic and M. A. Gundersen, "A superemissive self heated cathode for high power applications," IEEE Trans. Electron Devices, ED-36, 825, (1989).
4. R. H. Fowler and W. Nordheim, "Electron emission in intense electric fields," Proc. R. Soc. London Ser. A 119, 173, (1928).
5. "Electrical breakdown in gases," Edited by J. Meek and J. Craggs, Wiley 1978.
6. T. S, Sudarshan, Investigation of pulsed surface flashover phenomena along dielectric and photoconducting materials," Proceedings of the Third SDIO/ONR Pulse Power Meeting, August 1990, Norfolk VA.
7. M. J. Schonhuber, "Breakdown of gases below Paschen minimum: basic design data of high voltage equipment," IEEE Trans. Power Appar. Syst. PAS-88, 100, (1969).
8. W.C. Nunnally, B. L. Thomas, and G. Kirkman, "Development of an accelerator kicker magnet modulator using a back lighted thyratron, " in Conference Record of the Nineteenth Power Modulator Symposium, San Diego CA, June 1990, p. 87.
9. W. Zhang,S. Y. Zhang, A. V. Soukas, W. W. Frey, "A PFN and transmission line simulation method for energy discharge systems," in Conference Record of the Nineteenth Power Modulator Symposium, San Diego CA, June 1990, p. 74.
10. W. R. Cravey, T. . Burkes, and G. McDuff, Seventh Pulsed Power Conference, p. 116, Monterey CA, 1989.

G. Kirkman-Amemiya, photograph and biography not available at the time of publication.

N. Reinhardt, photograph and biography not available at the time of publication.

M. S. Choi, photograph and biography not available at the time of publication.

Martin A. Gundersen received the Ph.D. degree in physics from the University of Southern California, Los Angeles. From 1973 to 1980 he was with the Department of Electrical Engineering, Texas Tech University, and in 1980 he joined the Department of Electrical Engineering at the University of Southern California, where he is currently Professor of Electrical Engineering. He has been Visiting Professor at the University of California, Los Angeles (1986-1987), Visiting Scientist at the Massachusetts Institute of Technology (MIT) (1986-1987), CERN (1987), and MIT (1989). His research activities are in applied physics in the areas of pulsed power physics, quantum electronics, and semiconductor devices and physics. Quantum electronics research includes development of optically pumped and discharge lasers, and high pulse-energy single-mode IR lasers. Semiconductor research includes the investigation of the physical processes occurring during recombination in semiconductors, optoelectronic devices, and GaAs-based pulsed-power devices. Pulsed power physics research also includes the invention and development of the back-lighted thyratron switch, studies of super-emissive cathode processes in high-current plasma devices, and applications of high-density plasma-based devices to accelerator problems. Dr. Gundersen is a Fellow of the Optical Society of America and the IEEE. He has served as Chairman, IR Lasers Topical Meeting, 1980, Chairman, Power Conditioning Workshop (Dec. 1985), co-Chairman, SPIE Pulsed-Power for Lasers (Jan. 1987), Director of the 1989 NATO Advanced Research Workshop on High Power Glow Switches, Symposium Chair, Pulse-Power for Lasers, 1989 OSA Meeting, Technical Program Chairman, IEEE Power Modulator Symposium, 1990, and Program Chairman, 1991 SDIO/ONR Pulsed Power Meeting.

RECENT ADVANCES IN PLASMA CLOSING SWITCH TECHNOLOGY AT TEXAS TECH UNIVERSITY

T.G. Engel, M. Kristiansen, and A.L. Donaldson

Pulsed Power Laboratory
Department of Electrical Engineering
Texas Tech University
Lubbock, Texas 79409-3102

ABSTRACT

Highlights of recent advances in insulator and electrode performance of high current (up to 500 kA), gas discharge closing switches are reported. The report is taken from two recent Ph.D. dissertations at Texas Tech University and includes the results of surface discharge switch and (coaxial) spark gap studies. Both switches are operated in the self-commutating mode at atmospheric pressure (with a variety of gases) and have tested a wide variety of insulator and electrode materials. Various techniques to improve the performance of insulator and electrode materials have been developed and are also reported.

SUMMARY OF RECENT ADVANCES

Insulator materials research

Insulator performance in the surface discharge switch (SDS) has been the limiting factor of this switch. In terms of switch performance, the triggered SDS has a lower jitter and delay time than the triggered spark gap (SG)[1] (It is noted that reference (1) is an exceptional review of all gas discharge closing switches). However, few insulator materials have been found to withstand the thermal action of the arc discharge. The insulator materials will either decompose, becoming conductive or semiconductive, or melt, suffering severe mass erosion (with a comparable change in holdoff voltage due to switch geometry changes). The expected level of insulator performance is characterized by three parameters: 1) the holdoff voltage degradation resistance (HDR), 2) the mass vaporization coefficient (MVC), and 3) the holdoff voltage conditioning (HVC) figures of merit [2]. These figures of merit are related and given as[2]

$$\mathrm{HVC} = \alpha \mathrm{HDR}, \qquad (1)$$

where α is the water absorption (in % weight). The HDR figure of merit for a simple insulator material (i.e., one metal specie and one gas specie) is given as

$$\mathrm{HDR} = \left[\left(\frac{g}{m}\right)^{2g} w_M^m w_G^g\right]^{\frac{1}{2(m+g)}} e^{\frac{-\Delta G}{(m+g)RT}}, \qquad (2)$$

where w_M and w_G are the molecular weights of the metal and gas species, respectively, and ΔG is the free energy of formation of the generalized formation (or, equivalently, the decomposition) reaction of the insulator material. The variables, m and g, in Eq. (2) are the stoichiometric coefficients of the generalized formation reaction which is given as

$$mM(v) + gG(v) + \leftrightarrow cC(s), \qquad (3)$$

where v and s represent the vapor and gas phase of the specie, respectively. The MVC figure of merit for the simple insulator compound is given as

$$\mathrm{MVC} = \frac{g w_G \mathrm{N}_l}{m\mathrm{HDR}} \qquad (4a)$$

$$= \left[\frac{m}{g}\frac{1}{w_G \mathrm{N}_l}\mathrm{HDR}\right]^{-1}, \qquad (4b)$$

where N_l is the "lifetime" of the material (see below).

The HDR and HVC figures of merit are compared to the experimentally measured performance determined by the surface holdoff voltage response (SVHR) of the material in question. A typical SVHR and its phases are shown in Fig. 1. The HVC figure of merit is compared to the "conditionability" of the insulator material. The conditionability of the material is experimentally measured quantity, N_c, which is the number of discharges which occur at breakdown voltages higher than the

initial voltage, V_{init}. Conditioning effects are attributed to water absorption in the insulator. The HDR figure of merit is compared to the "lifetime" of the insulator material. The lifetime is experimentally measured by the quantity, N_l, which is the number of discharges required to reduce the surface holdoff voltage to the half-power level (i.e., $V_{init}/\sqrt{2}$) for three consecutive discharges. The reduction of the surface holdoff voltage is attributed to the decomposition of the insulator into conductive, or semiconductive, species. The MVC figure of merit is compared to the mass erosion of the insulator material. Vaporization is the only mechanism considered to cause mass erosion.

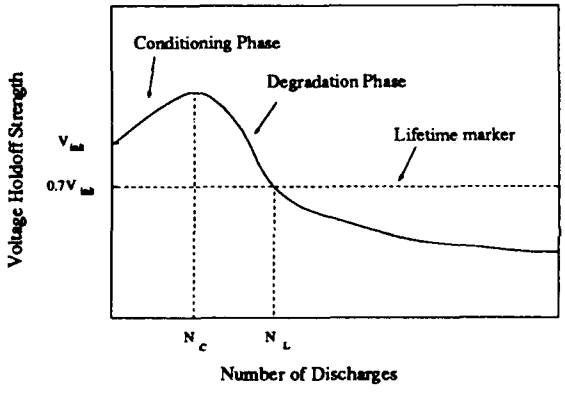

Figure 1. A typical SVHR, its phases, and the experimentally measured parameters of interest.

Many factors have been shown to affect the performance of a given insulator material[2]. In general, the performance of a given insulator material is affected by the level of U.V. radiation that reaches its surface. If the radiation level is decreased, then a corresponding decrease in the amount of chemical bond rupture and mass erosion can be expected. The polymeric and elastomeric materials are especially susceptible to changes in radiation levels. The radiation level is effectively reduced through choice of electrode material, ambient gas, or the use of U.V. absorbing chemicals (i.e., stabilizers). Graphite electrodes, due to a low atomic Z, produce lower U.V. levels in the spectrum of the discharge than do higher atomic Z materials, such as molybdenum and tungsten. Figure 2 illustrates the response of the G-10 thermoset polymer to changes in electrode materials. A similar type of effect is noted for discharges in various gases.

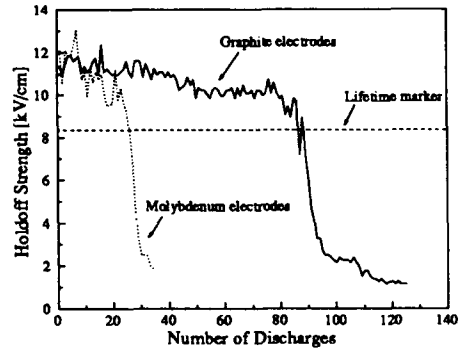

Figure 2. Illustrating the response of the G-10 thermoset polymer to changes in electrode material.

Other factors which affect the performance of a given insulator material include the discharge repetition-rate. This is illustrated in Fig. 3 for the aluminum titanate ceramic. In this experiment, the discharge rep-rate is varied from a continuous mode (~ one discharge per second) to a burst mode (5 discharges at ~one discharge per second, wait ~ 45 seconds, repeat).

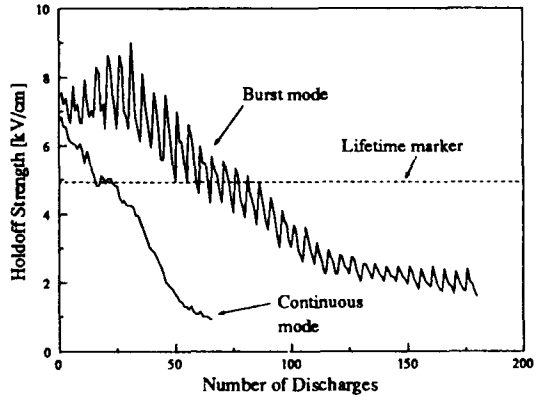

Figure 3. Illustrating the effect of discharge repetition-rate on the performance of the aluminum titanate ceramic.

Electrode materials research

The major mechanisms responsible for material melting, vaporization, and removal have been identified as functions of physical and design variables. These mechanisms have been incorporated into models that predict electrode erosion rates [3]. Figure 4 illustrates the typical "S" shaped curve obtained for a typical electrode material. This figure also illustrates the changes produced in the erosion curve by arc motion. Moving arcs have been employed to reduce electrode erosion. Reduced erosion rates of electrode materials have been noted in the rails of electromagnetic launchers after the armature (i.e., arc) has attained a certain velocity.

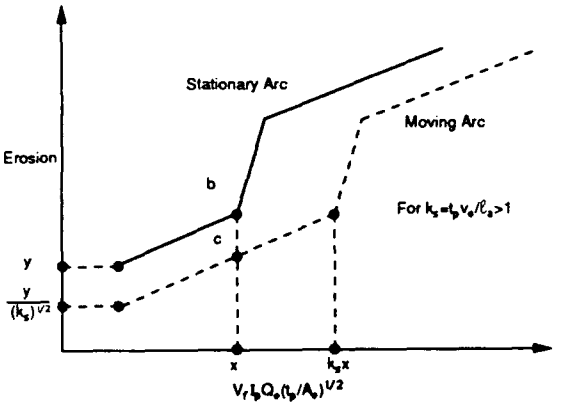

Figure 4. Illustrating an erosion curve obtained for a typical electrode material and the effects produced by arc motion (V_f, I_p, Q_e, t_p, A_e, y, and k_s are the cathode fall voltage, peak current, effective charge transferred, pulse length, effective arc attachment area, normalized volume erosion, and the coefficient of solid removal, respectively).

Techniques have also been developed to reduce the erosion of electrode materials up to an order of magnitude. Figure 5 illustrates the "shielding" technique applied to copper electrodes.

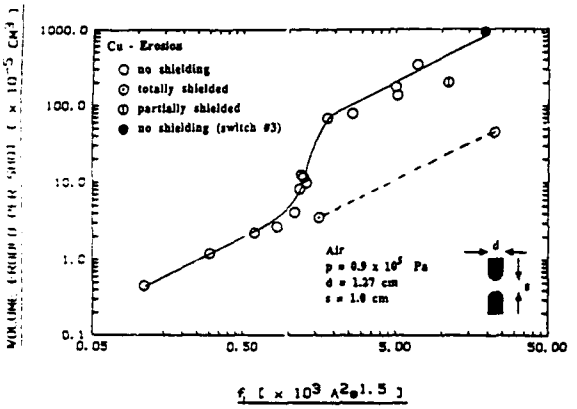

Figure 5. Illustrating the "shielding" technique applied to copper electrodes to reduce the erosion up to an order of magnitude.

Erosion and lifetime curves have been produced which reflect the state-of-the-art in electrode material performance from a variety of experimentalists. These curves are given in Fig. 6 (as a function of integrated charge) and in Fig. 7 (as a function of peak current). Models have also been refined and developed[4,5] which describe the expansion and resistance of high current, pulsed discharges.

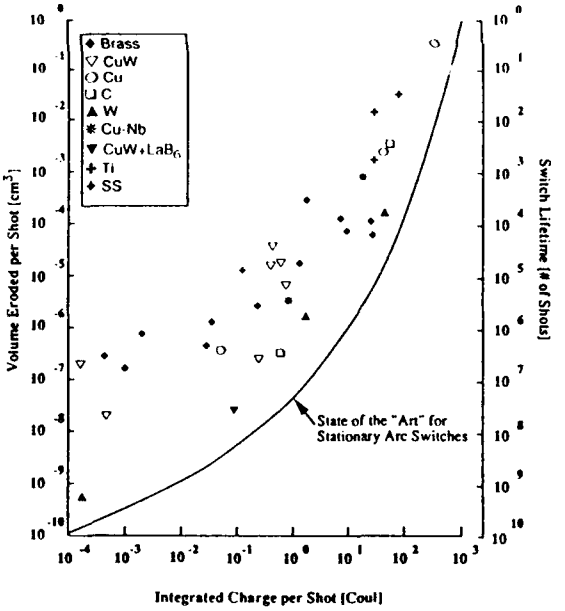

Figure 6. Comparison of the "best" electrode material erosion as derived from various experimentalists as a function of integrated charge.

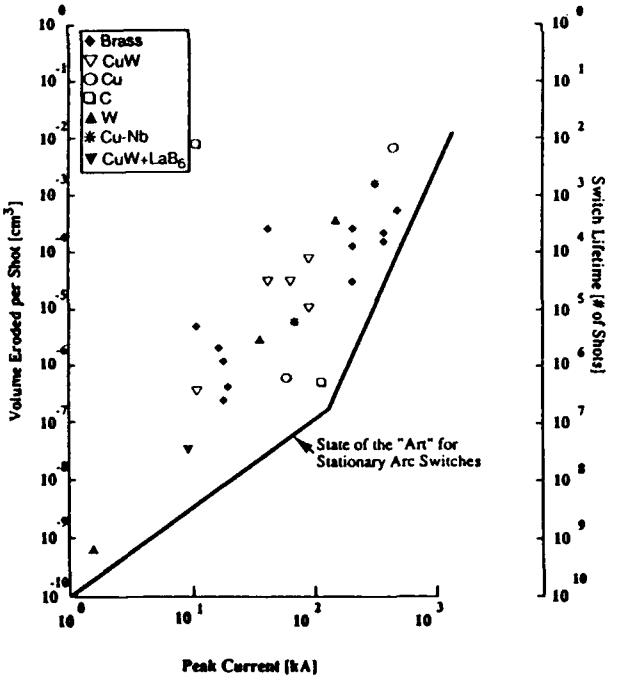

Figure 7. Comparison of the "best" electrode material erosion as derived from various experimentalists as a function of peak current.

FUTURE RESEARCH

Future research will be directed towards the development of state-of-the-art surface discharge (multi and single channel) and spark gap switches utilizing the techniques and advances outlined above. The switches will operate at higher currents (~ 1 MA), rep-rates (~ 10 pulses per second), higher coulomb transfers (~ 10^3 coulomb per discharge), and longer lifetimes (10^6 discharges). Future research will also be directed to better modeling of the arc discharge and its associated properties (i.e., expansion, resistance, etc.).

ACKNOWLEDGEMENTS

This work was supported by SDIO/T/IS through DNA/RAEV and the Texas Tech University Center for Energy Research.

REFERENCES

[1]. G. Schaefer, M. Kristiansen, and A. Guenther, eds., Advances In Pulsed Power Technology, Volume 2, Gas Discharge Closing Switches, Plenum Press, New York, 1990.

[2]. T.G. Engel, "Insulator degradation by high current discharges," Ph.D. Dissertation, Texas Tech University, December, 1991.

[3]. A.L. Donaldson, "Electrode erosion in high current, high energy transient arcs," Ph.D. Dissertation, Texas Tech University, December, 1991.

[4]. T.G. Engel, A.L. Donaldson, and M. Kristiansen, "The pulsed discharge arc resistance and its functional behavior," IEEE Trans. on Plasma Sci., vol. PS-17, no. 2, pp 323-329, 1989.

[5]. T.G. Engel, M. Kristiansen, and H. Krompholz, "Channel expansion in hydrogen arcs driven by oscillating currents," to appear in IEEE Trans. on Plasma Sci., October, 1991.

T. G. Engel, photograph and biography not available at the time of publication.

M. Kristiansen, photograph and biography not available at the time of publication.

A. L. Donaldson, photograph and biography not available at the time of publication.

BREAKDOWN CHARACTERISTICS IN NONPLANAR GEOMETRIES

Hoyoung Pak and Mark J. Kushner

University of Illinois
Department of Electrical and Computer Engineering
1406 W. Green Street, Urbana, IL 61801

***Abstract*-Breakdown voltages of gases in parallel plate geometries are well represented by Paschen's law, whose scaling parameter is pd (gas pressure x electrode separation). In nonplanar geometries, Paschen's law is not directly applicable due to the ambiguity in the distance between the electrodes and distortion of the electric field. In this paper, a Monte Carlo computer model is used to investigate breakdown characteristics in nonplanar geometries and hollow cathode switches in particular. The model tracks the trajectories of both electrons and ions, including ionizing collisions in the gas phase by electrons and ions, and secondary electron emission by ions on surfaces. We find that under typical operating conditions in helium (0.1 to a few Torr, voltages of 10s kV, effective electrode separation of mm's), approximately two-thirds of ionizing collisions are attributable to ion impact, of which half are due to ion impact in the gas phase.**

I. INTRODUCTION

The breakdown of gases in parallel plate geometries has been studied for many years [1], and has resulted in a well known characterization of the breakdown voltage called as Paschen's law. This relationship states

$$V_b = F(p \cdot d) \qquad (1)$$

where V_b is the breakdown voltage, p is the gas pressure, and d is the electrode separation.. The generalized breakdown condition is obtained by determining the voltage, for a given pd, at which the generation of electrons by direct electron impact (e.g., ionization, detachment) and secondary processes (e.g., photoionization, ion impact on electrodes), and the losses of electrons (e.g., attachment) result in at least a self sustaining current. In its simplest form, the current in a plane parallel gap in a nonattaching gas is given by

$$I = I_o \exp(\alpha d)/(1-(\omega/\alpha)(\exp(\alpha d)-1)) \qquad (2)$$

where α (cm^{-1}) is the first Townsend coefficient for ionization, and ω (cm^{-1}) is an effective secondary ionization coefficient. (ω/α) is the number of secondary electrons produced for every primary ionization in the gas phase. In most cases, α is a strong function of E/N (electric field/gas number density) while ω is a weak function of E/N. ω accounts for a number of secondary processes, including ion impact on the electrodes, photoionization, and ion impact in the gas phase. Breakdown is that voltage which satisfies

$$(\omega/\alpha)(\exp(\alpha d)-1) = 1. \qquad (3)$$

The dependence of V_b on pd for plane parallel electrodes shown in Fig. 1. Paschen's law specifies a minimum breakdown voltage occurs at a pd_o of a few Torr-cm. The increase in V_b at values of $pd < pd_o$ results from the decreasing likelihood of ionizing collisions caused by the decrease in the area density of gas. The increase in V_b at values of $pd > pd_o$ results from the requirement that one must have a critical value of E/N to achieve a self sustaining current.

Departures from Paschen's law results from both nonequilibrium and geometrical effects. The formulation of Paschen's law requires that the ionization coefficient be a well characterized function of E/N. If the electrons are not in equilibrium with the local value of E/N, then electron multiplication across the gap cannot be explicitly given by $\exp(\alpha d)$. A first order correction for this effect is to express electron multiplication across the gap as $\exp(\alpha(d-d_o))$ where d_o is the distance required for electrons to drift before coming in equilibrium with the electric field.

Geometrical effects are primarily manifested by E/N being a function of position between the electrodes, as in cylindrical or point-to-plane structures. Assuming that the electron energy distribution is in equilibrium with the local electric field (commonly called the local field

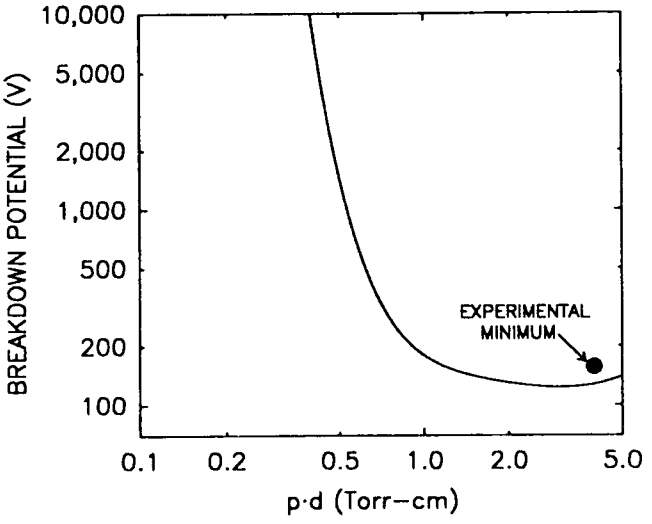

Figure 1. Simulated Paschen curve for breakdown between parallel plates in He. The experimental minimum breakdown voltage is at pd = 4 Torr-cm [Ref. 10].

approximation) the electron multiplication crossing the gap across in nonplanar geometries is given by

$$M = \int p(\vec{s}) \exp\left(\int_{\vec{r}(s)} \alpha(E(r)/N) d\vec{r}\right) d\vec{s} \qquad (4)$$

where $p(\vec{s})$ is the probability for electron emission occurring at location $\vec{s}$ on the cathode and $\vec{r}(\vec{s})$ is the path along the electric field from that location. In symmetric geometries, such as coaxial cylinders, $p(\vec{s})$ is a constant. In point-to-plane geometries, $p(\vec{s})$ is heavily weighted towards the high field region near the point. Under conditions where the local field approximation is not valid and geometrical effects are important, semianalytic expressions for V_b become increasingly less accurate.

In gases such as He and H_2, ion energies can reach many hundreds of eV for holdoff voltages of only a few kV. In recent work by Phelps and Jelenkovic [2], the importance of accounting for excitation and ionization by heavy particle impact (energetic ions and neutrals) was investigated at high E/N. They found that experimental observations of excited state emission could not be explained on the basis of electron impact excitation alone,and was largely attributable to ion impact. In He, the cross section for ion impact ionization exceeds that for electron impact at energies >200 eV [3]. In conventional dc or pulsed discharges, this condition is of little consequence since ions have a low probability of being accelerated to those energies. During high voltage holdoff in, for example, thyratrons ions can exceed those energies, and therefore significantly contribute to ionization.

The relative rate of secondary electron emission from the cathode by ion bombardment, γ, is also a strong function of ion energy. γ is nearly constant at energies of less than a few hundred eV. γ normally increases with increasing energy, and can exceed unity for energies greater than a few keV [4]. The rate of secondary electron emission by ion bombardment is also a sensitive function of the surface of the cathode. γ is typically small for clean surfaces, and larger for oxidized surfaces.

In this paper, we theoretically investigate the breakdown of gases in hollow cathode plasma switches where both geometrical and nonequilibrium effects are important. The particular switch of interest is the optically triggered pseudospark [5,6] which consists of opposing hollow cathode and anodes having central holes (see Fig. 2). The pseudospark has found application as both a particle beam generator and as a plasma switch. The optically triggered pseudospark has demonstrated high currents (I > 30 kA), high current densities ($I > 10^4$ A-cm^{-2}) and high rates of current rise ($dI/dt > 10^{11}$ A-s^{-1}). Its interesting properties include its compact size, thereby reducing inductance, and its ability to electrically float. Due to the nonplanar geometry of the pseudospark, Paschen's law is difficult to apply. This results both from the nonequilibrium nature of the electron transport and from the difficulty in defining an effective path length. Since pseudosparks operate on the "near side" of Paschen's curve (increasing V_b with decreasing pd), electrons having longer paths will decrease V_b due to their having more opportunity to avalanche before reaching the anode. Since the spatial distribution of the electric field, both in the gap and in the hollow electrode structures, depends on parameters such as the electrode separation, electrode thickness and electrode hole radii, V_b will also depend on these quantities.

II. DESCRIPTION OF THE MODEL

The model we have used in this study is a 3-dimensional Monte Carlo simulation. Since the sources of ionization in high voltage devices depend on the energy distributions of both electron and ions, the trajectories of both of these species are accounted for in the model. He is used as the gas in this study, a choice based on the observation that He has superior holdoff abilities compared to H_2 under many conditions. The geometry used in this study is that of the optically triggered pseudospark, and is shown in Fig. 2. The dimensions and thickness of all of the electrode structures, as well as their surface properties, can be specified in the model.

The simulation begins by calculating the electric field by solving Poisson's equation. Since during the breakdown stage deformation of the electric field by space charge is minimal, the vacuum fields are used in this study. Poisson's equation is solved using the method of successive over relaxation. The numerical mesh used for this purpose is nonuniform, with a higher density of mesh points in the gap and in the high field regions.

The mechanics of the Monte Carlo simulation will briefly be discussed. The trajectories of the electron and ion particles are advanced for a time Δt based on a number of criteria. The time step is chosen to be the smaller of the time required to travel a distance over which the electric changes by a specified amount and the time to the next collision. The null collision method is used to select the

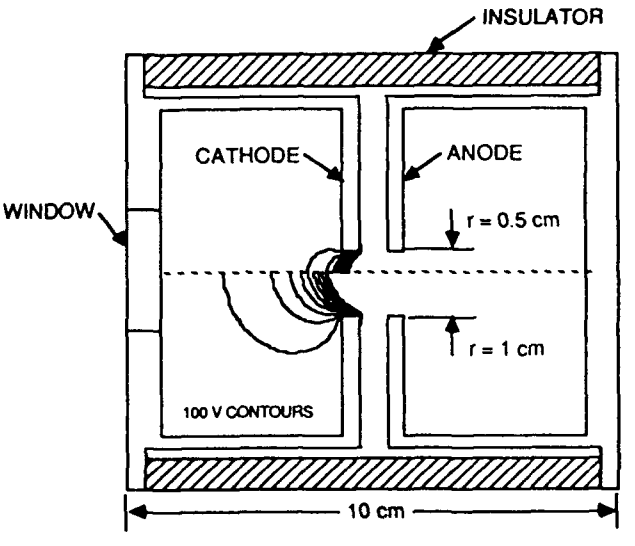

Figure 2. Schematic of the optically triggered pseudospark switch which consists of an opposing cylindrical hollow cathode and anode with central holes. The device is triggered by UV illumination through the window and typically operates at gas pressures of < 1 Torr. Two views are shown having cathode hole radii of 0.5 cm and 1 cm. Electric potential contours (0 - 1 kV, 100 V spacing) are shown for a holdoff voltage of 10 kV. More potential penetration into the cathode occurs with the larger hole.

time between collisions. This method is used because a particle's energy can change from thermal values to many keV between collisions and there is a commensurate change in the particle's collision frequency. This makes the initial choice of collision time ambiguous. In the null collision method, a fictitious cross section is added to the real cross section at every energy so that the total collision frequency appears to be a constant. With this condition the time to the next collision is given by

$$\Delta t = - (1/\nu_t)\ln(r) \qquad (5)$$

where ν_t is the total collision frequency including the null contribution and r is a random number evenly distributed on (0,1). At the time of the collision, a second random number is chosen. If $r < \nu(\varepsilon)/\nu_t$, where $\nu(\varepsilon)$ is the actual collision frequency at the current energy, then a collision occurs. If the inequality does not hold, the collision is said to be null, and the particle proceeds unhindered.

In case of a real collision, another random number is used to determine the type of collision. If the collision is an ionization by an electron, a secondary electron is placed at the site of the ionization. The energy of the secondary electron is given by an extrapolation of the data of Opal, Peterson and Beatty [7]. For an ionizing collision by an ion, the secondary electron is assumed to have only thermal energy. The energy of the primary particle is reduced by the inelastic energy loss and is anisotropically scattered. The scattering angle for electrons is energy dependent, being isotropic at low energies and becoming forward scattered at higher energies. In ion charge exchange collisions, the energy of the new ion is assumed to be thermal with an isotropic trajectory. In ion impact collisions resulting in an ionization, the scattering is assumed to be forward.

The flow of the computer model is as follows. A preselected number of electrons are uniformly released from the cathode surface having an average energy of a few eV. Electrons are then transported in the electric field while the number and location of ionizing collisions are recorded. The next step is to transport ions, with an ion being started at the location of each of the previous ionizations by electrons. The location of the heavy particle ionizing collisions are similarly recorded. When an ion strikes the cathode, an appropriate number of electrons are released as specified by the secondary electron emission coefficient. The transport of ions progresses until all ions are collected. Any electrons previously generated by ion impact are then transported. At this point, the first "wave" of particle transport has been completed. Breakdown is said to occur if the number of electrons generated by electron and ion impact compared to the initial number released indicates exponential multiplication. If breakdown does not occur, or better statistics are required, additional "waves" of electrons can be released.

Cross sections for electron impact processes were obtained from Refs. 8 and 9. Cross sections for ion impact processes in the gas phase were obtained from the compilation of Janev et al [3]. Secondary emission coefficients as a function of ion energy for the Mo cathode were scaled from Ref. 4.

III. BREAKDOWN CHARACTERISTICS

A. Breakdown Voltages

To validate our model, we simulated breakdown voltages for plane parallel geometries. Our predicted breakdown voltages as a function of pd are shown in Fig. 1. The minimum potential at which breakdown occurs is approximately 150V which corresponds to pd_o = 4.0 Torr-cm and agrees well with experiments [10]. On the left side of the minimum, commonly known as the near side of Paschen's curve, holdoff voltage increases with decreasing pd because of the increasing mean free path of electrons relative to the electrode separation. This results in a decreasing probability of ionizing collisions. At high gas pressures and large electrode separations, higher voltages are required to break down the gas because of the necessity to maintain a critical E/N.

As perturbations to the electric field are introduced due to nonplanar geometries, deviations from Paschen's law are expected. Using the geometry of the optically triggered pseudospark, the dependence of breakdown voltage on cathode hole radius is shown in Fig. 3 for various gas pressures. The electrode separation is 0.5 cm and the thickness of the cathode is 0.4 cm. For a given gas pressure, breakdown occurs above the curve while holdoff occurs below the curve. As the cathode hole radius increases, the holdoff voltage decreases due primarily to increased penetration of the anode potential through the cathode hole into the interior of the hollow cathode, as shown in Fig. 2. This increases the effective path length d through regions which have a high electric field. In this respect, increasing the radius of the cathode hole can be viewed as being equivalent to increasing the electrode separation of parallel plane electrode geometries. For a given cathode hole radius, the holdoff voltage decreases with increasing pressure, commensurate with operating on the near side of Paschen's curve.

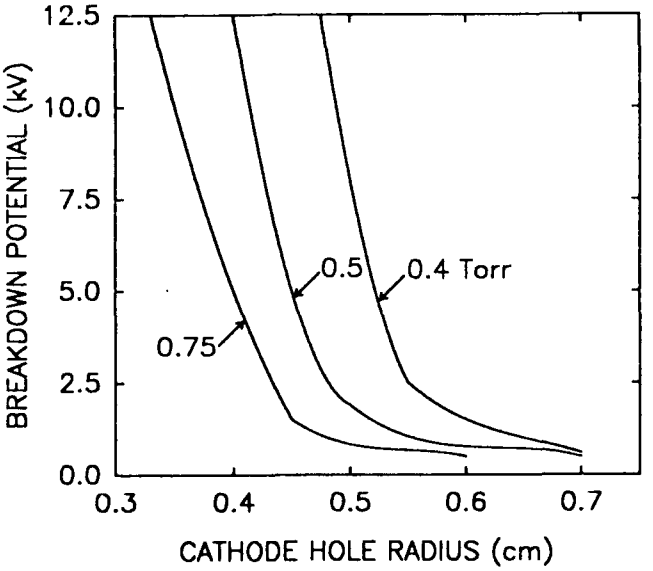

Figure 3. Breakdown voltage as a function of cathode hole radius for various He gas pressures. The electrode separation is 0.5 cm and the cathode thickness is 0.4 cm. Operating with large cathode holes effectively increases pd.

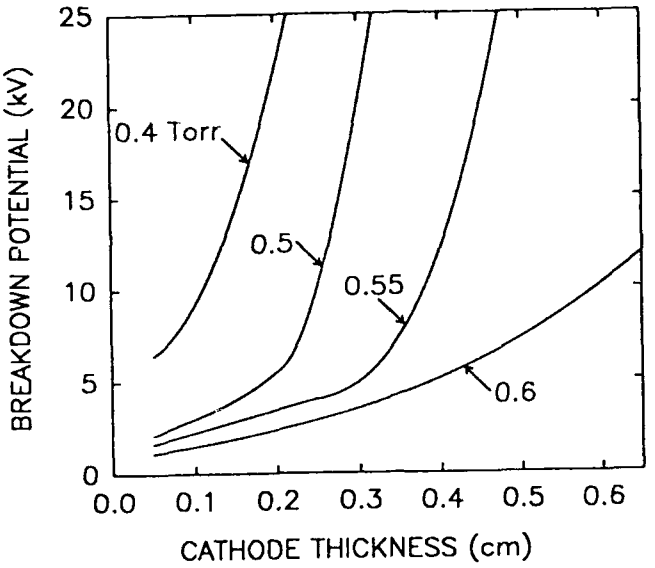

Figure 4. Breakdown voltage as a function of cathode thickness for various He pressures. The electrode separation is 0.5 cm. Increasing the cathode thickness decreases potential penetration, and effectively decreases pd.

The dependence of V_b on the width of the cathode at various gas pressures is shown in Fig. 4. The electrode separation of 0.5 cm and the radius of the electrode holes are 0.4 cm. V_b increases with increasing electrode thickness due to a reduction in the penetration of anode potential into the hollow cathode thereby effectively reducing d . Smaller cathode hole radii or larger cathode thickness cause the breakdown relationship to more closely represent Paschen's relationship. For cathode thickness exceeding 0.5 cm, breakdown is caused by electron avalanche occurring at the front face of the cathode. For thicknesses less than this value, avalanche occurs dominantly adjacent to the cathode hole in the interior of the cathode, an indication of long path breakdown (see below.)

B. Electron Impact Ionization

The locations of at which electron impact ionizations occur are shown in Fig. 5 for plane parallel and hollow electrode geometries. The gas pressure is 0.5 Torr and the holdoff voltage is 10 kV. In the plane parallel geometry, electron impact ionizations are randomly distributed as a function of radius, a consequence of their initial distribution being random across the face of the cathode. The locations of the ionizations are fairly close to the cathode within the gap. This latter point is a consequence of there being a maximum in the cross section for electron impact ionization at 130 eV. Therefore, electrons are more likely to undergo ionizations when they have lower energies, which occurs near the cathode.

In hollow cathode electrode structures, though, ionizations occur predominantly near the central hole by electrons initially emitted from the inside of the cathode. This behavior is a consequence of the electrons in the hollow cathode spending a longer time in the moderate electric fields resulting from potential penetration into the cathode. They also have a longer effective path length to the anode resulting in a large pd. Once the electrons convect into the high field region in the gap proper and accelerate to energies greater than the peak in the ionization cross section, the rate of ionization decreases. The amount of ionization which occurs in the hollow anode is minimal, since the effective mean free path there is many cm.

C. Ion Impact Ionization and Ion Energy Distributions

The contribution of ion impact processes to ionization can be substantial, and in some cases exceed that by electrons. The fractional contributions of electron impact, ion impact in the gas, and ion impact on surfaces are shown in Fig. 6 as a function of gas pressure. The holdoff voltage is 10 kV. At large values of V/p, the total contribution of ion impact to ionization is approximately twice that by electron impact, with the contribution by ion impact in the gas phase and on the cathode being nearly equal. As the gas pressure increases, the fractional contribution from electron impact increases primarily at the expense of ion impact on

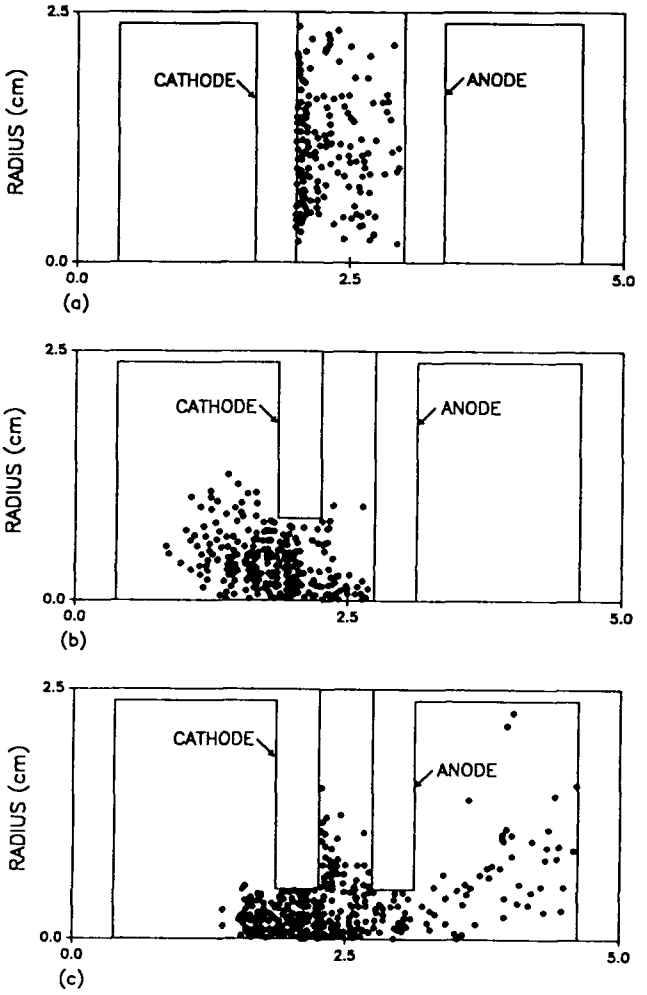

Figure 5. Locations of electron impact ionization events for a) plane parallel, b) hollow cathode and c) hollow anode geometries. The He gas pressure is 0.5 Torr and holdoff voltage is 10 kV. The locations of electron impact ionization are primarily on the cathode side of the gap.

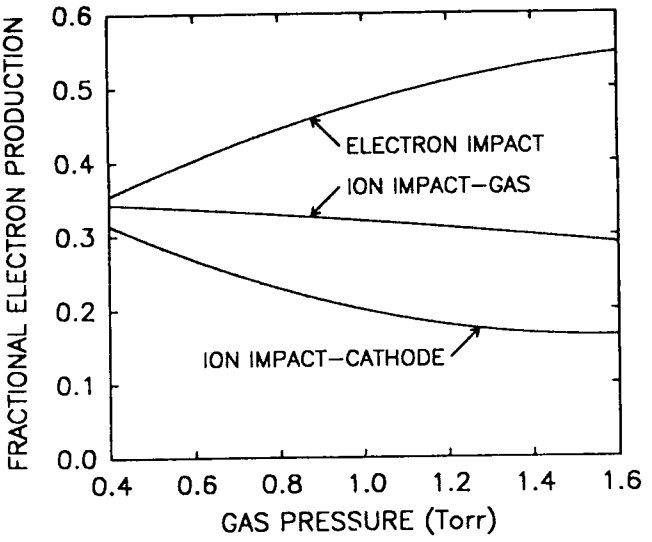

Figure 6. Fractional contributions to electron production by electron impact, ion impact in the gas and ion impact on the cathode for He with a holdoff voltage of 10 kV. For pressures below 1 Torr, the majority of electron production is due to ion impact processes.

the cathode. Under most conditions, the contribution by ion impact in the gas phase exceeds that by ion impact on surfaces.

These large contributions by ion impact to ionization are a consequence of the high ion energies which can be generated during holdoff. The distribution of ion energies striking the cathode for a pressure of 0.5 Torr, and holdoff voltage of 10 kV is shown in Fig. 7. The ion energy distribution is fairly broad, with a tail that extends to the full anode potential. The average ion energy striking the electrode is 630 eV for these conditions, which corresponds to a secondary electron emission coefficient of 0.6.

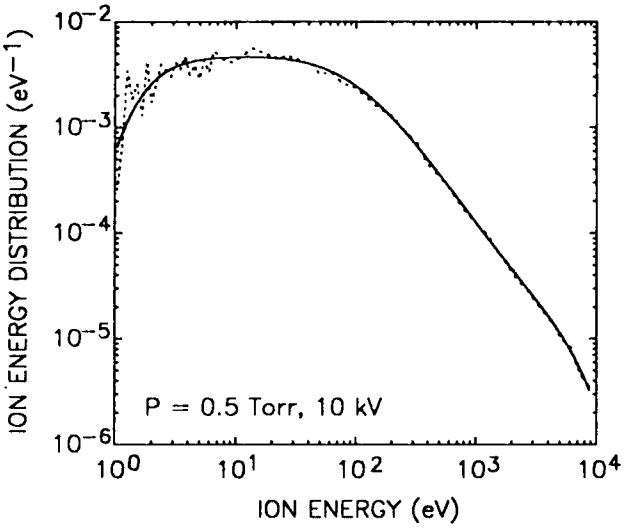

Figure 7. Ion energy distribution striking the cathode for a holdoff voltage of 10 kV in 0.5 Torr He. The dotted line is raw data and the solid line is a polynomial fit. The average ion energy striking the cathode is 630 eV, with the maximum ion energy extending to the anode potential.

IV. CONCLUDING REMARKS

A Monte Carlo model has been developed to study holdoff in nonplanar geometries, and in the optically triggered pseudospark in particular. Deviations from Paschen's curve resulting in lower holdoff voltages are caused by penetration of anode potential into the hollow cathode making a larger effective pd. Penetration increases with increasing cathode hold radius and decreasing cathode thickness, and so holdoff voltage decreases. The contribution of ion impact to ionization is substantial, and can exceed that due to electron impact. The average energy of ions striking the cathode during holdoff and the beginning of commutation is many hundreds of eV, and have maximum values of nearly the anode potential.

ACKNOWLEDGMENTS

This work was supported by SDIO/IST under management of the Office of Naval Research (N00014-90-J-1967) and by the National Science Foundation (ECS88-15781, CBT88-03170)

REFERENCES

[1] J. M. Meek and J. D. Craggs, *Electrical Breakdown of Gases* ,Wiley, Norwich, 1978; and references therein.

[2] A. V. Phelps and B. M. Jelenkovic, "Excitation and breakdown of Ar at very high ratios of electric field to gas density", *Phys. Rev. A* , vol. 38, pp. 2975-2990, 1988.

[3] R. K. Janev, W. D. Langer, K. Evans and D. E. Post, *Elementary Processes in Hydrogen-Helium Plasmas*, Springer, Berlin, 1987, ch. 2 and 5.

[4] B. Szapiro and J. J. Rocca, "Electron emission from glow discharge cathode materials due to neon and argon ion bombardment", *J. Appl. Phys.*, vol. 65, pp. 3713-3716, 1989.

[5] W. Hartmann and M. A. Gundersen "Cathode related processes in high current density low pressure glow Discharges" in *Physics of Pseudosparks*, edited by M. A. Gundersen and G. Schaefer, Plenum, New York, 1990, pp. 77-88.

[6] W. Hartmann, V. Dominic, G. F. Kirkman and M. A. Gundersen, "An analysis of the anomalous high current cathode emission in pseudospark and back-of-the-cathode lighted thyratron switches," *J. Appl. Phys.*, vol. 65, pp. 4388-4395, 1989.

[7] C. B. Opal, W. K. Petersen and E. C. Beatty, "Measurements of secondary electron spectra produced by electron impact ionization of a number of simple gases," *J. Chem. Phys.*, vol. 55, pp. 4100-4106, 1971.

[8] M. Hayashi, "Recommended values of transport cross sections for elastic collision and total collision cross section for electrons in atomic and molecular gases", Nagoya Institute of Technology Report IPPJ-AM-19, 1981.

[9] D. Rapp and P. Englander-Golden, "Total cross sections for ionization and attachment by electron impact: I. Positive ionization", *J. Chem. Phys.*, vol. 43, pp. 1464-1479, 1965.

[10] M. J. Schonhuber, "Breakdown of gases below Paschen minimum: Basic design of high-voltage equipment," *Trans. Power Apparatus Systems*, vol. PAS-88, pp. 100-107, 1969.

Hoyoung Pak was born on September 13, 1965 in Seoul, Korea. He received the B.S. degree in Electrical Engineering from the University of Illinois in 1987, where he also obtained the M.S. degree in 1988 and the Ph.D. degree in 1991. The subject of his Ph.D. thesis was on modeling nonequilibrium aspects of hollow electrode devices, particularly pseudosparks and back-lit thyratrons. Dr. Pak is currently a postdoctoral research fellow at Sandia National Laboratory (Albuquerque) where he is developing computer models for plasma etching reactors.

Mark J. Kushner was born in Los Angeles, California, on December 21, 1952. He received the BA degree in Astronomy and the BS degree in Engineering from the University of California at Los Angeles in 1976. His MS and PhD degrees in Applied Physics were received from the California Institute of Technology in 1977 and 1979, respectively, where he also held the position of Chaim Weizmann Postdoctoral Research Fellow. Dr. Kushner served on the Technical Staffs of Sandia National Laboratory and Lawrence Livermore National Laboratory before joining Spectra Technology Inc. (formerly Mathematical Sciences Northwest). At Spectra Technology, he was a Principal Research Scientist and Director of Electron, Atomic, and Molecular Physics. In August of 1986, Dr. Kushner joined the University of Illinois (Urbana-Champaign) where he currently holds the rank of Professor in the Department of Electrical and Computer Engineering. Dr. Kushner has published 70 refereed papers and presented more than 125 conference papers on topics related to gas and solid state lasers, pulse power plasmas, plasma chemistry, chemical lasers, plasma processing of semiconductors, plasma treatment of toxic gases, and laser spectroscopy. Dr. Kushner is a member of Phi Beta Kappa, Tau Beta Pi, Eta Kappa Nu, Sigma Xi, the Optical Society of America, and the Materials Research Society. He is also a Fellow of the American Physical Society and of the IEEE.

MAGNETIC CONTROL OF HOLLOW CATHODE DISCHARGE SWITCHES

K.H. Schoenbach and G.A. Gerdin

Physical Electronics Research Institute
Old Dominion University
Norfolk, VA 23529

ABSTRACT

The electrical breakdown of hollow cathode discharges in helium was studied by means of electrical and optical diagnostic techniques. The results indicate that the breakdown occurs in two stages. A filamentary, highly resistive discharge along the axis of the hollow cathode is first established by Townsend mechanism. The resulting distortion of the electric field causes a radial breakdown into a low resistance discharge at the orifice of the cathode hole. Through application of axial magnetic fields the transition into the high current discharge could be delayed or even inhibited. With an electrode geometry designed to enforce a continuing radial current flow after breakdown into the high current discharge, it was possible to modulate the discharge resistance by more than a factor of five using transient axial magnetic fields. It was shown experimentally and theoretically, by means of a Monte-Carlo code, that magnetic modulation of hollow cathode discharges is a threshold effect in magnetic field intensity. This and the fact that it is possible to run hollow cathode discharges in paralell could allow to use magnetically controlled multi-channel hollow cathode switches as high current modulators or opening switches with subOhm on-resistance, microsecond response time, and multi-kHz repetition rate.

INTRODUCTION

Although it is known for over 70 years that hollow cathode discharges can carry currents which are orders of magnitude higher than in discharges with plane cathodes, it is only in the past two decades that this effect is utilized in high current hollow cathode switches.[1,2,3,4] These switches allow high current densities with unheated cathodes without the usual erosion associated with an arc.

In order to fully utilize the potential of hollow cathode discharges as closing and possibly opening switches, it is important to understand the temporal development of the electrical breakdown and the physics of the steady-state phase of the discharge. Experimental investigations on the temporal and spatial development of the breakdown indicate that the buildup of hollow cathode discharges is well separated into a slow, low current predischarge and a fast high current main discharge.[5,6] Computer simulations of the breakdown phase[7,8] agree qualitatively with corresponding experimental results.

Optical and electrical studies of hollow cathode discharges suggest a simple two-stage model for the temporal and spatial development of the discharge[9] which describes the discharge up to the buildup of the super dense glow, the third and final stage. The results indicate a strong influence of axial magnetic fields both on the development and the sustainment of the hollow cathode discharge in at least the first two stages. Research results on the use of magnetic fields as a means to modulate the switch current and ultimately to open the hollow cathode switch are discussed in the following.

FORMATION OF THE HOLLOW CATHODE DISCHARGE

A. Experiment

1. Experimental setup. A linear discharge system was used to study the temporal development of a hollow cathode discharge in helium.[9] A cross-sectional view of the discharge chamber is shown in Fig. 1. The hollow cathode, made out of brass, incorporates a cylindrical hole of 0.86 cm diameter and a depth of 1.4 cm. The distance from the bottom of the cathode hole to the anode could be varied from 2.5 to 4.5 cm. The discharge was driven by a 50 Ohm pulse forming network (PFN) which can be charged up to 15 kV and provides a 10 μs pulse into a matched load.

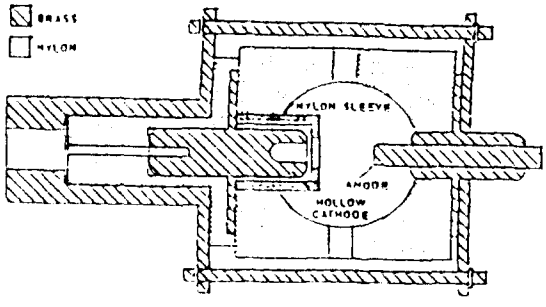

FIG. 1. Cross sectional view of the hollow cathode discharge chamber.

A semi-steady-state magnetic field along the discharge axis was generated by means of a magnetic field coil which was placed over the discharge chamber. The magnetic field circuit produces a critically damped current pulse with the current peak at approximately 700 μs and an e-folding decay time of 1.5 ms. The corresponding peak magnetic field is 0.3 T. Because of the long duration of the magnetic field pulse compared to the discharge duration, which is determined by the 10 μs electrical pulse, the magnetic field can be considered as constant for the time of the discharge. The amplitude of the magnetic field intensity can be adjusted to any value between zero and 0.3 T by simply varying the delay of the electrical discharge with respect to the onset of the magnetic field pulse.

2. Experimental results. The temporal development of the hollow cathode discharges was investigated by means of current and voltage measurements with the applied voltage and the gas pressure as variable parameters. The typical shape of the current signals is shown in Fig. 2. The discharge always begins with the breakdown into a high impedance mode. The maximum discharge current varies between 10's to hundred's of mA's, depending on the applied voltage and the operating gas pressure. The current decays exponentially with a time constant of about 800 μs. The breakdown voltage for this low current discharge, also called pre-discharge, is plotted in Fig. 3 (lower curve). If the applied voltage exceeds the pre-breakdown voltage by a certain amount (upper curve in Fig. 3) a transition into

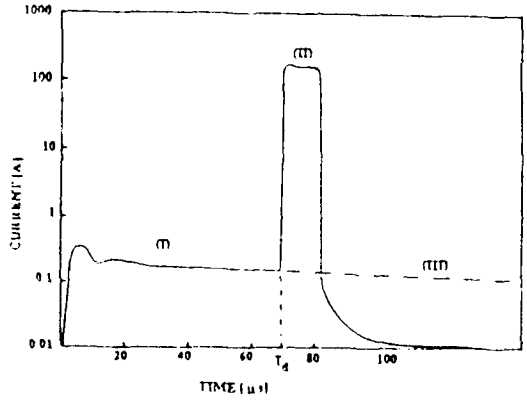

FIG. 2. Sketch of the temporal development of a hollow cathode discharge at a pressure of 735 mtorr and at an applied voltage (10 kV) where the transition pressure is 690 ± 10 mtorr. Region I: the predischarge current common to both modes. Region II: The transition was made to the main discharge mode. Region III: The discharge remained in the predischarge mode.

a low impedance, high current discharge is observed (see Fig. 2). The delay between the pre-discharge and the high current or main discharge decreases with increasing pressure and applied voltage as shown in Fig. 4. For voltages below the upper curve in Fig. 3 there is no transition into the high current mode.

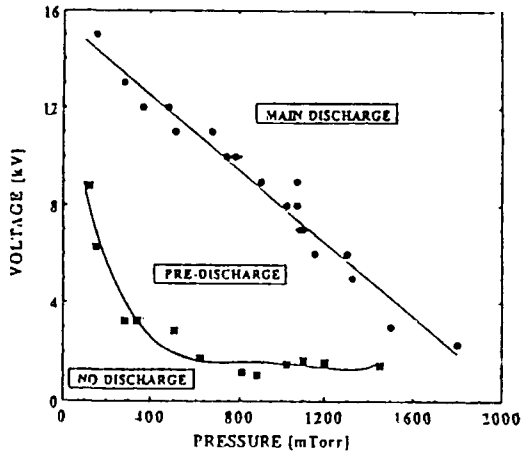

FIG. 3. Breakdown voltage versus pressure for the two modes of discharge.

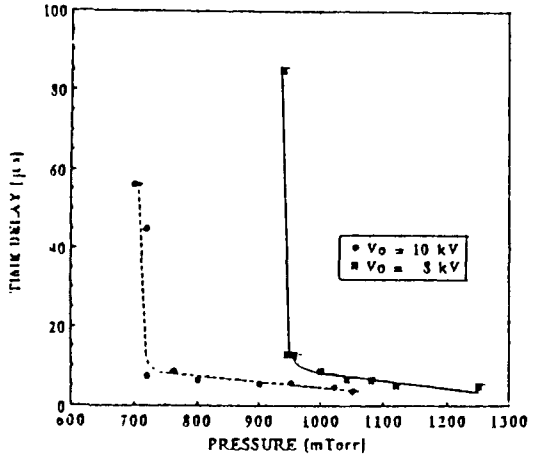

FIG. 4. Delay time versus pressure for applied voltages of 8 and 10 kV.

Static axial magnetic fields were found to delay or even inhibit the occurrance of the main discharge. This effect is strongly pressure dependent. This is demonstrated in Fig. 5, where the discharge current is plotted versus pressure for a two cases: B = 0, and B = 0.15 T. Up to a given pressure the hollow cathode discharge is of the predischarge type (high impedance discharge), in the range above this pressure a transition into the main discharge is observed, demonstrated by orders of magnitude higher current. The application of a magnetic field of 0.15 T causes a shift in the transition pressure to higher values, showing that magnetic fields can prevent the onset of the main discharge in a certain pressure range. In order to supress the main discharge the magnetic field intensity needs to exceed a certain value; in other words, the observed effect is a threshold effect. This is shown in Fig. 6, where the probability of discharge supression is plotted versus the intensity of the magnetic field. The magnetic field only affects the discharge development if its amplitude is above a threshold value, in this case 0.12 T.

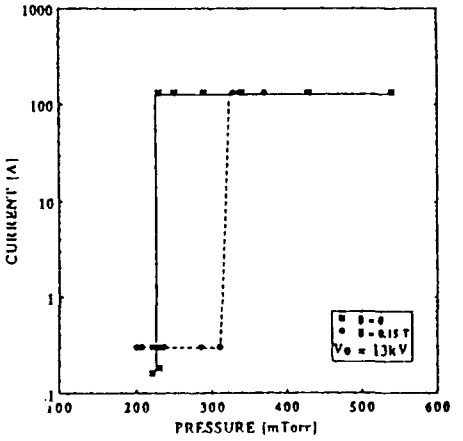

FIG. 5. Discharge current versus pressure without the axial magnetic field and with B = 0.15 T.

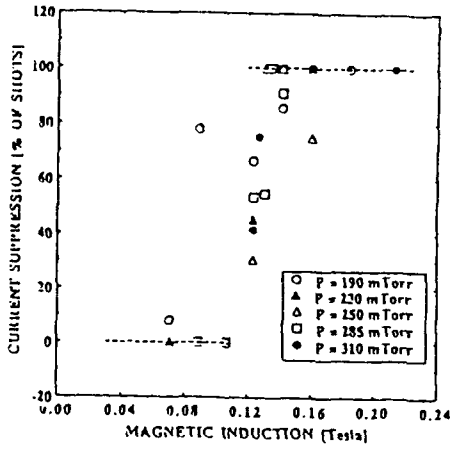

FIG. 6. Percentage of suppression of the high current main discharge as a function of the magnetic field intensity.

B. Breakdown Model for Hollow Cathode Discharges

The experimental results indicate that the breakdown into the high current hollow cathode discharge occurs in two steps. The breakdown is initiated by the formation of a low current predischarge which, after a voltage and pressure dependent delay time, transforms into a high current main discharge.

The predischarge is in our opinion initiated by the Townsend breakdown mechanism. In the pressure p times distance d range to the left of the Paschen minimum, where the discharge is initiated, the breakdown occurs over the longest possible path between the anode and the cathode. In the hollow cathode system shown in Fig. 1 the longest straight path is from the surface of the anode to the bottom of the cathode. Electrons accelerated through the cathode-fall region follow the electric field lines and travel to the anode, producing a collimated beam or a filamentary discharge. Such a radially confined discharge is actually observed on open shutter photographs of the predischarge.[9] In this regime the glow discharge carries currents of only fractions of amperes at high sustaining voltages. Because of the relatively long mean free path of the electrons, a certain percentage of the electrons do not suffer from any collision with gas atoms and therefore constitute an electron-beam with electron energies determined by the applied voltage.[10]

After the center plasma column (filamentary discharge) is developed, the potential on the discharge axis at the orifice of the cathode hole, which was almost the cathode potential, will approach a value closer to the anode potential. The electric field distribution in the hollow cathode region will change in such a way that there is a substantial increase in the radial component of the electric field at the orifice. For sufficiently high fields in this region (corresponding to high voltages as shown in Fig. 3, upper curve), a second breakdown can be expected from the cathode wall to the center of the plasma column. This assumption is supported by the fact that the development into the high current (radial) discharge can be prevented by the application of an axial magnetic field demonstrates that the breakdown into this mode must be radial. The breakdown into the main discharge will most likely occur between the center column and the edges of the cathode hole, because of the maximum radial electric field intensity in this plane.

The stages of the discharge development are schematically shown in Fig. 7. A possible third stage, besides the two discussed sofar, was observed in experiments at higher current levels.[11] It is a discharge determined by a hot cathode operation, the superdense glow discharge. The transition from the hollow cathode (main) discharge into the superdense mode might be caused by accumulative heating of the region about the hollow cathode egde through ion impact during the main discharge phase.

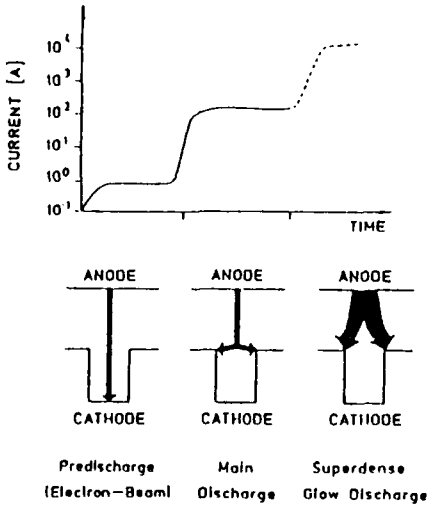

FIG. 7. Temporal development of the current in a hollow cathode discharge. The different related stages of the discharge are depicted graphically in the lower diagram.

The current gain of the main hollow cathode discharge over a standard glow discharge between plane paralell electrodes is assumed to be caused by "Pendel" electrons[12] These are electrons which are emitted from the cylindrical cathode walls, accelerated in the radial electric field inside the hollow cathode, gain so much energy that they traverse the plasma column in the center and then oscillate between the opposite cathode walls. Since most of their energy is deposited in the center region of the cathode hole they create and sustain a high plasma density on the axis of the hollow cathode system, which allows large currents to be carried by the hollow cathode main discharge (Fig. 7). In a later stage, after the electrodes are heated by ion impact, thermionic emission from the edges of the hollow cathode will provide enough electrons, such that discharge path from the edges right to the anode can develop. The radial field, which is required to generate "pendel" electrons will subsequently break down, and the current will flow in an axial, possibly hollow cylindrical discharge.

THE INFLUENCE OF AXIAL MAGNETIC FIELDS ON THE DISCHARGE IMPEDANCE

A. Experiment

1. Experimental setup. In order do study the influence of transient axial magnetic fields on the discharge in the on-state[13] the discharge chamber was modified as shown in Fig. 8. Since the cylindrical hollow cathode in the previous experiment, made of solid brass, allows the application of slowly varying magnetic fields only, it was replaced by a sqirrel cage electrode. (The characteristic time for magnetic field penetration through a conductor is given as $T = \mu_0 \sigma L^2$ where μ_0 is the permeability of free space, σ the conductivity of the material and L the thickness of the conductor. For brass electrodes with $\sigma = 1.5 \times 10^5$ Ohm^{-1}cm^{-1} and L = 0.5 cm, T is on the order of ten's of ms.) Secondly, in order to prevent the transition from the main discharge into the superdense glow, which is a thermionically sustained discharge in axial direction, a glass tube was inserted, which enforces a radial current flow in the discharge. The insulator plate at the bottom of the hollow cathode was also introduced to enforce radial current flow in the discharge.

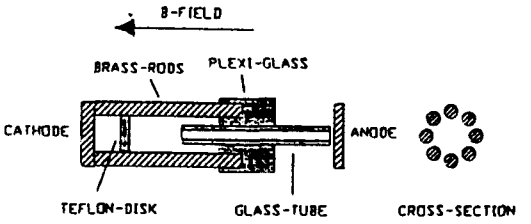

FIG. 8. View of the hollow cathode discharge chamber.

The magnetic circuit was modified to provide for magnetic fields with a risetime of 30 μs compared to 700 μs in the breakdown experiment. Magnetic fields with peak intensities of up to 2 T can be generated with

this circuit. The electrical circuit was also changed, such that it generates pulses comparable or longer in duration than the transients of the magnetic field. The new pulse forming network provides a 50 μs pulse into a 200 Ohm matched load, compared to a 10 μs, 50 Ohm PFN used for the breakdown studies. The complete electrical system in connection with the discharge is shown in Fig. 9.

2. Experimental results. The magnetic field pulse was applied to the discharge 10 μs after the electrical breakdown. The discharge current and voltage were recorded. The current is limited by the load resistance R_l, to $I_{max} = V_0/2R_l$ which for applied voltages of $V_0 > 4$ kV is in the range of less than 10 A. From voltage and current data the temporal change of the discharge resistance was computed for various magnetic field intensities and compared with the discharge resistance without magnetic field applied (Fig. 10). Figure 11 shows the corresponding magnetic field pulse and the relative change of the discharge resistance dR/R due to the applied magnetic field. The digrams indicate that the discharge resistance varies about linearly with magnetic field above a certain threshold field. This is more clearly visible in Fig. 12, where the relative increase of the discharge resistance is plotted as a function of the magnetic field intensity.

This magnetic field effect is strongly dependent on the gas pressure. Figure 13 shows the strength of the effect (the relative resistance change with an applied magnetic field of one Tesla) as it depends on the gas pressure. Highest rates of change were recorded at low pressures, with the lower limit determined by the breakdown condition, p > constant * V_0. The effect diminishes rapidly towards higher pressures. First experiments at higher current levels indicate that with

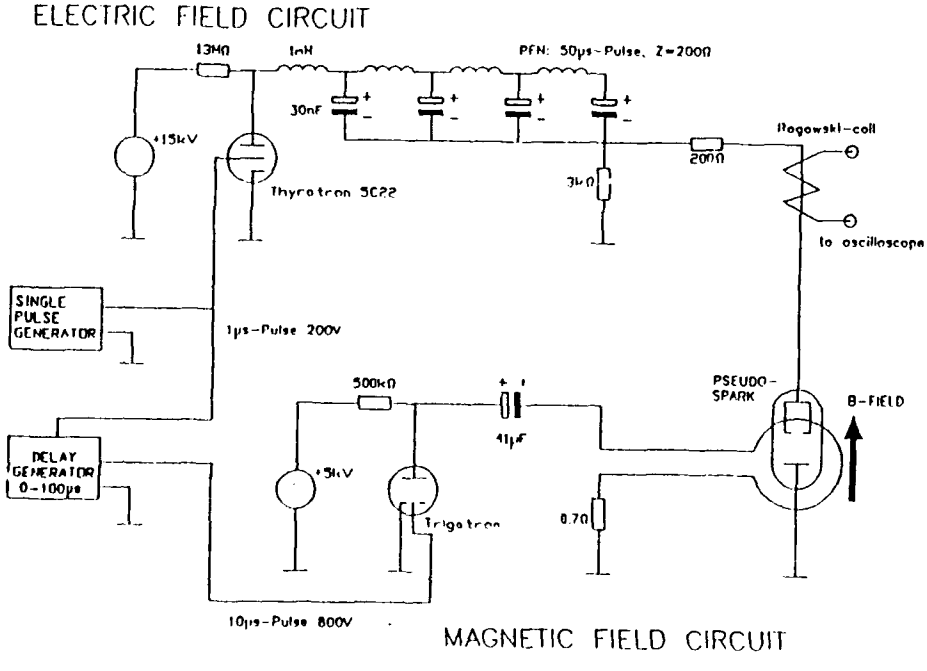

FIG. 9. (a) Electrical, and (b) magnetic-field circuit for the cathode discharge experiment.

increasing discharge current, the voltage across the discharge rises more than linear, that means the discharge resistance increases with current. The magnetic field effect on the other hand seems to have a higher threshold value.

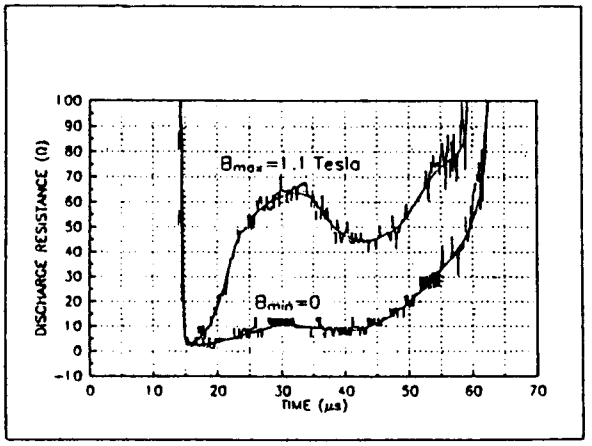

FIG. 10. Temporal development of the discharge resistance with and without magnetic field. The resistance rise at 45 μs is due to the recovery of the discharge after termination of the driving voltage.

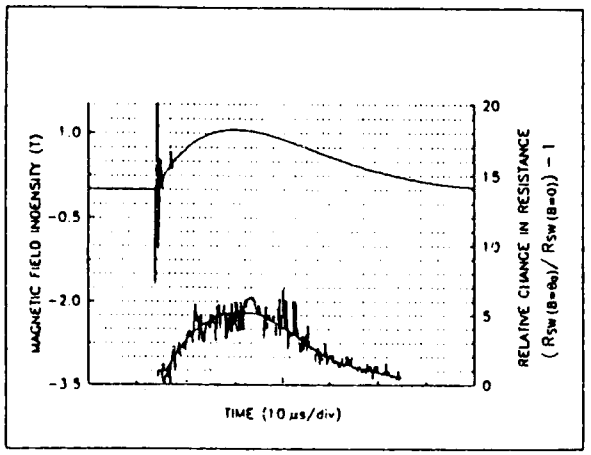

FIG. 11. Temporal Development of the magnetic field and corresponding relative change in discharge resistance.

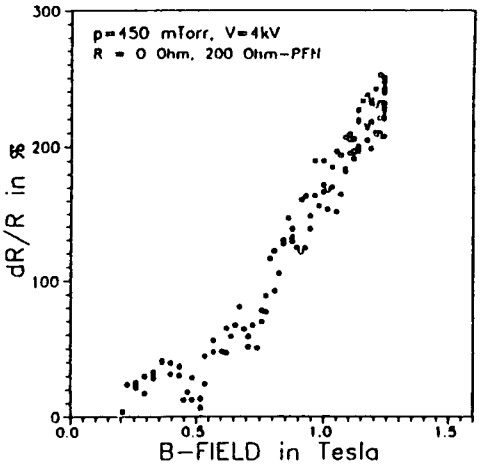

FIG. 12. The relative change in discharge resistance with applied axial magnetic field.

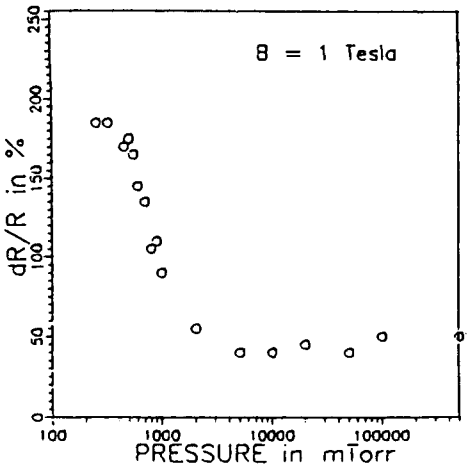

FIG. 13. The change in relative discharge resistance with pressure, for a magnetic field of Tesla.

B. Modeling of the Magnetic Field Controlled Discharge

The effect of an axial magnetic field on the resistance of the hollow cathode discharge can be qualitatively understood by considering its influence on the electron orbits in the cathode hole. At low pressures were the electrons are

magnetized the electrons emitted from the cathode wall will essentially move along trajectories as shown in Fig. 14. In this figure the outer circle represents the cathode and the inner circle the boundaries of the plasma column of the axial part of the main discharge. The maximum distance from the cathode walls is a function of the voltage and is inverse proportional to the magnetic field intensity. If the magnitude of the axial magnetic field exceeds a certain critical field, the electrons will not reach the center plasma column and therefore cannot sustain it through ionizing collisions. The critical value of the magnetic field intensity is given as:

$$B_e = (8mV_0/e)^{1/2}/(b(1-(a^2/b^2))) \qquad (1)$$

Below this value of B there is no effect of the field on the discharge impedance expected. At low magnetic fields the "pendel" electrons are able to enter the plasma column and sustain the discharge.

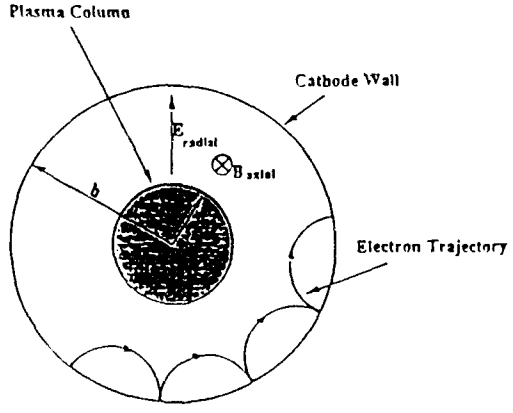

FIG. 14. Electron trajectories in a crossed electric and magnetic field in a cylindrical cavity.

However, if the magnetic field is increased beyond B_e, the pendel electrons can only reach the plasma column and sustain it if the discharge voltage, V_0, is also increased (according to eqn. 1), which corresponds to an increase in resistance at constant current. This is exactly what we observe in the magnetically controlled discharge: up to a certain value of magnetic field intensity there is no effect on the discharge, and then an increase in resistance with the magnetic field intensity is observed. Also that the effect has a higher threshold with respect to magnetic field intensity when the discharge voltage is increased is consistent with our model: B_e increases with voltage V_0. The condition that the pendel electrons in the hollow cathode region must be magnetized, that means that their Larmor frequency must be large compared to the collision frequency imposes a condition on the pressure range in which the magnetic field effect can be observed. Since the collision frequency scales with pressure the effect should diminish at elevated pressures. Again, this is what we observe experimentally.

Although this model explains the observed phenomena rather satisfactorily, a quantititave description of the magnetic field effect in hollow cathode discharges requires a more concise approach. Since the electrons are not in equilibrium with the electric field, Monte Carlo methods or Boltzmann codes need to be used to describe the electron kinetics in the hollow cathode. A first step in this direction has been done by calculating the energy distribution of electrons emitted from the cylindrical cathode and accelerated in radial electrical fields by means of a Monte-Carlo code.[14] The radial field which varies linearly with the radius is determined by a potential V_c at the cathode and zero potential in the center of the cathode hole with radius R_0.

Results obtained with this one-dimensional, steady state Monte-Carlo code are shown in Fig. 15 and Fig. 16 for B = 0 and B = 0.25 T, respectively. The cathode voltage was assumed to be 12 kV, the cathode radius is 0.5 cm, and the He-pressure was set to 200 mTorr. The calculation showed that at zero magnetic field there is a well defined region on the axis

with high electron density. This is the region of the center plasma column. With an axial magnetic field applied, the electron density in the center decreases and a ring shaped region with high concentration of electrons is formed as seen in Fig. 16. With increasing magnetic field this ring expands more and more, and the probability that electrons reach that center and contribute to the formation of a plasma column which carries an axial current (through the glass tube shown in Fig. 8) becomes smaller. At constant voltage the current decreases, or to keep the current constant the voltage needs to be increased. Both changes correspond to an increase in resistance.

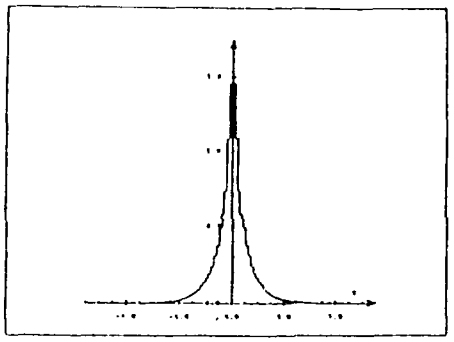

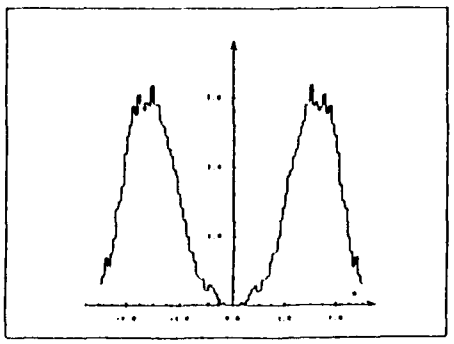

FIG. 15. and FIG. 16. The radial electron density profiles for an applied voltage of 3 kV, a gas pressure p_0 = 200 mTorr, and a cathode hole radius R_0 = 0.5 cm. The vertical center line is the center axis of the hole, and horizontal distances are in mm. In the top figure, the axial magnetic field B_z = 0, and the vertical scale is linear in units of $10^{10}/cm^3$. In the bottom figure, the axial magnetic field B_z = 250 mT, and the vertical scale is linear in units of $10^9/cm^3$.

Though this Monte-Carlo code allows to get a better picture of the physics in the hollow cathode discharge than the simple orbit model discussed in the first part of this section it is far from beeing complete. A better model must be two-dimensional to include the axial motion of the charge carriers, and it must be self consistent. Attempts to improve our Monte-Carlo code in this direction are under way.

SUMMARY

The experimental studies performed with a hollow cathode discharge in He suggest the following breakdown mechanism: The initial breakdown occurs between the anode and the bottom of the hollow cathode. After the formation of a plasma column on the axis of the discharge, a stronger radial electric field is induced at the hollow cavity. With sufficient high voltage supplied, a second, radial, breakdown occurs between the center plasma and the inside wall of the hollow cathode. This breakdown model is supported by the results of measurements with applied magnetic fields, which showed that the breakdown into the main discharge can be prevented with sufficiently strong axial magnetic fields.

The hollow cathode discharge is assumed to be sustained by "pendel" electrons, electrons which oscillate between the cathode walls inside the hollow cathode and which contribute to an enhanced ionization rate in the vicinity of the axis. Due to this mechanism a current carrying plasma column along the axis is developed. This plasma column which reaches from the anode into the hollow cathode is sustained by the "pendel" electrons, which gain their energy in the radial cathode fall. Controlling this radial flow of electrons, should therefore allow to control the ionization rate in the center column and consequently the discharge current.

Experiments with transient axial magnetic fields in a discharge geometry which was particularly designed to provide for radial

current flow have proven the validity of this model. With magnetic fields in the range of hundred's of mT to 1.2 T it was possible to modulate the discharge impedance by up to a factor of six. The experiments indicate a threshold in magnetic field intensity for this effect and, above this threshold, a linear dependence of the discharge resistance on the magnetic field intensity. The effect is strongly pressure dependent. A maximum change in resistance was observed at pressures close to breakdown pressure for a given applied voltage. The results of these experiments agree with theoretical results obtained with a one-dimensional, steady-state Monte-Carlo code. The calculations show that with increasing magnetic field the ionization rate in the center of the discharge geometry diminishes and a ring shaped plasma around the axis is generated. The reduction in the density of electrons and ions in the center region reduces the discharge current in a properly designed discharge geometry.

The experimental and theoretical results show that magnetic fields can be used to control the breakdown as well as the conduction phase of hollow cathode discharges. Because the magnetic field effect was found to be a threshold effect, it is possible to "bias" the discharge with a static magnetic field (using a permanent magnet) and apply transient magnetic fields of lower intensity than the ones used in these experiments to control the discharge. The discharge resistance, which in our experiments (in the main discharge mode) was on the order of 10 Ohms with no magnetic field applied can be reduced by using a multi cathode system. It was shown that it possible to run pseudo spark discharges paralell to each other.[15] Using a large number of hollow cathodes in form of a honeycomb allows to reduce the discharge resistance to values in the subOhm range.

Though only a relatively small number of experiments were performed sofar to explore the effect of transient magnetic fields on the discharge impedance it became obvious that the strength of this effect depends on a multitude of discharge and geometry parameters. More elaborate experimental studies and improved modeling could lead to the design of a powerful current modulator or eventually to an opening switch with subOhm on resistance, opening time in the μs range. and multi-kHz repetition rate.

ACKNOWLEDGEMENTS

This work was supported by SDIO/IST and managed by ONR under contract number N00-14-86-K-560. The program monitor is Gabriel Roy.

REFERENCES

1. E.A. Koltypin, A.I. Nastyukha, and P.A. Smirnov, "Rectification in a low-pressure arc with a hollow cold cathode, I. and II.," Sov. Phys. - Tech. Phys. 15, 1703, and 1710 (1971).

2. J. Christiansen and C. Schultheiss, "Production of high current particle beams by low pressure spark discharges," Z. Physik, A290, 36 (1979).

3. G.F. Kirkman and M.A. Gundersen, "Low pressure light initiated glow discharge switch," Appl. Phys. Lett. 49, 494 (1986).

4. For general information on hollow electrode discharge switches see "Physics and applications of Pseudosparks", M.A. Gundersen and G. Schaefer, eds., NATO ASI Series B., Vol. 219, Plenum Press, New York and London, 1990.

5. K. Frank and J. Christiansen, "The fundamentals of the Pseudospark and it's applications," IEEE Trans. Plasma Science 17, 748 (1989).

6. G. Kirkman-Amemiya, H. Bauer, and M.A. Gundersen "Analysis of the high current glow discharge occuring in the BLT and

Pseudospark switch," Bull. Amer. Phys. Soc., 31st Plasma Phys. Meet., Anaheim, CA (1989).

7. H. Pak, and M.J. Kushner, "Simulation of the switching performance of an optically triggered pseudo-spark thyratron," J. Appl. Phys. 66, 2325 (1989).

8. K. Mittag, "A physical model of prebreakdown in the hollow cathode Pseudospark discharge based on numerical simulations," in "physics and applications of Pseudosparks," M.A. Gundersen, and G. Schaefer, eds., NATO ASI Series B, Vol. 219, Plenum Press, New York and London, 1990, p. 233.

9. M.T. Ngo, K.H. Schoenbach, G.A. Gerdin, and J.H. Lee, "The temporal development of hollow cathode discharges," IEEE Trans. Plasma Science 18, 669 (1990).

10. B. Wernsman, H. Ranea-Sandoval, J. Rocca, and H. Mancini, "Generation of pulsed electron-beams by simple cold cathode plasma guns," IEEE Trans. Plasma Science 14, 518 (1986).

11. W. Hartmann, and M.A. Gundersen, "Origin of anomalous emission in superdense glow discharges," Phys. Rev. Lett. 60, 2371 (1988).

12. K.H. Schoenbach, L.L. Vahala, G.A. Gerdin, N. Homayoun, F. Loke, and G. Schaefer, "The effect of pendel electrons on breakdown and sustainment of a hollow cathode discharge," in "physics and applications of Pseudosparks," M.A. Gundersen, and G. Schaefer, eds., NATO ASI Series B., Vol. 219, Plenum Press, New York and London, 1990, p. 293.

13. T. Tessnow, K.H. Schoenbach, and G.A. Gerdin, "Magnetic Control of the Impedance of Hollow Cathode Discharges," Rec. 18th IEEE Intern. Conf. Plasma Science, Williamsburg, VA, 1991, paper 5P15.

14. G.A. Gerdin, K.H. Schoenbach, L.L. Vahala, and T. Tessnow, "Mode transitions in hollow-cathode discharges," Proc. 6th Intern. Symp. on Gaseous Dielectrics, Knoxville TN, September 1990.

15. J. Christiansen, "The properties of the Pseudospark discharge," in "physics and applications of Pseudosparks," M.A. Gundersen, and G. Schaefer, eds., NATO ASI Series B., Vol. 219, Plenum Press, New York and London, 1990, p. 1.

K. H. Schoenbach, photograph and biography not available at the time of publication.

G. A. Gerdin, photograph and biography not available at the time of publication.

SUPER-EMISSIVE CATHODE DEVICES

M. A. Gundersen, G. Kirkman, R. Liou, and Y. Hsu

Department of Electrical Engineering-Electrophysics
University of Southern California
Los Angeles, CA 90089-0484

ABSTRACT

This paper reviews recent research to design, test and implement new pulse power thyratron-type switches for operation at high voltage, high power, high current, and high repetition rate with lower housekeeping, weight and volume. The most important single result of the last few years is the delineation of the high current cathode emission mechanism in the pseudospark and back-lighted thyratron (BLT) – the super-emissive cathode. These switches are based on the super-emissive cathode. Success will produce valuable laser, accelerator, and other switches, modulators, and pulse generation devices for ground and space based pulse power systems, and will form the basis for a new generation of pulsed power devices. Results reviewed here include understanding of basic processes, development of specific switching devices, new applications in other areas, and transfer of the technology to applications and to the marketplace.

INTRODUCTION

This paper reviews recent research performed on the BLT device. Results include 1) determination of the super-emissive cathode process, 2) development of new applications, and 3) transfer of the technology to applications. The most important single result of the last few years is the delineation of the cathode emission mechanism in the pseudospark and back-lighted thyratron (BLT) – the super-emissive cathode.

By way of review, a schematic of a typical BLT is shown in Figure 1. Two cylindrical cap electrodes face one another end-on and hold off the applied voltage across a narrow (typical 3 mm) gap. The device contains a low pressure (<0.5 torr) gas, such as hydrogen, nitrogen or argon. Electrons are generated by a trigger pulse – optical or electrical – and pass through the small aperature in the cathode and initiate a discharge which closes the switch[1,2].

Super-emissive cathode

The BLT and pseudospark have been shown to operate with a self-heated super emissive cathode (SEC) producing electron emission current densities $>10 kA/cm^2$. The high cathode emission (>> externally heated cathodes) and current densities obtained in a non-arcing mode and with a simple, robust structure, strongly encourage consideration of new applications. The emission occurs over a surface area $\approx 1\ cm^2$, and the cathode operates without forming a constricted arc.

This is in contrast to the high current densities achieved over very small areas in field emission devices and the high, yet rather disruptive, currents achieved in arc discharges. Although in the past comparable but localized current densities have been achieved through the formation of filamentary arcs, devices used for applications (e.g. spark gaps, felt cathodes, and field emission devices) tend to be life-limited. Problems associated with arc discharges include the melting, sputtering and cratering of electrode material, and addition of electrode material to the arc plasma. This new cathode supports currents that formerly required arc-type devices, such as spark gaps. It appears feasible to extend performance to devices requiring peak currents over 100,000 A, and these results suggest that high brightness cathode design may be significantly improved.

The plasma is initiated with a Townsend avalanche discharge in a low pressure gas (typically 0.1-0.5 torr) that develops on axis due to the focusing effect of the electric field. A positive space charge builds up inside the hollow cathode region as a result of low mobility of the ions produced by electron-neutral collisions. The release of a sufficient number of starting electrons inside the hollow cathode initiates a transient Hollow Cathode Discharge (HCD).

This work was supported by the SDIO through the ONR.

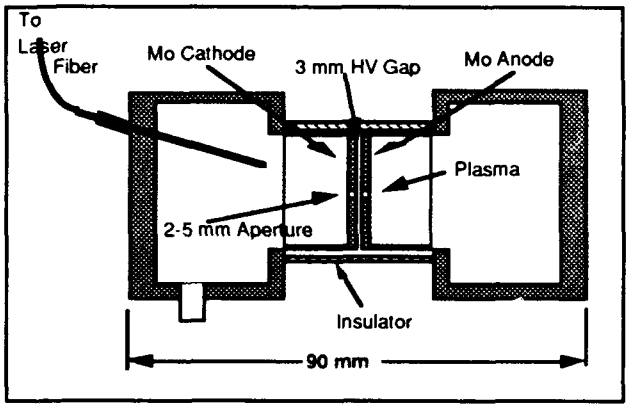

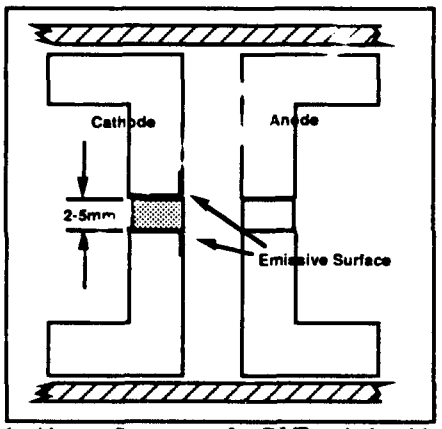

Figure 1. Above: Structure of a BLT switch with optical triggering through an optical fiber. The switch is filled with low pressure (0.01-0.3 Torr typical) gas and is triggered by unfocused UV light incident on the back of the cathode surface. Below: Detail of super-emissive cathode electrode structure indicating the region that is ion-heated. The super-emissive area is approximately 1 cm^2, and is the surface indicated in and around the cathode aperture.

During this growth phase of the discharge, before the plasma is fully formed, a transient high voltage remains across the electrodes, and an electron beam is produced that passes through the anode aperture. These HCD beams are reported to have kA peak currents and very good emittance and brightness properties (55 mm·mrad and $2*10^{11}$ $Am^{-2}rad^{-2}$, respectively at 20 kV with 1 kA beam current). The electron beam will propagate and hence interact with the discharge plasma. The plasma density can be $\approx 10^{12}$ cm^{-3} to> 10^{15} cm^{-3}, which is appropriate for the production of radiation in the millimeter range.

If the plasma density is allowed to increase to > $\approx 10^{14}$ cm^{-3}, the electric field will be shielded from penetrating into the hollow cathode and terminate the HCD. The cathode then makes a transition to a different phase, the super-emissive phase. This phase has extraordinary emission properties, including production of current densities 10^4 to 10^5 A/cm^2, generated over a macroscopic area $\approx 1cm^2$.

The Super-emissive cathode (SEC) switch is thus fundamentally different in operation from externally heated cathode switches, such as previous thyratrons, hollow cathode switches, and spark gaps. A super-emissive cathode is defined here as one which produces uniform current emission ≥10,000 A/cm^2 from a macroscopic area ($\approx 1cm^2$). Thus the current emission characteristics are very large in comparison with conventional heated thermionic cathodes. The pseudospark and back-lighted thyratron are switches that can operate in this highly emissive mode. This mode is to be distinguished from hollow cathode behavior, which also occurs in these switches, but which produces lower current, and is distinguished by other processes as well. It is specifically the super-emissive behavior that makes possible the improved operating characteristics of the switch.

Reviewed below are results of development of the BLT as a pulsed power switch. These include high voltage, high current, low inductance and compact size for pulsed power applications. In addition, a summary of some of the related fundamental physical processes is presented. Some new applications are discussed, including electron beam production. Finally, a summary of results of an active technology transfer program are presented.

SEC SWITCH APPLICATIONS TESTED AT USC

The USC project has demonstrated a variety of applications of the BLT switch. These include:

Marx bank operation

This is important because it is a proof of principal experiment that demonstrates a method of optical control that is potentially very important for high power modulators. If modulators controled through optical fibers can be used for large systems

with many modulators, the methodology for design will change.

The BLT-based Marx bank offers attractive possibilities for improved pulsed power performance for a number of applications. The BLT has been implemented in a Marx bank at USC, and has demonstrated switching of > 100 kV, with unsophisticated BLT switches. There are various possibilities for implementation. For example, high current can be straightforwardly achieved in a small device, and improved isolation can be obtained by optical triggering. At USC a small, single aperture device has been operated that switched 81.6 kA peak current in a relatively short (≈ 400 nsec) ringing pulse (≈ 75% reverse current) at 20 kV. Of related importance is that the USC results do not show arc-type behavior during this experiment.

High current and high voltage operation

We report successful operation of flashlamp-switched multiple-stage back-lighted thyratrons at very high pulsed power levels, including 100 kV stand-off voltage and >70 kA switched peak current. Simultaneous optical triggering of each gap for precision timing, and plasma triggering, are also discussed. The results suggest that fairly simple multiple-gap configurations of the device will be useful for applications such as multiple high power modulator systems for accelerators.

Although operation of a single-stage 100-kV thyratron has been reported by Mancebo, this interesting switch has not been implemented as a commercially engineered device. Multiple-stage commercial switches have been reported for reliable operation at voltages up to ~250 kV. The size of these high-voltage multiple-stage thyratrons is proportional to the number of grids required and other factors. The BLT switches described are simpler and smaller than these multiple-stage thyratrons.

FUNDAMENTAL PHYSICAL PROCESSES IN THE BLT

Super-emissive cathode background

As discussed above, the pseudo-spark and back lighted thyratron operate with a large-area (~1cm^2) superemissive cathode (~10^4 A/cm^2). The discharge is a superdense glow with a cross-section of the order of 1cm^2, rather than an arc. Data includes the following: Streak camera recordings show that the plasma extends radially outward from the center aperture and is homogeneous. Studies of the cathode with a scanning electron microscope indicate that the discharge produces a uniform surface melting. The data supports the mechanism wherein the cathode surface is heated to the melting point by an intense ion beam present during the avalanche phase of discharge. This high temperature, together with the high field across the cathode sheath, is responsible for the extremely large and uniform field-enchanced thermionic emission over a large area. Cathodes studied with a scanning electron microscope following operation at 6-8KA, ~1msec pulse length, 10^5 pulses in a low-pressure (~27Pa) H_2 discharge show evidence of melting of a thin surface layer within a radius of ~4mm.

Previous studies show that a mechanism, wherein the cathode surface is heated by an intense ion beam present during the avalanche phase of a discharge, is responsible for the cathode emission[3]. In the avalanche phase this ion beam will have an energy related to the initial voltage of the electrode gap, while during the steady-state phase the beam will have a lower energy related to the cathode fall voltage. An ion beam with 10-20MW/cm^2 lasting ~100 nsec was shown to be sufficient to heat a thin surface layer (several mm deep) to a temperature near the melting point of Mo. A high field (~10^8V/cm) could exists at the surface in the plasma sheath. The combination of high temperature and field can be a possibility for this extremely large field-enchanced thermionic emission after the initial cathode surface heating.

Modeling of the BLT plasma

Part of the research has been directed towards understanding fundamental plasma properties, so that fundamental limitations and new applications can be understood and developed[4]. Temperature, energy, and densities of two electron distribution function components, including an isoptropic "bulk" part and an anisotropic beam, have been analyzed for a hydrogen pseudospark and/or back-lighted thyratron SEC switch plasma with peak electron density of 1-3x10^{15} cm^{-3} and peak current density of 10^4 A/cm^2. Estimates of a very small cathode fall width during the conduction phase and high electric field strengths lead to injection of an electron beam with energies ≥100 eV and density of 10^{13}-10^{14} cm^{-3} into a Maxwellian "bulk" plasma. Collisional and radiative

processes of monoenergetic beam electrons, "bulk" plasma electrons and ions, and atomic hydrogen are modeled by a set of rate equations and line intensity ratios are compared with measurements. Under these high current conditions, for an initial density $n_{H2} \approx 10^{16}$ cm^{-3} the evaluated "bulk" plasma parameters are electron density of 1-3x10^{15} cm^{-3} and electron temperature of 0.8-1 eV, the estimated "beam" density is $\approx 10^{13}$ - 10^{14} cm^{-3}.

These results suggest the possibility of producing in a simple way a very high density electron beam. Consideration of the current density and electric field strength lead to the assumption of a cathode fall produced electron beam. Electron densities of 1-5x10^{15} cm^{-3} and an estimated electron temperature of about 1 eV cause a very small cathode fall width of several μm during the conduction phase which results in a high electric field inside the cathode fall which is estimated to about 10^6 V/cm. Hence, because the device geometry is confined and the cathode fall is close to the "bulk" conducting region, it is necessary to consider a strong anisotropic electron component, e.g. an electron beam. Considering only electron-electron encounters the mean free path of electrons with initial energies of 100 eV is estimated to be ≈ 1-5 cm for ionization degrees of 0.1 - 0.5. Because the gap spacing is much smaller than this mean free path, injected electrons will not become thermalized during the gap penetration, i.e., their distribution function becomes not too broadened and is therefore assumed to be a Dirac delta function in energy.

The model thus consists of two electron groups: a monoenergetic electron beam, which penetrates a Maxwellian "bulk" plasma, directly excites and ionizes atomic hydrogen, and a 'background' Maxwellian "bulk" plasma. Collisional processes of both electron-groups with hydrogen ions and atoms and radiative transitions were considered. The solution of the appropriate set of rate equations yields the population of atomic levels and the "bulk" electron density as a function of electron beam density and energy and electron temperature of the "bulk" plasma. It is shown that a steady state assumption fails for the process of impact-ionization due to a pulse beam electrons with a pulse duration of 100-300 ns. Once the beam dissapears the relaxation of excited states occurs immediately and a steady state condition is applied to the remaining "bulk" plasma. Comparision of calculated and measured line intensity ratios of H_α and H_β lines yields the "bulk" electron temperature and electron density.

A result of this is the prediction of a new electron beam source. The beam is estimated to traverse the device without thermalization if the plasma density is ≤ 2.5x10^{15} cm^{-3}. High brightness electron sources are necessary for various new plasma based devices, and these results encourage consideration of this electron beam as a new candidate for applications including microwave generation sources, electron sources for accelerators and plasma based accelerators which require improved cathodes.

Current quenching

In high current density, low pressure glow discharges, current quenching has been found to exist within a limited range of discharge parameters[5]. The quenching phenomenon occurs at the transition of a pulsed high - voltage hollow cathode discharge to a superdense glow discharge. A lower current limit was found as well as an upper limit, above which no quenching occurs although the discharge plasma remains diffuse and does not show arcing. The quenching process is explained in terms of limited cathode emissivity after electrostatic shielding of the hollow cathode by the rapidly expanding discharge plasma. Ion pumping in the cathode fall leads to a strong reduction of the net discharge current despite the increased cathode fall voltage drop during the quenching process. Gas replenishment, caused by ion impact desorption and/or thermal desorption due to surface heating of the cathode surface, can temporarily weaken the quenching process, which is supported by experimental findings. Sufficient surface heating of the cathode surface due to ion bombardment, with a consequently high thermal desorption rate of the adsorbed gas layer, finally transforms the discharge into a superdense glow discharge. This mechanism opens the possibility of constructing opening switches at the MW power level.

The phenomenon of current quenching is well known for hot cathode glow discharge switches like conventional thyratrons. Various mechanisms have been discussed for its explanation, like ion pumping, pinch effect, cathode double sheath, plasma instabilities, etc. In all cases, quenching is observed to occur at current densities of up to several 100 A/cm^2 on a time scale of some microseconds, not allowing a charge transfer of more than ~10^{-3} Asec/cm^2 without arcing. Quenching, therefore,

imposes an upper limit for the charge transferred in a single shot in conventional thyratrons. In contrast to this behavior, it is found that quenching occurs at lower, rather than higher, currents in cold cathode, low pressure diffuse discharge switches like the pseudo-spark switch and the BLT. We observed quenching only in a small range of parameters: pressure between 15 and 40 Pa H_2, current 1-2 kA, cathode thickness < 2 mm. Above these limits, no quenching is observed although the discharge is still a spatially homogeneous glow. We think that quenching is caused by the lack of ions (which are the main charge carriers within the cathode sheath) due to intense ion pumping at current densities of the order of several 100 A/cm^2.

Current quenching was observed mainly in a setup with thin (2.5 mm nickel sheet) cathodes; in a similar setup with thick cathodes (5 mm molybdenum) , the quenching effect was very weak and could hardly be observed. Therefore, the experimental findings reported hereafter all belong to experiments where the above-mentioned Ni cathodes had been used. (In cases where quenching could be observed with thick cathodes, the time at which quenching occurred did not vary too much from that observed with thin cathodes; the 'degree' of quenching - that is, the percentage of current drop and the duration of the phase of reduced current flow -, however, was much less pronounced with thick cathodes. An interpretation and discussion of this result will be given in the next paragraph.

The rate of current drop during the onset of quenching is of the order of $5*10^9$ A/sec and does not vary very much with a variation of the other discharge parameters (pressure, voltage, and current). Therefore, the voltage spike induced during this phase is fairly independent on voltage, current, and hydrogen pressure and amounts to the order of 1 kV.

The experimental data are interpreted in terms of a 2-stage discharge mechanism, which finally leads to the reduction or even interruption of the discharge current. As to the first stage, a hollow cathode discharge (hcd) is initiated in the region behind the cathode hole. The main processes for electron release at the surface of the hollow cathode are the photoeffect due to VUV photons from the hcd plasma, and secondary electrons produced by the impact of fast ions (and neutrals) which have been accelerated in the cathode fall. Due to the inefficiency of these processes, the cathode fall voltage drop is rather high (of the order of several hundred volts), and consequently an electron beam is produced which leaves the cathode region towards the anode, creating a plasma on axis because of ionizing electron - gas atom encounters.

The second stage of the discharge begins when this plasma 'contacts' the walls of the cathode hole (that is, when its radial dimension becomes equal to or larger than the cathode hole due to the thermal expansion of the plasma in the radial direction). If the cathode fall width is, at the same time, small compared to the cathode hole diameter, the hollow cathode suddenly becomes electrostatically shielded from the main discharge region between anode and cathode, and the cold cathode surface which is facing the anode has to take over most of the discharge current. As the active cathode surface from this moment on is largely reduced, and the electron emission from the cathode is even more reduced because of the undesirable discharge geometry in comparison to the favorable geometry of a hollow cathode, the total discharge current can drop by an order of magnitude or even more, depending on the specific discharge conditions. At that time, the discharge current is determined mainly by the ion component of the cathode fall current balance, as the field emission and the secondary electron emission components are considerably less than the ion current drawn from the cathode-side of the discharge plasma. Heating of a thin surface layer of the cathode surface due to the ion current can lead to the desorption of the adsorbed surface gas layer at a temperature above ~ 1600 K, if the surface power load due to the ion current is of the order of ~10 MW/cm^2 for durations of several 10 nsec. In the case of a limitation of this power density due to a high impedance of the discharge circuit, or a discharge voltage too low to sustain such a high ion current density in the cathode fall, a gas starvation at the cathode side of the plasma will occur due to the ion pumping effect of the cathode fall, and a permanent strong reduction of the discharge current occurs. If the cathode surface temperature would be increased to > 1600 K, however, the thermally desorbed gas layer provides a very effective gas replenishment; it is expanding with a velocity corresponding roughly to the surface temperature of the cathode, and can provide enough gas even for rather long pulse durations and at ion current densities of the order of several kA/cm^2. The discharge will still remain highly resistive, however, due to the low efficiency of secondary electron release at the cathode surface, and a noticeable quenching

effect can be observed.The total power into the discharge, given by

$$P = U_C * I$$

where U_C is the anode - cathode voltage drop of the switch, gives an upper limit for the maximum possible power input into the cathode surface. In the experiments described herein, P is of the order of ~MW , and the peak power density at the cathode surface therefore is of the order of several MW/cm^2 at the lower end of the voltages of these experiments. Hence, the cathode surface temperature does not reach a temperature which is high enough for thermal desorption of the gas adsorbat, and consequently quenching is very pronounced. Due to the lack of reliable cathode fall voltage drop measurements during the early part of the pulse, however, a more detailed analysis of the cathode surface temperature can not readily be made, and the comparison of the actual cathode temperature with that needed for the onset of thermal desorption remains an open question.

NEW APPLICATIONS

Plasma based devices are under consideration for applications include not only practical high power switches, but also advanced accelerator technology, improving accelerator beam luminosity, and as sources of electrons, ions and electromagnetic radiation. The USC effort addresses practical device implementation problems in the development of these plasma based devices.

We have developed a reliable plasma source that meets many of the conditions required for a wakefield accelerator, or plasma lens – including reliability, durability, high repetition rate, shot-to-shot reproducibility, and negligible jitter. The BLT appears to be scalable to increased plasma densities without compromising performance. Applications to electromagnetic wave generation in several ways, including plasma loaded free electron lasers, other pulse generation applications, such as EMP, excimer and other laser development, will also be affected. The electron and ion beams may also be expected to be of interest for microwave, accelerator, and other technology, such as X-ray generation.

The superemissive cathode is robust, self-heated, produces very high, uniform current, and operates in a low pressure plasma environment. These data indicate that the electron beam produced by the superemissive cathode should be considered for applications such as electron beam generation and high power microwave generation.

Microwave and millimeter wave generation in the BLT

We have observed micrometer and millimeter wavelength radiation (1 to >100 GHz) produced by the BLT. The device generates the electromagnetic wave radiation directly from the beam-plasma interaction without a slow-wave structure. In the conventional slow-wave device, the characteristic dimension decreases with increasing frequency resulting in a shrinking of device dimension and reduction of available power output. Also, the tolerance imposed by the specific device size makes it virtually impossible to fabricate the higher-frequency sources. Two main advantages for our approach, first, radiation directly from the beam-plasma interaction can overcome the mechanical constraint on the conventional slow-wave structure and, secondly, the beam neutralization provided by the background plasma permits the beam current to be larger than is possible in space-charge-limited devices. These two advantages directly address the possibility of generating both higher-frequency and higher-power radiation.

Shown in Fig. 2 is the experimental setup for the millimeter wavelength radiation and electron beam measurements conducted at USC. In one version, a two-gap BLT (consisting of cathode, a floating electrode and anode) was used. The structure is detailed in the inset of Fig. 2. The hollow cathode region was a copper a cup structure. The electrode hole size, electrode-to-electrode distance and thickness of quartz insulator are 3 mm. A quartz window with thickness of 1/8" was used behind the hollow cathode region for a radiation transmission and visual observation. A conventional thyratron was used to control the applied voltage on the BLT, and the BLT was operated in an over-voltaged (self-breakdown) mode. The repetition rate was variable and was not limited by the BLT– repetition rates in the kHz range shoud be straightforwardly achievable. The total current through the discharge was measured with a 5 mΩ current viewing resistor. Time-resolved measurements were made with a fast transient digitizer with 500 MHz bandwidth. The 330 nH inductance is a lumped parameter value for the circuit. The 4-Ω load resistor limits the discharge current.

Radiation was measured from the cathode side through the quartz window with the horn antenna and detector combinations for various bands without bandpass filters. (Ka band: 26.5~40 GHz, V band: 50~75 GHz, F band: 90~140 GHz) In order to avoid noise all detectors were located inside a double-shielded screen room.

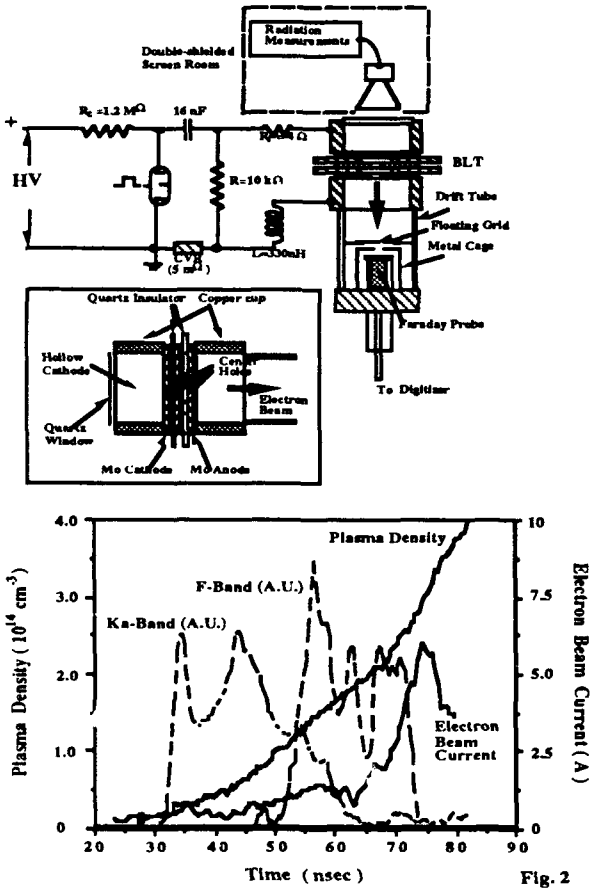

Figure 2-a. Experimental Set-up for initial millimeter wave observations. The BLT structure is shown in the inset. Figure 2-b. Observed radiation at Ka and F band, and correlation with plasma density and electron beam current.

Fig. 2-b shows the radiation and estimated plasma density versus time at 120 mTorr Ar and 20 kV applied voltage. The radiation was measured in several bands including Ka-Band and F-Band. The Ar plasma density was estimated from the discharge current using results from a previous experiment done in a hydrogen gas. A comparison of the differences in ionization cross section and neutral density between H_2 and Ar suggests that the accuracy of this estimation is within a factor of 2. The cutoff frequencies of various waveguide horns were used to determine the time of onset of radiation for three different bands (Ka, V and F).

An electron beam with peak current ~ 30 A and energy in the range about 15~20 keV has been measured during the hollow cathode discharge. The electron beam is described further below. These time resolved measurements show a strong correlation between the presence of the electron beam and the production of radiation. The sequence of the observed radiation in different bands (Ka, V and F) also is strongly correlated with the temporal variation of the plasma density. The correlation between the electron beam and radiation suggests that beam-plasma interaction(s) may be responsible for the electromagnetic waves generation.

The length of the electron beam pulse and corresponding millimeter wave emission, can be controlled by modifying the electrical circuitry. By adjusting circuit impedence either actively or passively, we expect to vary the pulse length from ns to steady state.

The results of these measurements lead to the conclusions that 1) a single BLT device should produce radiation by a beam-plasma interaction and that 2) two BLT devices can be used in a counter-propagating beam experiment to produce high frequency mm-wavelength radiation through two beam-plasma interactions and beam-beam interactions.

The BLT electron beam

An essential issue in the development of a millimeter wave device is the quality of the electron beam produced by the hollow cathode. The electron beam properties are key to utilizing the BLT structure and producing a rugged, simple device.

Electron beam measurements include time resolved beam current, current density, gap voltage, beam energy, emittance, brightness, beam profile, and dependence of these values on applied voltage, gas pressure and external circuit have been made. The BLT electron source and diagnostic sections were mounted on conflat high vacuum flanges to allow interchange of diagnostic sections and secure high vacuum sealing.

The BLT device can be electrically or optically triggered. For optical triggering the BLT is dc or pulse charged to the desired voltage and then a flashlamp produced UV light pulse is used to initiate the electron beam producing discharge. The flashlamp used is a simple triggered bulb type lamp operating with an electrical input energy of ~200mJ.

Beam current: Preliminary measurements of the beam current have been made with a fast Faraday cup which was designed and fabricated specifically for this application. The Faraday cup is welded to a high vacuum feedthrough on a conflat flange and then connected to a current viewing resistor and BNC connector. The current viewing resistor risetime <1nsec as quoted by the manufacturer and we have verified this to be <3nsec using an available pulse generator with 3nsec risetime. The current was also monitored by a current transformer although these measurements were bandwidth limited.

An electron beam current density of $\approx$1kA/cm^2 has been produced by the BLT with a total current of ~100A. This current was produced from an electrode structure with a 3mm diameter aperture. The total beam current can be increased by adding multiple apertures or by using an annular aperture. In a preliminary experiment using an annular aperture at USC total beam currents as high as 260A have been observed.

The beam current produced is a function of gas pressure in the discharge gap and has been modeled in hydrogen (Bauer and Gundersen, 1990). We have measured beam current as a function of gas pressure in argon and find an increase in beam current and beam fraction with decreasing gas pressure. Both the temporal behavior and pressure dependence agrees with these modeling results.

An electron beam current of 105A peak current is observed at 25kV when discharging a total current of 3.5kA. The $\approx$3% efficiency of beam production agrees with the modeling results. The beam current pulse begins before the discharge current and has a shorter pulse length. A transverse magnetic field is applied to deflect the beam away from the faraday cup verifying that the measured current is due to the beam and not conduction current through the ionized gas or noise. Typical data are shown in Figure 3.

We have investigated several approaches to increasing the beam current and energy including voltage dependence, pressure dependence, annular apertures, differential pumping, hollow cathode field shaping and multiple gap structures. The highest current and voltage obtained has been 230A and 70kV respectively. Further increases are expected in this project.

The total beam current and beam current fraction increases with increasing voltage and decreasing pressure. This behavior has been predicted by modeling and our experimental results agree. A beam current of 350A and beam fraction of >6% is expected at 100kV.

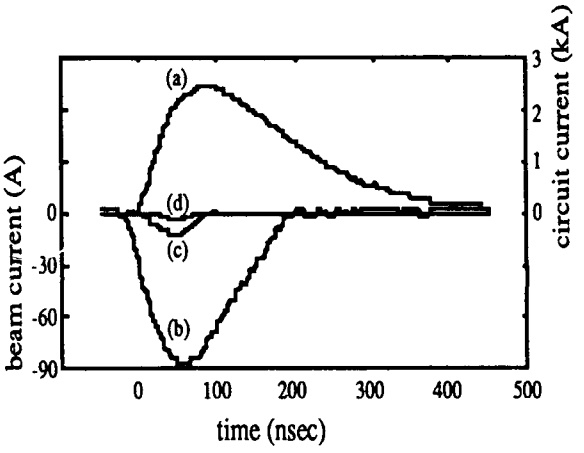

Figure 3. (a) The main discharge current and the beam currents at 7 cm downstream when (b) no magnetic field, (c) low magnetic field, and (d) higher magnetic field applied.

The temporal behavior of the beam indicates at least two components of beam current separated in time. The first component is a 20nsec low current ~2A pulse associated with the discharge of the self capacitance of the electrode structure the second begins 40nsec later, has much higher current >70A and is associated with the discharge of the external capacitance. Although the first beam pulse is low current it is of interest due to its efficiency of production, >50% of the total stored charge is converted to beam current with energy of the full applied voltage. The total current in this beam may be increased by increasing the self capacitance of the structure or by more closely coupling the external capacitance. Increasing the total current of both components will be investigated.

Beam energy, brightness and emittance: The beam energy has been estimated by measuring its deflection in a magnetic field. The beam passes through a drift tube and is deflected by a transverse magnetic field applied by a solenoid, there is a further drift region after which the beam is observed on a phosphor screen. The screen phosphor is P-11 and is photographed using a polaroid camera. During the project we will use a digitizing camera to record electron beam data from the phosphor screen, and obtain temporally resolved quantitative data of beam density distribution. With no magnetic field applied the radial current distribution can be observed while with the magnetic field the energy is measured and the energy distribution can be estimated from the deformation of the beam shape. For beam emittance measurements the magnetic field is removed and a "pepper pot" emittance mask is used with the phosphor screen and camera system (Fig. 3).

The electron beam energy was measured to be on the order of the applied voltage 10 - 25kV and have a small energy spread. The electron beam energy was measured by deflecting it in a transverse magnetic field and measuring its displacement on a phosphor screen. The energy was calculated by approximating the vXB force to be perpendicular to the drift tube which is correct when the beam is not deflected much in the region of interaction with the magnetic field (Larmor radius >> length of interaction region). In this approximation the beam energy is given by $E=0.5\ (e^2/m_e)\ (BLD/x)^2$ where B is the transverse magnetic field, L is the length of the region of interaction with the field, D is the drift distance from the interaction region to the phosphor screen and x is the displacement on the screen, e and m_e are electron charge and mass.

Repetition rate capability and lifetime of the electron source can be estimated from test results obtained with BLT switches. In one test the BLT was operated continuously at 280Hz and 120Hz, 20kV, 7.2kA with 100nsec pulselength for $2x10^7$ pulses with no degradation of performance. In another test the BLT switch was operated in burst mode at repetition rates of 5kHz.

The lifetime of the cathode can be estimated as a function of total c rge transfered. In our continuous operation tests a total charge of 15,000 C has been transfered with no degradation of performance. After extended operation with high discharge current, the electrode structure was opened and erosion of the molybdenum surfaces observed. The electrode erosion observed was not large enough to affect operation and it appeared that at least 10 times more erosion could be tolerated without degradation of performance. An additional 2 orders of magnitude in lifetime could be obtained by using electrodes made from tungsten which will have a much lower erosion. A lifetime $>10^{10}$ pulses is expected from a BLT with tungsten electrodes operating at 10kA with a 70nsec pulselength.

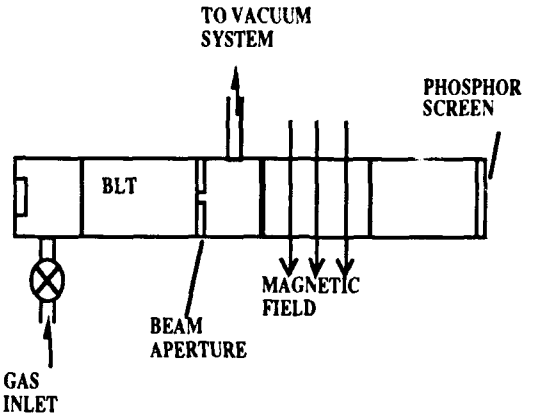

Figure 3. Schematic of electron beam energy measurement apparatus, as described in text.

A preliminary measurement of the beam density in phase space was made using the pepperpot emittance diagnostic. In our implementation of this method the beam passes through a pepper pot mask with an array of 300μm diameter holes each separated by 1mm, then drifts freely 18.7cm to a phosphor screen where it is photographed. The raw data is used to generate a plot of $x'=v_x/v_z$ against x. The emittance ε_o is defined as $1/\pi$ times the area of the ellipse in x'-x space that encloses >90% of the beam electrons. Our estimate of the emittance using this method is $\approx 80\pi \cdot mm \cdot mrad$. This may be compared with the measurements of the Maryland group, which are comparable, using a different structure. The normalized emittance $\varepsilon_n=\beta\gamma\varepsilon_o$ is about $20\pi \cdot mm \cdot mrad$. The normalized beam brightness defined as $B_n = 2I/(\pi\varepsilon_n)^2$ is estimated using our measured beam current of 50 - 70A to be $\approx 1.5x10^{10} A/m^2 \cdot rad^2$. This brightness value verifies that the BLT discharge is a source of high brightness electron beams and agrees with the previous measurement in a demountable multiple gap structure by Rhee et. al. verifying that a single gap

structure can produce similar low emittance beams as multiple gap structures operated at the same voltage. An x'-x plot are shown in Fig. 4. The electron beam parameters measured at USC are summarized in Table 1.

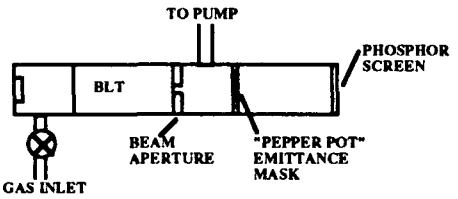

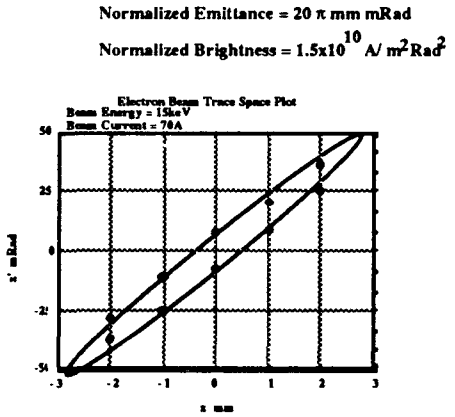

Figure 4. Emittance measurement. The ellipse has been drawn to enclose all the measured points.

Peak Current	≈100A
Diameter	<0.3cm
Current Density	>1kA/cm^2
Pulse Length	≈100nsec
Energy	10-70keV
Emittance rms	80 π mm mrad
Normalized Emittance	20π mm mrad
Normalized Brightness	10^{10} A/m^{2}Rad^2
Repetition Rate	5kHz
Lifetime Estimate	>10^{10} pulses

Table I. High Brightness Electron Beam Results

These results indicate that the BLT is a practical source of high brightness electron beams. The present value of brightness, >10^{10} A/m^{2}rad^2, is directly applicable for an electron injector for a high power induction linac. The value of brightness exceeds the requirements for the induction linac based MTX microwave experiment at LLNL. The current required for the MTX experiment is over 1kA and the repetition rate over 1kHz. The BLT is expected to produce those values of current and repetition rate. The value of beam brightness achieved in the BLT is possibly sufficient for use in a LLNL experiment at infrared wavelengths (10μm). Further development of the BLT as an electron injector could lead to improved performance of linac-based free electron lasers at visible to microwave wavelengths.

TECHNOLOGY TRANSFER

BLT devices have been fabricated by ITT and Integrated Applied Physics inc. as well as by laboratories in Europe and Japan. Testing is underway at University of Texas at Arlington, Naval Surface Warfare Center Dahlgren VA, at the Super-Collider, SLAC, and in Europe and Japan. The BLT is being studied in Japan for laser fusion applications, and for laser isotope separation. ITT has built a BLT that has switched 30 kA at 60 kV in testing at NSWC Dahlgren. Versions of the switch are now being tested by a number of laser companies for excimer laser and other applications. Prototypes have been purchased by Lumonics, Hughes and Northrop.

A Workshop was conducted by Lawrence Livermore Laboratory in October 1990 to consider future directions for developing pulsed power switches for accelerators and other applications. A talk was presented ("Super-emissive cathode switches", M.A. Gundersen, High Average Power Switching Workshop, Lawrence Livermore National Laboratory, Livermore, CA, October 10-11 1990., and Proceedings were prepared[6]. Several SEC switches are of interest for applications considered at this workshop. One switch is an 'input' switch (≈ 25-50 kV, high current), a second is as an 'output' switch (≈ 250 kV, 100 ns pulse, ≈ 50 kA, to replace magnetic pulse compression in order to achieve reliable jitter), and a third is as a trigger switch for a spark gap.

The development of the pseudo-spark switch in Europe and the further development (and patenting) of the back lighted thyratron or BLT in the U.S. by Integrated Applied Physics has spawned a switching technology with the potential to exceed available switching parameters. The electrically triggered, single gap, pseudo-spark switch, much smaller than a conventional thyratron, has demonstrated fast switching at peak currents and rates of current rise at least an order of magnitude superior to conventional

thyratrons at voltages up to 100kV. A back lighted thyratron can be operated at higher voltages because multiple series stages can be switched simultaneously (sub-ns jitter) with only tens of microjoules of optical energy per stage cathode. Marx-bank operation with the BLT has been demonstrated. The optical triggering advantages of the BLT enable new and innovative power conditioning strategies to be pursued that potentially reduce system weight and cost while reducing the complexity and increasing the redundancy and reliability.

However, the application of the BLT technology is presently limited by the development funding required to produce commercially available devices that utilize the BLT advantages. Presently, development of commercial devices is being conducted in the U.S. and other nations such as Japan and in Europe. The BLT technology, patented in the U.S. by a U.S. company, is attractive for many applications because of the optical trigger system that permits innovative system designs.

The New Switches - Comparison with the State of the Art

Types of switches under development include

1. High Voltage, series stage BLT
2. High Current, parallel aperture, BLT
3. High Average Power BLT (> 10 MW)
4. Related specialized switches

Important middle steps are necessary to carry a these switches to applications and the marketplace.

An approximate comparison is made here to existing switches. This is done in a 'generic' fashion, in order to provide information about the fundamental differences in types and applications. In addition to making possible state of the art comparisons, this approach provides a little better overview of what actually exists, and what type of switch can be expected to impact and produce new applications breakthroughs. There is at present no industry 'standard' that makes it possible to readily compare switching and modulator requirements for pulsed power applications. Such standardization would be very useful, as it would go beyond classification of switches, and would facilitate understanding of where new applications would be most productive.

Cathode comparison

The heart of the BLT is the super-emissive cathode. The cathode is perhaps the most critical element for many applications, and it is often the least considered. The super-emissive cathode is described above, and shown schematically in figure 5.

In order to make an adequate comparison, the BLT cathode is shown in figure 2 in comparison with a cathode that provides comparable peak current, the EG&G MAPS 40, or HY 5.

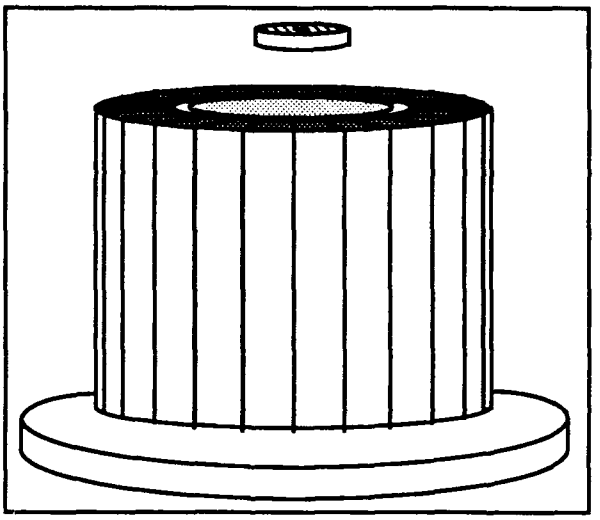

Figure 5. Comparison of 40 kA cathodes. Top. BLT cathode, with emissive area of ≈ 1 cm^2. Bottom. EG&G MAPS 40 cathode, with 5000 cm^2 emissive area. Both cathodes produce emission reliably into a *glow*, not arc, mode.

The BLT cathode is much smaller, is much simpler to fabricate, and is fabricated from a refractory metal, such as molybdenum. Shown in Table 2 is a comparison with several other high power thyratron cathodes for which data is available.

Input switch for accelerator modulator

The modulators for accelerators such as the ATA, ETA II, DARHT, SLAC, and others are commonly configured as class 'C' modulators (following Guillimin), and require switching in several stages. Normally there is an input switch that is a high power thyratron. At present, testing of the EEV CX 1536R and ITT F257 at Ft. Monmouth is to address input switch requirements for ETA II - type applications.

The input switch requires low jitter, because there are many modulators, and for some of the above must operate at high repetition rate. Typical current and voltage requirements are 25 to 40 kV, 3 to 6 kA, with a 5 μs pulse length. Repetition rates vary from a few Hz to several kHz. These requirements in combination, especially at high repetition rate, are very difficult to achieve, and along with the output stage (discussed below) are very critical limitations to the development of these accelerators. Testing at high repetition rates (>kHz) of these switches has been limited to 30 to 100 second bursts, with total number of pulses of the order of 10^6 (well below life goals in excess of 10^9 to 10^{11}).

Type	Area (cm^2)	Power (heater)	Peak Current (kA)
HY-5	500	158 W	25
HY-7	5000	1120 W	40
1802	100	88 W	2 - 10
BLT-250	**1**	**None**	**> 50**

Table 2. High current cathode comparisons. Peak currents for EG&G tubes are listed for repetition rates < 50 pps, and are less for higher repetition rates.

Shown in figure 6 is a size comparison for a BLT 250 and a typical high power thyratron. As a fairly typical example, test condition goals for an SEC switch include (not necessarily occurring during the same run), epy = 42 kV (stand-off voltage), i_b = 20 kA (peak current), t_p = 20 μs (pulse length), PRR = 200 Hz (repetition rate), P_{ave} = 375 kW (average power), I_{ave} = 25 A (average current), I_{rms} = 1.26 kA (rms current).

The BLT (right, figure 6) has the potential to be used for applications now requiring the larger switch. Potential advantages include lower parts count, more accessible thermal control, no cathode heating and much less cathode size, and considerably less overall size. The BLT has already realized peak current, stand-off voltage, pulse length, and repetition rates comparable to and in excess of those listed, and development is to achieve life and higher repetition rate, and these ratings taken in combination.

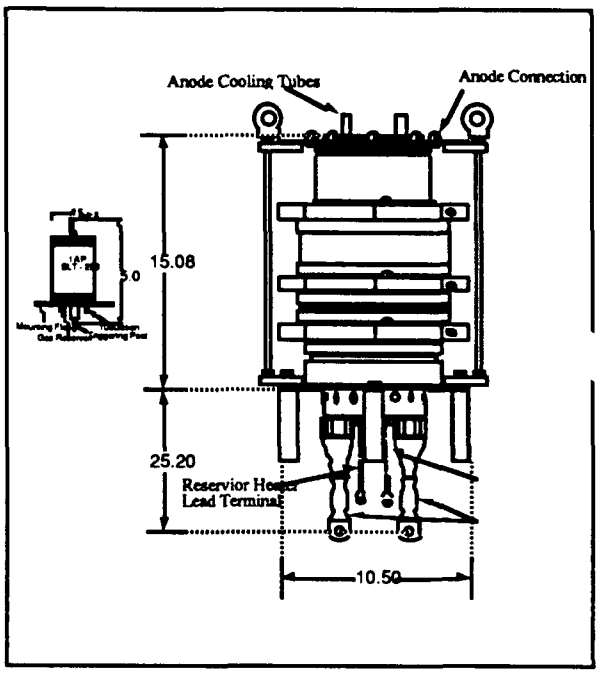

Figure 6. Rough size comparison of prototyper BLT and high power thyratron, which have comparable peak current, stand-off voltage and pulse length ratings.

Output switch for power conditioning

In order to provide an appropriate, high voltage (250 kV is a typical voltage) pulse to an induction accelerator cell, such as one of the accelerators cited above, it is usually necessary to either use a spark gap, or use a technique known as magnetic pulse compression (Fig. 7). With either of these techniques, low jitter is very difficult to achieve for high power, high repetition rate operation, and thus the output stage for a power modulator for these applications is a very serious limitation that effects the development of existing systems, and limits the options for new systems planning.

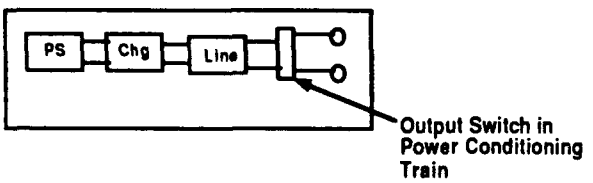

Figure 7. Output switch for power conditioning.

Typical operating characteristics would be multi kA, ≥ 250 kV, very fast current rise, and for some applications very high (> 1000 Hz) repetition rate. For example, the output of the ETA II system requires 250 kV, 63 kA, 70 ns, $6x10^{12}$ A/sec dI/dt, nsec jitter, 5000 pps, and 1200 A rms current.

Several versions of the switch offer advantages including low jitter, high voltage, high current and fast di/dt. Therefore, the development of a BLT or pseudospark for these applications would considerably change the options available to the system planner.

High voltage, high current switch

At the limit of present thyratron state of the art is the CX 1812 (EEV) thyratron designed for operation at 100 kV stand off voltage and 100 kA peak current. Versions tested to date have achieved 70 kV and 70 kA at a repetition rate of 5 Hz in testing at Los Alamos National Laboratory. Work at USC has demonstrated BLT operation, using flashlamp switching, at low repetition rate, but at 100 kV and 70 kA. Peak currents were limited by safety considerations, not by any observed switch limit. Shown in Figure 8 is a comparison of the EEV 1812 and the BLT that was tested at 100 kV.

The laboratory BLT has not demonstrated high average power; however, the EEV switch has also not performed well at high voltage. Part of the difficulty is the problem in braze sealing the large diameter (10") EEV tube – a difficulty that is obviously less of a problem with the much smaller BLT utilizing the super-emissive cathode.

The BLT offers higher current capability in a smaller package with low jitter, optical or electrical control, and what is also now observed is that these simplifying factors also affect stand-off voltage. The high stand-off voltage is apparently easier to achieve in the BLT or pseudospark configuration.

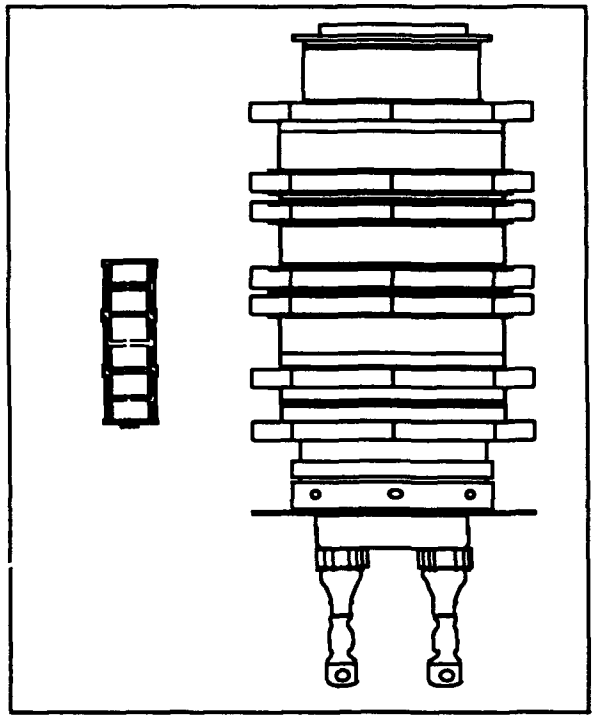

Figure 8. Rough size comparison of the EEV CX 1812 (right) and a three gap flashlamp triggered BLT that has been operated at 100 kV.

High coulomb, ignitron-type switch

Certain applications – such as kinetic energy weapons – require switching of very high current, and multi-coulomb charge in a single pulse. Most present switching devices for these applications are limited to low repetition rates, and have additional drawbacks. For example, the ignitron is somewhat heavy, and requires special housekeeping in order to manage a supply of mercury. It is also a low repetition rate switch for most applications.

The BLT offers the prospect of much higher repetition rates in a simple device. Important preliminary data exists regarding operation of this multichannel switch. The initial concept was developed under Mechtersheimer at St. Louis, France, where it was operated in a 10 channel configuration at peak currents ≈ 10 kA. It is significant because the device was operated at repetition rates in excess of 10 kHz. Subsequently, the concept was used in a 20 channel prototype device developed at the Siemens Kraftwerk Union in Erlangen, West Germany. This

device was designed for higher peak current, and was observed to switch 100 kA, 40 kV at the astonishing repetition rate of 40 Hz[7],[8]. Thus, the concept is clearly of importance for this application because it offers a means of combining high current operation with high repetition rate operation.

Research must assess the feasibility of a multichannel structure that would also switch in the long pulse regime. Although there will be a trade-off in long pulse operation and repetition rate, one can readily consider structures that would nevertheless dramatically improve operating repetition rates while retaining the intrinsically simple housekeeping.

As discussed above, data for high peak current from single aperture switches of the type to be developed is now available in the literature from numercus sources. The high current pseudospark data from CERN[9] demonstrated up to 200 kA peak current with a 5 μsec pulse in a single aperture switch. The switch has been operated in parallel with three others to switch 0.5 MA at 1/3 Hz for ≈400,000 pulses[10].

At USC, A small, single aperture device has been reported[11] that switched 81.6 kA peak current in a relatively short (≈ 400 nsec) ringing pulse (≈ 75% reverse current) at 20 kV. Of related importance is that the USC results do not show arc-type behavior during this experiment -- it should be possible to extend the glow-type operation to these very high currents.

Space application high power switch

Very small high power switches are envisaged. Shown in figure 9 is a design for a switch that is under development as part of the technology transfer effort associated with this project. The super-emissive cathode allows this exceptional small body to be developed for applications previously requiring 5000 cm^2 area cathodes, and hence large volume and weight. The switch shown has no cathode heater requirement, and, depending on application, little or no gas reservoir heater requirement. By moving beyond the present day possibilities, it is possible to consider such a switch for a range of space applications.

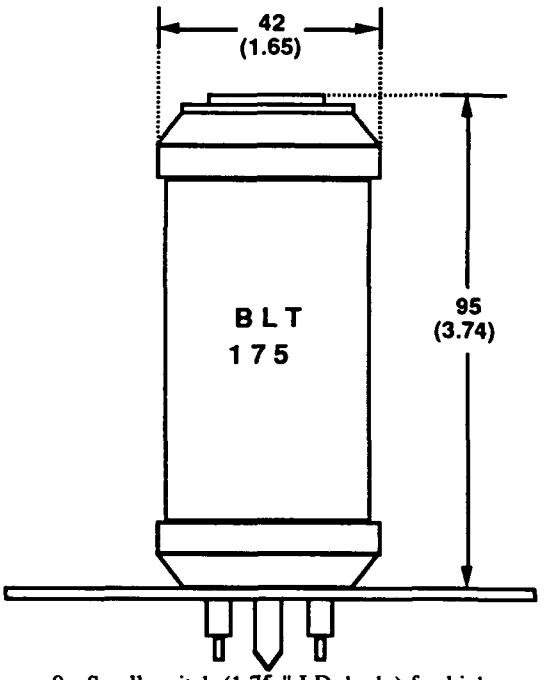

Figure 9. Small switch (1.75 " I.D. body) for high power applications. This switch is expected to conduct peak currents in excess of 30 kA, and stand off voltages comparable to present day high power thyratrons.

Summary

A range of switch applications exist that will be fostered by this technology. These include:

- Input switch for power modulator (ETA II, high energy physics)
- Output switch for power modulator (ETA II, high energy physics)
- Space based systems
- Multi kHz switch, such as Hitachi is developing
- Excimer, other laser switch - Limiting industrial applications
- Industrial applications for accelerators - FEL's, medical, other beams
- Opening switch potential - Inductive energy store, power industry
- High voltage, high current switches for microwave generation

- Accelerator, Los Alamos - Input, Output, Optical Control
- Simple, high rep rate ignitron
- Fusion systems
- High energy physics applications for injection accelerators and kickers

There is significant fallout for robust, industry worthy applications of pulsed power with successful implementation of the new technology.

Breakthrough aspects – technical reasons that BLT and pseudospark development will significantly impact pulsed power applications – of the project include the following:

1. dI/dt – current rise rate is being significantly improved.
2. Jitter – will be low, and should be low over a long life.
3. Life – the cathode offers the prospect of long life.
4. Peak current – order of magnitude improvement.
5. High coulomb – long pulse, ignitron competition.
6. Variations in combination provide basis for **new systems concepts.**

REFERENCES

1. M. A. Gundersen and G. Schaefer, Eds., "The Physics and Applications of Pseudosparks," NATO ASI Series B: Physics Vol. 219 (1990).
2. K. Frank, E. Boggasch, J. Christiansen, A. Goertler, W. Hartmann, C. Kozlik, G. Kirkman, C. Braun, V. Dominic, M. A. Gundersen, H. Riege, and G. Mechtersheimer, "High-power pseudospark and BLT switches," IEEE Trans. on Plasma Science **16** (2), 317 (1988).
3. The emission processes are discussed in detail in "A super-emissive self-heated cathode for high-power applications," W. Hartmann, G. F. Kirkman, V. Dominic, and M.A. Gundersen, IEEE Trans. Elect. Dev. **36** (4), 825 (1989), "Origin of anomalous emission in superdense glow discharge," W. Hartmann and M.A. Gundersen, Phys. Rev. Lett. **60**, (23), 2371 (1988), "Evidence for large-area superemission into a high current glow discharge," W. Hartmann, V. Dominic, G.F. Kirkman, and M.A. Gundersen, App. Phys. Lett. **53** (18), 1699 (1988), and "Cathode-related processes in high-current density, low pressure glow discharges," W. Hartmann and M. A. Gundersen, in "The Physics and Applications of Pseudosparks," M. Gundersen and G. Schaefer, Ed., Plenum Press, 1990. The last-cited book also reviews other aspects of pseudosparks.
4. H. Bauer, G. Kirkman, and M. A. Gundersen, "A two-component model for the electron distribution function in a high current pseudo-spark or back-lighted thyratron," IEEE Trans. Plasma Sci. **18** (2), 237 (1990).
5. W. Hartman, G. Kirkman, and M. A. Gundersen, "Current quenching in the pseudospark," Appl. Phys. Lett. **58**, 574 (1991).
6. These proceedings are available from Lawrence Livermore National Laboratory, UCRL-JC-106836.
7. H.J. Cirkel, "High power excimer laser", presented at Lasers '87, Lake Tahoe, CA, Dec. 1987.
8. G. Mechtersheimer, R. Kohler, T. Lasser, and R. Meyer, "High repetition rate, fast pseudo-spark switch," J. Phys. E: Sci. Instrum. **19**, 466, 1986.
9. E. Boggasch, V. Brueckner, and H. Riege, "A 400 kA pulse generator with pseudo-spark switches", Proceedings of the 5th IEEE Pulsed Power Conference, Arlington, VA, pp. 820, 1985.
10. H. Riege and E.P. Boggasch, "High power, high current pseudospark switches", IEEE Trans. Plasma Science **17**, 775 (1989).
11. G. Kirkman, T-Y. Hsu, R-L. Liou and M. A. Gundersen, "Recent experimental studies of the BLT switch", Proc. seventh IEEE Pulse Power Meeting, June 1989.

Martin A. Gundersen, received the Ph.D. degree in physics from the University of Southern California, Los Angeles. From 1973 to 1980 he was with the Department of Electrical Engineering, Texas Tech University, and in 1980 he joined the Department of Electrical Engineering at the University of Southern California, where he is currently Professor of Electrical Engineering. He has been Visiting Professor at the University of California, Los Angeles (1986-1987), Visiting Scientist at the Massachusetts Institute of Technology (MIT) (1986-1987), CERN (1987), and MIT (1989). His research activities are in applied physics in the areas of pulsed power physics, quantum electronics, and semiconductor devices and physics. Quantum electronics research includes development of optically pumped and discharge lasers, and high pulse-energy single-mode IR lasers. Semiconductor research includes the investigation of the physical processes occurring during recombination in semiconductors, optoelectronic devices, and GaAs-based pulsed-power devices. Pulsed-power physics research also includes the invention and development of the back-lighted thyratron switch, studies of super-emissive cathode processes in high-current plasma devices, and applications of high-density plasma-based devices to accelerator problems. Dr. Gundersen is a Fellow of the Optical Society of America and the IEEE. He has served as Chairman, IR Lasers Topical Meeting, 1980, Chairman, Power Conditioning Workshop (Dec. 1985), co-Chairman, SPIE Pulsed-Power for Lasers (Jan. 1987), Director of the 1989 NATO Advanced Research Workshop on High Power Glow Switches, Symposium Chair, Pulse-Power for Lasers, 1989 OSA Meeting, Technical Program Chairman, IEEE Power Modulator Symposium, 1990, and Program Chairman, 1991 SDIO/ONR Pulsed Power Meeting.

George Kirkman, photograph and biography not available at the time of publication.

Rong-Lin Liou was born in Taipei, Taiwan in 1961. He received the diploma from the National Taipei Institute of Technology, Taipei, Taiwan in 1981 and M.Sc. degree from the State University of New York at Stony Brook in 1987, both in Electrical Engineering. He is presently working towards the Ph.D. degree in Electrical Engineering-Electrophysics at the University of Southern California, Los Angeles, California. His current research interests are the electron beam generation in the Back-Lighted Thyratron and its interaction with plasma for the generation of millimeter wave.

Tseng-Yang Hsu was born in Taipei, Taiwan, in 1958. He was awarded the Bachelor of Science degree in atmospheric science from the National Taiwan University in 1981, the Master of Science degrees in physics and in electrical science from the University of Michigan, Ann Arbor, in 1986. He is presently a Ph.D. candidate of the Department of Electrical Engineering-Electrophysics, at the University of Southern California. His current research interests are in the fundamental physics of the superemissive glow discharge and its applications to particle beam generations.

INVESTIGATIONS OF PULSED-POWER SYSTEMS USING HIGH-RESOLUTION SPECTROSCOPIC METHODS

G. Davara, R.E. Duvall, A. Fisher*, M.E. Foord, A. Fruchtman, K. Gomberoff, Ya. Krasik, C. Litwin, Y. Maron, L. Perelmutter, M. Sarfaty, E. Sarid, and L. Troyansky.

Department of Physics
Weizmann Institute of Science
Rehovot, 76100, Israel.

Abstract-Recently developed spectroscopic diagnostic methods are being used to investigate the plasma behaviour in three pulsed-power systems: a Plasma Opening Switch, a Magnetically Insulated Ion Diode, and gas-puffed Z-pinch. For the plasma opening switch a novel gaseous plasma source was developed which is mounted inside the inner conductor. High spatial, spectral, and temporal resolution measurements were achieved. The methods allow for reliably determining important plasma properties such as the magnetic field penetration, electron heating, turbulent electric fields, and particle velocity and density distributions. Our theoretical modelling is time-dependent and accounts for the nonequilibrium features of these highly dynamic plasmas. We believe that such detailed and systematic microscopic investigations of plasmas interacting with strong electric and magnetic fields are essential for improving the operation of various pulsed power devices.

I. INTRODUCTION

Obtaining high resolution measurements in pulsed-power system plasmas and studying the microscopic processes in these plasmas are important because the plasma properties crucially affect the operation of such systems. For systems in which plasma carries high-density currents the system impedance is critically influenced by the plasma parameters (density, temperature, resistivity). The plasma expansion, magnetic field penetration, and plasma pushing are all factors which control the pulse sharpening and voltage and power multiplication in power-conditioning devices. The plasma pushing, magnetic field penetration, and plasma turbulence determine the properties of pinching plasmas. In systems in which the plasmas serve as sources for ion beams, the time dependent plasma composition and the particle transport in the plasma determine the ion beam composition. The plasma nonuniformities affect the emittance of the generated ion beams. Our measurements are supported by a theoretical modelling which addresses these issues.

In our plasma laboratory we investigate the behavior of plasmas in three different pulsed-power devices: a Magnetically-Insulated Ion Diode (MID), a Plasma Opening Switch (POS), and a Z-pinch. Until recently, such plasmas had been little diagnosed because the strong electric fields ($\simeq$1 MV/cm) that prevail over a relatively narrow gap spacing ($\simeq$1 cm) and the high currents ($\simeq$1 MA) inhibit the use of common plasma diagnostic methods. The understanding of the complicated phenomena that take place in a high power device can be improved only if high-resolution non-intrusive diagnostic methods are used to observe many physical quantities inside the device. We have gained insight into the physics of the magnetically-insulated diode plasma in the last few years by developing high-resolution spectroscopic methods which were combined with collisional-radiative atomic modelling calculations[1-8,10,11]. We are currently extending these methods for the study of the POS and Z-pinch plasmas. In this report, we describe our diagnostic systems (Sec. II), our recent spectroscopic observations in the MID (Sec. III), and the newly built POS and Z-pinch experiments (Sec. IV and V) together with preliminary measurements.

II. DIAGNOSTIC SYSTEMS

Fig. 1 summarizes the various features of our diagnostic systems. In brief, our laboratory is equipped with a few 1-m and 1.3 m spectrographs. Until recently, the spectral line profiles have been measured in a single dis-

* University of California, Irvine, and Naval Research Laboratory, Washington D.C.

charge by optically dispersing a spectral line at the output of the spectrograph, projecting its image on a rectangular array of 12 fibre-bundles, and measuring the light signal transmitted in each fibre by a photomultiplier tube and a digital oscilloscope.

The temporal resolution in these systems is $\simeq$5 ns. In the near future, we plan to couple the image plane at the spectrograph exit window to a high resolution streak camera detector system. A high resolution low-noise CCD camera records the streak camera image and the CCD is readout to a 386-PC for processing and analysis. The highest spectral resolution that can be achieved is 0.05 Å with a 15 Å wide spectral window. Employing a sweep speed of 1 μs, the time resolution of the streak camera is 5 ns. At the fastest sweep of 10 ns, 100 ps time resolution is possible. The spatial resolution is determined by the input optics and is typically 0.5 mm.

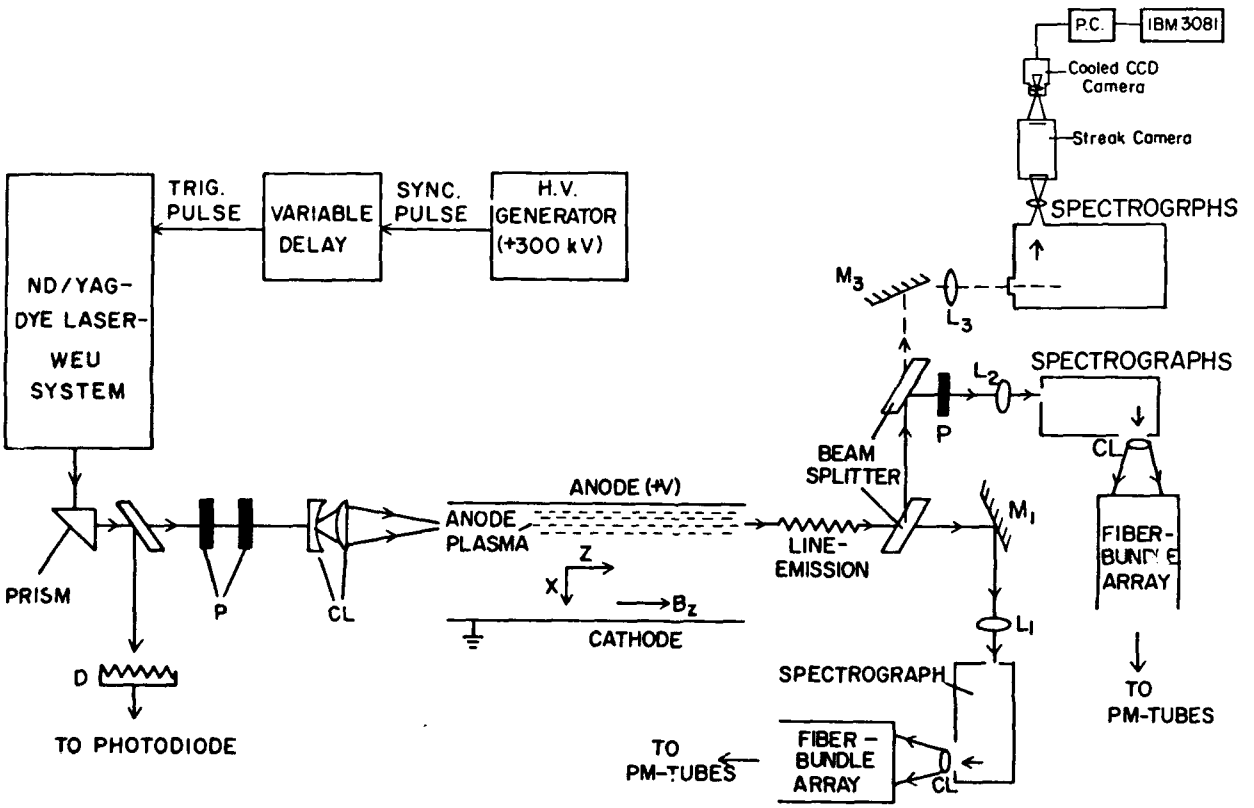

Fig. 1. The laser system and the diagnostic arrangement. WEU, D, Cl and M denote a wave extending unit, a diffuser, a cylindrical lens, and a mirror, respectively. The laser light, synchronized with the diode voltage pulse, can be directed into the diode in the x and y directions. Laser light, induced fluorescence, and spontaneous emission can be collected in various directions by the two spectroscopic systems. The polarizers P are used for the polarization spectroscopy. For cylindrical plasmas the line-emission is imaged on a cylindrical fibre array. For observing the spectral line profile as a function of time in a single discharge either a fibre-bundle-PM-tube-digitizer system or a fast streak camera system are used.

The spectrographs are equipped with 2400 grooves/mm gratings allowing for a spectral resolution down to 0.06Å. The fused-silica optics, the photo-multiplier tubes, and the streak camera allow for sensitivity in the range 2000-7000Å. Absolute calibration of the systems over the entire spectral range provides the absolute particle level populations in the plasma. Usually two spectroscopic systems are used simultaneously in order to measure a few quantities in a single discharge.

Our laboratory is also equipped with a high-power pulsed (6 ns) dye laser pumped by a Q-switched Nd:Yag laser equipped with a unit that extends the wavelength range to 216-900 nm. The laser pulse energy is up to 120 mJ. This laser system is used for diagnostics based on resonant laser absorption or on laser induced fluorescence. With this system the particle density and velocity distributions were determined with a resolution down to $\simeq$30 μm, as described in Sec. III.

We have also constructed time-dependent collisional-radiative models of many atomic systems, such as carbon, magnesium, and silicon in order to interpret the absolute and relative spectral line intensities. These calculations are especially important for diagnosing short lived pulsed power plasmas whose level populations are far from being in a steady state.

III. HIGH-POWER DIODE EXPERIMENT

The behavior of the electrode-plasmas in high power electron or ion diodes, transmission lines, and microwave-sources significantly affect the device operation. Recently, we have investigated the anode plasma in the MID. The expansion and magnetic field penetration in the anode plasma in intense ion diodes determine the time-dependent actual diode acceleration gap and the magnetic field flux in this gap.

Previously we used Zeeman splitting[5] to determine the magnetic field penetration into the anode plasma as a function of time throughout the 100-ns-long voltage pulse. From the fast field penetration we inferred a plasma resistivity significantly higher than the classical one. This led us to develop experimental methods to search for turbulent electric fields in the plasma that could be associated with the inferred anomalous conductivity. Development of experimental techniques

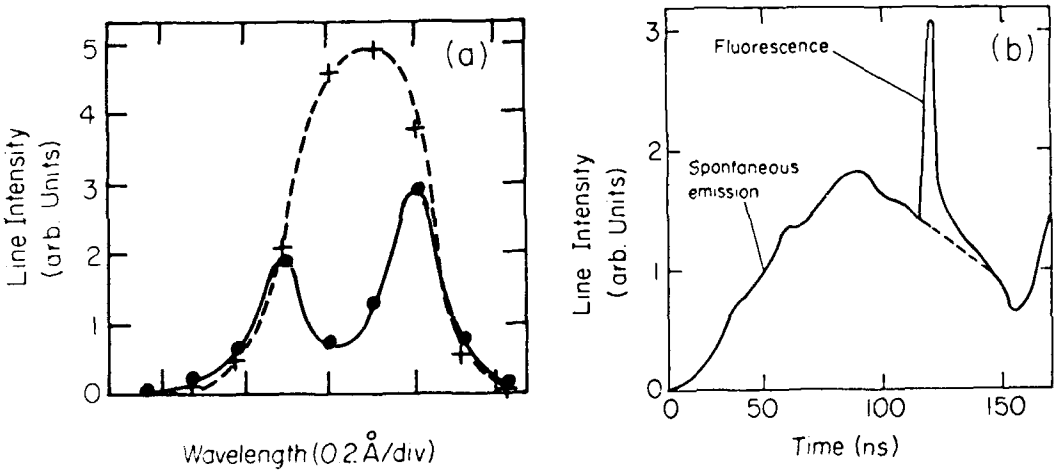

Fig. 2. (a)Typical spectral profile of the laser light transmitted through the plasma for light wavelength λ=2795.53Å corresponding to the MgII $3S_{1/2} \rightarrow 3P_{3/2}$ transition (solid curve). Also shown is the spectral profile with no plasma in the diode (dashed curve).
(b)Spontaneous emission of the $3P_{3/2} \rightarrow 3S_{1/2}$ transition together with the fluorescence resulting from the same transition induced by the laser saturated excitation of the MgII $3S_{1/2} \rightarrow 3P_{3/2}$ transition. Here, the laser beam energy was $\simeq$30 μJ, the time was 115 ns and the observation distance from the anode surface was 0.1 mm.

to determine the amplitude, direction, and frequency range of fluctuating collective electric fields in pulsed-power plasmas is believed to be of great importance since the plasma turbulence can affect the plasma heating, flow, and hydrodynamic evolution in time. We investigated the anisotropic fluctuating electric fields in the anode plasma by the use of polarization spectroscopy of the Stark broadened hydrogen lines. The method utilizes the effect that when the emission line spectral profiles are affected by collective anisotropic fields the observed profiles are dependent on the directions of the polarization and of the line of sight as was first used for longer duration plasmas in a mirror machine[9]. In our experiments, the spectral profiles of the H_α and H_β lines were measured for two lines of sight and two different polarizations[10]. The data is being analyzed using detailed calculations of the Stark broadening for these lines under the influence of the collective fields in the plasma. Turbulent electric fields with an amplitude of a few kV/cm and a direction mainly perpendicular to the anode surface and to the externally applied magnetic field are inferred[10]. Bounds on the turbulent-field frequencies were also obtained. We are presently formulating a mechanism that could be responsible for the inferred fluctuating fields[12]. The modified two-stream instability, driven by the ion drift that was observed in the experiment, leads to electrostatic oscillations with frequency and saturated amplitude comparable to the measured ones.

In a previous study [7] we have shown that the particle fluxes from the anode surface into the plasma in our magnetically insulative ion diode are considerably affected by the plasma properties at the immediate vicinity of the anode surface. Since studying the plasma properties very close to electrodes is highly important for various applications we developed methods, based on laser absorption and laser-induced-fluorescence, to investigate the plasma near the anode surface[11].

We first note that the use of emission spectroscopy to determine the particle densities can be considerably erroneous since in short-duration plasmas or in plasmas near electrodes most of the particles lie in the ground state

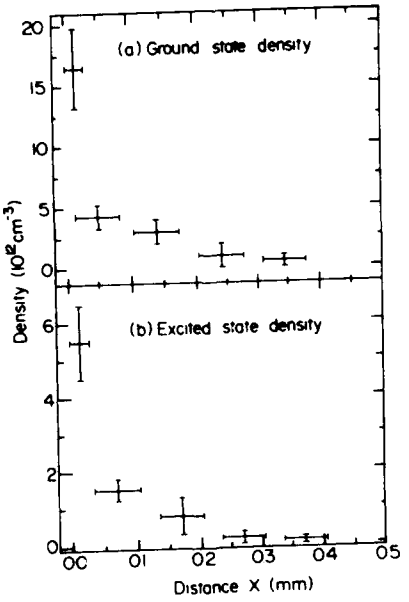

Fig. 3. (a)The MgII ground state density as a function of the distance x from the anode surface obtained from the laser absorption at 2795.53Å for t=55 ns. The spatial resolution near the anode surface is $\simeq$30 μm. The data reveal a large density gradient of MgII ions near the anode surface (see the data point at $x \simeq 0$; (b) Similar to (a) for the density of the MgII excited state, $3P_{3/2}$, obtained from the laser absorption at 2798Å.

and the densities of the latter cannot be reliably determined from excited level populations. Laser absorption and laser-induced fluorescence allowed us to directly determine the densities of the particle ground states or of states that radiate in the VUV region. Furthermore, Doppler broadening of the absorption line allowed the particle velocity distribution to be obtained. In addition, these methods enabled us to achieve a high spatial resolution and to determine, for the first time, the particle density and velocity distributions within a few tens of μm near the surface. Fig. 2 gives a sample of our spectroscopic measurements, in which the laser-light resonant absorption in the plasma and the laser-induced-fluorescence are shown, and Fig. 3 shows the inferred ground state and excited-state densities.

The densities of the MgII ground and first-excited states and of the LiI ground state were observed to be much larger within $\simeq$50 μm from the anode surface than further away in the plasma, as shown in Fig. 3. This dense layer probably serves as the source of particles previously observed to be injected throughout the pulse into the plasma[7]. Hydrogen atoms were found to be distributed much farther than MgII ions and LiI atoms. The MgII Doppler broadened absorption profile showed that the MgII velocities seen in the plasma are acquired by the ions mainly within $\simeq$30 μm near the anode surface. This shows that a significant fraction of the MgII velocities seen in the anode plasma[4] is acquired by the ions within $\simeq$30 μm from the anode surface. This is a complement to our previous data[7] which suggested that the ion kinetic energies in the plasma result from the presence of electric fields at the immediate vicinity of the anode surface.

The use of our data in the explanation of the previously observed absolute fluxes of various charge states injected from the surface and in obtaining estimates of the particle ionization rates at the immediate vicinity of the anode surface is currently under study[11]. This will enable us to estimate n_e and T_e close to the surface and to compare them to the values inferred from the measured ratio between the ground and the first-excited level densities. This ratio can also give information on the material release from the surface into the adjacent plasma layer. We believe that such studies may help to improve the understanding of various phenomena in plasma-surface interactions.

It has been suggested that an ionizing neutral layer near the anode surface makes a major contribution to the initial plasma buildup[13]. Several theoretical models are currently being used to study the general problem of ion flow through an ionizing layer and the resulting plasma buildup and screening of the electric field[14]. Our analysis indicates that electron flow to the anode plays a crucial role in the electric field time evolution. Comparison to measurements of the electric field in the MID will, therefore, allow us to estimate the dominant mechanisms of electron flow from the plasma. Comparisons between theory and experiment will also provide an estimate of the initial neutral layer density, which can then be compared with that value inferred from the measured electron density in the fully ionized plasma.

IV. THE Z-PINCH EXPERIMENT

A Z-pinch device, recently constructed, is powered by a 16 μF, 50 kV capacitor bank that is switched through a low inductance transmission line, delivering 400 kA with a 1 μs rise time, as shown in Fig. 4. High pressure gas is released through an electromagnetic fast valve to an annular nozzle, producing a well collimated uniform gas profile between the anode and cathode. The high voltage is then applied across the anode-cathode region which initiates the discharge.

Various diagnostics have been developed for monitoring many characteristics of the plasma. Framing and streak photography are used to observe the uniformity of the initial breakdown. This has directed our nozzle design and resulted in well formed uniform discharges. The plasma shell thickness and radius is also determined, which is necessary for in interpreting line-integral spectral intensities. A four-headed Penning probe was also used to verify the initial neutral gas uniformity and collimation.

PIN photodiodes with metallic filters and

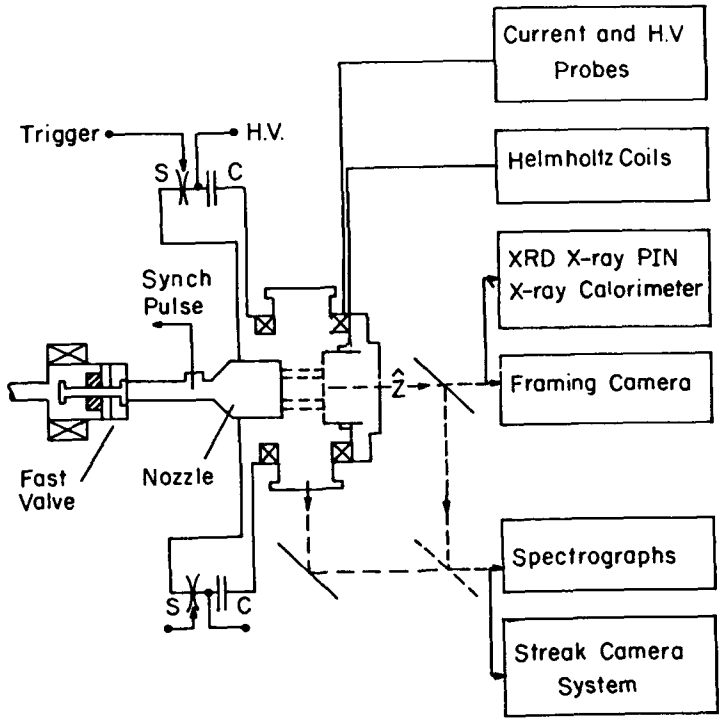

Fig. 4. Experimental arrangement of the Z-pinch and the diagnostic systems. The nozzle injects an annular gas shell in the anode cathode region which forms the initial plasma geometry. S denotes a switch. Helmholtz coils generate $\simeq$2 T axial magnetic field.

high voltage XRDs are routinely used to monitor the high(1-3 kev) and low(10 eV-1 keV) x-ray emission emitted during the pinch. The signal is used to determine the total x-ray yield and to monitor the pinch conditions. Magnetic probes are located in various positions in the experiment to measure the plasma current and monitor the switching.

Presently, as we prepare for the streak-camera detector system to arrive, a single channel PMT detector is used to investigate the intensity of emission lines from various transitions. Using CO_2 gas we have observed strong line emission from CI-CIV ions during the entire discharge, see Fig. 5. These preliminary results are important in allowing us to estimate the plasma temperature and density by single shot spectral scans and to select appropriate transitions for our streak camera detector system. During the pinch phase, continuum emission, which is strongly dependent on the electron density is also used to monitor the pinching.

Spectral line profiles will be used to characterize the plasma density and temperature. Stark broadening measurements will directly determine the electron density over a large density range(10^{15}-10^{18} cm^{-3}). The electron temperature will be determined by use of the collisional radiative codes and measurements of spectral line intensity ratios. Ionization dynamics will be studied by determining the rate of neutral and ion production from the collisional radiative calculations and spectral line measurements.

A preionization source is being developed in order to extend the range of operation to lower densities. This will allow better control of the initial plasma density and allow changes in the initial plasma conditions to be studied experimentally and theoretically.

An axial magnetic field will be applied in order to study Megagauss field compression and strong field diffusion. The field coils and

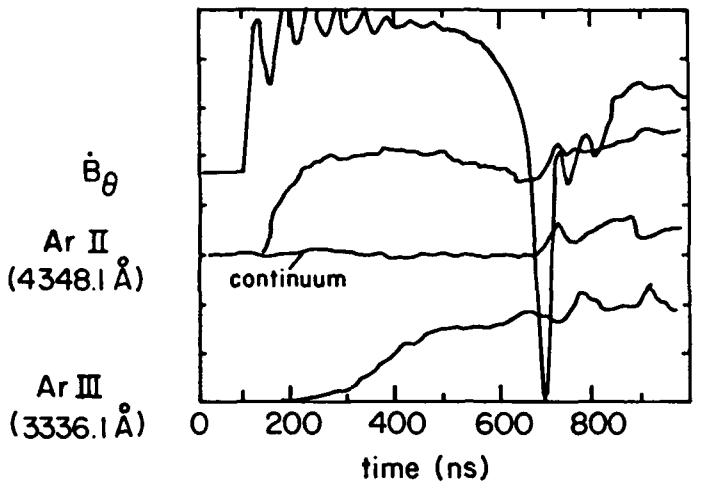

Fig. 5. Spectral emission from ArII (4348.1Å) and ArIII (3336.1Å) transitions from the Z-pinch plasma. The $\dot{B}_\theta$ trace shows strong pinching at 700 ns. Also shown is emission near 4358Å due to continuum radiation. The ordinate is in arbitrary units.

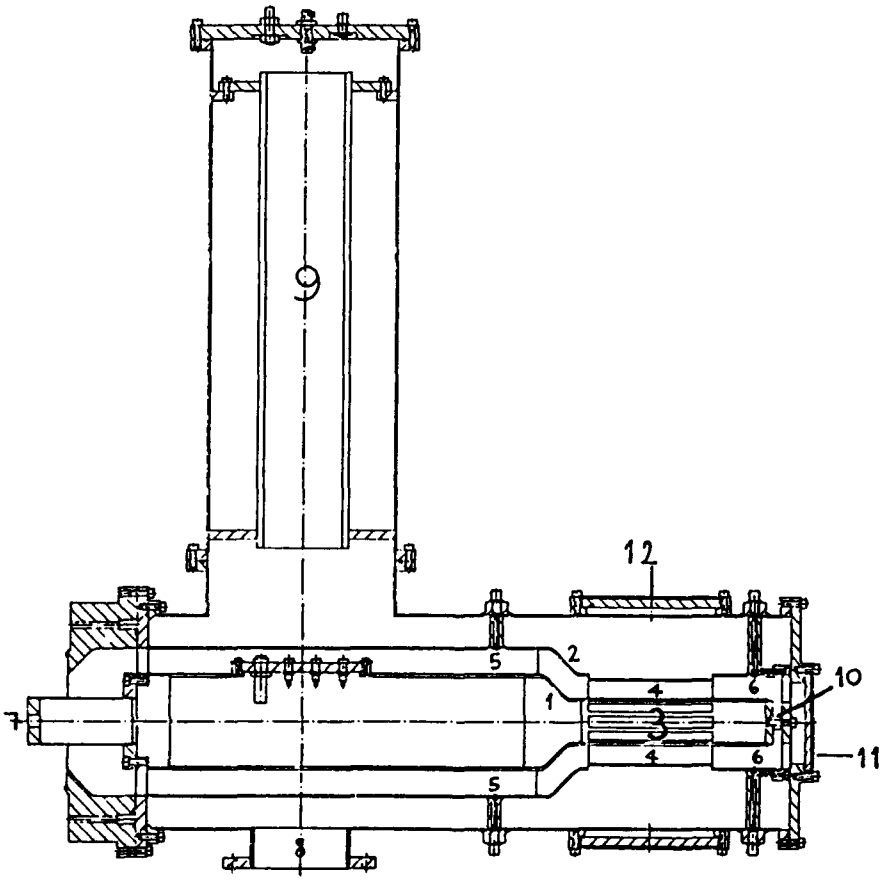

Fig. 6. Plasma Opening Switch experimental arrangement: 1-Anode; 2-Cathode; 3-Plasma gun; 4-POS region; 5-upstream $\dot{B}$ loops; 6-downstream $\dot{B}$ loops; 7-to Marx generator; 8-Vacuum pump exit; 9-Inductive coupling tube; 10-Downstream Load; 11-Axial access; 12-Transverse access.

circuit are tested and ready for installation. The magnetic field will be measured using Zeeman splitting of spectral line emission. Polarization spectroscopy of Stark profiles will be used to estimate fluctuating electric field amplitudes which will be correlated with the possible anomalous magnetic field diffusion.

V. THE PLASMA OPENING SWITCH EXPERIMENT

The plasma opening switch concept is relevant to various pulsed-power applications. Although considerable progress in the switch operation has been made in the recent years, experimental investigations are still highly required in order to examine the various underlying theories and to suggest improvements in the device operation. The distribution of the magnetic field and the particle flow in the switch plasma are of major importance. We have built a novel POS experiment for systematically studying these two phenomena using spectroscopy. The main distinct feature of our experiment is that the plasma is injected radially from the inside of the inner conductor. Also, we use a gaseous source in order to control the plasma species, as required for the spectroscopic observations and for examining models. Our present experiment is designed for the 100-ns time scale regime, however experiments for longer times can be built in the future. The designed POS system is shown in Fig. 6.

The plasma source is composed of a fast valve connected to a hollow cylindrical tube having $\simeq$100 capillary outlets for radial plasma injection, see Fig. 7. The fast opening allows the gas to propagate quickly into the hollow cylinder and uniformly fill the capillary channels. The inner coax surface consists of a stainless steel mesh (50%) connected through a 50 Ω resistor to the outer surface of the cylindrical tube. A graphite cathode brush is mounted inside the hollow cylinder along the axis. A 20-kV pulse is supplied to the brush, lowering the mesh potential to -20 kV and initiating the capillary breakdown from the fast electrons emitted from the brush. The capillaries are without surface breakdown. The high current density through each capillary (a few kA/cm^2) creates highly ionized plasma which is then injected into the POS region.

The gas parameters were measured by special Penning probes and the plasma density and temperature were measured by three double floating probes used for simultaneous measurements in various locations. The plasma source will be mounted on a Marx-water-line generator (1.5 kJ, 600 kV, 1.9 Ω line impedance) that charges positively the switch inner conductor, delivering a peak current of 200 kA. The magnetic fields produced in the plasma will be up to 8 kG and 16 kG at the switch cathode and anode sides, respectively.

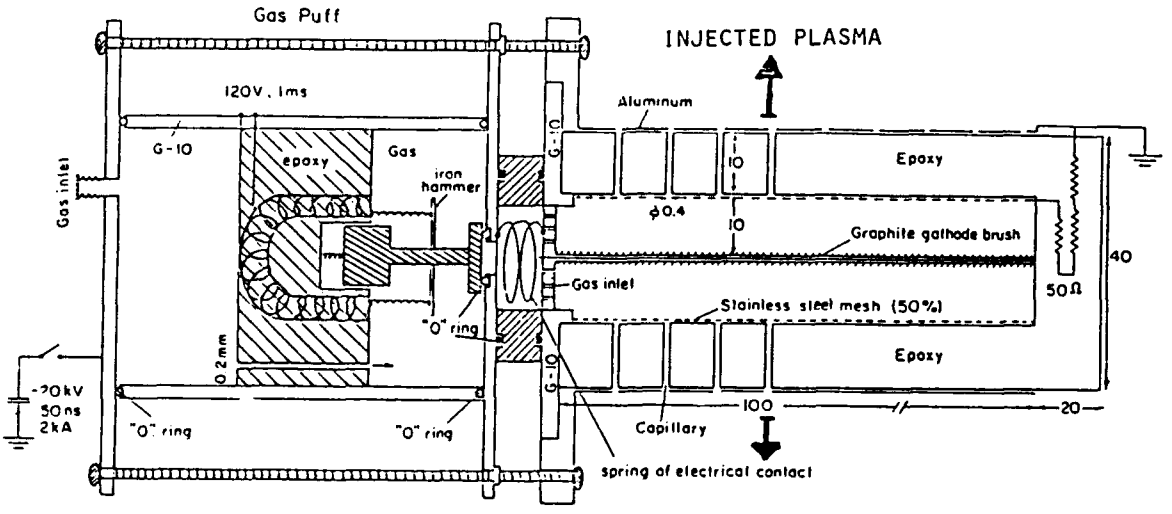

Fig. 7. Schematic sketch of the plasma gun developed.

The plasma source is installed inside the inner conductor and its power feed and gas supply are inductively decoupled from the generator, as shown in Fig. 6. The POS chamber has four transverse and one axial quartz windows, allowing for radial and axial optical accesses to the plasma. Axial measurements will provide radial and azimuthal resolutions. The upstream current I_g and the downstream load current I_l will be measured by calibrated $\dot{B}$ loops that have been already installed and calibrated.

An extensive study has been made for optimizing and characterizing the plasma source. The effects of the source length, the number of capillaries, the tube dimensions, and the kind of gas were assessed. The data given in this section were obtained with a 10-cm-long plasma gun containing 50 capillaries of 0.51 mm I.D. and 10 mm length filled with argon gas and the applied current is 1.6 kA. Typical values for the plasma electron temperature and density are given in Fig. 8. The plasma electron density was found to be 1×10^{12} - 3×10^{12} cm^{-3} and the electron temperature 5 - 10 eV. The plasma gun reproducibility was found to be ±20%.

The plasma radial propagation velocity determined from time-of-flight (TOF) measurements of probe signals, was found to be 2.0 - 5.0 cm/μs. The plasma ion current density in the radial direction was measured by negatively biased charge collectors facing the radial direction. These measurements, together with the plasma velocity, allow us to estimate the plasma ion density. Assuming a singly charged argon plasma an ion density of $5.0 \pm 2.0 \times 10^{11} cm^{-3}$ was inferred.

In the near future we intend to improve the source reproducibility and to increase the plasma density by increasing the number of capillaries per unit area and the current density for each capillary. We will then mount the plasma source on the high voltage generator and optimize the switch operation. In this stage we will use electrical diagnostics and streak photography to study the macroscopic operation of the POS. Ways to seed the plasma with various elements will be examined. The spectroscopic system, including imaging of the plasma on fibre array of different geometries, will be arranged, in order to proceed for the detailed spectroscopic observations planned.

In our theoretical study we investigated the magnetic field evolution in the POS. It has been shown that when the cathode is in the inner conductor, the Hall field enables the magnetic field to penetrate into the plasma as a shock wave[15,16]. We completed a 2D study

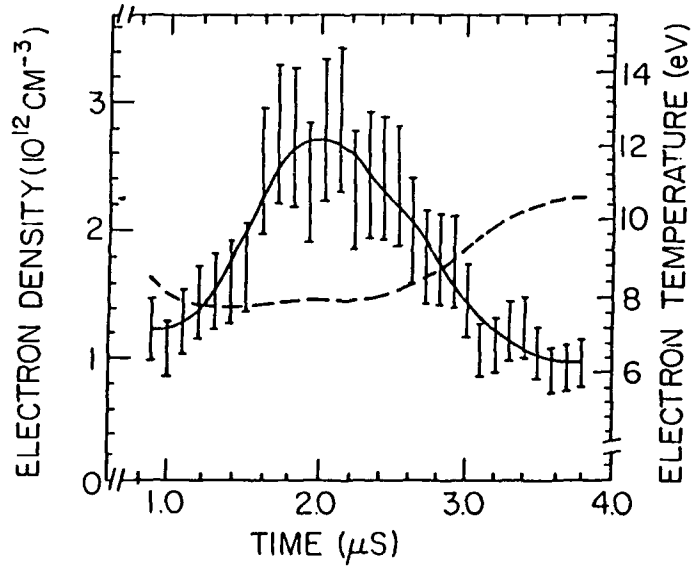

Fig. 8. Argon plasma electron density (solid) and electron temperature (dashed) as a function of time at 25 mm from the plasma source surface.

of the magnetic field evolution[17]. The energy flow was analyzed, and the dissipation, determined by the nondissipative Hall field, was shown to be large both near the conductors and in the bulk of the plasma. Our measurements of the magnetic and electric fields and of the plasma temperature will provide a test of our theoretical model. We have also studied other mechanisms of magnetic field penetration into plasmas which might bear relevance to the POS[18].

VI. SUMMARY

Recently developed spectroscopic diagnostic methods are being used to investigate the plasma behavior in an intense ion diode, a plasma opening switch, and a Z-pinch. In the diode experiment the magnetic field, turbulent electric fields in the plasma, and, the particle density and velocity distributions at the immediate vicinity of the anode surface were observed using emission-line Zeeman splitting, polarization spectroscopy of Stark broadened lines, and Doppler effects in laser spectroscopy, respectively. These methods will be used to investigate the magnetic-field penetration, the particle velocity distributions, the electron heating, and turbulent electric fields in the newly built Plasma Opening Switch and Z-pinch experiments described in the above.

ACKNOWLEDGMENT

This work is partially supported by the SDIO/IST managed by ONR. The authors are grateful to Dr. Y. Shiloh for valuable discussions and to P. Meiri, Y. Macabi, Y. Danino, and D. Liram for their skilled technical assistance.

REFERENCES

[1] Y. Maron and C. Litwin, J. Appl. Phys. **54**, 2086 (1983).

[2] Y. Maron, M.D. Coleman, D.A. Hammer, and H.S. Peng, Phys. Rev. Lett. **57**, 699 (1986) and Phys. Rev. **A36**, 2818 (1987).

[3] Y. Maron, M. Coleman, D.A. Hammer, and H.S. Peng, J. Appl. Phys. **61**, 4781 (1987)

[4] Y. Maron, E. Sarid, O. Zahavi, L. Perelmutter and M. Sarfaty, Phys. Rev. A., **39**, 5842 (1989).

[5] Y. Maron, E. Sarid, E. Nahshoni, and O. Zahavi, Phys. Rev. A., **39**, 5856 (1989).

[6] Y. Maron, M. Sarfaty, L. Perelmutter, O. Zahavi, M.E. Foord and E. Sarid, Phys. Rev. A, **40** 3240 (1989).

[7] Y. Maron, L. Perelmutter, E. Sarid, M.E. Foord, and M. Sarfaty, Phys. Rev. A. **41**, 1074 (1990).

[8] M.E. Foord, Y. Maron, and E. Sarid, J. Appl. Phys. **68**, 5016 (1990).

[9] E.K. Zavoiskii, Yu.G. Kalinin, V.A. Skoryupin,V.V. Shapkin and G.V. Sholin, JETP Lett. **13**, 12 (1971).

[10] E. Sarid, Ph.D. Thesis, to be published; E. Sarid, L. Troyansky, C. Litwin and Y. Maron, "Investigation of turbulent electric fields in a high-power-diode plasma", Bull. Am. Phys. Soc. **35**, 2006 (1990).

[11] L. Perelmutter, G. Davara, and Y. Maron, "Spectroscopic investigations of particle velocities and densities on a dielectric surface undergoing flashover", 14th Int. Symp. on Discharges and Electrical Insulation in Vacuum, Sante Fe, New Mexico, USA, Sept. 17-20, 1990; L. Troyansky, M.Sc. Thesis.

[12] C. Litwin, E. Sarid, and Y. Maron, in preparation.

[13] C. Litwin and Y. Maron, Phys. Fluids **B1**, 670 (1989).

[14] R.E. Duvall, C. Litwin, and Y. Maron, in preparation.

[15] K.V. Chukbar and Yan'kov, Sov. Phys. Tech. Phys. **33**, 1293 (1988).

[16] A. Fruchtman, Phys. Fluids B, to be published (Aug. 1991).

[17] A. Fruchtman, WIS Report 91/20/Apr.-Ph.

[18] A. Fruchtman and Y. Maron, Phys. Fluids B, to be published (July 1991).

G. Davara, photograph and biography not available at the time of publication.

R. E. Duvall, photograph and biography not available at the time of publication.

A. Fisher, photograph and biography not available at the time of publication.

M. E. Foord, photograph and biography not available at the time of publication.

A. Fruchtman, photograph and biography not available at the time of publication.

K. Gomberoff, photograph and biography not available at the time of publication.

Ya. Krasik, photograph and biography not available at the time of publication.

C. Litwin, photograph and biography not available at the time of publication.

Yitzhak Maron was born on April 12, 1948 and was brought up in Israel. He received his Ph.D. from the Weizmann Institute of Science, Rehovot, Israel. He has worked at the Weizmann Institute and Cornell University at Ithaca, N.Y. Since 1988 he has been Professor of Physics at the Weizmann Institute and he is currently heading the Plasma Laboratory there. The experimental work at this laboratory concentrates on the investigations of pulsed-power systems with special emphasis on the use of spectroscopic diagnostic methods.

L. Perelmutter, photograph and biography not available at the time of publication.

M. Sarfaty, photograph and biography not available at the time of publication.

E. Sarid, photograph and biography not available at the time of publication.

L. Troyansky, photograph and biography not available at the time of publication.

DEVELOPMENT OF HIGH ACTION SPARKGAPS FOR LARGE CAPACITIVE ENERGY STORES

John T. Naff, D. Bhasavanich, J. Hammon, S. Hitchcock, I.S. Roth, and F.T. Warren

Physics International Company
2700 Merced Street
San Leandro CA 94577

***Abstract*—Sparkgap switches have been developed that are capable of switching large capacitive energy stores. This paper describes the development of high action sparkgaps for use in megajoule-class capacitor banks. Switches that are used both as the capacitor bank output switch and to crowbar the bank after transfer of the stored energy to an inductor have been developed.**

The requirements driving the development and the results of the development effort will be described.

I. INTRODUCTION

In May of 1983 the first 22 kJ per unit capacitors arrived at Physics International Company (PI) for use in an upgrade of a Marx bank (designated LINK[1]) from 1 MJ to 3.2 MJ. Reference 1 describes the original 1 MJ system. The new capacitor ratings were nominally 29.5 μF at 40 kV each. The configuration of the LINK Marx generator was arranged in a six-stage configuration with 12 capacitors connected in parallel for each half-stage of the Marx (each stage was charged to maximum voltage of ± 40 kV, i.e., a stage voltage of 80 kV). The maximum charge transfer per shot for the non-oscillatory discharge application was 14 Cb. The Marx switches were strengthened versions of the PI T-508 switches. The PI T-508 switch is the switch used in the AURORA simulator, the PITHON simulator, most of the large simulators at Sandia National Laboratories, and in large pulsed power machines at other laboratories in the United States and in Europe.

This work was supported by the Defense Nuclear Agency and Physics International Company.

In the course of operating the Marx generator for a substantial number of shots, a standard maintenance cycle was established in which the plastic (acrylic) switch envelopes were replaced after 20 shots. The replacement was necessary as the switch envelopes would typically fail catastrophically due to wall tracking if they were allowed to remain in service for as long as 25 shots. The symptom leading to failure was a large amount of metallic debris that accumulated in the switches due to the "large" charge transfer. The switch used at different times both dry air (at about 3 to 4 atmospheres) and sulfur hexafluoride (at just over atmospheric pressure). The switch envelope replacement cycle was similar for both gases.

Sparkgap switches that had been used for more than a decade in all types of large pulsed power systems proved to be inadequate for the LINK pulser application. A new switch needed to be developed, or a different way to switch large energy systems containing high energy density capacitors needed to be discovered.

Fifty kilojoule per can capacitors appeared in 1986 and PI received a contract to design and produce a 60 MJ bank to drive the Thunderbolt EM Launcher.[2] At this date (June 1991), 32 megajoules are in operation at Thunderbolt. In 1986, development of high charge transfer, high action switches was underway, but testing of a large number of switches had not been completed so there was no basis for choosing sparkgaps for Thunderbolt. Ignitrons were, therefore, chosen to be the switches for the Thunderbolt bank.

The Thunderbolt pulsed power system has been successful in delivering the required energy to the gun. Ignitron reliability, however, has not been as high as is desirable. Wetting of the igniters of the ignitrons occurred frequently, causing failure to fire when triggered. The use of a thermal management system to cool the

cathodes and heat the ignitron insulators was necessary to keep the mercury in the ignitrons in the cathode region. The thermal management system for the ignitrons proved to be expensive and complex.

Series switch requirements for gun banks are driven by fault modes of the system such as the possibility of flashover of the buss work or a fault at the gun breech. Typical switch requirements for a recent EM Launcher design that is currently being manufactured are given in Table I.

TABLE I
ELECTRIC GUN REQUIREMENTS
TYPICAL RATINGS FOR EACH SHOT

Peak Current	Max.dI/dt	Action	Charge Transfer
250 kA	$1 \cdot 10^9$ A/s	>100MJ/Ω	>1000 Cb

In high energy circuits, action:

$$A = \int I^2 \, dt$$

is a measure of the stress that a components must endure.

Prior to the development of the high action switches described here, the use of spark gaps for such high charge transfer per shot and high action duty would not have been possible. Currently, the high action sparkgap switches are in use in a multi-megajoule bank design and two more such systems are in the manufacturing process.

II. EARLY DEVELOPMENT

With the appearance of 50 kJ/can capacitors and the need to use the capacitors economically in large banks, the need for switches to handle larger charge transfer and higher action was apparent. The Defense Nuclear Agency responded to this need by supporting switch development subtasks to the SREMP Test support contracts that were in progress at the time. A 560 kJ Marx stage in the 3.2 MJ LINK pulser was used as the first test bank. A bank storing 850 kJ was used for some tests and was formed by adding an extra half stage from the LINK Marx. The first switch tests were begun using the LINK Marx switches as the test switch. The bank produced an oscillatory discharge using the switch as the load. An inductor was constructed so as to have two test conditions:

a. High current without the added inductance
b. Higher charge transfer at lower current with the inductor in the circuit

A circuit diagram representing the first test circuit is shown in Fig. 1.

The original LINK switches failed mechanically at actions between 5 and 10 MJ/Ω. Switch stress rods were broken and envelopes were shattered. Additionally, a large amount of debris in the form of vaporized electrode material was deposited in the switch and in the gas lines to the switch.

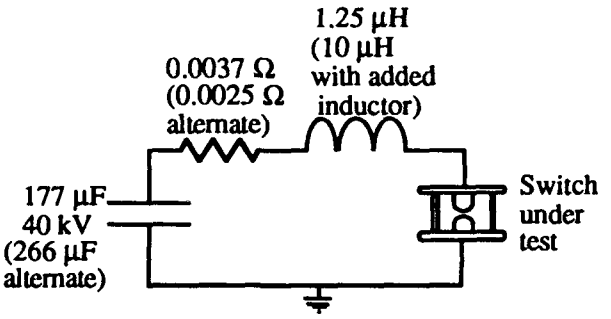

Fig. 1. Equivalent circuit of initial high action switch test bank.

A new three electrode switch was designed to be a very high strength pressure vessel using wound fiberglass as the switch insulator and Permali Super Stud™ as the stress rods. The strengthened switch mechanically survived in excess of 10 MJ/Ω shots. The switch electrode erosion remained very high and the switch, upon opening after a very few shots, was filled with a black power consisting of vaporized and recondensed electrode material. On one occasion, a new switch was opened after only one shot and had essentially the same amount of debris as one with multiple shots. A large amount of vaporized electrode material was pushed out of the switch and into the gas lines each shot. The gas lines were made of nylon and had to be replaced after about 10 shots as they became too thin to sustain the gas pressures.

The switch was again redesigned, this time using Poco™ ACF-10-Q graphite tips for the electrodes and the same high strength housing that was as previously

described. The results of these tests were very encouraging. The amount of debris was reduced considerably and the switch would survive several shots without attention. The maximum operating conditions for this initial test series is shown in Table II and represented a substantial gain over the original Marx switches.

TABLE II
SWITCH PERFORMANCE FOR TEST SERIES #1

Peak Current	Max.dI/dt	Action	Charge Transfer
250kA	$4.25 \cdot 10^9$A/s	5MJ/Ω	14 Cb*
780 kA	$4.25 \cdot 10^{10}$A/s	17MJ/Ω	35 Cb+
270 kA	$6.4 \cdot 10^9$A/s	7.5 MJ/Ω	59 Cb#

*Original LINK Switch
+Graphite @ 560 kJ + Inductor added
#Graphite @ 850 kJ and no added inductance.

The maximum action was improved by a factor of three and the total charge transfer was increased by more than a factor of 4. Some problems remained at the end of these tests. There was still a considerable amount of debris accumulating in the switch due to electrode holder erosion because the arc did not always stay on the carbon electrode tips. Additionally, the fiberglass switch insulator would char or burn internally during the accumulation of tens of shots and eventually it was believed that the charring would cause flashover.

III. DEVELOPMENT DURING LINK PULSER TESTING

The initial development tests of the high action switches described above were conducted while the LINK pulser was located in at the SREMP Test Facility in San Diego, California. At the conclusion of these tests, the pulser was moved to Kirtland, AFB in Albuquerque, New Mexico, for continued SREMP tests requiring high action. Although the amount of debris that was produced in the switch was much reduced after converting to graphite electrodes, it had been assumed for some time that the remaining debris was caused by the arc being pushed off of the graphite electrode tips by magnetic forces on the arc. During the course of the Kirtland tests, magnetic force was confirmed as the reason for arc movement by the erosion pattern observed in using the improved switches for a relatively large number of shots. A further improvement was conceived consisting of a current return cage around the switches to provide a co-axial current path with the graphite electrode tips located on axis. Although co-axial geometry does not guarantee arc stability for very short times, the long term average position of the arc should be at the axis position and on the graphite electrode tips.

The co-axial modification was implemented. When the switches were put back into service and a substantial number of shots were fired, almost no debris was noticed exiting the gas lines. When the switches were opened for inspection, they were essentially clean.

During this period of testing, new switch envelopes were manufactured. A study of the burning of the switch fiberglass insulators resulted in choosing an aliphatic resin coating as a non-charing coating for the inside wall of the switch insulators. The aliphatic resin coating was applied and the insulators installed on the LINK Marx switches. After a relatively large number of shots, the switches were again examined and no further charing was evident.

At the end of the Kirtland AFB test and for the duty encountered in those tests (~ 200 kA peak current and 14 Cb maximum for shots with no fault conditions) the switches were adequate in every way for the required service. The wear rates of the switches in this duty was not measured, but did not appear to be a problem.

The lessons learned during this testing were used in the later continued switch development.

IV. INSTALLATION OF THE SWITCH TEST FACILITY

In 1985, as a result of an upgrade to the DNA PITHON simulator, surplus capacitors with a total energy storage capability of 1.3 MJ became available. DNA supported using the capacitors to assemble a Switch Test Facility at PI. The Switch Test Facility capacitors were derated from 60 kV to 55 kV in order that air insulation could be used for the bank. The resulting test facilty capacitance is 686 μF and at 55 kV the test bank stores 1.03 MJ. The internal resistance of the bank was set at 0.005 Ω at 68° F by the use of liquid capacitor isolation resistors on each capacitor (a safety feature). Under repetitive use on hot summer days the internal resistance drops to 0.0045 Ω or less.

The capacitors are capable of high reversal without damage and the bank can achieve high charge transfer per shot by adding low resistance inductance to the circuit and using a switch as a load, which results in an oscillatory discharge. With care, actions of up to about 200 MJ/Ω can be achieved in the oscillatory mode and

charge transfers of 250 Cb or more are achievable. (The charge on the bank at full voltage is 37.7 Cb.)

A schematic of the oscillatory configuration is shown in Fig. 2. Not indicated in Fig. 2 is the resistance introduced by the switch itself. The switch resistance is variable as a function of current and is an important circuit parameter.

In another test configuration, the switch test facility can be used to charge an inductor, which when crowbarred can provide much higher action and charge transfer than the bank alone. The crowbar circuit arrangement is shown in Fig. 3. A description of the crowbar circuit operation follows.

With the bank at the desired charge voltage, the bank switch is closed and current begins to increase in the inductor. When peak current is reached, the majority of the bank energy has been transferred to the inductor. When the energy in the inductor is at a maximum, the crowbar switch is triggered and caused to close. In the circuit loop formed by the current charged inductor and the crowbar switch, the switch resistance plus the inductor and connection resistances are the only loss elements in the circuit. The amount of bank energy transferred to the inductor compared to the initial bank energy is the ratio of the inductor value to the total circuit inductance. For component values similar to those shown in Fig. 3, the resistance has little effect on the peak current reached as the peak current is essentially determined by the circuit inductance.. The current in the inductor is unidirectional and decays with a falltime of L/R, the ratio of the inductor value and the crowbar loop resistance. The switch resistance is a function of current and as a result the current decay is somewhat nonlinear. Careful measurements and data reduction are required to ascertain the performance of the switch due to the nonlinear nature of the discharge.

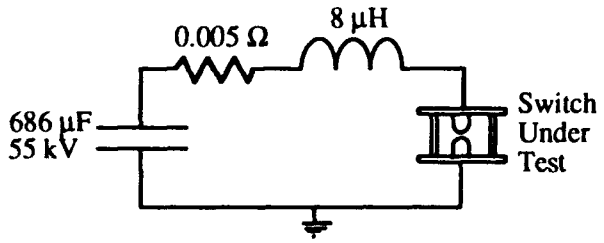

Fig. 2. Schematic of the Switch Test Facility in the oscillatory configuration.

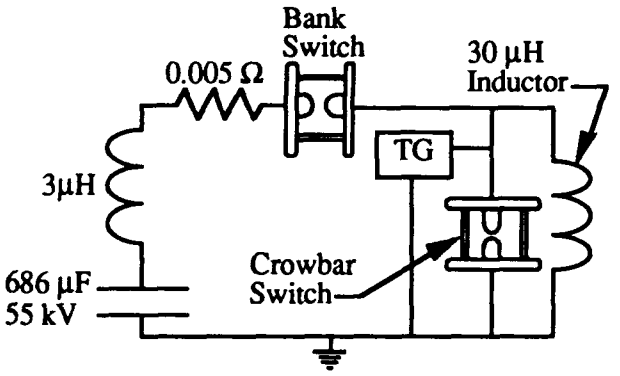

Fig. 3. Crowbar circuit arrangement to provide high action and charge transfer for switch testing.

Another circuit arrangement of the Switch Test Facility that has been used for switch testing is shown in Fig. 4. In Fig. 4, both the bank switch and the crowbar switches are in the crowbar circuit loop and are subjected to high action and large charge transfer. The charge transfer and action available in the circuit of Fig. 4 is less than that of the circuit of Fig. 3 because the resistances of both switches contribute to the crowbar loop resistance. When using the circuit of Fig. 4, the nonlinear behavior of the resistance of both switches in series causes visually apparent distortion of the data traces. The decay of current is not a simple exponential waveform.

The advantage of using the circuit of Fig. 4 is that both switches are being subjected to high action and large charge transfer at the same time, which allows more rapid accumulation of test data. Both switches are test objects.

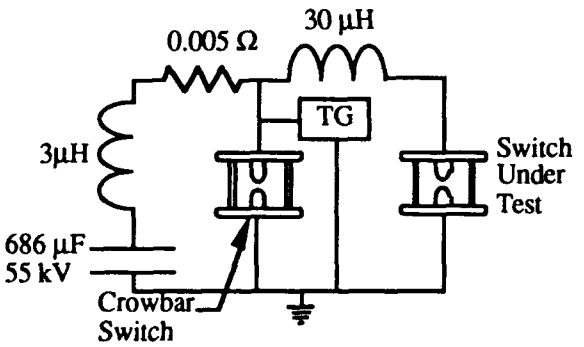

Fig. 4. Alternate crowbarred switch test circuit with both the bank switch and the crowbar switch in the crowbar cicuit loop.

The levels of action, total charge transferred per shot, and peak current achieved to date with the switch test bank are reflected in the switch performance parameters presented in Section V.

V. SWITCH DESIGNS TESTED AND THE PERFORMANCE ACHIEVED TO DATE

The original LINK switch was a mid-plane triggered three electrode switch. The switch when closed was topologically two separate two electrode switches in series. The switch resistance is in large part due to electrode losses. In some self-break tests of two-electrode switches, the circuit losses were noticably less as evidenced by the circuit Q. In order to minimize losses, the final high action switch design was a two electrode switch.

Many of the large capacitor banks that are used for launchers and the like are similar to the Thunderbolt bank and have added inductors to shape the current pulse. For such banks, transiently increasing the voltage on the inductor with a trigger generator also overvolts the switch causing the switch to breakdown and therefore allows the use of two electrode switches. In fact, by using two elctrode switches operated at less than 50% of self-breakdown voltage and using a sufficiently high voltage trigger generator, the incidence of switch prefires is essentially eliminated. This method of triggering is termed "series injection triggering" and with a sufficient trigger generator two electrode switches can be fired with zero volts on the switch as is required for the crowbar switch application.

The only disadvantage to series injection triggering is that the inductor must be designed to withstand the trigger pulse without flashover.

The design of the two-electrode switches for use in large energy stores used the lessons learned from the previous testing using the LINK pulser. An integral coaxial current return was provided that also moved the switch gap into a metallic region and away from the switch insulator. The switch insulator was made using the non-charring aliphatic resin wound fiberglass construction that was found to be effective in the earlier testing. The entire switch was designed as a very strong pressure vessel.

Two versions of the switch have been developed to date. The first version that was constructed is shown in Fig. 5. This switch was designated the PI ST-4196 and was tested as both a bank switch in the oscillatory mode (Fig. 2) and in the crowbar mode (Fig. 3 and Fig. 4). The ST-4196 is 28 cm in diameter has a length of 53 cm. The ST-4196 weighs 110 kg (50 lbs). The maximum operating parameters of the ST-4198 are given in Table III. The peak current and maximum dI/dt shown for the ST-4196 in Table III is for an oscillatory case (see Fig. 2). The action and charge transfer conditions are for tests in the crowbar case (see Fig. 3 and Fig. 4).

Some switch users indicated a need for a smaller and lighter switch. The ST-300 resulted from this need and is shown in Fig 6. The ST-300 is 23 cm in diameter and has a length of 27 cm. The ST-300 weighs 44 kg (20 lbs). The tested operating parameters for the ST-300 are given in Table III and all the conditions for the ST-300 are for a single test setup—that is, except for the electrode life, the listed conditions all occurred on a single shot.

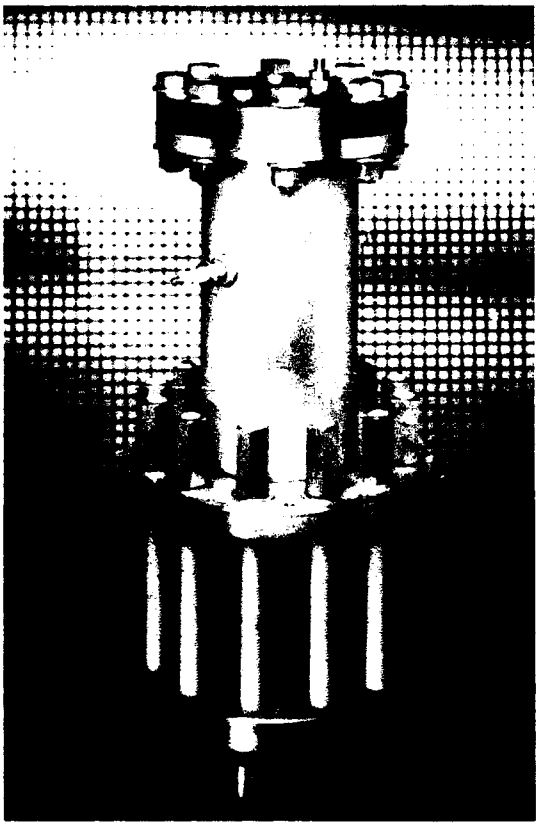

Fig. 5. The PI ST-4196 high action capable sparkgap.

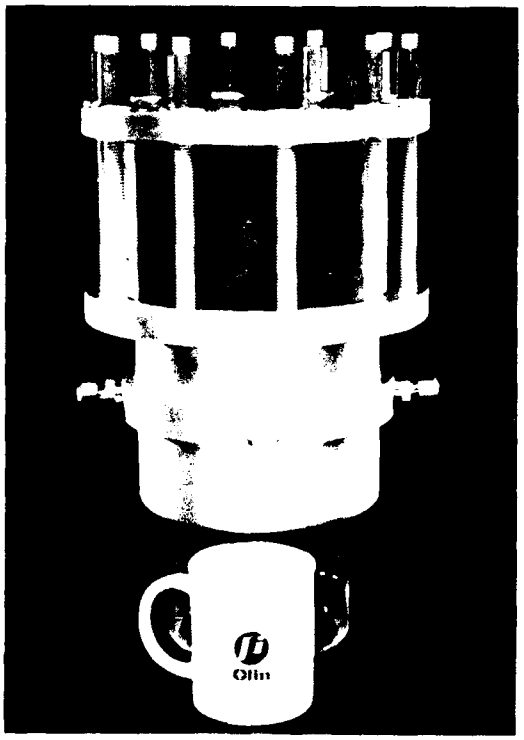

Fig. 6. The PI ST-300 high action capable sparkgap.

TABLE III
DEMONSTRATED OPERATING PARAMETERS OF PI SWITCH DESIGNS

	ST-4198	ST-300
Peak Current, kA	850	280
dI/dt, A/s	$8.5 \cdot 10^{10}$	$5.6 \cdot 10^{10}$
Action, MJ/Ω	220	220
Charge per Shot, Coul.	800	800
Electrode Life, Coul	150,000*	150,000*

*Estimated

The electrode life listed for both switches reflects that both switches have the same graphite electrodes and the life is estimated from observing the wear on test series that totaled 20,000 to 30,000 Cb. Because of the series injection method of triggering, the gap spacing is not critical and the gap life is arbitrarily taken as the coulomb totals required to double the original gap. The shape of the electrode tips is a quasi-Rogowski shape. The Rogowski shape is chosen to provide a large erosion volume.

Spherical electrodes have been used and the erosion is much faster with the gap doubling in 20,000 to 30,000 Cb.

Several runs were made for the purpose of determining electrode erosion rates. Erosion rates were estimated by measuring the change in gap length and observing the erosion pattern. Then the shapes were sketched on grid paper and the volume removed was calculated. The erosion was very uniform, smooth, and almost symmetrical. Even so, the accuracy is probably only ± 25%.

In addition, some low repetitition rate tests were run[3] at one to two shots per minute and found that the erosion rates appear to be almost an order of magnitude higher with very hot electrodes and flowing gas. (The electrode holders were required to be cooled.)

The performance indicated in Tables III and IV are more than an order of magnitude greater in the charge transfer and action capability than the switches that were available at the beginning of the program and have performance capability to serve as the switches in present day large capacitive energy stores using high energy density capacitors.

TABLE IV
OPERATING AND PERFORMANCE PARAMETERS FOR AN ELECTRODE EROSION TEST FOR GRAPHITE

	ST-4198	ST-300
Peak Current	170 kA	170 kA
Charge per shot	700 Cb	700 Cb
dI/dt (max)	1.1•109	1.1•109
Action	71 MJ/Ω	71 MJ/Ω
Electrode Dia.	3.8 cm	7 cm
Gap Length	0.96 cm	0.63 cm
Electrode Shape	hemi	Rogowski
Erosion Rate *		
Anode	100 µg/Cb	100 µg/Cb
Cathode	50 µg/Cb	50 µg/Cb
Period	933 µs	933 µs
Waveform	Crowbar	Crowbar
Pressure	0 - 8 psig	0 -20 psig

*Estimated

VI. LIMITATIONS OF GRAPHITE ELECTRODE SWITCHES

In the tests reported here, there were no failures of the switches. For the highest action tests, often the high current buss work of the bank required repair on almost every shot, but the switches survived.

The peak current capability of the switches has not been determined nor has the maximum charge transfer per shot capability. The performance parameters that were tested were the highest available from the Switch Test Facility.

One performance parameter limitation has been discovered. The same Poco™ACF 10-Q electrode material (3.8 cm diameter) was used in a fast capacitor bank that had a zero to peak current risetime of 1 μs. When the peak current equaled or exceeded 230 kA, the tips of the electrodes exhibited a spalling. The electrode would eject a well formed conical shaped piece of the electrode tip that was about 2 cm in diameter and about 2 cm deep. On a single test where several of the switches were used in a fast bank, essentially all of the electrodes failed in this manner on the same shot. This failure is reproducible.

The failure is apparently associated with the maximum dI/dt to which the electrode is subjected. First reported here, other tests with different peak currents have shown similar failure at the same dI/dt. For example, Pulser F,[4] used in SREMP tests for BMO/DNA was a fast (10 ns) risetime 5 Ω output impedance pulse generator. Pulser F is described in the design stages in Reference 4 as using Poco graphite in the output switches and that was the intention. Pulser F achieved fast risetime and low impedance by running 10 each 50 Ω output cables in parallel and used 10 parallel output switches. During checkout of the pulser, when the pulse output voltage was raised from 120 kV to 150 kV, all 10 switch sites spalled simultaneously. The peak current was 3 kA per switch site and the dI/dt was calculated to be some what over $3.5 \cdot 10^{11}$. This is the same dI/dt at which the fast bank spalled the switch electodes (at 230 kA per switch site). The size of the electrodes in Pulser F was only 1.27 cm diameter and ejected the conical electrode tip fragments were smaller than the tip diameter.

Similar failures of other switches using the same electrode material have occurred. It has been found that the maximum dI/dt is higher for spherical electrodes with relatively large gaps than for Rogowski shaped tips with close spacing. In the case of close spaced Rogowski shaped electrodes the expansion of the shock wave from the arc is cylindrical whereas in the spherical electrode case with a large gap, the expansion is more spherical and the peak pressures fall off more rapidly..

A tenative explanation based on stress caused by rapid differential thermal expansion due to transient heating as a result of skin effect has been proposed.[5] The threshold for the spall to occur appears to be very precise for a particular electrode shape and gap spacing.

Another limitation is that the switches can be adversely affected by magnetic fields from inductors or other nearby high currents. The co-axial current return balances the magnetic forces from the switch and the buss work connected to the switch. If the switch, however, is placed too close to an inductor, the arc in the switch can be blown off of the graphite electrode tips and a large amount of electode metallic debris results. Almost all switch designs including ignitrons are similarly adversely affected by excessive magnetic fields.

In selecting switches for high action duty applications, if the dI/dt is below $3.5 \cdot 10^{11}$, the ST-4196 and the ST-300 are the best choices for many present day applications.

VII. SUMMARY

The appearance of high energy density capacitors and the need to assemble the high energy density capacitors into large energy stores to drive electric guns and the like have made necessary the development of high current, high charge transfer, high action switches.

PI has developed switches that are reliable in handling charge transfer per shot, total charge transfer, and actions that are an order of magnitude higher than was available at the start of the development program. The switches are now being used in applications for large capacitive energy stores and are the switch of choice for such applications.

ACKNOWLEDGEMENT

The authors wish to thank Jeff Banister, Dennis Creely, Rod Everson, Steve Hogue, Mike Klatt, and Larry Sanders and to acknowledge the hard work and technical contribution of these PI Scientific Associates and Technicians that made this effort successful.

REFERENCES

[1] Donald F.Strachan, "LINK, A 1 MJ, 1 MV, 20 Ω, 2 ms HIGH ENERGY PULSE GENERATOR", Joint International IEEE/APS Symposium National Radio Science Meeting, and Nuclear Electromagnetic Pulse Meeting, Albuquerque, New Mexico, May 24-28, 1982

[2] McNab, Ian R., *et al.*, "THUNDERBOLT", IEEE Transactions on Magnetics, Vol. 27, No. 1, January 1991.

[3] Roth, I., *et al.*, "LINK Pulser Operations 1985-1989", DNA-TR-89-145, December 1990.

[4] Naff, J. T., "High Energy LINK Pulser Tests", PIFR-3189-D (Draft Final Report), August 1985.

[5] Physics International Technical Report PITR-3412-1-6, September 1986.

John T. Naff was born in Monroe, Louisiana, on February 21, 1934. He received the B.S. in Physics Degree from Louisiana Polytechnic Institute, Ruston in 1956. From 1956 until 1960 he was with Lockheed Missiles Systems Research Laboratories, Palo Alto, CA. From 1960 until 1967 he was with MHD Research, Inc. He was with Maxwell Lab from 1967 until 1970. He was a co-founder of Pulsar Associates, Inc., in 1970. He joined Physics International Company in 1978. He has been involved in all areas of pulsed power technology since joining industry in 1956. He is currently Chief Scientist of Electromagnetic Systems at Physics International Company where he directs developments in pulsed power. He specializes in switching systems, including fast risetime EMP systems and high coulomb, high action capacitor bank systems.

Daun Bhasavanich (S'71-M'78) was born in Bangkok, Thailand, on October 2, 1951. He received the B.S. and M.E. degrees in electric power and electrical engineering from Rensselaer Polytechnic Institute, Troy, NY, in 1974, the Ph.D. degree in electrical engineering from University of Liverpool, England, in 1977, and the MBA degree from the University of Pittsburgh, Pittsburgh, PA, in 1982.

From 1978 to 1989, he worked at the Westinghouse R&D Center in Pittsburgh, PA. His principal interests included a study of high current discharges and switching in gases and vacuum, high temperature lead vapor Raman cell for excimer laser frequency conversion, thallium-cesium atomic line filter as a narrow-band receiver for blue-green laser communications with submarines. He joined Physics International Company, San Leandro, CA, in 1989. His current activity is in the design and analysis of switching components for electromagnetic launchers, electromagnets for high power microwave, and high repetition rate modulator for compact linear induction accelerator.

H. George Hammon, III (**"Jud"**) received the A.B. degree in physics from the University of California at Berkeley, in 1969, the M.S. degree in physics from the University of Washington, Seattle, in 1970, and the D.A. degree in physics in 1975, also from the University of Washington.

He is Manager of the Pulsed Power Engineering Department at Physics International Company, San Leandro, CA. His responsibilities include technical and programmatic supervision of the development and systems for domestic and international customers. In his thirteen years of experience at Physics International, he has developed a broad range of advanced pulsed power systems, ranging from spark gap and magnetic switches to compact, low-jitter trigger generators, and on to very large systems providing the pulsed electrical energy for high-power lasers, high-power microwaves, electromagnetic guns, and nuclear weapon effects simulation.

Sherry S. Hitchcock received the B.S. and M.S. Degrees in Electrical Engineering from the State University of New York at Buffalo in 1983 and 1987, respectively.

In 1983 she joined the U.S. Army LABCOM, Pulsed Power Branch where she was involved in high power thyratron evaluation, small caliber railgun development and transient computer modeling techniques. In 1985, she joined Physics International where she has been involved with flash

X-ray machines, flashlamp pulser design, trigger generator development, and high current switch testing. She is the author of several technical articles in the area of high power electronics design and modeling.

I. S. Roth received the A.B. Degree in Physics from the University of California, San Diego, in 1976. He joined Physics International, where he has worked on fast Z-pinches. In 1980, he entered Cornell University and received a Ph.D. Degree in Electrical Engineering in 1987. His graduate research covered propagation of a kiloampere proton beam in a linear induction accelerator. He returned to Physics International, where he has designed a fast, high current Marx generator and contributed to the development of the high action, high coulomb transfer switch. He is currently working on plasma opening switches. I. S. Roth is a member of the American Physical Society.

F. T. Warren, Jr. received the B.S., M.S., and Ph.D. degrees in electrical engineering from the University of South Carolina, Columbia, SC, in 1979, 1980, and 1985, respectively. During his graduate work, he studied the electrical breakdown of vacuum and low-pressure gas with particular application to laser-triggered, electrically triggered, and pulse-over-stressed switching. His work covered the span from DC to 50 ns pulse excitation in the 100 kV and 50 kA parameter regimes.

In 1985, he joined Physics International where he has been engaged in the design, development, and testing of various high-voltage, pulsed power devices. Some of these projects include a 6-MV, 75-ns pulse generator, a 12-MV Marx generator system, a 60-kV, 10-kHz modulator system operating at 1.5-MW average power, a 16-kV, 8.5-MJ pulse forming network, and a 750-kV, 100-Hz dual pulse generator. Throughout this work, he has continued his interest in many varieties of switching: 12-MV, multi-channel oil switches; multi-gap, high-power thyratrons; and high-current, high-charge-transfer spark gaps.

Dr. Warren is a member of Phi Beta Kappa, Tau Beta Pi, Eta Kappa Nu, Sigma Xi, and IEEE.

INTERACTIVE SPACE TECHNOLOGIES CONSORTIUM RESEARCH

C. R. Johnson

Space Power Institute
Auburn University, Alabama 36849

ABSTRACT

Auburn University's new four-year research program sponsored by the Strategic Defense Initiative Organization (SDIO) features basic research by eight investigators from the United Kingdom, Canada, and Tuskegee University organized under a Consortium concept. Eight Auburn investigators complement the group by collaborating in examination of the chemical and mechanical effects on materials in the space environment, in assessing thermal management issues on spacecraft, and in determining proper electrical materials for space applications.

INTRODUCTION

Need for the Research

Researchers agree that SDIO spacecraft designs stress one's knowledge of the interactive effects of the space environment on the specialized materials to be used. A primary lesson from LDEF has been the need to clearly quantify the synergism between various aspects of the space environment and a host of multipath interactions affecting systems. Materials must be created, and engineering guidelines modified, to ensure the reliability, weight/volume limits, durability, and long life of SDIO platforms. Full understanding of the space environment requires a multidisciplinary approach. Figure 1 depicts some major environmental aspects of space and highlights the Consortium's four inter-dependent areas of research.

Benefits of Consortium Concept

The effects of the environment and the classes of technologies employed in analyses are too complex and broad in scope for any one research institution to possess all of the requisite expert talent and facilities to adequately address the issues. Well-equipped laboratories, and a Consortium of talented researchers, offer the best approach to finding economical solutions, promoting cross-fertilization of ideas, and inserting competitive

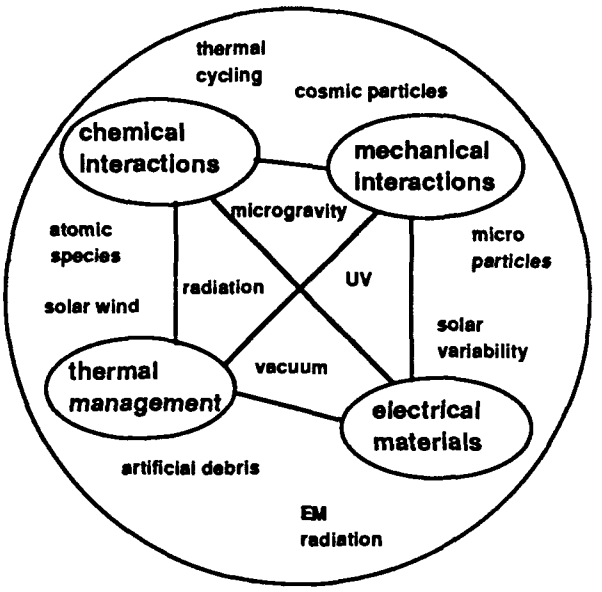

Figure 1: Interactions in the Space Environment

opportunities and innovative approaches to complex issues. In a brief review of the current research program, one will recognize the importance of a multidisciplinary, international approach to space environmental challenges. Members of the consortium are actively engaged in space research, often with support from other sponsors. This involvement effectively leverages the SDIO funds, providing even more return on the research investment.

RESEARCH OBJECTIVES

The technical program is divided into two parts, the first related to the effects of the space environment and the second focusing on the technologies to address operation in that environment. Some key technical objectives in each of these areas are discussed in the paragraphs which follow.

Effects of the Space Environment

In chemical effects, the team determines the reaction rates, the activation energies, and mechanisms due to attack by atomic oxygen and other chemical components on films of selected polymers, metals, carbons, diamond coatings, and cerarnics. The team determines the extent of protection offered by static, self-healing, and auto-polymerizing coatings. In mechanical effects, the team studies underlying mechanisms for damage initiation and propagation during hypervelocity impact, and develops mechanisms, methods, and models to minimize such damages. It develops techniques for the periodic generation of protective coatings on surfaces damaged by micrometeoroid impacts. Finally, it characterizes impact directional anisotropy from LDEF surfaces, establishing impact morphology and developing bumper efficiency data.

Electrical / Thermal Conduction and Insulation

In thermal management, the team develops and assesses the feasibility of innovative electrically-insulating, high thermal-conductivity heat-rejection structures using either CVD diamond thin films deposited on coolant-carrying microchannel plates or micromachined poly-crystalline diamond films permeated with coolant-carrying microchannels. It assesses such fundamental issues as interfacial bonding, thermal mismatch, contact thermal resistance, and micromachining. It assesses the degradation, failure, and etching of high-resistivity diamond insulators, and studies adherent, self-passivating coatings which retain hardness in erosive and chemically corrosive environments. In the electrical materials area, the Consortium is expanding its knowledge of the outgassing characteristics of space-rated polymers and the role of outgassing in the surface charge deposition mechanisms, especially at triple junctions. It studies and models mechanisms by which local micro-perturbations promote parasitic "cold" emission of electrons under high electric field stress. It investigates new classes of materials for electrical transmission and conditioning in the space environment with emphasis on compact, high-voltage pulse conditioning in geometries compatible with operation in the space environment. It determines and models the responses of space-rated and innovative polymeric insulating materials to a multi-stress simulation of the space environment.

DESCRIPTION OF RESEARCH AREAS

Chemical Effects on Materials - Task 1

Collaborative studies, with a focus on chemical effects on materials, are underway within the Consortium laboratories, in Auburn, in Swansea, and in Toronto. Several research issues and the related research efforts are discussed below in the first sub-task area on materials and thin films.

Materials / Films in Multistress Environment

Background: The space environment is hostile to numerous materials used on space platforms. The role of atomic oxygen (AO) in the erosion of materials exposed to the space environment at Low Earth Orbit (LEO) is well established. Atomic oxygen concentration varies with altitude and solar activity. Concentrations of 10^9/cc are common at LEO, so that the effective flux, due to the platform orbital velocity of 7 km/s, is about $10^{15}/cm^2$-s. The kinetic energy of impact of the oxygen atom is approximately 5-6 eV. Polymers, including Kapton and epoxies, are severely affected as are some metals, particularly silver.

Space systems operating in a LEO environment for long periods of time require materials which are stable in that environment[1]. Shuttle flight experience has shown that certain organic (polymeric) and metallic materials, used in structural, thermal, and electrical applications, are attacked and eroded by AO. Short term exposure can harm spacecraft surfaces, if those surfaces are composed of or covered with organic materials. Organic polymers are important to future generations of spacecraft power systems. Oxidizing O-atoms cause irreversible degradation of materials' physical characteristics (optical, electrical, or mechanical).

At higher altitudes, charge buildup due to impinging electrons and ions in the Van Allen Belts and solar wind (e.g., in geostationary orbit) has other deleterious effects on insulating spacecraft materials such as organic polymers. When charge build-up on an exterior surface reaches a specific level, the result is surface discharge arcs or flashover, which can permanently damage the polymer structure and integrity. Furthermore, electrical transients associated with these discharge events can perturb or destroy electronic circuitry aboard the space vehicle. These events have been shown to cause loss or near loss of spacecraft.

It is possible to apply very thin coatings onto the exposed surfaces of organic and inorganic materials in order to protect them against the harmful effects just described. The following statements define the properties required for such protective barrier coatings.

- The barrier must, of course, itself be resistant to atomic oxygen bombardment;
- The barrier should be flexible, abrasion-resistant, and allow adhesive bonding;
- The barrier should be UV tolerant, but not alter the substrate's properties;
- Finally, surface conductivity should be high in order to prevent the buildup of harmful potential gradients which result from surface charging.

Next, there are other species in the pristine environment of space, including nitrogen atoms and oxygen ions. A number of these species, including ozone (O_3) and the hydroxyl radical (HO), can readily be formed around a platform as a result of interaction with platform effluents. Various stress factors, including the solar ultraviolet flux and solar heating of exposed surfaces, also play a role in the chemistry which occurs. In summary, fundamental understanding of the chemical bases for the reactions and accurately determined kinetic data are needed in order to develop means for control. Auburn's program, combined with contributions from researchers in the United Kingdom and Canada, is directed toward these ends.

Photothermal Studies of Reactions

At the University College of Swansea in Wales (Aled Williams), the research focus is on a photothermal depth profiling system using both photoacoustic cells and piezoelectric films as the detecting system[2]. Past profiles of samples such as Kapton and Teflon coated with aluminum, silver, tin, gold and silicon, clearly show the metal-polymer interface. Thus, the homogeneity and the damage of samples can be readily determined. The technique has recently developed interest, as there is some evidence that damage, caused by AO to a polymer with a protective coating of metal, occurs preferentially at pin-holes or other imperfections in the metal coating. Results from the photothermal depth profiling work have been compared with other techniques and found quite useful. Tasks assigned to Williams include conducting extensive three dimensional photothermal depth-profiling analyses of surfaces and interfaces of an expanded family of sample materials, pre- and post-examination of samples exposed to atomic oxygen, study of the effects caused by defects in the materials from manufacturing, hostile attack, folding, and pin-holes, and development of a procedure or technique for damage assessment of coatings.

Space Environmental Effects

At the University of Toronto's Institute for Aerospace Studies (Rod Tennyson), another research team has extended its previous work in AO erosion of dielectric materials used for spacecraft applications. In the most recent work, the team measured erosion rates that compared well to known space flight test data, showed that the surface morphology of samples was identical to that found in space flight specimens, proved the validity of accelerated testing in the AO simulator, and demonstrated that the dielectric properties and surface charge characteristics were altered due to AO exposure[3].

Barrier Coatings: Current investigation involves evaluation of the performance of thin barrier coatings on the behavior of thin film and composite materials subjected to prolonged exposure to AO, UV radiation and thermal cycling. Test protocols also include dielectric materials subject to power loading. Tennyson is assessing the major factors and worst-case conditions which will impact system designs from a materials viewpoint. As additional flight data becomes available from LDEF analyses and Space Transportation System mission experiments in 1991, 1992, and onward, the team will continue to validate its space simulator data, developing a theoretical model of AO interaction with material surfaces.

SDIO Emphasis on Materials: Materials and coatings of primary interest to SDIO include the traditional substrates (Kapton, Mylar, Teflon, polyethylene, carbon / epoxy composites) and coatings (organosilicones, inorganic silicon compounds, and amorphous hydrogenated silicon). Tennyson's focus on materials properties includes mass loss rates, UV degradation, thermal cracking of coatings, presence of defects, dielectric and optical property changes, surface morphology changes, outgassing and reaction products, surface discharges, and others. Specific tasks underway, or planned, include UV radiation and long-term exposure to AO tests on uncoated and coated combinations of the materials discussed previously, documented comparative analyses of property changes on different dielectric materials and composites, and extensive validation of accelerated testing.

Mechanical Effects of the Environment - Task 2

In terms of materials, the danger to spacecraft posed by artificial space debris has been rapidly increasing over the past 20 years. The recent return of LDEF has afforded researchers the opportunity to gain much empirical data on this aspect of the near-earth environment. Efforts will draw heavily on the LDEF data base and augment it with selected experiments carefully designed to understand the underlying mechanisms governing impact processes, the macroscopic effects these produce on systems, and techniques for mitigating their ill effects.

Hypervelocity Impact Capability

The research at the University of Kent at Canterbury (J. A. M. McDonnell) complements on-going research at Auburn, since the Space Power Institute and the Unit for Space Science at the University of Kent operate uniquely different hypervelocity launching facilities for environment simulation. McDonnell, as project leader for this part of the work, is Principal Investigator (PI) of the LDEF (meteoroid) Micro-Abrasion Package (MAP), and is also responsible via the European Space Agency for analyzing the erosion of some 18 square meters of FEP Teflon thermal blanket covers from the Ultra High Energy Cosmic Ray Experiment.

Initial LDEF Data: Initial studies of the flux anisotropy on the Canterbury LDEF MAP experiment have shown that a separation of the relative number of orbital debris and cosmic particulates can be performed.(4) As a result of data and differing geometric configurations / pointing directions, LDEF's unique records permit careful evaluation of the resultant damage observed from space exposure. LDEF's "lessons learned" on the harsh effect of the environment were evident even to the casual visitor to the Kennedy Space Center de-integration facility. Results showed a heavily-biased impact erosion environment toward the ram direction (forward), AO erosion in the vicinity of impact sites and even beyond the "ram accessible" exposure directions, modification of the surface properties of space materials, and a "zone of modification" surrounding impacts which greatly exceeded expected hypervelocity impact crater dimensions. These are significant findings. Another surprise was the severe discoloration due to outgassing and subsequent radiation modification which radically affected the absorptivity / emissivity ratio (α/ε) or thermal characteristics. This valuable data base is being recorded and applied to the future development of space-hardy systems. Canterbury's technical tasks are divided into six areas below.

Projectile-System Interactions: A series of experiments are being conducted from which underlying mechanisms governing impact processes may be extracted. Three types of system materiels (ceramics, metals, and polymers) are being investigated for their response to hypervelocity impact. The various interatomic forces (ionic, covalent, metallic, and Van der Waals) that these three types of systems possess provide the necessary freedom to properly identify the governing parameters for impact energy dissipation. At Auburn's Space Power Institute, in parallel research, selected materials and components are being bombarded with particles from the Hypervelocity Impact Facility (HIF). Velocities exceed 7 km/s. The differences in the physical properties of these materials together with those of the target will provide the necessary variations needed for mechanistic determination and collaboration.

Modeling: Back at Canterbury, three dimensional computer codes are being used to model various impact responses, using both Lagrangian and Eulerian codes. Results from the controlled experiments in the projectile-system interactions area will provide the necessary information on the mechanisms with which deformation and energy loss occur during hypervelocity impact. This is an opportunity to expand the data base and establish collaborative efforts abroad. Also, the experiments involved are designed to extract critical parameters governing impact processes. Selecting three types of materials to be investigated provides the necessary variations for definitive correlation of impact response with system properties.

Protection Schemes: As a direct consequence of the effort described above, various protection schemes are being explored to minimize meteoroid damage. These methods include both intrinsic and extrinsic considerations. Intrinsic aspects include the choice of materials according to their basic materials physical properties (both at the atomic and bulk levels). The possibility of minimizing damage by enhancing energy loss due to very localized melting (function of thermal properties) will be explored. The concept of toughening (enhanced energy absorption) by deformation-induced transformation will be examined.

Extrinsic control of damage includes the use of multiple bumper protection. The effects of meteoroid damage on the response of critical SDI components (subjected to atomic oxygen and UV attack) will also be analyzed.

LDEF Data Characterization: Particulate impact directional anisotropy is being characterized from existing data on LDEF surfaces, resulting in a definition of the size distribution of natural and artificial space debris particulates from 0.2 μm diameter upwards to the region of 1 mm diameter. Over the next several years of the program, the impact crater morphology will be established for thin foil perforations including multilayers and for thick targets for several hundred target sites. Impact scaling relationships on thin foil and thick target sites will lead to meteoroid bumper efficiency.

Space Erosion: Finally, at Canterbury, the combined effects of AO erosion and hypervelocity impact are being studied using an existing light gas gun, an existing 2 MV microparticle accelerator, and a new (low cost) atomic oxygen erosion beam. The effect of the thermal parameters will be established at or near impact sites, both with, and without atomic oxygen erosion using high resolution α/ε mapping. Modeling of the impact data will be performed to better understand the dynamics of near Earth natural / artificial space particulates.

In summary, McDonnell's ultimate goal is to develop design parameters (guidelines) for extended deployment of properly engineered space systems. These new design guidelines include key criteria, such as the dependence of α/ε degradation of the target material for a given AO dosage, the measurement and predictions of the dependence of α/ε degradation on exposure pointing direction in LEO, and the minimizing of exposure degradation by AO and hypervelocity impact through configurations of multilayer structures, open honeycomb, porous finished, and furrowed materials. The successes of the program being initiated will lead to a better understanding of the formation of fragmentation and vapor plumes during impact and the resulting interactions with SDI space systems. Protection mechanisms can then be developed.

Thermal Management on Spacecraft - Task 3

Electron and Phonon Scattering: For completeness in the discussion of the four major research areas, one must include the work of Tuskegee University (Prakash Sharma). This investigation is an extension of his previous work on electron and phonon scattering processes and their role in the mechanism of heat transport in semiconductors[5]. The program involves a four-year effort to enable Sharma to further examine the thermal conduction problems associated with pure and doped semiconducting mediums. So that spacecraft designers may better manage excess thermal energy, Sharma is studying the flow of heat energy within portions of electronic devices, and the resultant flow of heat energy out of the device to, and within, the mounting material. Polycrystalline diamond's role as a mounting material, or as an inclusion within the device, is analyzed through theoretical modeling of the phonon interactions and their impact on thermal transport within devices fabricated of many materials, specifically, pure diamond, germanium, doped germanium, pure silicon, doped silicon, mercury telluride, germanium doped indium, antimonide, and zinc-doped gallium antimonide. Sharma's theoretical calculations will be used to predict the exact temperature dependent lattice thermal conductivity. In future years, the contribution of electron-phonon scattering in the intermediate concentration region will be determined, and the results will be combined so that ways and means can be proposed to control the temperature and heat content within electronic devices fabricated of such materials as gallium arsenide, gallium antimonide, diamond and silicon.

Electrical Materials / Space Applications - Task 4

Background: The requirements for electrical power in space have increased significantly in recent years. Earlier power levels were limited to 15 kW with voltage levels at 200V. New applications, however, will require power levels from 10's of kW up to MWs, and voltage levels for such power systems will likely be several kV to minimize resistive losses. Special applications may require 100's of kV. Reducing the mass of insulating dielectrics will require utilization of the space vacuum as an electrical insulator. This fact will result in the direct exposure of energized systems to the space environment. It is important, therefore, to understand and predict breakdown mechanisms. It is also important to understand the interactions between the space environment and typical high voltage systems. Four programs, at Aston University, the University of Strathclyde, and Oxford University, complement one another and the objectives of Auburn's program. The basic approaches

address known deficiencies in our understanding of the behavior of electrical materials in space.

State of the Art: Electron field emission is central to the space insulation issue. It has been said that, from a technological perspective, the only reliable procedure that is currently available for improving the insulating performance of electrodes is to invest heavily in expensive "clean room" assembly techniques so as to minimize the presence of contamination, coupled with high-temperature (in excess of 1200C) in situ processing to "pacify" residual emission sites. The technological goal is to develop an "ambient" electrode processing procedure that is reliable and cheap. It is necessary to make a further investment into studies of the fundamental nature of the emission mechanism. This investment is centered about the research being done in field emission phenomena and electrode stability at Aston University (Rod Latham) (6).

Micro-particle Bombardment: In space deployment, emission characteristics of electrode surfaces will be adversely affected by bombardment from several sources of micro-particles: contaminants from the local spacecraft, space-generated contaminants (cosmic dust and micro-meteoroids), and Earth-generated contaminants (orbital debris from previous spacecraft activities). Contamination sources include surface particulates, friction generated wear, impact induced particles, adhesives, electrical insulators, and thermal blankets. Contamination exists throughout the spacecraft lifetime as components wear and materials degrade due to interactions with the space environment.

Vacuum Breakdown: There are several important effects that particulate contamination may have upon the breakdown characteristics of vacuum gaps. Low velocity contaminants (spacecraft generated) will enhance large gap breakdown by classical microparticle breakdown processes, and alter small gap emission processes by surface contamination. High velocity contaminants (orbital and cosmic debris) can cause any vacuum gap to fail when the secondary particles and plasma/gas plumes are injected into the inter-electrode region by impact with an electrode surface. Cratering and contamination of electrode surfaces from impacts also enhances electron field emission.

Aging and Degradation: Other space environmental factors can affect solid insulating support structures. Aging and degradation of a wide range of electrical insulating materials have been studied for many years under a variety of conditions such as heat, electric stress, atmosphere and nuclear radiation. Various methodologies determine the influence of specific parameters and the synergism of different stresses. One particular type of methodology in wide use consists of stressing the sample of material to a required limit and subsequently conducting post-stress testing, very often in a different environment. A great deal of work on radiation effects has been carried out in this manner. This technique could suffer from the lack of realistic environmental stresses. For example, much of the information available in the literature documents single stimuli such as thermal or radiation effects, but single stimuli may not be directly applicable to the multistressed space environment. There is a need for study of multifactor stressing, for establishment of accelerated aging procedures, and for scaling parameters. This deficit is addressed in the Consortium's programs.

Surface Charge Accumulation: Surface charge accumulation and migration are believed to play an important role in creating the necessary field distortion conditions to initiate breakdown. Previous research has been conducted under relatively benign laboratory conditions, and the applicability of the results to the hostile conditions of space is in doubt. During a four-year investigation at Auburn University (Lloyd Gordon, Charles Neely) as well as in the United Kingdom, considerable progress was made in assessing the detailed outgassing characteristics of a number of space-qualified polymers, the effect of these outgassed products upon the dielectric integrity of vacuum insulated systems, and the deposition of surface charge on stressed polymeric spacers.

Aston's Research in Field Emission

The problems outlined above are linked in this next research program in the United Kingdom portion of the Consortium. Field emission phenomena are being pursued at Aston University through parallel lines of investigation. Both efforts contain fundamental and technological themes, employing a unique and dedicated equipment base which Latham developed under a previous SDIO contract.

Fundamental Studies: Latham is undertaking further investigations into the physical nature of the basic electron emission mechanism, e.g. he intends

- To determine the relative importance of microgeometry and material composition in creating an emission site;
- To make a comparative investigation into the switch-on behavior of emission sites under dc and pulsed field conditions, at varying (a) temperatures, (b) residual gas pressures and gas species, and (c) UV radiation levels;
- To follow an on-going theoretical program aimed at modeling the emission mechanism under both dc and pulsed field conditions; and
- To experimentally evaluate simulated metal-insulator-vacuum (MIV) and metal-insulator-metal-vacuum (MIMV) emission regimes, ideally fabricated in situ, based on a silicon substrate.

Technological Studies: First, Latham is investigating how the stability of electrodes, as measured by the incidence of emission sites, their current-voltage characteristics, and their ultimate breakdown behavior are influenced by external parameters and processes, i.e.

- Material composition and electrode processing;
- Long and short-term thermal cycling under both zero and high electric field conditions;
- UV radiation, under a range of field conditions;
- Simulated microparticle impact;
- Influence of various residual gas atmospheres at elevated temperatures;
- Effectiveness of commercial sputter-cleaning techniques in removing emission sites;
- Evaluation of vapor doping techniques as a means of "pacifying" emission sites.

He is investigating the practical potential of a "local" conditioning procedure, where a laser probe can be used to successively pacify individual emission sites as the applied field is incrementally increased, an interesting option.

Finally, he will build upon previous studies in which the basic emission mechanism has been harnessed in the development of a large-area, low-field, cold-cathode electron source for device applications. This investigation will be particularly concerned with the:

- Influence of substrate electrode material;
- Influence of the dielectric matrix material on the use of a "non-gassy" glass-like media;
- Influence of the size, shape and material composition of the suspended particle species;
- Cathode response to dc, ac, and pulsed fields;
- Cathode stability and lifetime characteristics.

Dielectric Bulk Characteristics

The University of Strathclyde program (Hamish Banford), an investigation of dielectric bulk characteristics, consists of a series of experiments in which two space-qualified polymeric insulating materials, namely polyimide and an epoxy resin formulation, are being subjected to detailed analyses. Various aspects of their electrical behavior are being scrutinized during and following exposure tc different combinations of electromagnetic nuclear radiation, atomic oxygen bombardment, vacuum and temperature. Banford's most current research is an extension of his earlier work[7]. A portion is done in a space simulation chamber, permitting electromagnetic radiation studies. The real time electrical investigations are measurements of dielectric loss over a frequency range of six orders of magnitude (10^{-3} - 10^{3} Hz) and analyses of pre-breakdown activity under a direct electric field.

The Strathclyde program is being conducted in two phases. In Phase I, samples are placed in the space simulation chamber and subjected to a combination of vacuum (10^{-7} mbar), thermal cycling (80-420 K) and electromagnetic (^{60}Co and X-ray) nuclear radiation (10^{-3} to 10^{-1} Gy/hour), measuring pre-breakdown electrical pulse activity, dielectric breakdown strength, and other parameters. In Phase II, samples are placed in a high vacuum chamber and the thermally stimulated discharge current and thermoluminescence are monitored. Following Phases I and II, infrared spectroscopy and differential scanning calorimetry techniques are applied in materials analyses.

The initial work is being carried out with fresh test specimens, and the bulk of the work will be undertaken with "aged" material. The aging conditions are definitive, and include specific gamma doses, AO flux rates, temperature regimes for periods of time, periodic cycling of temperatures over a temperature range, and a period of exposure for a given set of samples (from 6 to 42 months duration, in multiples of six months). Samples are to be withdrawn during the aging process, split into two groups, and analyzed under Phase I or Phase II criteria.

In summary, the overall aim of the project is to correlate the degradation of the electrical performance of the materials with their environmental treatment. Clear results permit recommendations to be made about the proper

use of materials in a space environment, the methodology of aging for a space environment, and improved fabrication of future materials. Comparisons and conclusions will be reported in the technical reports and appropriate literature.

Dielectric Surface Studies

In still another University of Strathclyde program (Ian Chalmers), dielectric surface studies involve surface charge measurement by means of an electrostatic probe feeding a high impedance op amp configured as an integrator. Chalmers has developed a special drift compensation technique which allows the probe to be used without any shuttering of the tip, thus permitting better spatial resolution. Other advantages are being exploited.

A portion of Chalmers' work investigates the effect of space environmental factors on stressed insulating structures such as might exist in space-borne power systems. The factors of immediate interest to SDIO are temperature, UV irradiation and space plasma. The first sub-task involves the development of a system in which these environmental conditions can be simulated while a dielectric sample is stressed. Chalmers' collaboration with others in the Consortium (Banford, Gordon, Neely) enables him to assess the effect of exposure to atomic oxygen and gamma irradiation.

Articles on the effects of the space environment on existing dielectric surface charge now appear in the literature[8]. This research effort stresses a sample of dielectric in such a way as to produce a known charge distribution on its surface, and then exposes it to a specified (tailored) environment. The subsequent behavior of the charge in terms of variation in magnitude and distribution is monitored as a function of time from the instant of exposure and from the quality of the tailored environment. This investigation is done for conditions of elevated temperature, UV irradiation and the presence of low energy plasma. The three environmental factors are studied synergistically, since interactions of charge, the environment, and the dielectric is the set of conditions relevant to space systems.

In summary, after Chalmers quantifies the environmental effects previously discussed, he conducts a dynamic study in which the samples are actively stressed in specific "hostile" environments. One should not speculate on results, as there are many possible variations of the outcome. It is this uncertainty which demonstrates the value of the research. The goal is to ascertain the extent and the means by which the space environment affects the insulation integrity of stressed systems.

Pulsed / DC High Voltage Power Supplies

The Oxford University (Paul Smith) program provides an interface between the dielectric materials work and the application to on-board pulsed power and dc generation. It has become clear as a result of his previous work, that, by utilizing novel materials which combine high dielectric strength coupled with high permittivity, and by designing novel circuit configurations, one may develop devices with impressive characteristics[9]. One such configuration involves a lumped element Blumlein pulse forming line (PFL) driving a simple four-stage transmission line transformer (TLT), the result of which is rectified and smoothed to give a dc output. Since some development work is required before such a configuration can be made reliably operational, the new research program is divided into four sub-tasks.

TLT Development: The first sub-task of the program investigates the optimum techniques that should be used in constructing TLT's for use in both high pulsed power systems and in high repetition rate converters. This part of the program investigates the best geometries and materials for building the lines used to construct the TLT's, the most effective way of suppressing the secondary transmission line modes within these devices, the prospect of using air-core windings to suppress the secondary modes (to produce ultra-lightweight devices), insulation problems associated with the top stages of TLT structures, and the optimizing of gain by development of the TLT voltage gain formula (reported last year in his SDIO Final Report to Auburn University).

Non-linear, Low-Impedance PFL/PFNs: In another sub-task, Smith is further developing the low impedance, non-linear pulse forming lines and networks (PFLs/PFNs) which are needed to drive the low impedance inputs of the TLT's. Numerical computer codes and materials analysis are used in search of improved non-linear magnetic and dielectric materials. Criteria for selection is simple. These materials must be stable, have low loss characteristics, and show strong nonlinear behavior.

Test Generators: Smith's future plans involve building a series of experimental pulsed power generators to explore the efficacy of "scaling up" techniques in terms of power, output voltage, size, impedance characteristics, pulse lengths, repetition rate capabilities, etc.

Capacitor Charging Unit: At least one prototype high voltage capacitor charging unit will be built based on the high-frequency switched TLT circuit. Plans are to initiate this phase by constructing a "fairly low output power" high voltage supply (1 kJ s^{-1}) with an output potential of around 20 kV. This supply will demonstrate proof-of-principle and highlight any problems that may arise in this type of circuit. Larger units may follow, funds permitting.

SUMMARY

In the review of Auburn's international research program, one recognizes the importance of a multidisciplinary, international approach to space environmental challenges. The Consortium consists of investigators from nine institutions of learning in Canada, the United Kingdom, and the United States, all bound by common goals. Members of the Consortium meet frequently to share research achievements and to consult with the Program Director. Specific tasks are shared among the group, closely coordinated to meet the major task areas outlined in the four-year Statement of Work. The Consortium members enjoy funding support from a variety of sources, government agencies, other academic institutions, and industry. In many instances, the SDIO "seed money" provides the researcher with the first look at a space-related problem. Leveraged funding and dual-use facilities provide extraordinary opportunities for achievements in basic research. The benefits are unlimited, from spin-off products and technologies to spin-off companies. Through enrichment in knowledge and experience in new space technologies, the ultimate winners in this international Consortium are the graduate student researchers, the research associates, and Principal Investigators.

ACKNOWLEDGMENTS

The author thanks each Consortium member cited in the paper for sharing those research achievements and objectives. This work is supported by the Strategic Defense Initiative Organization's IST Office under contract number N60921-91-C-0078 with NSWC.

REFERENCES

1. Carolyn K. Purvis, D. C. Ferguson, et. al., "Environmental Interaction Considerations for Space Station and Solar Array Design," Preliminary - December, 1986.

2. Aled W. Williams, "Photothermal Studies of Material Interfaces," University College of Swansea, SDIO Report to Auburn University, Contract N60921-86-C-A226, December, 1990.

3. Rod C. Tennyson, "Effect of Space Environment on Electrical Materials for Spacecraft Power Systems," SDIO Report, Contract N60921-86-C-A226 to Auburn University, December, 1990.

4. J. A. M. McDonnell and T. J. Stevenson, "First Results From LDEF's Multiple Foil Microabrasion Package," Lunar and Planetary Science Conference, Abstracts Volume, March, 1990.

5. Prakash C. Sharma , "Thermal Conduction in Germanium at Low Temperatures in Intermediate Concentration Region of Doping," American Physical Society, Volume 35/3, March, 1990.

6. S. Bajic, N. A. Cade, A. D. Archer and Rodney V. Latham, "Stimulated Cold-cathode Emission from Metal Electrodes Coated with Langmuir-Blodgett Multilayers," Institute of Physics Conference, Series 99/6,1989.

7. Hamish M. Banford, R. A. Fouracre, G. Chen and D. J. Tedford, "Current Pulse Activity in Irradiated Low-Density Polyethylene," Proceedings of the Conference on Electrical Insulation and Dielectric Phenomena, October, 1989.

8. Ian D. Chalmers, "Dielectric Surface Charge Phenomena in Vacuum," 14th International Symposium on Discharges and Electrical Insulation in Vacuum, September, 1990.

9. C. R. Wilson, M. M. Turner and Paul W. Smith, "Electromagnetic Shock Wave Generation in a Lumped Element Delay Line Containing Nonlinear Ferroelectric Capacitors," Applied Physics Letters, June, 1990.

Calvin Johnson received his BSE from the United States Military Academy, West Point, in 1960 and an MSE degree from Arizona State University, Tempe, in 1970. He served 28 years in the USAF, taught Engineering Mechanics at the USAF Academy, and served in Viet Nam.

Calvin Johnson received his BSE from the United States Military Academy, West Point, in 1960 and an MSE degree from Arizona State University, Tempe, in 1970. He served 28 years in the USAF, taught Engineering Mechanics at the USAF Academy, and served in Viet Nam.

High Average Power Switching for Linear Induction Accelerators

A Summary of the Workshop held at the Wente Conference Center in Livermore, California on October 10-11, 1990

by:
M. S. Di Capua
Lawrence Livermore National Laboratory
Livermore, CA 94550

Workshop organized by:
W. W. Hofer
T. J. Orzechowski
Lawrence Livermore National Laboratory
Livermore, CA 94550

ABSTRACT

This report summarizes the presentations and the findings of the Workshop on High Average Power Switching (WHAPS) that took place in Livermore, CA on October 10–11, 1990. The WHAPS discussed switching technologies that could meet requirements that arise in applications of linear induction accelerators also known as induction linacs. Induction linacs require a switch that will hold-off 250 kV, conduct 30 kA for 150 to 200 ns, operate at 1 to 2 kHz for several second bursts, have better than 1 ns jitter, and last in excess of 10^8 pulses. The workshop reviewed the state-of-the-art of Super-Emissive Cathode Switches, Magnetically Delayed Vacuum Switches and Solid State Switches and considered research and development steps that would allow these technologies to meet these requirements.

1 High Average Power Switching for Linear Induction Accelerators

1.1 Introduction

This report summarizes the presentations and the findings of the Workshop on High Average Power Switching (WHAPS) convened by W. Hofer and T. Orzechowski, Lawrence Livermore National Laboratory at the Wente Conference Center, Livermore, CA on October 10–11, 1990.

The WHAPS discussed switching technologies that could meet requirements that arise in applications of linear induction accelerators also known as induction linacs. Certain induction linac designs require switches that hold-off 250 kV, conduct 30 kA for 150 to 200 ns, operate at 1 to 2 kHz for several second bursts, have better than 1 ns jitter, and last in excess of 10^8 pulses .

The workshop organizers chose to explore three technologies:

- Super-Emissive Cathode Switches
- Magnetically Delayed Vacuum Switches
- Solid State Switches

1.2 Purpose of the Worksl.op

The purpose of the Workshop was to:

- Familiarize the HAPS community with the pulse power requirements of induction linacs
- Acquaint the induction linac user community with selected HAPS technologies
- Establish a common ground through discussions between HAPS researchers and users of these technologies
- Acquaint other specialists of the pulse power community with HAPS techniques and solicit their comments
- To explore research and development paths leading from the present state-of-the-art in HAPS to devices that meet the induction linac requirements.

1.3 Format of the Workshop and this Summary

This report, which follows the format of the workshop, consists of a summary of presentations on:

HAPS in Induction Linacs

Applications of Induction Linacs	V. George, LLNL[1]
Switching Requirements for Induction Linacs	T. Orzechowski, LLNL
Switch Configurations for Induction Linacs	H. Kirbie, LLNL

State of the Art in Selected HAPS Technologies

Super Emissive Cathode Switches	M. Gundersen, USC W. Nunnally, APERC-UTA H. Riege, CERN
Magnetically Delayed Vacuum Switches	R. Dougal, U. of So. Carolina
Solid State Switches	R. Druce, LLNL K. Schoenbach, Old Dominion U.

After these presentations, the participants assembled into three working groups,[2] one for each technology. Each group explored paths that would lead to a HAPS that would fill induction linac requirements. Leaders from the groups presented their findings to all workshop participants in a plenary session.

R&D Path Leading from Present Capabilities to Induction Linac Requirements

Super Emissive Cathode Switches	M. Gundersen, USC M. Di Capua, LLNL
Magnetically Delayed Vacuum Switches	R. Dougal, U. of So. Carolina M. Newton, LLNL
Solid State Switches	R. Druce, LLNL M. Pocha, LLNL

In addition there was a presentation on High Repetition Rate Hydrogen Spark Gaps by S. Moran from the Naval Surface Warfare Center, Dahlgren, VA. A summary of this presentation appears at the end of this report.

---

[1] Appendix 1 provides complete affiliations and addresses of participants

[2] Appendix 1 also identifies participants in the working groups

2 Applications of Induction Linacs (V. George)

2.1 The Induction Linac

Induction linacs, interchangeably known also as linear induction accelerators [Humphries, 1986], rely on pulsed voltage sources to deliver a voltage across a gap in parallel with an inductor. Charged particles in the gap then accelerate in the electric field across the gap. A linear sequence of n gaps can then accelerate charged particles to an energy equal to n times the gap voltage.

Since the induction linac behaves like a transformer with a multi-turn primary and a single turn secondary (the beam), and since pulsed sources can deliver 10's of kA at 100's of kV for 100's of ns to the primaries (the gaps and ferromagnetic core inductors), induction linacs with 100's of gaps are very attractive to accelerate ~ 100 ns pulses of a few kA's of charged particles to 10's of MeV.

Therefore, the switches, key components that deliver the electrical pulse to the primaries, must hold off 100's of kV and conduct 10's of kA for 100's of ns. Moreover, as the gaps stack sequentially, the voltage pulses must appear at the appropriate time in successive gaps as the particle beam propagates along the induction linac.

The maximum current in the switch limits the number of gaps that a pulse source can feed in parallel. Therefore, timing of the pulses in successive sections of the linac, places an additional constraint on the switch jitter between pulses which must remain below 1% of the length of the pulse, i.e., 1 ns or less. Finally, demand for a burst of pulses sets the requirement for a switch repetition rate that can be as high as a few kHz.

In an ideal induction linac, the current that drives the primary and the beam current should be equal. In practical devices, however, the primary current exceeds the beam current because:

- Leakage currents magnetize the core
- There are energy losses in the magnetic material
- Current flows in compensation networks in parallel with the primary. These networks are necessary to make most effective use of the volume of ferromagnetic material of the core and to deliver a flat topped accelerating voltage [Caporasso, nd].

Therefore, the current required to drive the primaries can exceed the beam current by factors as large as two. This factor can become even larger in accelerator designs with a premium on flat topped gap voltage waveforms rather than energy efficiency.

The requirement to deliver a current to the primary that exceeds the current in the beam, increases the demands on the switch.

2.2 Induction Linacs and Generation of High Power Microwaves

The Beam Research Program in the Advanced Applications Group within the Laser Directorate of LLNL has identified amplification of microwaves using intense electron beam pulses delivered by induction linacs as an advantageous application of these accelerators.

The group is considering two techniques for microwave amplification:

- Free electron maser sources for heating of Tokomak plasmas at harmonics of the electron cyclotron resonance frequency (ECRH)
- Relativistic klystron microwave sources to power a new generation of high gradient electron accelerators

2.2.1 Free Electron Maser Configuration

The free electron maser amplifies microwaves as an electron beam and microwave radiation from a master oscillator co-propagate in a wiggler magnetic field. The wiggler imparts a periodic transverse momentum to the beam that aligns with the electric field component of the microwave radiation field. When the phase of the transverse momentum and electromagnetic field are appropriate, as the electron beam bunches, energy is transferred from the beam to the radiation field.

Experiments at LLNL have already demonstrated single pulse microwave production at 140 GHz (2 mm) in a free electron maser at peak powers of 0.2 GW with a 1.5 kA, 6 MeV beam delivered by the ETA-II induction linac [Sheaffer, 1990]. In a 35 GHz FEL, the radiated power exceeded 1 GW with extraction efficiencies (beam power to microwave power) of 40% in a 3 m-long wiggler (ETA, E_b = 3.5 MeV, I_b = 850 A).

A new set of experiments called the Intense Microwave Prototype will have a 5.5–m-long wiggler with a 0.1–m-period that operates continuously at a maximum field of 0.45 T. This FEL using an electron beam generated by ETA-II will produce 250 GHz microwaves in a 10 ms burst of 50 pulses with 70 ns duration each, at peak powers of 12 GW, with expected extraction efficiencies of 40%.

To produce these microwave pulse trains, the ETA II accelerator configuration is expected to deliver 10 MeV, 3 kA electron beam pulses to the wiggler in bursts. Electron acceleration in ETA-II takes place in a 1.2 MeV injector followed by eighty

100 kV gaps. Table 2.1 gathers the present switching requirements for the MAG 1-D modulators that power ETA II.

Peak cell voltage	(kV)	100	
PFL impedance	(Ω)	2	
Peak switch current	(kA)	50	
Load impedance	(Ω)	2	(20 cells)
Load voltage	(kV)	100	
Pulse length	(ns)	70	
Pulses in burst		50	
Burst duration	(ms)	10	(5 kHz)
Risetime	(ns)	~20	
Frequency	(kHz)	5	
Interval between bursts	(s)	few s	

Table 2.1: Switching Requirements for the MAG 1-D Modulator

Since the magnetic output switch of the present MAG 1-D modulator configuration now accounts for the largest fraction of the energy loss in the modulator [Turner, 1990], future switches that are expected to handle voltages that are 20% higher, pulse lengths that are twice as long and repetition rates that are twice as fast, will require substantial improvements in switch performance (See Table 2.2).

2.2.2 Relativistic Klystron Microwave Sources to Drive High Gradient, High Energy Accelerators

Powering of relativistic klystrons is another promising application of electron beams delivered by induction linacs. The short pulse, high power, 11.4 GHz microwave output of such klystrons could drive RF linear accelerators with gradients as high as 200 MV per meter and peak powers as high as 1 GW per meter [Sessler, 1988].

In one RF-driven linear accelerator concept, the relativistic klystron extracts electromagnetic energy (microwaves) from a lower energy (~3 MeV), high current (~3 kA) electron beam. The microwave energy, delivered to a more conventional RF linac, then accelerates a low current (few 100 mA) to energies that could be as high as a TeV.

The beam requirements to power relativistic klystrons are:

Beam energy	(MeV)	3
Beam current	(kA)	3
Pulse duration	(ns)	100
Beam emittance	(rad m)	3.0×10^{-4}

Induction linacs to drive such a klystron would require:

Number of gaps		12
Gap voltage	(kV)	250
Switch voltage	(kV)	250
Switch current	(kA)	30
Pulse duration	(ns)	100
Pulse risetime	(ns)	<20
Pulse flatness	(%)	<1
Pulse interval	(ms)	3

In recent experiments [Allen, 1989], a relativistic klystron powered by a 1.3 MeV, 0.6 kA induction linac produced 290 MW of RF power at 11.4 GHz to drive a high gradient RF linac accelerator. The accelerator attained an 84 MV m^{-1} accelerating gradient with 80 MW of RF microwave power.

References

Allen, M., et al., "High Gradient Electron Accelerator Powered by a Relativistic Klystron," Physical Review Letters, Volume 63, Number 22 (1989) 2472-75.

Caporasso, G., et al., "Design of Long Induction Linacs," (nd).

Humphries, S., Principles of Charged Particle Acceleration, J. Wiley, NY, NY (1986) 283-325.

Sessler, A., Physics Today, Volume 41, January 1988.

Sheaffer, M.S., Orzechowski, T. J. "Free Electron Lawers" in: Energy and Technology Review, July August 1990, UCRL-52000-907.8 (1990) 48.

Turner, W., "Critical System Issues and Modeling Requirements - The Problem of Beam Energy Sweep in an Electron Linear Induction Accelerator," International Magnetic Compression Workshop Proceedings, H. C. Kirbie, ed. (1990); also UCRL-JC-104643 (1990).

3 Switching Requirements for Future Induction Linacs (T. Orzechowski)

To reduce beam instabilities in induction linacs, it is desirable to minimize the number of cells and operate them with the smallest possible gap. Therefore, a large accelerating voltage per gap is desirable, subject to constraints that result from field emission (vacuum breakdown) in the gaps. Since the admissible penetration of wake fields from the beam into the cavities behind the gaps sets an upper limit to the gap opening, at present this tradeoff yields a maximum voltage of 250 kV per gap. These tradeoffs are an area of active research.

High energy accelerators would require a continuous stream of 100 ns pulses repeating at 3.3 ms intervals (0.3 kHz) for 1 or 2 s with a 300 s period, are desirable. In plasma heating applications, the energy content of the burst is important. Therefore, even a longer pulse would be desirable (300 ns) to reduce the pulse repetition rate of the accelerator.

Requirements on the peak microwave power set a lower current limit in the kA range. Lower beam currents are unproductive because the shunt impedance of the cell draws a parallel current, independent of beam current, that results in a lower efficiency. Limitations arising from beam transport and stability set a few kA upper limit on beam current [Caporasso, nd].

To fulfill these beam requirements, the pulse sources that drive the induction linac will need switches with the performance specified in Table 3.1.

Voltage hold-off	(kV)	250	
Current transfer	(kA)	>10	
Conduction time	(ns)	>100	
Risetime	(ns)	<20	
Jitter	(ns)	~1	
Repetition rate	(Hz)	300-1000	
Efficiency	(%)	>70	(for the whole pulse power chain)
Lifetime	>	10^8	
Burst duration	(s)	2-5	
Burst interval	(s)	~200	

Table 3.1: Specifications for High Average Power Switch, a Focus of the HAPS Workshop Discussions

The requirements in Table 3.1 constituted the focal point of the presentations and discussions of the workshop. The next section discusses these switching requirements within the context of proposed driver circuits.

References

Caporasso, G., et al., "Design of Long Induction Linacs," (nd).

4 A Switch Configuration for Future Accelerators (H. Kirbie)

This section examines a switch configuration for the induction linac driver for free electron masers. The design proposed for the driver circuit appears in Figure 4.1. A thyristor switched capacitive resonant circuit feeds a non-linear magnetic element that drives the primary of a 1:6 air core transformer. The secondary feeds a second circuit that drives the primary of a 1:4 transformer. The output of this transformer charges the center conductor of a Blumlein circuit. The Blumlein delivers the voltage pulse to three cells through six-parallel 68 Ω coaxial cables. The charging voltage of the intermediate conductor of the Blumlein circuit will have a 1 - cos ωt time dependence peaking to 270 kV at about 4 μs. Table 4.1 specifies the circuit parameters in more detail.

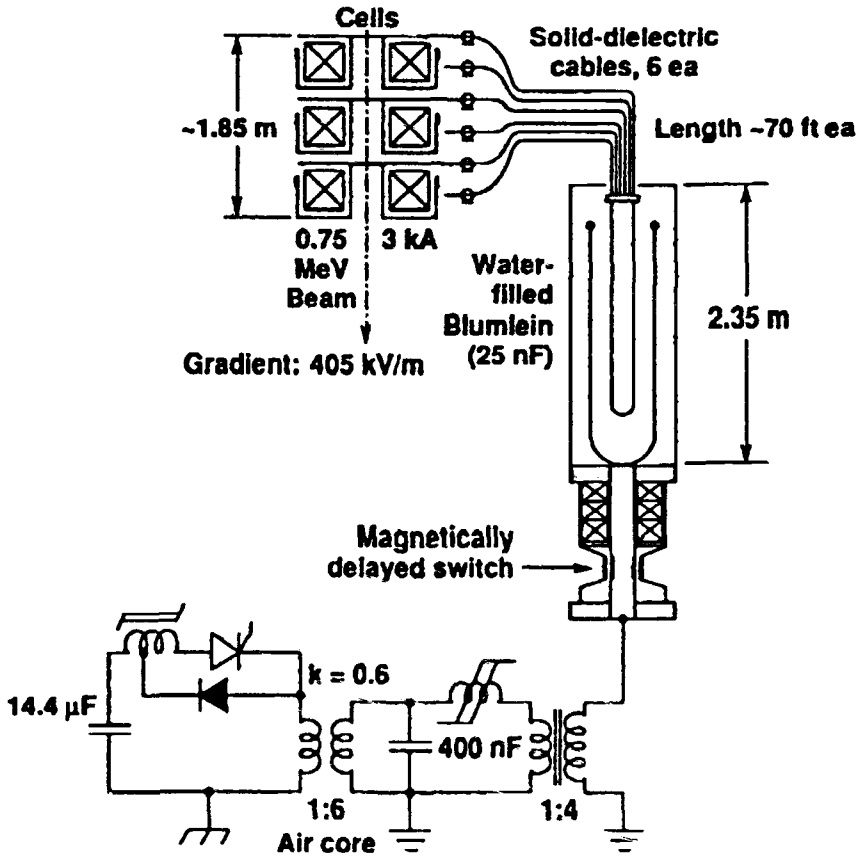

Figure 4.1: Blumlein circuit driver for induction linac. The circuit at the bottom charges the intermediate conductor of the Blumlein. The Blumlein delivers a pulse to the accelerator cells at the top through coaxial cables. The sketch shows the location of the HAPS. This example chose a magnetically delayed switch for illustration.

Blumlein load impedance	(Ω)	11
Center conductor voltage	(kV)	250
Blumlein capacitance	(nF)	25
Stored charge	(mC)	6.2
Switch current	(kA)	44
Switch inductance (max.)	(nH)	51
Minimum di/dt	(MA/μs)	4.9
Output pulse length	(ns)	140
Output current	(kA)	22
Output voltage	(kV)	250
Cable impedance (1 of 6)	(Ω)	68

Table 4.1: Circuit Parameters of Blumlein Driver for Induction Linac Cell

It is evident from Table 4.1 and Figure 4.1 that the circuit delivers 7.4 kA to each cell while the beam current is only 3 kA. The remainder of the current flows in a compensation resistor. To maintain an acceptable shape of the voltage pulse at the output, the Blumlein of Figure 4.1 incorporates a magnetically delayed switch. The other switch options discussed at this workshop could be incorporated in this design as well.

Figure 4.2 displays the predicted output voltage across the load of a circuit (Table 4.1 and Figure 4.3) that simulates the behavior of a magnetically delayed vacuum switch in a Blumlein circuit with a resistive load. The most significant features of the load voltage waveform are:

- A small initial jump that arises from the current flowing in the inductor of the magnetically delayed switch before the vacuum, or low pressure gas, switch fully closes
- The current that will eventually saturate the inductor causes the "foot" in the voltage
- As the inductor saturates, there is a surge of current at the load, producing the sharp rise in voltage
- Reflection of the "foot" from the open end of the Blumlein (with an opposite polarity) rounds-off the flat-top portion of the voltage waveform.

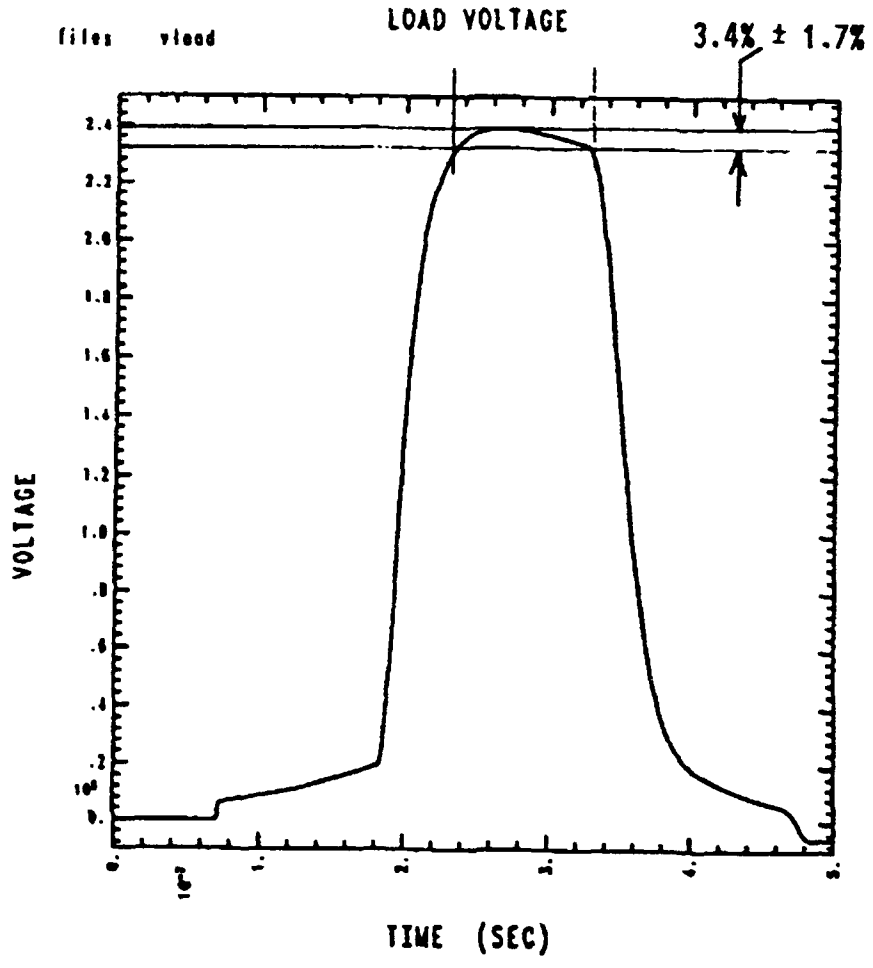

Figure 4.2: Accelerating voltage waveform of a cell fed by a Blumlein circuit switched by a magnetically delayed switch. (Voltage range is 0 to 2.4 x 10^5 V; time range is 0 to 5 x 10^{-7} s.)

This simple calculation illustrates some concerns that arise in the application of magnetically delayed vacuum switching:

- Will the leakage current in the magnetic switch degrade the voltage waveform at the output?
- What is the optimum delay (core saturation time) to reduce electrode erosion in the low pressure or vacuum switch to an acceptable level?
- Is there an optimum choice of Blumlein impedance, delay time, pulse length, charging time and cell compensation that accompanies this, or any other, switching technique?

The Switch Test Stand

The switch test stand that appears in Fig. 4.4 is under construction. In this stand a resonant transformer charges a 12 Ω, 250 kV, 70 ns Blumlein circuit. At present there is a provision to install a magnetically delayed switch. The stand could host other switch concepts as well.

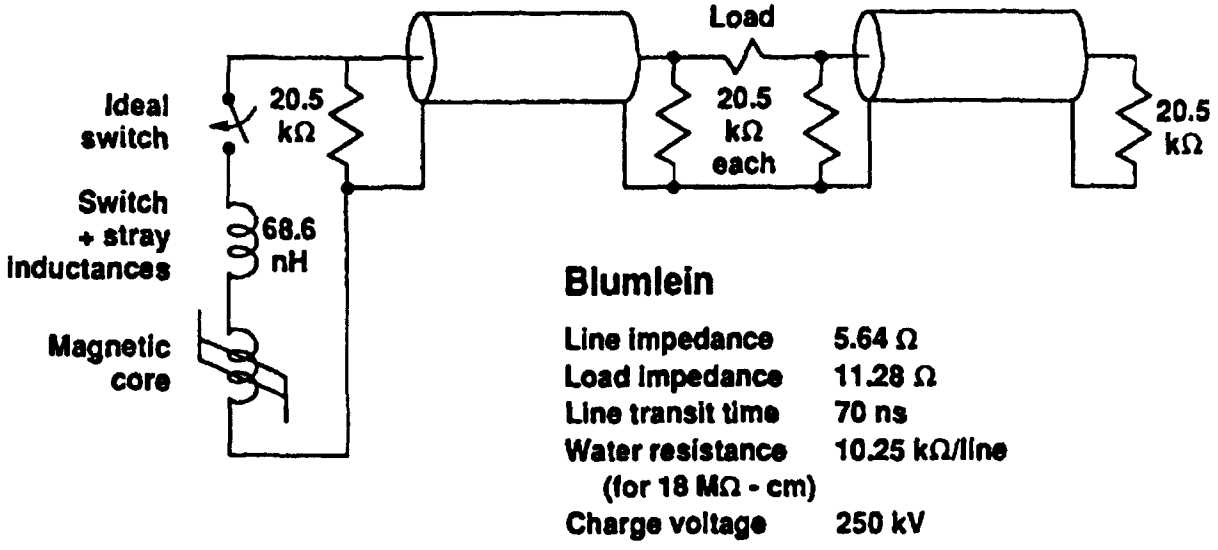

Figure 4.3: Network model for Magnetically Delayed Switch Blumlein circuit simulations for waveforms of Figure 2. Ideal impedance simulates accelerator cell load. Circuit parameters appear in inset.

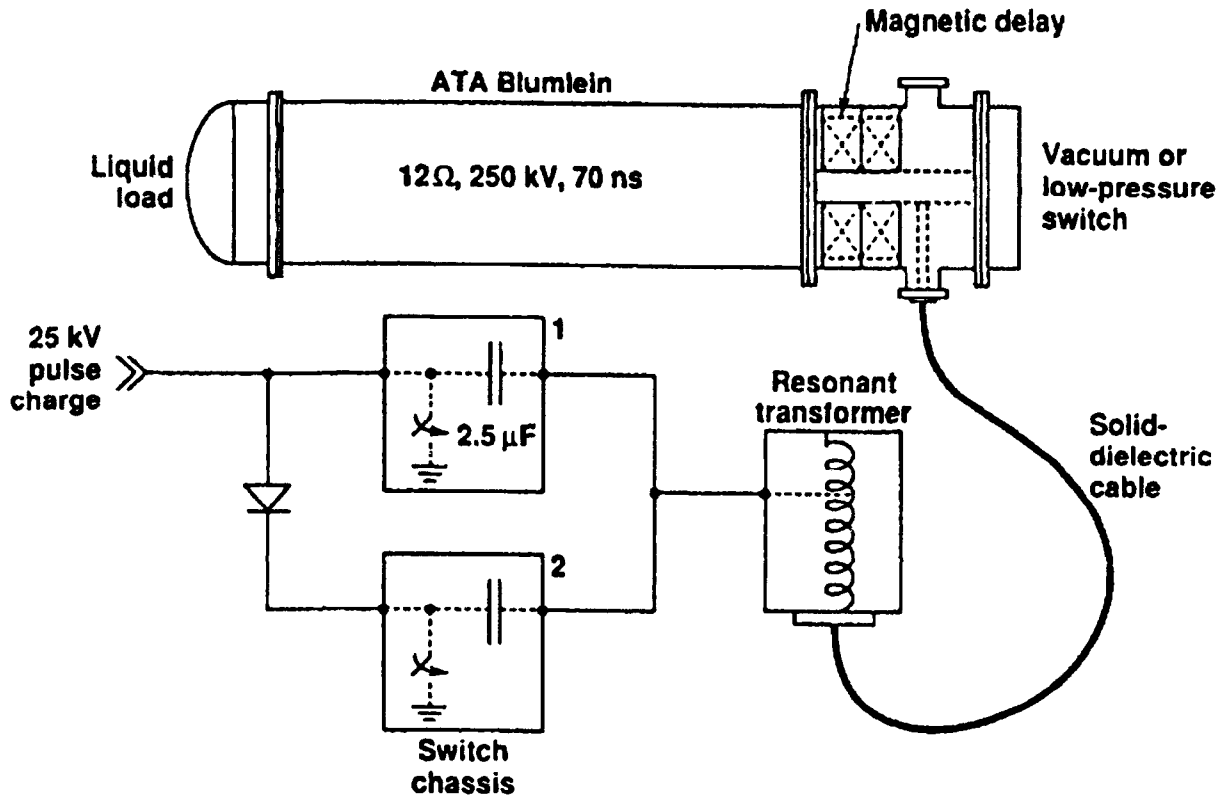

Figure 4.4: Switch test stand. Double charging supplies allow testing of switch recovery time.

5 Magnetically Delayed Vacuum Switching (R. Dougal)[3]

5.1 Introduction

Triggered vacuum gaps are attractive for repetitive power systems because they exhibit:

- Large hold-off field (<100 kV cm^{-1})
- Wide triggering range (5 % to 100 % of self-break voltage)
- Fast recovery (< 10 μs)
- High repetition rate (> 10 kHz)

In a magnetically delayed vacuum switch (MDVS), a saturable inductor in series with the vacuum gap drops most of the voltage in the switch as the anode and cathode plasmas cross the gap and establish ohmic current conduction. Once conduction takes place, the inductor saturates and the switch closes. The delay in the saturable inductor can circumvent some of the limitations associated with the transient process of vacuum gap turn-on:

- Large jitter
- Energy losses during turn-on
- Anode deterioration during turn-on
- Energy losses during conduction

We discuss the physical basis of these limitations below.

5.2 Limitations of Switch Performance in the Closure Process

In a vacuum gap, there is a time interval between trigger plasma injection at the cathode and bridging of the cathode-anode gap by the plasma. In this interval, a negative space charge extends between the boundary of the expanding trigger plasma and the anode. This space charge limits the current in the vacuum gap at a time when the full voltage already appears across the gap.

The onset of full conduction current (and shorting of the electric fields across the gap) can only take place once the expanding cathode trigger plasma and the anode plasma meet. This anode plasma results from energy deposition at the anode by the space charge electrons that accelerate across the gap. These electrons also vaporize local regions of the anode and eject materials from it as they dissipate their energy.

---

[3] Work supported by the Center for Commercial Development of Space Power and Advanced Electronics at the Space Power Institute, Auburn University

However, with a saturable inductor in series with the vacuum gap, most of the voltage drops across the inductor, decreasing the voltage across the gap during the plasma expansion phase. A lower voltage decreases the energy the electrons acquire during space charge limited conduction, therefore lowering energy dissipation at the anode. Lower energy dissipation reduces electrode erosion and reduces recovery times for the gap.

In addition to this first role of reducing the electron energy, the saturable inductor plays two other important roles. The second one is to reduce the initial time rate of change of the current allowing sufficient time for uniform and reproducible anode and cathode plasmas [Lauer, 1981] to form and bridge the gap before the time the switch is required to conduct full current. This delay produces a more uniform plasma luminosity. Researchers believe a uniform plasma luminosity correlates with uniform current conduction and a lower voltage drop when the switch carries the main current pulse. Experimental evidence suggests a third role. Observations show that the jitter of a vacuum switch in series with a magnetic switch is lower than the jitter of the vacuum switch by itself.

		Single Pulse	5kHz Rep rate	Best (Non sim*)
• Switch Voltage	(kV)	36	30	>45
• Switch Current	(kA)	3	2.5	>3
• Circuit		PFN	RLC	
• Pulse duration	(ns)	300	400	>500
• Current risetime	(ns)	40	80	<15
• Repetition rate	(kHz)	--	5	>10
• Burst duration	(μs)	--	20	>20
• Magnetic delay	(ns)	100	100	<85
• Trigger sites		1	1	--
• Prepulse current**	(kA)	.04-.05	--	--
• Leakage current***	(kA)	.01	.01	--
• Gap	(mm)	5	3	(100 kV/cm)

* Not simultaneous
** Discharges stray capacitance of the vacuum gap. Does not flow through load.
*** This current saturates the inductor.

PFN: 6 Ω Source and 6 Ω load.
RLC: R = 5 Ω, L = 400-500 nH, C = 20 nF.

Table 5.1: Switch Parameters for Repetitive Operation of MDVS

5.3 The State of the Art of High Average Power MDVS

The sketch of an MDVS appears in Figure 5.1 [Volakakis, 1989]. Table 5.1 lists the parameters of the switch.

Fig. 5.2.a shows the voltage across the vacuum gap and the current in the switch when the switch discharges a 12 Ω PFL charged at 33 kV into a 12 Ω load. The Al cathode and Cu anode are separated by a 5 mm gap in vacuum. The magnetic delay is 120 ns. A waveform that shows the prepulse and leakage currents appears in Fig. 5.2.b. At first, a ~50 A, 20 ns prepulse flows in the vacuum gap. This prepulse discharges the stray capacitance shunting the vacuum gap and does not flow through the network. A low (~10 A) current leakage current foot follows. This is the current flowing through the external circuit which will saturate the inductor.

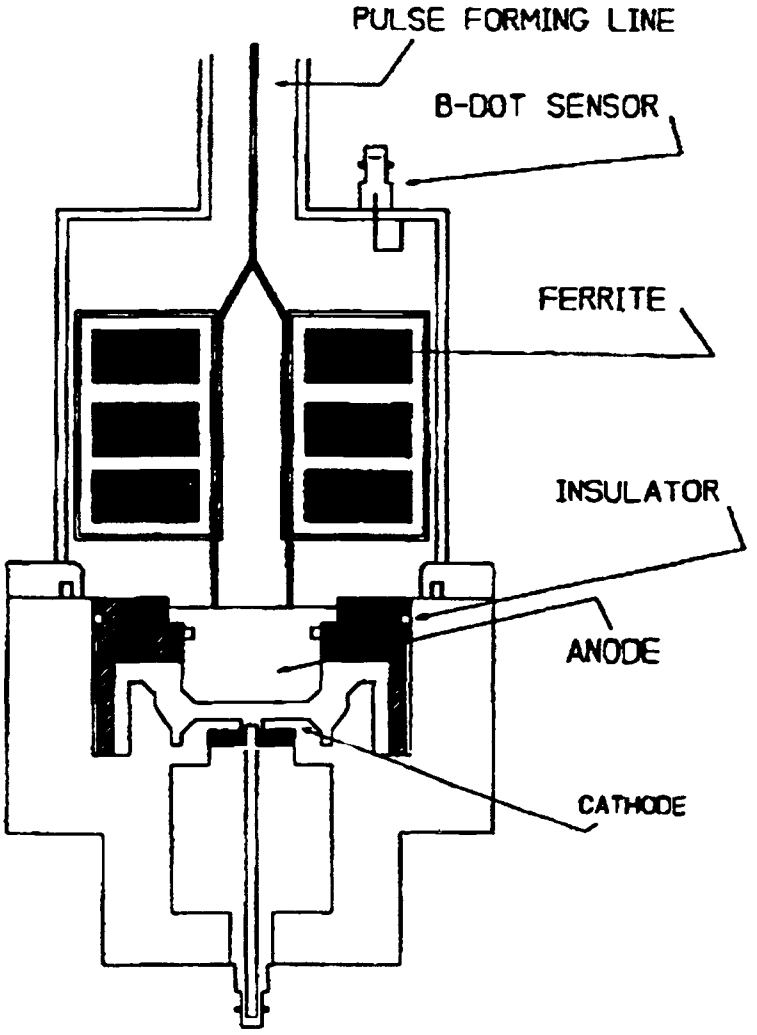

Figure 5.1: A Magnetically Delayed Vacuum Switch

5.2.a

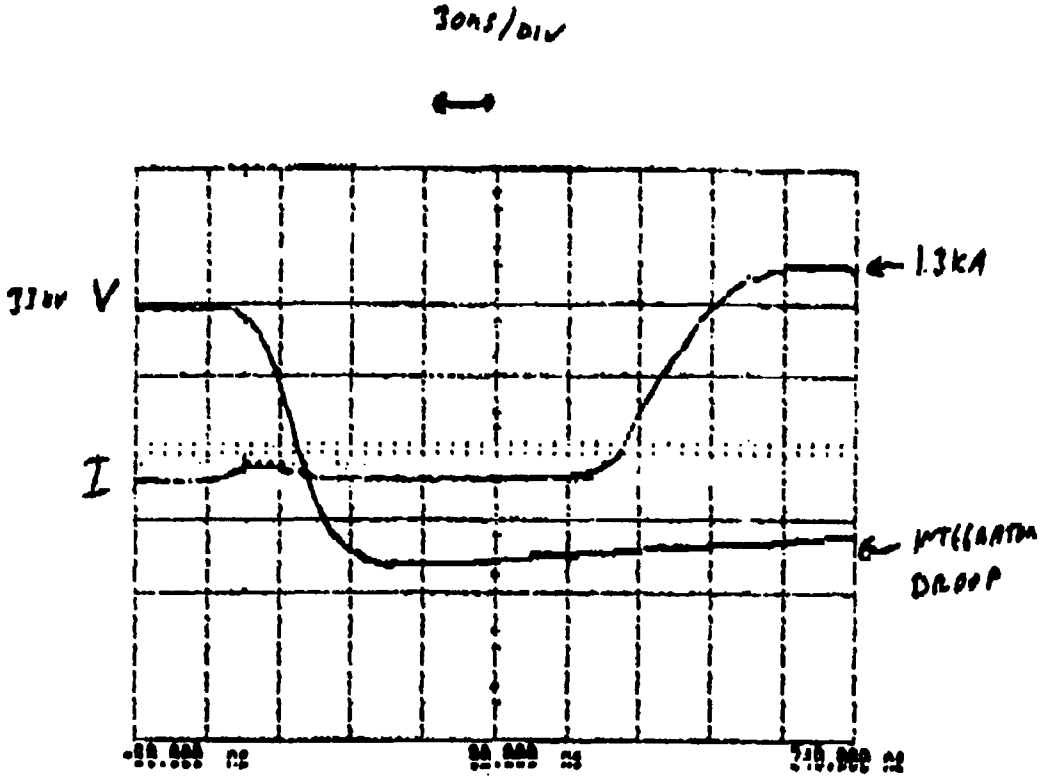

5.2.b

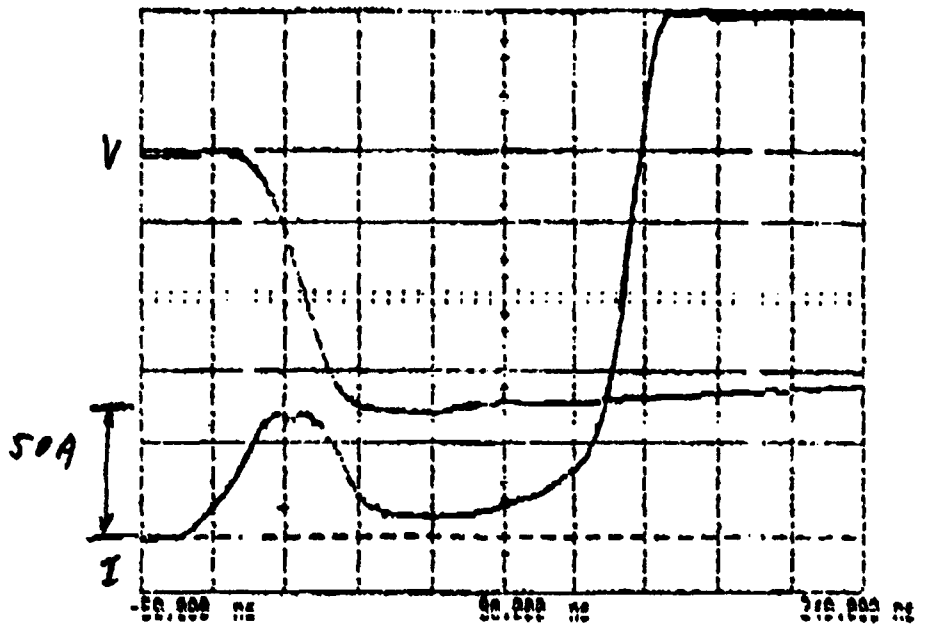

Figure 5.2: Voltage and current waveforms across the switch. (a) Displays current rise after magnetic delay (20 ns e-fold). (b) Displays leakage current during voltage collapse (50 A / 30 ns) and current that saturates inductor (10A / 90 ns)(Δ V=33 kV, Δ I=1.3 kA, time scale is 30 ns/div).

5.4 Present Research in Magnetically Delayed Vacuum Switches

Present research in MDVS involves:

- Determination of the optimum amount of magnetic delay that will result in reliable switching
- Determination of the optimum trigger, electrode and insulator geometry so that vaporized electrode material redeposits on the electrodes rather than on the trigger insulator or the vacuum envelope
- Choice of anode materials that absorb energy without forming droplets
- Choice of cathode materials whose plasmas sustain a high current discharge.

Challenges in meeting the specifications outlined in Section 4 are:

- Satisfying the conflicting constraints between magnetic delay and allowable switch inductance
- Providing multiple triggering sites
- Preventing current constriction by magnetic forces.

References

Dougal, R.A., et al., "Magnetically Delayed Vacuum Switching," Proceedings of the 1987 Pulse Power Conference (1987) 21-24.

Lauer E.J., et al., "Tests of a Low Pressure Switch Protected by a Saturating Inductor," LLNL UCID-19230 (1981); also: Lauer, E.J., et al., "Low Pressure Switch Progress Report," UCID-18848 (1980).

Volakakis, G.D., et al., "10 kHz Operation of the Magnetically Delayed Vacuum Switch," Proceedings of the 1989 Pulse Power Conference (1989) 678-680.

6 Super Emissive Cathode Switches (M. Gundersen, H. Riege, W. Nunnally and G. Kirkman)[4]

6.1 Introduction

The Electrophysics Department, University of Southern California, coined the term Super Emissive Cathode Switch (SEC) to describe an electronic device (switch) that incorporates a Super Emissive Cathode electron source [Hartmann, 1989]. The SEC switch definition encompasses devices such as the electrically triggered pseudo-spark switch and the optically triggered back lighted thyratron (BLT).

There is a clear distinction between the electron emission processes that take place in SEC and those that take place in the cathodes of thyratrons and spark gaps. In thyratrons thermionic emission ($J < 100$ A cm^{-2} over a few cm^2) occurs at 800°K from alkali-oxide cathodes in a tungsten matrix. In spark gaps and ignitrons, localized thermionic emission at $J \sim 10^4$ A cm^{-2} takes place from 10^{-4} cm^{-2} cathode spots of filamentary arcs.

In contrast, a SEC delivers **uniform current densities greater than 10^4 A cm^{-2}** from macroscopic areas of the order of 1 cm^2 of a **cathode in a glow discharge plasma**. This emission process which hinges upon a unique configuration of the cathode and anode, occurs when **the surface of pure refractory metal cathodes such as Mo and pure W is heated by ion bombardment.** Current conduction takes place in a **low pressure gas** fill so, that breakdown of the gap occurs on the **left branch of the Paschen curve** [Hartmann, 1989].

The SEC regime is a new regime [Christiansen, 1979; Bloess, 1983] that could have important new device applications (see [Frank, 1988; Gundersen, 1990] for a review of research on SEC devices).

The keynote speakers on SEC switches were:

- M. Gundersen, Electrophysics Department, University of Southern California (USC), Los Angeles, CA
- H. Riege, CERN, Geneva, Switzerland
- W. Nunnally, Applied Physical Electronics Research Center (APERC-UTA), University of Texas, Arlington, TX
- G. Kirkman, Integrated Applied Physics (IAP), Arcadia, CA

In addition, research on SEC switches and related phenomena takes place at the following centers [Di Capua, 1990a; Gundersen, 1990]:

---

[4] Work supported by: CERN, PS Division (H.R.); SDIO/ONR, DOE (M.G. and G.K.); and SDIO/IST/DNA (W.N.)

- University of Erlangen/Nuremberg, Federal Republic of Germany (J. Christiansen)
- Centre de Physique Atomique de Touluse, France (J. P. Boeuf/L. Pitchford)
- Karlsruhe Nuclear Research Center, Karlsruhe, FRG (K. Mittag)
- Institut Saint Louis (ISL), St. Louis, France

6.2 The Super Emissive Cathode Switch

A sketch of an SEC switch appears in Figure 6.1. The bottoms of the cup-like electrodes are refractory metal disks with 3 - 12 mm-diameter holes at the center.

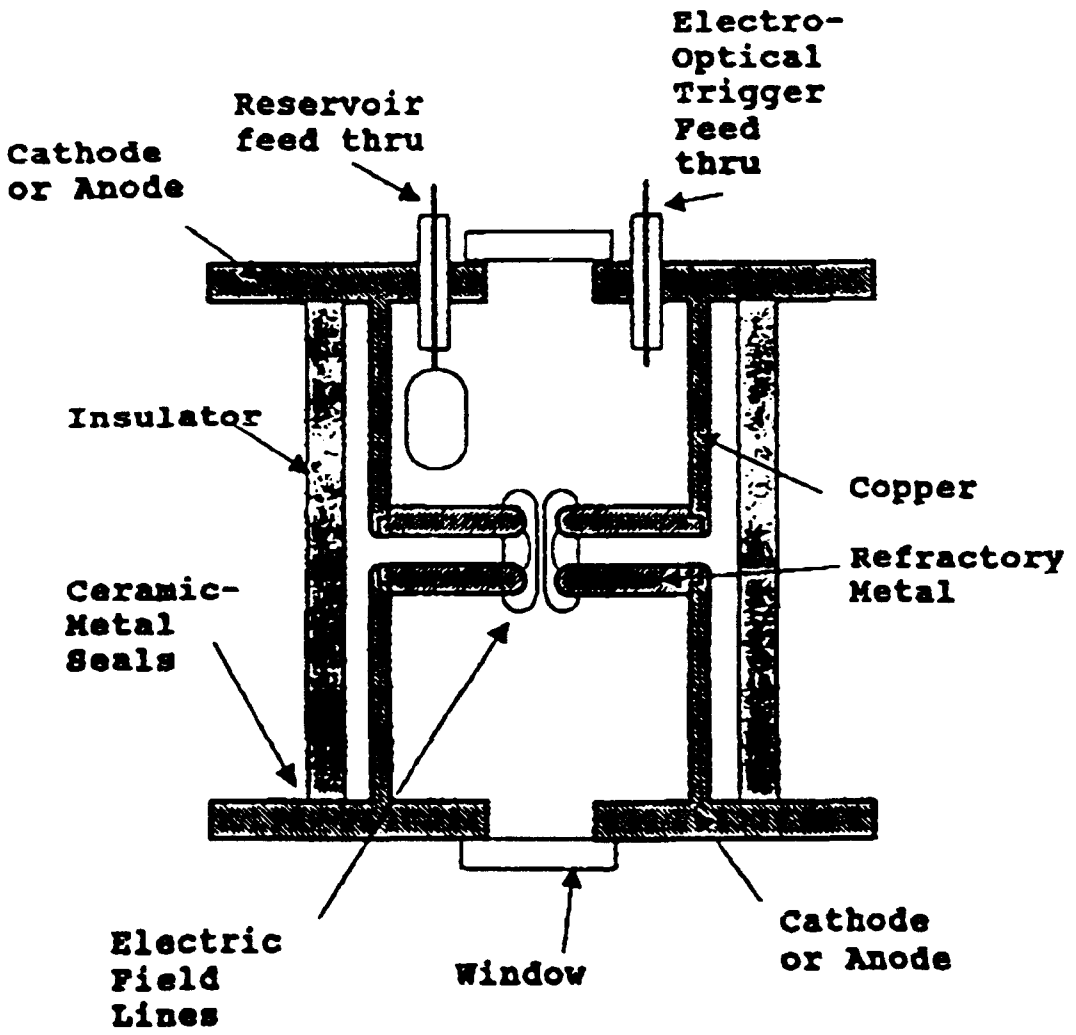

Figure 6.1: A generic super emissive cathode switch. This version incorporates an electro optical trigger feedthrough. Other trigger options are also available. Triggering takes place at the cathode side (W. Nunnally, APERC-UTA).

The two disc electrodes face each other across a 2 to 3 mm gap. The edges of the cups attach to the ends of a ceramic or glass cylinder which is the insulator, vacuum envelope, and structural element of the switch. The cups fit snugly in the envelope so that the gap between the cups and the envelope is smaller than the gap between the refractory metal disks. Gas at 10-30 Pa (H_2 or He) fills the envelope so that the pressure-distance product for the gap is lower than the product at which the Paschen curve has a minimum. Therefore breakdown initiates on the longest path which occurs in the region of the central holes of the electrodes.

We can understand the switching process with the aid of Figure 6.2 which displays conceptually the pre-breakdown field geometry in the cathode-anode region. About 10^9 electrons [several mA for 10 or 100 ns according to Hartmann, 1989a; μA according to Riege] are delivered at the back of the cathode by a pulsed glow discharge, a pulsed ferroelectric, which according to Riege can deliver several amperes [Gundel, 1989; Gundel, 1991], or unfocused UV laser light [McKinley, 1990]. These electrons initiate the breakdown process. The electrons accelerate along the electric field in the region of the central aperture of the gap and collisionally ionize the neutral background gas. The same electric field accelerates the resulting positive ions which in turn impact the cathode, heating a thin surface layer to a temperature that can reach 3000-4000°K [Hartmann, 1989a] in the later stages of the discharge. The thermionic emission electron flux from the ion impact heated cathode promotes the formation of a diffuse discharge in the gas fill that carries the conduction current. Anode heating by electron flux produces an anode plasma that also allows the electrode to emit when the voltage reverses on the device.

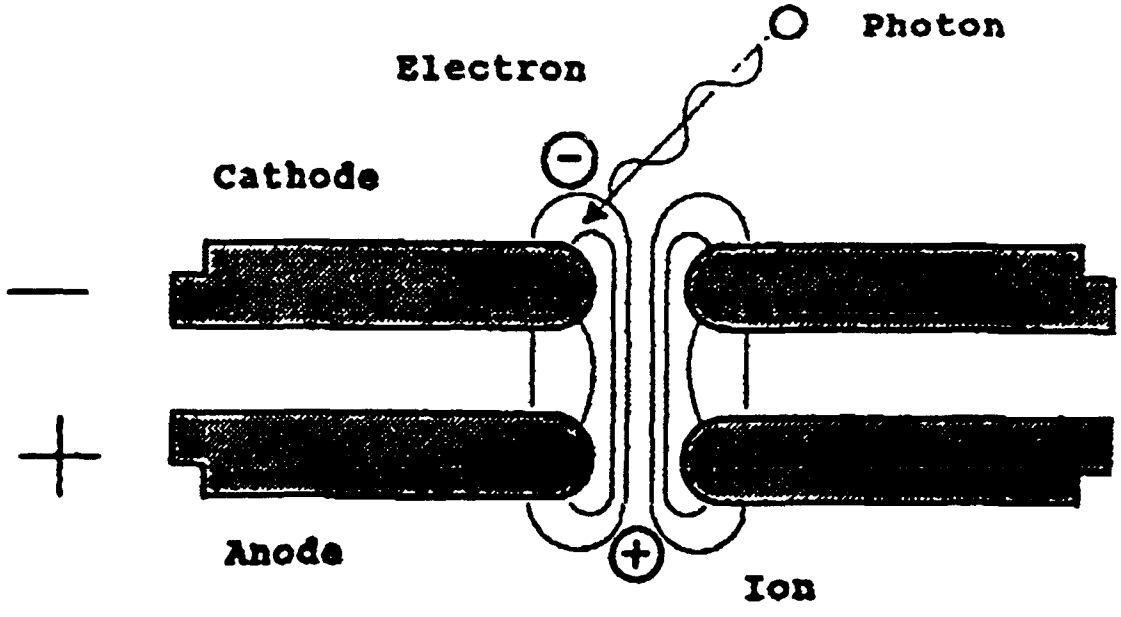

Figure 6.2: Conceptual view of electrode region of SEC switch. Other sources could deliver electrons on the back side of the cathode. Acceleration of electrons along the long path is the critical triggering mechanism (W. Nunnally, APERC-UTA).

Current conduction in an SEC switch takes place in a plasma with two components of the electron distribution function [Bauer, 1990]. In a device with a neutral H_2 fill of 10^{16} cm^{-3}, a peak current of 10^4 A and a 0.5 μs pulse length, one component is the "bulk" plasma with an electron density of 1 - 4.0 x 10^{15} cm^{-3}, an ionization degree of 0.4, and 0.8 - 1 eV electron temperatures with a Maxwellian distribution. The second component is a beam-like electron distribution with a density of 0.1 - 1.0 x 10^{14} cm^{-3}, an energy of 100 to 500 eV, and a duration of 100-300 ns that participates in current conduction with current densities in the range of 0.1 - 1.0 x 10^4 A cm^{-2}.

6.3 The State of the Art on Super Emissive Cathode Switches

Table 6.1 summarizes the state of the art of SEC switches as discussed at the workshop:

		CERN	USC	USC	IAP
Switch voltage	(kV)	16-20	17.5	100	40
Peak current	(kA)	100-200	60	76	20
Resistance	(mΩ)	0.6	<60	--	<100
Charge transfer	(C)	0.5	0.022	0.024	0.003
dI/dt (circuit limit)	(TA s^{-1})	0.06	0.34	0.3	0.6
Pulse duration	(μs)	15	0.4	0.5	0.15
Repetition rate	(Hz)	0.3	5	<1	--

Table 6.1: State of the Art of Switches with SEC

Table 6.2 summarizes existing data for continuous SEC operation at USC

Voltage (kV)	Current (kA)	Energy (J)	Frequency (kHz)	Power (kW)	Mode
7	3.5	2	5	10	Burst
20	10.5	--	0.12	--	Continuous
25	9.4	1.7	1.8	3	Continuous

Table 6.2: Continuous operation data for SEC switches at USC.

6.3.a

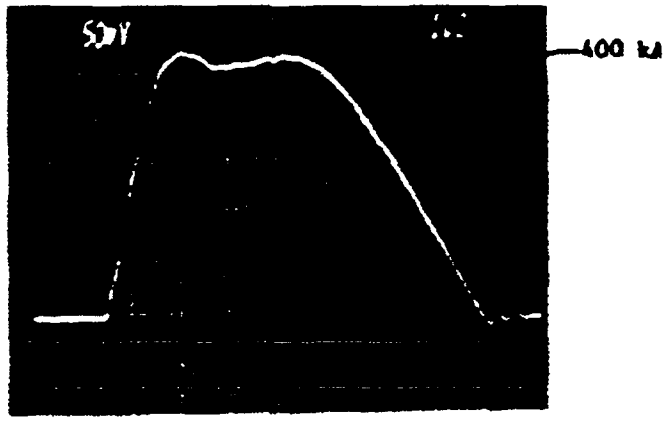

Total plasma lens current = sum of four pseudo-spark switch currents.

6.3.b

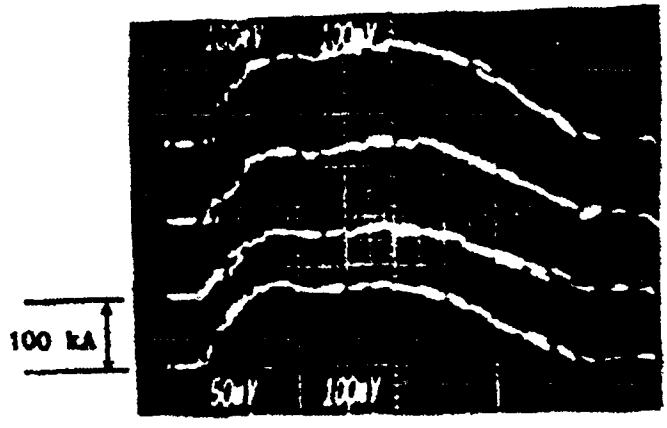

6.3.c

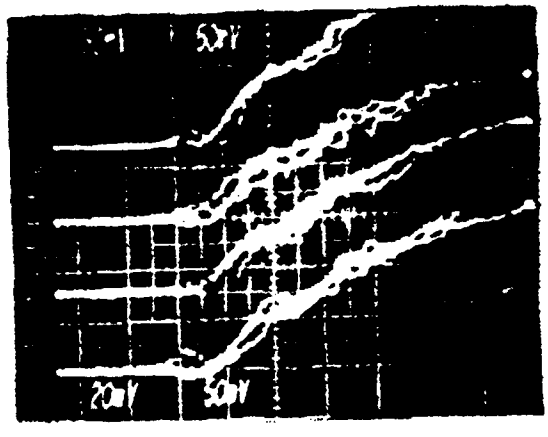

Figure 6.3: Currents in the CERN 100 kA switch: 6.3a - Sum of 4 switch currents (base to base width is 7 μs); 6.3b - Currents through each switch on the same timescale; 6.3c - Five current pulses through each switch on a fast timescale (200 μs/div) [Brillault, 1987].

Figure 6.3 displays the currents in the CERN 100 kA switch [Brillault, 1987]. Four SEC switches in this experiment fed a plasma lens. Figure 6.3.a displays the total current in the plasma lens which is the sum of currents from four switches. The base to base width is 7 μs (1 μs/div). Figure 6.3.b displays the currents through each switch on the same timescale. Fig 6.3.c with a timescale that is five times as fast displays five current pulses for each switch. The waveforms show the variability of the waveforms delivered by the switches in this "slow" current risetime application.

Figure 6.4 displays a current waveform for the IAP BLT-250 switch operating at 25 kV with a 1 Ω pulse forming network source in a fast kicker application. The waveform displays a foot with a 50 ns duration and a sub-10 ns risetime thereafter ($di/dt > 0.6$ TA s^{-1}). The conjecture is that the foot is the ion current the switch requires for bombardment of the cathode so that super emission from the heated cathode can take place.

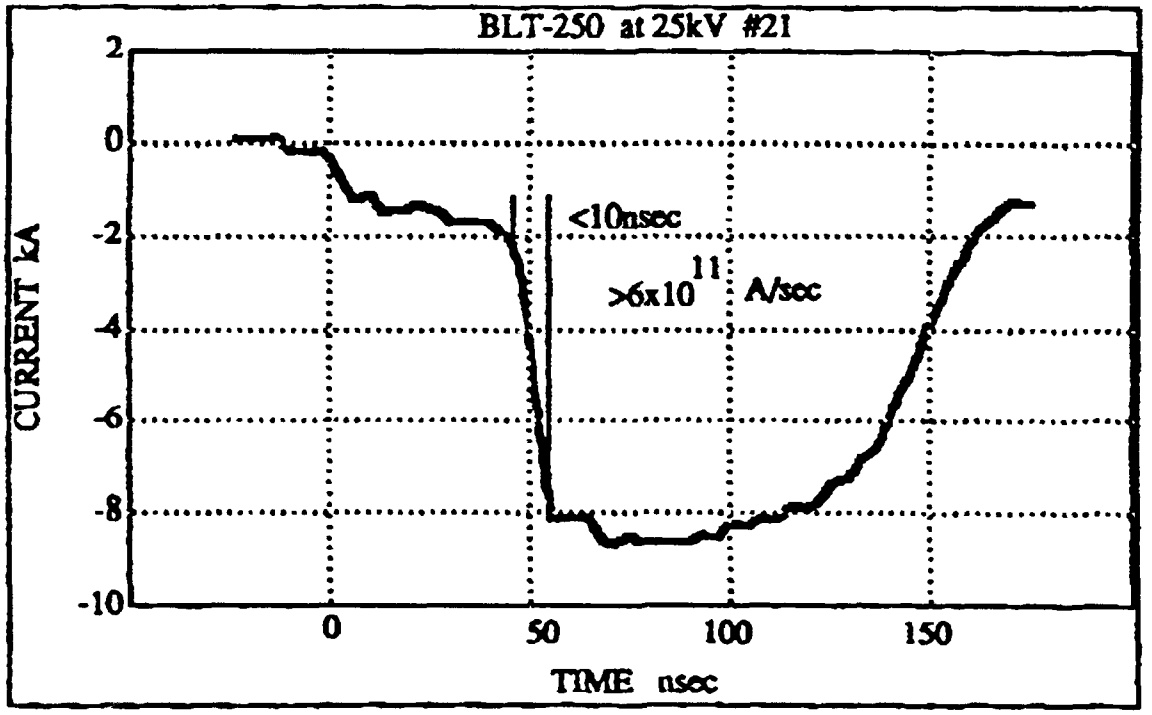

Figure 6.4: Current for a BLT 250 SEC switch operating at 25 kV. Foot in current pulse is ion current that heats the cathode (M. Gundersen, USC; Nunnally, 1990).

The turn-on of SEC switches depends strongly on the triggering driver and the circuit energy switched. Weak triggering and/or low circuit voltage/high circuit impedance causes a long heating phase of the SEC. Vigorous triggering and higher energy circuits greatly reduce the magnitude and duration of the heating current to a value that can become negligible compared to the total current flowing in the circuit. Figure 6.5.a displays this feature in a 1 Ω PFN, 1 Ω load circuit at 20 kV/16 J and Fig. 6.5.b at 2.5 kV / 0.25 J. At 20 kV the 150 A heating current is barely noticeable

(about 2% of peak) and lasts 30 or 40 ns. At 2.5 kV the heating current rises linearly from zero to 300 A in 100 ns. When the switch "closes" this current has reached 33% of the peak current in the circuit.

6.5.a

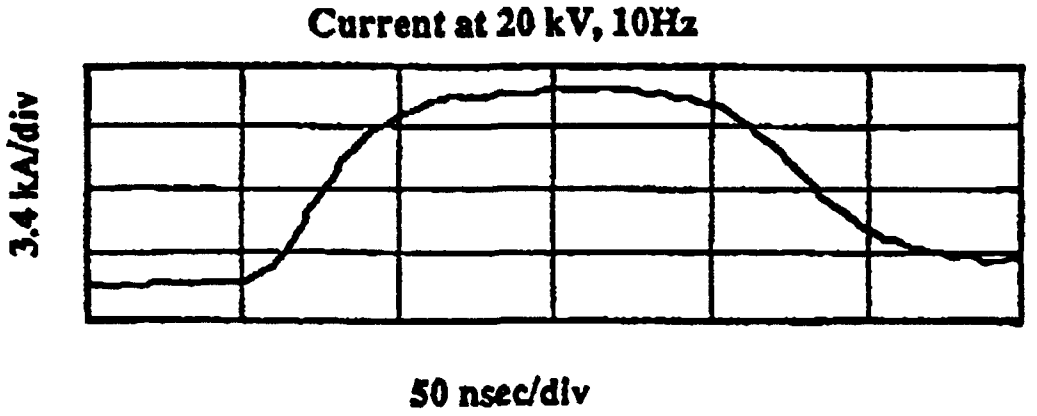

6.5.b

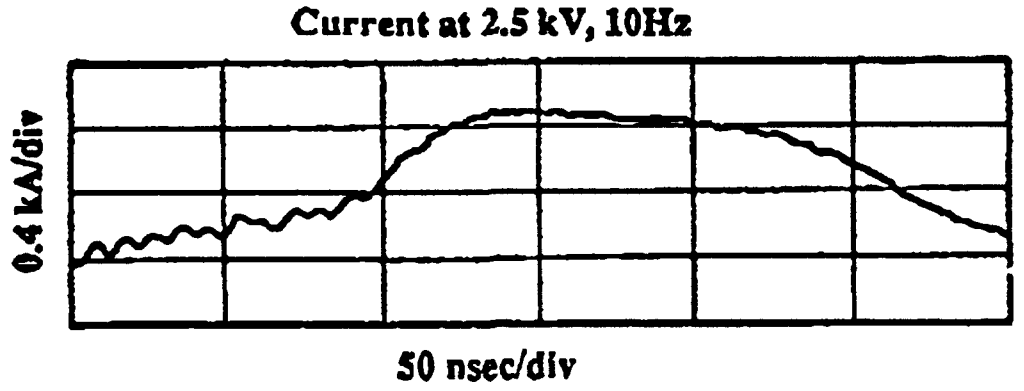

Figure 6.5: Turn-on of SEC switches. At low voltage (current), the turn on current is a larger fraction of the total current that at higher voltages (currents) (G. Kirkman-A., IAP).

Figure 6.6 displays high current (60 kA) operation with large current reversals in a flashlamp-triggered BLT that discharges a 17.5 kV, 0.8 μf capacitor without additional series resistance (1 μs period, 5 Hz). In this experiment, the sensitivity of the measurement is too low to record the heating current.

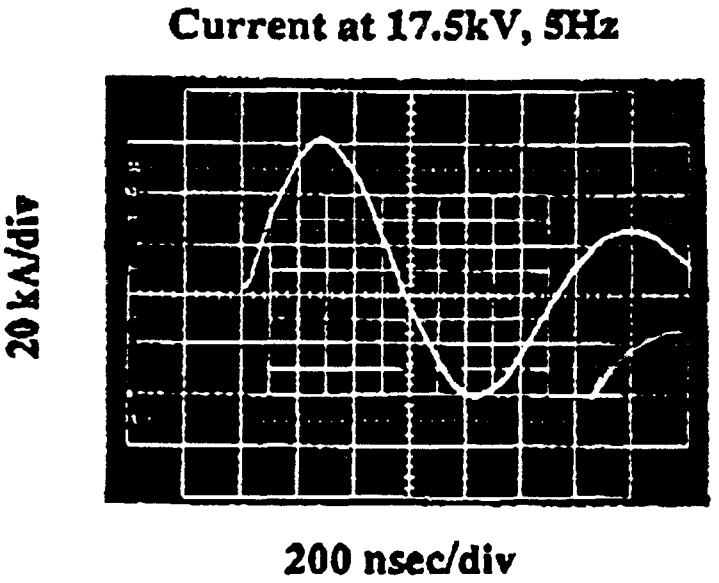

Figure 6.6: SEC high current operation. Light from a flash lamp triggers the switch. Sensitivity of measurement is too low to record the heating current (G. Kirkman-A., IAP).

Figure 6.7 displays the charging voltage waveforms for continuous operation (7 kV entry of Table 6.2). The waveforms show the 200 μs pulse interval and a fast recovery (<20 μs) for the switch voltage.

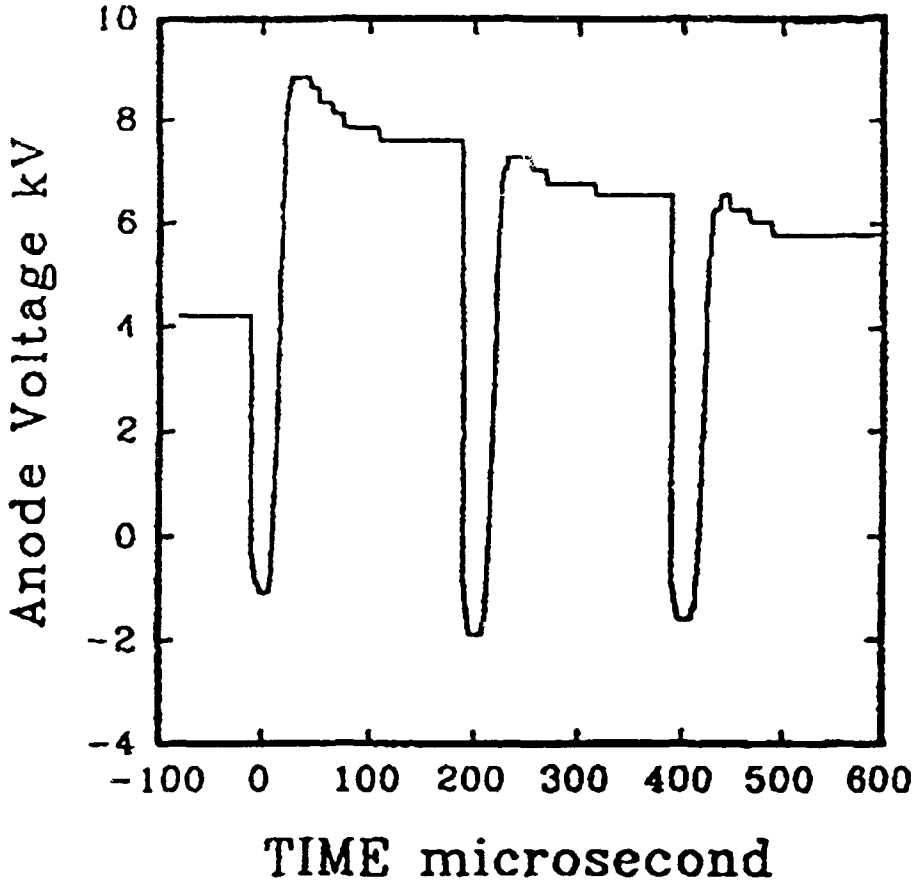

Figure 6.7: Charging voltage waveforms display a very fast (20 μs) switch recovery (G. Kirkman-A., IAP).

6.4 Research Directions in SEC Switches

This section outlines research directions discussed at the workshop.

6.4.1 Gas Reservoir, Supply and Flow.

- Improve methods to maintain a constant gas composition and pressure in a sealed SEC switch during repetitive operation at high C transfer. Direction is to activate gas dispensing reservoirs and gas gettering alloys [Di Capua, 1990] within the envelope once the switch envelope is under vacuum (USC, IAP).

6.4.2 Triggering

- Optical triggering at visible wavelengths to reduce the trigger part count and the energy required for triggering (APERC-UTA, IAP)
- Improve the lifetime of surface discharge and ferroelectric emitter electron sources (CERN)
- Increase electron beam trigger current from ferroelectric emitters (CERN)
- Protect the trigger from discharge accelerated beam ions (CERN, USC)
- Develop a fast, low jitter, highly reliable, thyratron-like electrical triggering method (IAP).

6.4.3 Electrode Development

- Measure average and peak thermal profiles of the electrodes during high C repetitive operation (IAP)
- Measure the SEC switch power dissipation and average power handling capability
- Develop internal switch baffling to prevent deposition of vapors on the insulator and triggers (CERN, APERC-UTA). Figure 6.8 shows a APERC-UTA concept for a baffled low inductance SEC switch
- Optimize the electrode geometry to reduce trigger energy and dwell current prior to full switch closure (APERC-UTA).

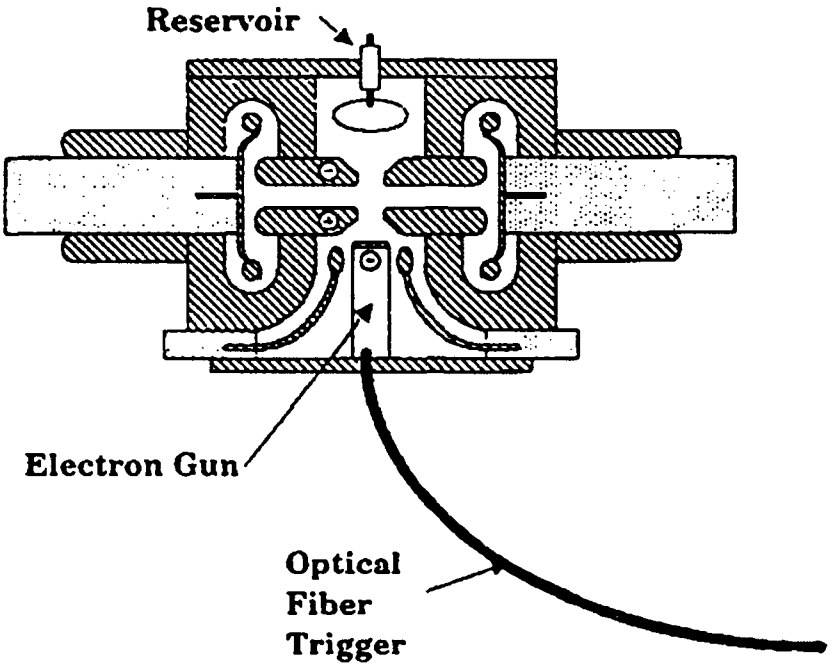

Figure 6.8: Concept for a low inductance SEC switch (W. Nunnally, USC).

6.4.4 System Studies

- Establish the limits on the maximum voltage a single gap can withstand (IAP/USC; Hsu, 1989)
- Configuration of devices with multiple gaps for voltage hold-off (UTA, USC, IAP)
- Series connection of multiple devices (APERC-UTA)
- SEC applications to High Energy Particle Accelerators (CERN, APERC-UTA).

References

Bauer, H., et al., "A Two Component Model For the Electron Distribution Function in a High Current Pseudospark or Back Lighted Thyratron," IEEE Transactions on Plasma Science, Volume 18 (1990) 237-245.

Bloess, D., et al., "The Triggered Pseudo-Spark Chamber as a Fast Switch and as a High Intensity Beam Source," Nucl. Instrum. Meth., Volume 205 (1983) 173.

Brillault, P., et al., "Pseudospark Switches," Yellow Report, CERN 87-13, Geneva, Switzerland (1987).

Christiansen, J. et al., "Production of High Current Particle Beams by Low Pressure Spark Discharges," Z. Phys., Volume A290 (1979) 35.

Di Capua, M.S., "Getter Metallurgy, Vacuum Technology and Gas Purification at SAES Getters in Milano, Italy," European Science Notes Information Bulletin, Office of Naval Research, ESNIB 90-05 (1990) 27-29.

Di Capua, M. S., "Transient Hollow Cathode Discharge Phenomena," European Science Notes Information Bulletin, Office of Naval Research, ESNIB 90-06 (1990a) 53-56.

Frank, K., et al., "High Power Pseudospark and BLT Switches," IEEE Transactions on Plasma Science, Volume 16 (1988) 317-323.

Gundel, H., Riege, H., Wilson, E. J. N., Handerek, J., Zioutas, K., "Ferroelectrics 100," 1 (1989).

Gundel, H., Handerek, J., Riege, H., J. Appl. Phys., Vol. 69, No. 2 (1991).

Gundersen, M.A., et al., "The Physics and Applications of Pseudosparks," Plenum Press, New York (1990).

Hartmann, W., et al., "A Super Emissive Self-Heated Cathode for High Power Applications," IEEE Transactions on Electron Devices, Volume 36 (1989) 825-826.

Hartmann, W., et al., "An Analysis of the Anomalous High Current Cathode Emission in Pseudospark and Back of the Cathode Lighted Thyratron Switches," Journal of Applied Physics, Volume 65 (1989a) 4388-4393.

Hsu, T. Y., "Studies of Multigap BLT's for High Power Applications," Proc. 7th IEEE Pulse Power Conference, IEEE 89-CH2678-2 (1989).

McKinley, M. C., "UV Triggering of Remote BLT's Using Optical Fibers, and Neodymium Glass, Neodynium:YAG, and Copper Vapor Lasers," Proc. 19th Mod. Symp., IEEE 90-CH2839-9 (1990) 411-413.

Nunnally, W. C., et al., "Development of an Accelerator Kicker Magnet Modulator Using a Back Lighted Thyratron," Proc. 19th Mod. Symp., IEEE 90-CH2839-9 (1990) 87-90.

7 Solid State Switches (R. L. Druce, K. Schoenbach)

The workshop discussed two solid state switching technologies that differ in the method of carrier generation. Section 7.1 discusses photoconductive solid state switches (PCSS) where photons from a laser generate the carriers. Section 7.2 deals with electron beam controlled semiconductor switches. In these switches an external electron beam produces photons in a thin layer of the semiconductor. These photons then generate the carriers in the bulk of the material.

7.1 Photoconductive Switching[5]

Photoconductive solid-state switches (PCSS) are optically controlled devices. As shown in Figure 7.1.1, a PCSS is a block of semiconductor with electrodes attached at opposite faces. Current conduction takes place in the applied electric field when light of the appropriate wavelength produces free charge carriers in the semiconductor material. The carriers then move in the semiconductor under the action of the electric field as a conduction current, thereby closing the switch.

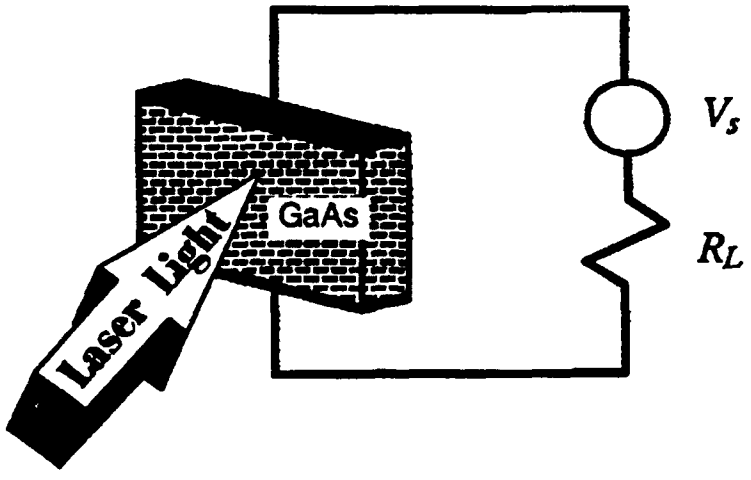

Figure 7.1.1: PCSS concept showing the basic components of a photoconductive switching system

[5] Contributed by R. L. Druce, Lawrence Livermore National Laboratory. Work supported by USDOE

7.1.1 Laboratories Performing PCSS Switch Research

The most active laboratories performing research in PCSS are:

- Lawrence Livermore National Laboratory (LLNL)
- University of Maryland (U of M)
- U.S. Army LABCOM ET&DL (ETDL)
- University of Texas at Arlington (UTA)
- Sandia National Laboratories, Albuquerque (SNLA)
- Old Dominion University, Norfolk, VA
- University of Rochester, Rochester, NY
- Naval Surface Warfare Center, Dahlgren, VA
- University of Southern California (Optothyristors) [Hur, 1990]
- Some industrial concerns performing proprietary work

7.1.2 Solid State Junction Devices and PCSS Switches

Solid-state junction devices, with their fast recovery times, match the high rep-rate requirements of linear induction accelerators quite well. However, for operation at 250 kV or above and tens kA, accelerators would require an inordinate number of junction devices (open-state voltage - a few kV, closed-state current - a few kA).

PCSS's do not share the voltage and current limitations of junction devices because these switches are bulk in nature. There is data spanning an order of magnitude in semiconductor length and area that suggests PCSS switches scale to larger values of open-state voltage and closed state current.

7.1.3 The State of the Art in PCSS Performance

The clear advantage of PCSS for generating very fast-rise pulses has motivated most of the effort in this direction. Figure 7.1.2 is a typical fast-rise wave form [Druce, 1989]. The laser duration for Figure 7.1.2 is 100 ps. Table 7.1.1 shows some of the switching parameters that have been achieved by several laboratories.

SNLA has achieved over 50 MW on a single event where the switch did not survive. Table 7.1.1 also shows that most work to date has been done with solid-state lasers, constraining the overall efficiency of switching.

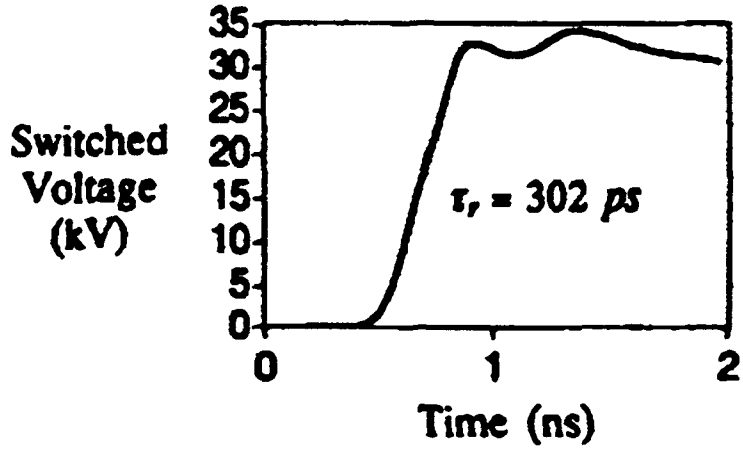

Figure 7.1.2: PCSS waveform showing the fast rise time and lock on for a GaAs device

Laboratory*	ETDL	U of M	LLNL	UTA	SNLA
Peak Power (MW)	> 2	> 1	25	> 1	1
Rise Time (ps)	300	100	200	200	600
Load Impedance (Ω)	50	150	50	50	50
Pulse Length (ns)	1-2	< 1	3	0.8	--
Rep-rate (pps)	1	1	1	1	1000
Device Life (shots)	NA	NA	~100	NA	10^5
Material	GaAs	GaAs, Si	GaAs	GaAs	GaAs
Configuration	Radial line	Strip line	Strip line	Blumlein	Strip line
Laser	Nd:YAG	Nd:YAG	Nd:YAG	Alexandrite	AlGaAs Diode
Mode	Linear	Linear	Lock-on	Linear	Lock-on [Loubriel, 1990]

NA - not attempted

* see page 36

Table 7.1.1: State-of-the-art at several laboratories for short-pulse PCSS. There is some additional work on SiC and ZnSe [Loubriel, 1990]

The advantages of PCSS for generating slower, very high rep-rate pulses have not been fully explored experimentally. The experimental data that are available indicate that there are definite potential advantages for PCSS in generating longer pulses. Figure 7.1.3 shows plots of longer pulses obtained at LLNL [Pocha, 1989] and SNLA [Zutavern, 1989]. The laser pulses in both cases were much shorter than the output pulses (5 ns at LLNL and 10 ns at SNLA). These pulses take advantage of lock-on, which is discussed below. Voltages to > 35 kV have been switched in this manner [Pocha, 1990].

a. Diode laser triggered wave form, 440 μm device gap (LLNL, 5 ns laser)

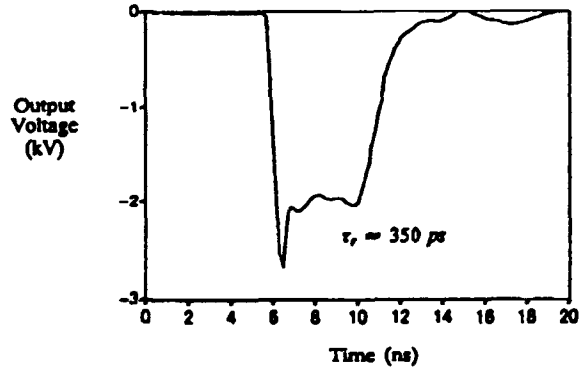

b. Nd:YAG laser triggered wave form, 1.5 cm device gap (SNLA, 10 ns laser; Zutavern, 1989)

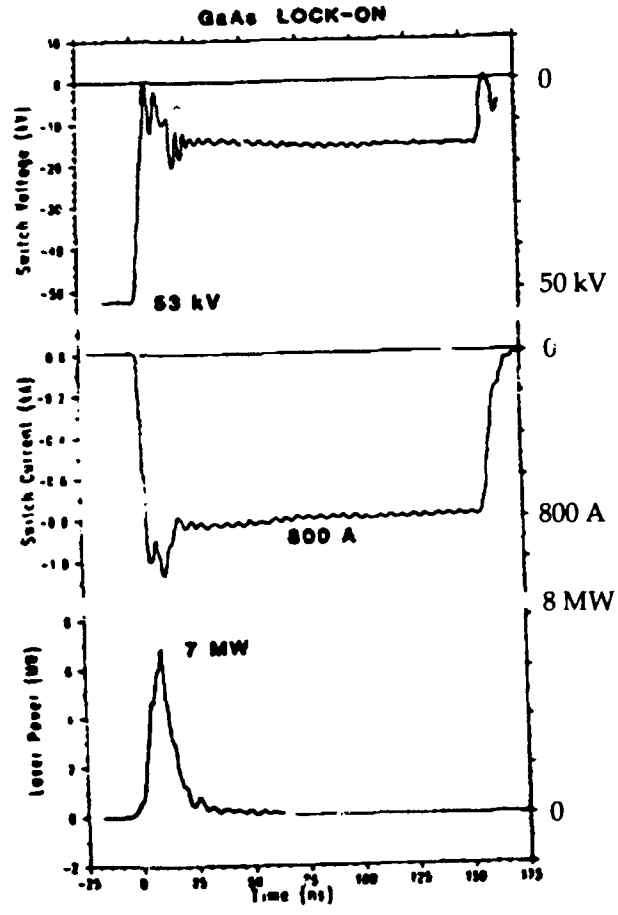

Voltage, current, and laser waveforms for a 1-in. diameter Cr:GaAs switch triggered with a 532-nm laser pulse at high voltages (above lock-on). Although the laser pulse is only 10-ns wide, the switch stays on for 160 ns, at which time the storage line energy has been completely dissipated (Time scale range is -25 ns to 175 ns).

Figure 7.1.3: Slow wave forms showing the longer times attainable with lock-on mode

7.1.4 Inherent Limitations to Device Performance.

Table 7.1.2 summarizes the semiconductor materials being studied and some of the pertinent parameters of those materials.

Diamond would seem to be the ideal choice for PCSS. However, reasonable sized diamond crystals are very expensive to produce. There are hidden costs with diamond as well: the combination of a large band gap and low mobility require a large number of UV photons, which are quite expensive to generate. In addition, the high breakdown fields associated with diamond must extend to the entire switch system (edges, packaging, etc.) to be effectively exploited. Designing systems for such high field holdoff is difficult.

Material	Band gap (eV)	Mobility(μ) (cm^2/V-sec)	E_{bd} kV/cm	ρ electrical (MΩ-cm)	σ thermal (W/cm-°C)
Si	1.1	1000	170	0.11	1.41
GaAs	1.4	1000	200	28	0.54
InP	1.35	1000	200	28	0.68
Diamond	5.3	<1000	2000	10^5	15

Table 7.1.2: Semiconductor materials being studied for PCSS.

Silicon (Si) was initially studied as a photoconductive switch. Silicon's low dark resistivity requires pulse charging from a low impedance source to overcome the high leakage current and eliminate thermal runaway in the "open" state.

Gallium Arsenide (GaAs) is the material currently being studied most extensively for PCSS. We explore some of its properties in more detail below.

7.1.5 Gallium Arsenide as a PCSS Material

Voltage Hold-off - Table 7.1.2 shows that the breakdown field increases with increasing band gap of the material so the maximum open-state voltage for PCSS materials is essentially a linear function of the breakdown electric field (E_{bd}) and device length. However, practical values of open-state voltage are limited by surface flashover and charging pulse length. At present, GaAs must be pulse charged at high fields. Open-state voltages of over 200 kV (140 kV/cm) have been attained with pulse charging [Loubriel, 1990]. Small devices have been consistently biased (500 ns pulse) to > 150 kV/cm with careful consideration of the surface path of the devices.

Switching the devices at these high field levels usually limits the device life. Repeatable, reliable operation requires much lower applied fields. Fields of 50 kV/cm or less seem to be safe. Continued research will certainly increase the open-state voltage for reliable switching to values near the maximum hold-off voltage achieved to date.

DC charging of > 80 kV/cm (2.7 kV) has been achieved in 330 μm-thick Cr doped GaAs devices. Ongoing research with Cr doped GaAs may alleviate the need for pulse charging in the future.

Maximum Current - The maximum current attainable is a function of the number of carriers generated in the semiconductor and the ease with which they move about the crystal lattice (mobility).

- **Carrier Generation**

  Carrier generation can take place through intrinsic or extrinsic absorption. Photons with energies larger than the band gap will directly ionize the crystal structure, generating free electrons and holes (intrinsic absorption). Photons with energies lower than the band gap will only ionize defects in the crystal, generating free electrons (extrinsic absorption). The time for carrier generation in PCSS is very fast [10^{-14} sec] making these devices capable of low jitter and fast rise operation.

  In extrinsic absorption, the density of defects in the crystal structure determines the maximum density of carriers photons can generate. The density of defects in LEC grown, El2 compensated GaAs is generally 10^{15} - 10^{16} defects/cm^3. Carrier generation by Nd:YAG laser photons depends entirely on extrinsic absorption. Extrinsic absorption depth (sub-band gap light) is 4 mm for 1.06 μm radiation.

  While intrinsic absorption can produce orders of magnitude larger densities of carriers than extrinsic absorption, the intrinsic absorption depth is small and wavelengths are shorter (< 10 μm for 532 nm radiation in GaAs). Al:GaAs diode lasers, Alexandrite lasers, and Ti:Sapphire lasers can all operate at intrinsic absorption wave lengths, albeit at low powers.

  The relative merits of extrinsic and intrinsic absorption carrier generation in the quality of switching are a topic of research. A tradeoff arises between generation of a lower density of carriers over a larger volume (extrinsic absorption) or a larger density of carriers over a smaller volume (intrinsic absorption). Since high energy, short pulse Nd:YAG lasers are better developed than shorter wavelength lasers at this time, the majority of PCSS data exists for extrinsic absorption switching. As the technology of short wave length lasers improves, more data on intrinsic absorption

switching is becoming available. Closed-state resistances of less than 1 Ω are fairly easily attainable in both regimes.

The number of carriers generated by each incident photon and the mobility of the carriers determine the switch gain [ratio of electrical power/energy switched to optical power/energy required for control]. Optical considerations such as reflections at the interfaces and relative sample thickness compared to absorption depth affect the gain in a straight forward manner; any photon lost by reflection or transmission will not contribute conduction carriers. Calculated maximum gain without lock-on approaches 100. Experimental values are more in the range of 5 - 20 [Donaldson, 1987; Loubriel, 1987].

- **Carrier Mobility**

Mobility is usually a complicated function of field and material and changes over the range of switched fields encountered in high-voltage devices. Figure 7.1.4 is a plot of electron velocity vs. electric field for GaAs [Loubriel, 1987]. Note from Figure 7.1.4 that the electron velocity is not monotonic with field. The high-field portion of the curve is generally referred to as velocity saturation. Values for mobility are normally quoted for the low-field region. For pulsed power switches, the entire curve must

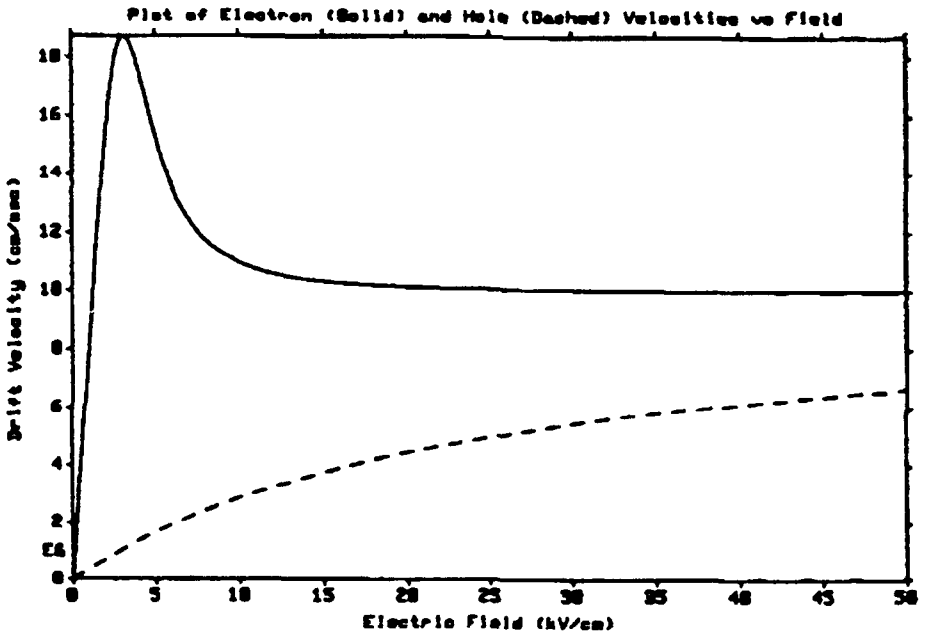

Figure 7.1.4: Plot of electron and hole velocities vs. field for GaAs [White, 1990]. Velocity scale is 2×10^6 cm s^{-1} per division, electric field scale is 5 kV cm^{-1} per division.

be considered. Optimum switch gain will occur for a closed-state field between zero and the field that results in the peak velocity. To complicate matters further, Figure 7.1.4 shows that the electron and hole velocities are not equal.

- **Carrier Recombination**

  Recombination depends on the type of semiconductor, the processing of the material, and the type of carriers generated. Recombination times as long as milliseconds or as short as 10's of picoseconds have been demonstrated. Recombination in GaAs is typically quite fast, from a few ns for intrinsic material to as short as a few ps for correctly prepared material. If the device operates below the lock-on field (discussed below), the switch will open with the characteristic recombination time of the material when the light is removed. During low-field operation output pulse durations are limited approximately to the durations of available laser outputs.

Lock-On - GaAs (and at least one other direct band gap semiconductor material, InP) exhibit behavior dubbed lock-on by researchers at SNLA. In lock-on, high field operation defeats the normally fast recombination processes in GaAs. Depending on the material preparation and, somewhat less on the time scale of switching, lock-on will take place above a threshold field of 4-60 kV/cm.

While the exact mechanism of lock-on is not yet fully explained, lock-on has the advantage that it increases the range of possible switch gain by reducing the incident light requirement in two ways: the PCSS material requires fewer photons to initiate conduction (multiplication) and switch conduction continues after the incident light is removed from the material. Gains of 10^3-10^4 [Loubriel, 1989; Zutavern, 1989; Pocha, 1989] are easily achievable in lock-on. The disadvantage is that a residual field of 4 - 8 kV cm^{-1} (see [6] below), depending on device preparation, remains across the device during lock-on. This residual field may be very weakly dependent on current density. The lock-on field results in higher power dissipation in the switch [Lobriel, 1989; Zutavern 1989; White, 1989; Pocha, 1989].

Repetition Rate - Repetition rate is limited by switch recovery, switch heating, charging considerations, and indirectly by switch life. Experiments [LLNL, SNLA] indicate that a switch in lock-on recovers in < 70 ns after the voltage is removed; switch recovery should not limit performance until repetition rates of > 1 MHz are attempted.

Switch heating - Switch heating is a more stringent limitation since energy dissipated in the semiconductor must be removed by external cooling. Figure 7.1.5 shows a diagram of a microchannel cooled PCSS. Using parameters of 250 kV, 10 kA,

---

[6] Literature quotes values a high as 60 kV cm^{-1} for material that has been neutron damaged to enhance recombination. Such a material is very inefficient for long pulse applications

100 ns pulse length, GaAs thermal capacity = 1.8 J/cm^3-°C, thermal conductivity = 0.54 W/cm-°C, and heat removal at the switch face of 1 kW/cm^2 yields a switch that is 2.7 cm-high in the field direction, 14 cm wide for the cooled face and 2 mm thick in the direction of laser propagation. The foregoing calculation assumes state-of-the-art for all switch parameters. The laser energy required to drive such a switch into lock-on would be about 38 mJ/pulse with no power gain (the device is triggered hard and lock-on is used only to stretch the pulse length). Commercially available lasers will produce these parameters now.

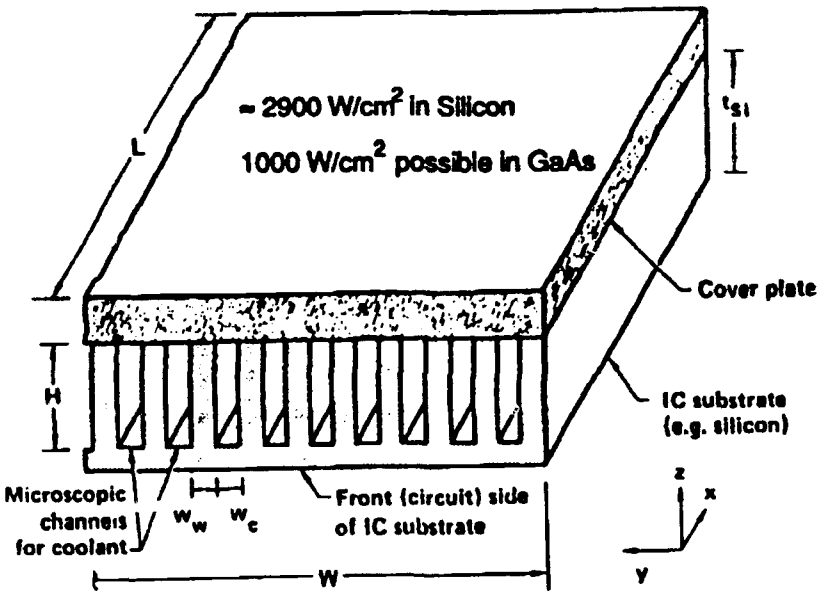

Figure 7.1.5: Microchannel cooling concept applied to a photoconductive switch

Efficiency - Figure 7.1.6 shows a strawman design that provides a feel for the efficiency that can be expected for a PCSS system. The system depicted in Figure 7.1.6. relies on lock-on for pulse stretching (and gain). Note that lock-on allows reasonable efficiency from the switching system even though the laser is a very low efficiency component.

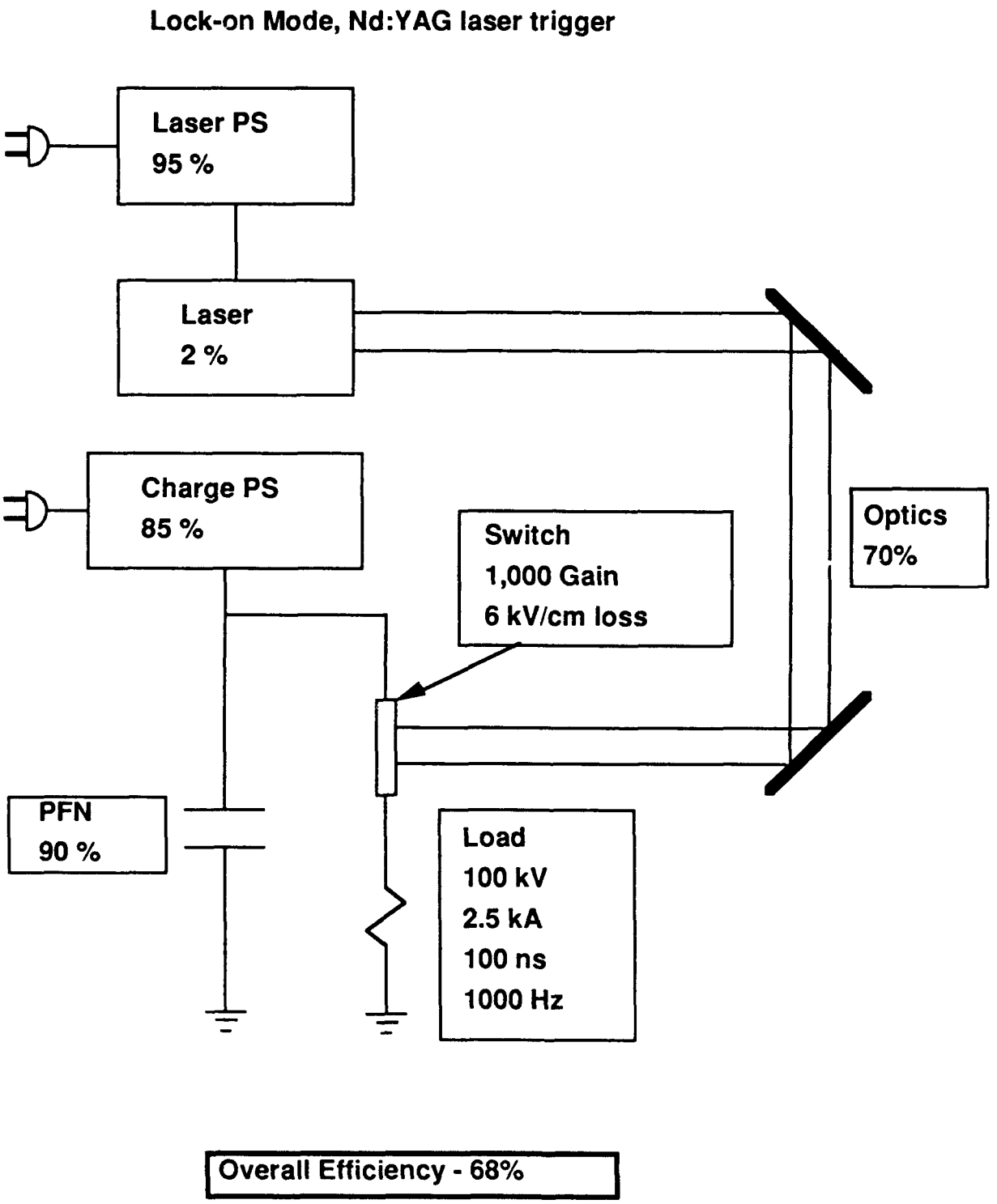

Figure 7.1.6: Overall efficiency diagram showing estimated efficiencies of components and their impact on the efficiency of the switching system

Switch Life - Switch life is a serious concern for PCSS at high peak and average powers. Possible filamentation, contact and defect migration, mechanical shock, quality assurance of the GaAs, and doping near contacts and throughout the bulk may all play a part in switch life. At present, switch life ranges from a few hundred to many hundreds of thousands of actions depending on the electrical parameters of operation and the switch being used.

7.1.6 References

Donaldson, W., et al., "Characterization of High-Voltage Photoconductive Switches," Proceedings of the 6th IEEE Pulsed Power Conference (1987) 141-144.

Druce, R.L., et al., "Subnanosecond Linear GaAs Photoconductive Switching," Proceedings of the 7th IEEE Pulsed Power Conference (1989) 882-886.

Hur, J., et al., "GaAs Optothyristor for Pulsed Power Applications," IEEE Trans. El. Dev., 37 (1990) 2520-26.

Loubriel, G. M., et al., "Toward Pulsed Power Uses for Photoconductive Semiconductor Switches: Closing Switches," Proceedings of the 6th IEEE Pulsed Power Conference (1987) 145-148.

Loubriel, G. M., et al., "Closing Photoconductor Switches," Proceedings of the 7th IEEE Pulsed Power Conference (1989) 365-367.

Loubriel, G. M., et al., "Triggering GaAs Lock-on Switches with Laser Diode Arrays," Proc. 19th Mod. Symp., IEEE 90-CH2839-9 (1990) 352-56.

nn, Special Issue, IEEE Trans. El. Dev., 37 (1990) 2425-2553.

Pocha, M.D., et al., "Avalanche Photoconductive Switching," Proceedings of the 7th IEEE Pulsed Power Conference (1989) 866-868.

Pocha, M. D., "35 kV GaAs Subnanosecond Photoconductive Switches," IEEE Trans. El. Dev., 37 (1990) 2486-2493.

White, W.T., et al., "Analysis of the Performance of Gallium Arsenide Photoavalanche Switches," Proceedings of the 7th IEEE Pulsed Power Conference (1989) 422-425.

White, W. T., et al., "Modeling GaAs High-Voltage Subnanosecond Photoconductive Switches in One Spatial Dimension," to appear in [nn, 1990].

Zutavern, F.J., et al., "Photoconductive Semiconductor Switch. (PCSS) Recovery," Proceedings of the 7th IEEE Pulsed Power Conference (1989) 412-417; also: Proc. 19th Mod. Symp., IEEE CH 2839-9 (1990) 385-390.

Additional References

Goeller, R.M., et al., "Investigation of Cryogenic Photoconductive Power Switches," Proceedings of the 6th IEEE Pulsed Power Conference (1987) 157-156.

Litz, M.S., et al., "Photoconductive Switching of a Blumlein Pulser," Proceedings of the 6th IEEE Pulsed Power Conference (1987) 153-156.

Mazzola, M.S., et al., "Investigation of a Photoconductive Closing and Opening Bulk GaAs Semiconductor Switch," Proceedings of the 7th IEEE Pulsed Power Conference (1989) 418-421.

Stoudt, D.C., et al., "The Electrical Characteristics of Semi-Insulating GaAs for High Power Switches," Proceedings of the 7th IEEE Pulsed Power Conference (1989) 348-351.

Thomas, B.L., et al., "Investigation of Surface Flashover in Silicon Photoconductive Power Switches," Proceedings of the 6th IEEE Pulsed Power Conference (1987) 149-152.

7.2 Electron-Beam Controlled Semiconductor Switches [7]

Electron-beam controlled GaAs switches operating either in the linear mode or triggered into a semi-permanent conductive state, can switch, like photoconductive switches at high powers, with nanosecond risetimes and very low jitter. Since electron beam sources have higher efficiencies, higher repetition rates, and are less expensive than lasers at comparable power levels, electron beam controlled semiconductor switches could be competitive with photoconductive switches in high average power switching applications. In addition the use of electron beams as drivers for switches operated in the linear mode allows pulse shaping by modulating the electron beam current in a gated vacuum tube.

7.2.1 Electron-Beam Sustained GaAs Switch

The concept of electron-beam sustained semiconductor switches (1, 2) is based on irradiating a wide-bandgap, direct semiconductor material, such as GaAs or ZnSe, with a high energy electron-beam. The electron-beam creates a high density

[7] K. Schoenbach contributed this section. Work supported by USARO and AFOSR

electron-hole carrier in a surface layer with a depth in the range of several tens to hundreds of micrometers. The electron-beam-generated secondary ionizing radiation (x-rays and band-edge radiation from recombining electron-hole pairs) can penetrate deep into the bulk of the semiconductor. Band-edge radiation, with an emission characteristic which is well matched to the absorption spectrum of the semiconductor, is the dominant source of ionization. The physics of the switching process is therefore similar to that of a laser-driven photoconductive switch.

A sketch which shows schematically how the switch can be integrated in an electron-beam driver is shown in Figure 7.2.1. The switch consists of a cylindrical piece of semi-insulating GaAs or any other wide-bandgap, direct semiconductor. It is doped on the cathode side with acceptor material to a depth equal to the penetration depth of the electron-beam. For 200 keV this depth is on the order of 100 μm. At the anode the semiconductor is doped with a donor material, generating a P-layer, intrinsic, N-layer (PIN) structure.

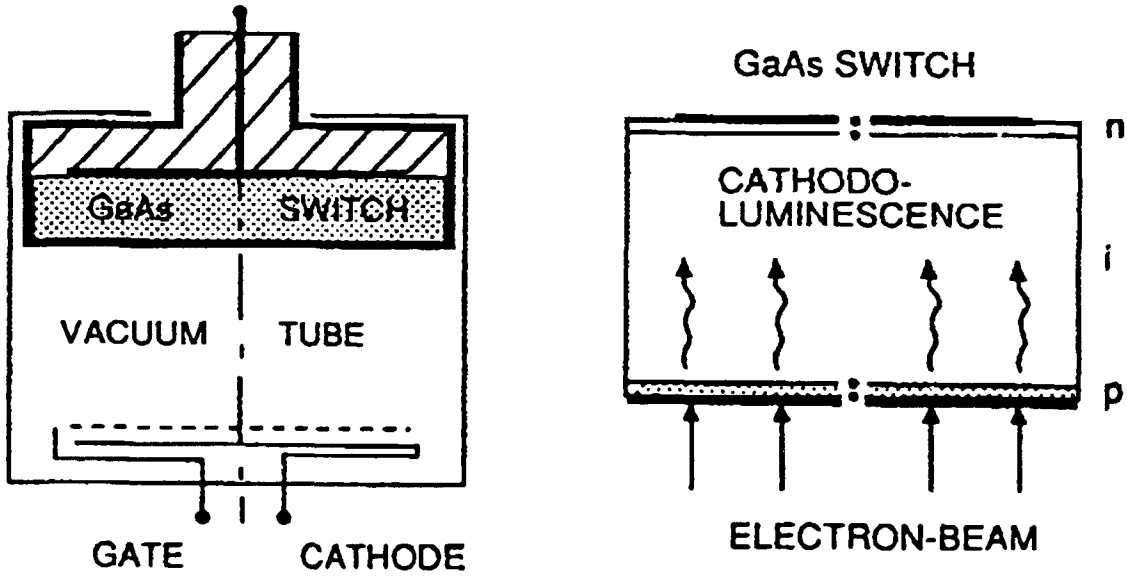

Figure 7.2.1: Schematics of an electron beam controller switch with the GaAs switch integrated in a gated electron tube. The figure on the right shows the design of the solid state switch (PIN structure) and indicates the process of electron energy conversion into band edge radiation.

In the open state (no irradiation), the bulk material has a high resistivity, with measured hold-off field strengths of more than 150 kV/cm. The PIN structure prevents current injection into the bulk of the switch and insures therefore a low dark current.

To turn the switch into the conducting state, closing the switch, an electron-beam with an energy below the damage threshold of 250 keV, is injected at the cathode side of the sample. Due to the small penetration depth of the electron-beam, the

electrons that stop in the p-type layer of the switch create a high concentration of electron-hole pairs by direct ionization. Subsequently, these pairs recombine emitting band-edge radiation (in GaAs: $h\upsilon$ = 1.42 eV) which then penetrates deep into the material, ionizing the bulk of the switch. The electron-hole plasma in the bulk zone allows large currents to flow during electron-beam irradiation. Modulation of the electron-beam current will cause linear changes in electron-hole plasma density and therefore the switch current.

The strong p-type doping of the electron impact region has two effects on the switch efficiency. First, it enhances the probability of electron energy conversion into photon energy and second, it reduces the bandgap. Consequently, the resulting band-edge radiation undergoes less absorption in the intrinsic material and penetrates deeper into the bulk. Proper doping of the p-type layer allows tailoring of the 1/e depth of the band-edge radiation with respect to the switch geometry, in a similar way to that attainable with a tunable laser.

Early experiments were performed with 0.5 mm thick semi-insulating GaAs wafers without the PIN structure. Electron-beam current densities were in the range of 10 mA / cm^2 with pulse durations in the 10 μs range. Figure 7.2.2 shows the results of the electrical measurements. In the linear range, currents of up to 10 A have been switched with 36 mA electron beams corresponding to a current gain (switch current/electron-beam current) of about 300. Gains of more than 10,000 have been reached in the nonlinear range at applied fields in excess of 5 kV/cm. Also shown in this figure are results of modeling (solid lines) which indicate that linear switch operation, where the switch current is proportional to the applied voltage, is well understood.

Improvements in current gain by more than an order of magnitude are possible by using PIN structures. Also, modeling results indicate that it should be possible to extend the linear range to much higher field strengths, avoiding the lock-on effect [3], and therefore keeping the switch controllable over a wide range of voltages. This would allow the switch to open even at high applied voltages by turning off the electron-beam. Experiments with GaAs in a PIN structure have confirmed this prediction [3a]. It was possible to apply five times higher voltage to the switch than to an intrinsic one without going into the lock-on state. Also, the switch gain improved by about a factor of four, even though the p-type layer in the GaAs did not have the optimal thickness. Because the proposed switch would operate in the linear regime, currents and voltages should scale linearly with switch dimensions and source intensities. Modeling results [2], which are experimentally verified for lower current and voltage levels, led to the scenario generated by the discussion group on solid state switches [Table 10.1].

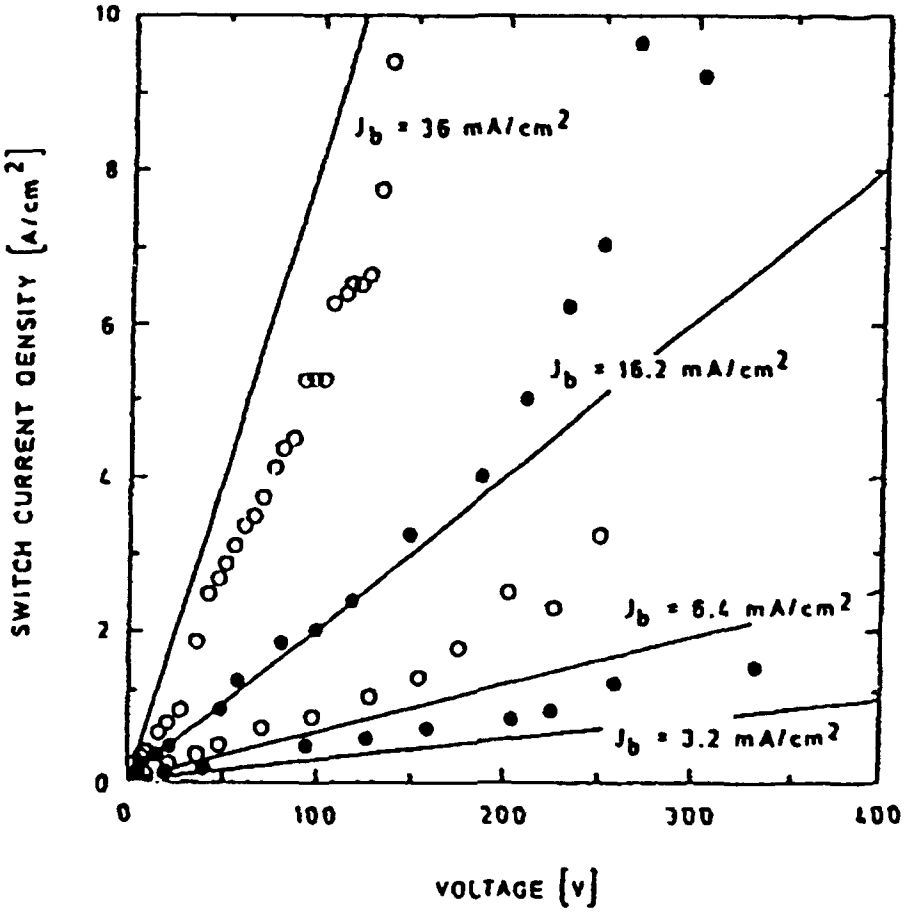

Figure 7.2.2: Comparison of experimentally obtained J-V characteristics with computed J-V curves for 0.5 mm-thick semi-insulating GaAs switches. The modeling results hold for low voltages only.

7.2.2 Electron-Beam Triggered GaAs:Si:Cu Switch

The development of a new type of semi-insulating GaAs at Old Dominion University (ODU), which has decay time constants far exceeding those of GaAs and even Si, offers the possibility to use this material as a low jitter closing switch. This switch can be triggered with either a Nd:YAG laser, as it was done at ODU, or with an electron beam. It has hold-off voltages and dark currents comparable to those at GaAs, but the current decays with 1/e times that are long compared to the pulse duration requirements of Linear Induction Accelerators (Figure 7.2.3). This persistence of the current after switching into the conducting state is *not* due to the lock-on effect. Rather, it is a linear effect, which results from the slow trapping of electrons into ionized deep Cu centers. Unlike the lock-on case, where the switch current is locked to a certain voltage, the forward voltage is only determined by the source function and can therefore attain very low values. The new material, silicon doped, copper compensated GaAs (GaAs:Si:Cu) and its applications are discussed in [4, 5, 6, and 7]. One of the most attractive features of this new material is its use as an

opening switch, where the current is optically quenched: GaAs:Si:Cu switches can be closed *and* opened by means of laser radiation.

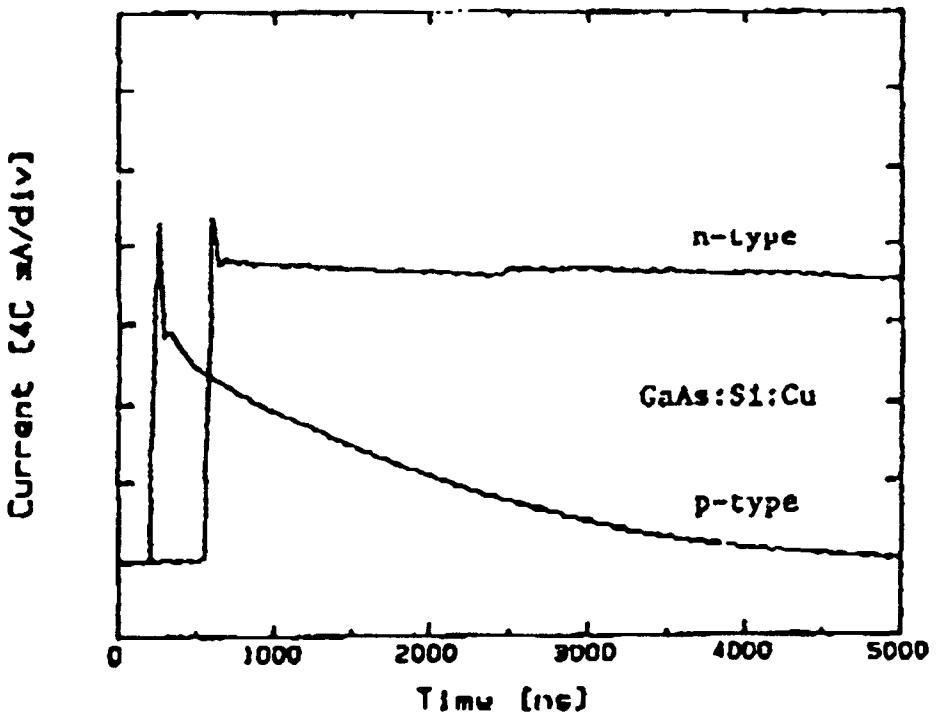

Figure 7.2.3: Photocurrent decay curves for slightly undercompensated (n-type) GaAs:Si:Cu and slightly overcompensated (p-type) GaAs:Si:Cu. Un-doped GaAs or chromium doped GaAs has decay times of nanoseconds and less. Current scale is 40 mA div^{-1}, time scale is 1000 ns div^{-1}. (M. Mazzola, Dissertation, ODU, 1990)

The properties of GaAs:Si:Cu, its high optical gain together with its low dark current, make it the best available switch material for photoconductive closing switches, operating at voltages far below the lock-on voltage. The closing switch based on e-beam triggering of the GaAs:Si:Cu has been modeled and results are discussed in [8]. Results show that subnanosecond switching of a GaAs:Si:Cu switch into a conductive state with less than 0.1 Ω/cm^2 (Figure 7.2.4) is possible with electron-beam pulses which generate carriers at a rate of 10^{25} cm^{-3} s^{-1}. This corresponds to an electron current density of 100 A/cm^2 at an electron energy of 150 keV. Although these values seem high, it should be considered that handheld, battery driven e-beam guns with 2 ns e-beam pulses, which generate several hundred amperes at the required electron energy are available [10, also: M. Kristiansen, Texas Tech University].

The calculation of Figure 7.2.4 was performed for a 0.5 mm sample. However, it can be expected, that by relaxing the condition for the risetime from ps to ns, it becomes possible to switch thick samples with about the same e-beam flux as used in the

model. The advantages of using such a switch in Linear Induction Accelerators would lie in the relatively inexpensive (compared to lasers) construction of switch drivers, which allow precise switch triggering at high repetition rates. In addition, the reduced thermal loading of the switch due to the low forward voltage (far below the lock-on voltage) and the small amount of trigger energy should allow easier thermal management of the repetitively operated solid state switch.

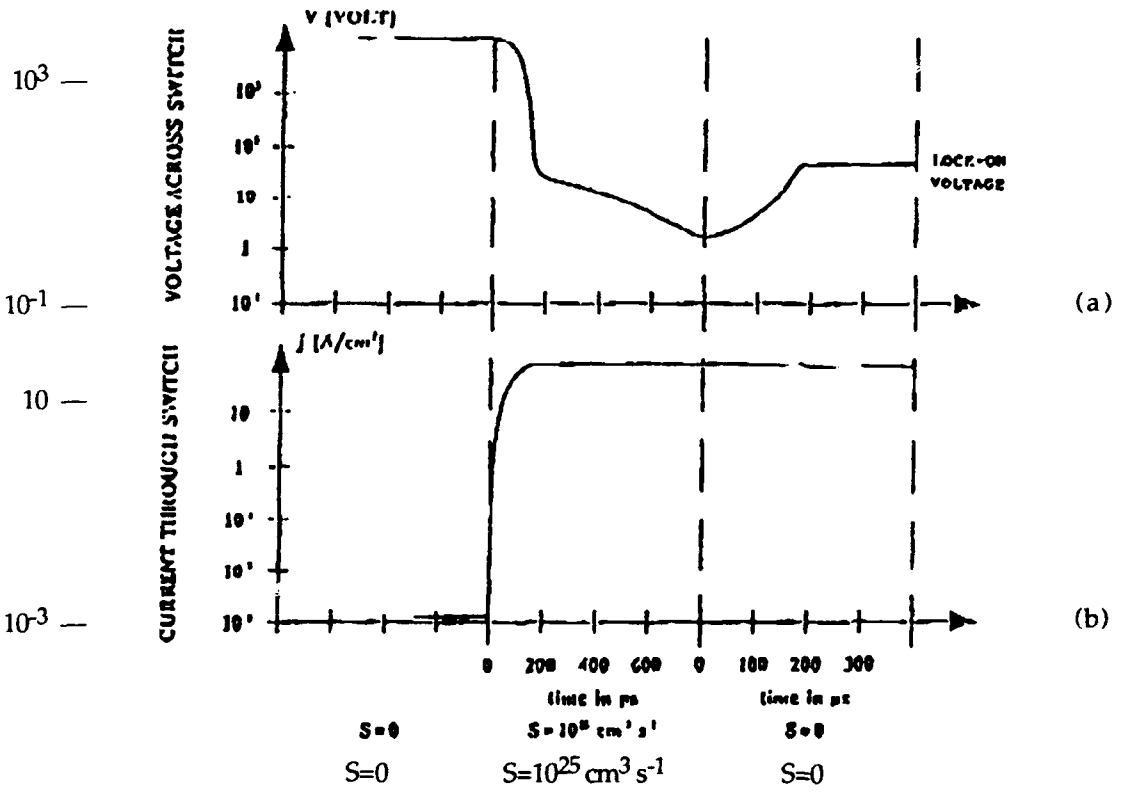

Figure 7.2.4: Calculated temporal development of switch voltage (a) and current density (b) in a 0.5 mm GaAs switch during (time scale 200: ps div^{-1}) and after (time scale 100: μs div^{-1}) electron beam radiation. The forward voltage during the first 100 μs is far below the lock-on voltage. It reaches the lock-on voltage level after about 200 μs.

Although this switch concept, as the first one, is not yet tested at high power levels, it should be scalable because it does not rely on nonlinear effects, such as the lock-on effect, for the conduction phase. The novel idea in both type of switches is the use of electron-beams with their inherent high efficiency and controllability, and in the triggered switch case, the utilization of "tailored" switch materials. In both cases it is not even necessary to generate the cathodoluminescence in the switch itself. It is possible to have the electron-beam controlled light source separated from the switch and to couple the light through fibers from source to switch [9]. This, although less efficient than having the light source integrated in the switch, might have advantages in switching parallel systems with low jitter.

References:

[1] Schoenbach, K., Lakdawala, V., Stoudt, D., Smith, T., and Brinkmann, R., "Electron-beam Controlled High Power Semiconductor Switches," IEEE Trans. El. Dev. 36, 1793 (1989).

[2] Brinkmann, R. P., "Modeling of Electron-Beam Controlled Semiconductor Switches," J. Appl. Phys. 68 (1990) 318.

[3] Brinkmann, R., Stoudt, D., Schoenback, K., Lakdawala, V., and Gerdin, G., "The Lock-On Effect In Electron-BEam Controlled GaAs-Switches," Proc. 19th Mod. Symp., IEEE 90-CH2839-9 (1990) 334-338.

[3a] Stoudt, D. C., et al., "The Recovery Behavior of Semi-Insulating GaAs in Electron Beam Controlled Switches," IEEE Trans. El. Dev., 37 (1990) 2478-2486.

[4] Schoenbach, K., Lakdawala, V., Germer, R., and Ko, S., "An Optically Controlled Closing and Opening Semiconductor Switch," J. Appl. Phys. 63 (1988) 2460-2463.

[5] Mazzola, M., Schoenbach, K., Lakdawala, V., Germer, R., Loubriel, M., and Zutavern, F., "GaAs Photoconductive Closing Switches with High Dark Resistance and Microsecond Conductivity Decay," Appl. Phys. Lett. 54 (1989) 742.

[6] Mazzola, M., Schoenbach, K., Lakdawala, V., and Ko, S., "Nanosecond Optical Quenching of Photoconductivity in a Bulk GaAs Switch," Appl. Phys. Lett. 55 (1989) 2102.

[7] Roush, R., Mazzola, M., Schoenbach, K., and Lakdawala, V., "Optical Quenching of Lock-On Currents in GaAs:Si:Cu Switches," Proc. 19th Mod. Symp., IEEE 90-CH2839-9 (1990) 334-338; also: M. S. Mazzola, et. al., "Infrared Quenching of Conductivity at High Electric Fields in a Bulk, Copper-Compensated, Optically Activated GaAs Switch," IEEE Trans. El. Dev., 37 (1990) 2499, 2506.

[8] Brinkmann, R., Schoenbach, K., Roush, R., Stoudt, D., Lakdawala, V., and Gerdin, G., "High Power Switching with Electron-Beam Controlled Semiconductors," Proceedings of the OPTCON '90, Boston, November 1990.

[9] Gerdin, G., Schoenbach, K., Lakdawala, V., Smith, T., and Brinkmann, R., "A Band Edge Radiation Generator for Pulsed Power," Proceedings 7th IEEE Pulsed Power Conference, Monterey, CA (1989) 857.

[10] Di Capua, M., "The Institute of High Current Electronics in Tomsk, U.S.S.R.," European Science Notes Information Bulletin, ESNIB 90-08 (1990) 16-24.

8 Magnetically Delayed Vacuum Switching[8] Working Group Report (R. Dougal and M. Newton)

The discussions on the Magnetically Delayed Vacuum Switch (MDVS) working group centered upon five topics: voltage hold-off, peak current handling, jitter, high power operation, and lifetime. This section examines these topics in some detail.

8.1 Voltage Hold Off

8.1.1 The Vacuum Gap. - Vacuum gaps that hold 150 kV/cm DC are the present state-of-the-art. Somewhat higher voltages may be possible through pulse charging. Stresses can reach 150 kV cm^{-1} with good bakeout and cleaning techniques.

Difficulties arose with insulator breakdown, triggering and cooling of the electrodes in conceiving multigap configurations.

8.1.2 The Magnetic Core. - The design of the saturable inductor is more subtle because the time integral of the voltage on the core (flux) must be equal to the flux swing of the core (change of B times the area). The core must not saturate during the time the plasma crosses the vacuum gap (switch gap divided by a characteristic plasma velocity). The vacuum gap is the ratio of the applied voltage divided by the allowable electric field. Therefore the switch requires a core area proportional to the square of the applied voltage and inversely proportional to the plasma closure velocity, the allowable electric field and the flux swing of the core.

The maximum inductance allowed at saturation yields the mean core diameter which in turn yields the volume of the core. The saturated inductance places a limit on the maximum cross-section of the core. Table 8.1 summarizes the magnetic core scaling parameters.

Table 8.2 displays the core requirements of the switch considering three options:

Option 1	1 gap	25 mm, single	1300 ns delay
Option 2	6 gaps	4 mm each	210 ns delay
Option 3	6 gaps	4 mm each	100 ns delay

[8] This section relies upon a record of the discussions by Mark Newton, LLNL

Magnetic Core Scaling

Saturation Time	=	$\frac{V}{N\bar{v}E}$
Core Area	=	$\frac{V^2}{N\bar{v}E\Delta B}$
Mean Diameter	=	$\frac{V^2}{N\bar{v}E\Delta B}\ \frac{\mu_s}{\pi L}$
Core Volume	=	$\frac{V^4}{(N\bar{v}E\ \Delta B)^2}\ \frac{\mu_s}{L}$
Leakage Current	=	$\frac{V^2}{N\bar{v}E}\ \frac{H}{\Delta B}\ \frac{\mu_s}{L}$

V = Switch Voltage
N = # of Sections
$\bar{v}$ = Plasma Velocity
E = Gap Electric Field
ΔB = Core Flux Swing
μ_s = Saturated Permeability
L = Switch Inductance

Table 8.1: Scaling of core parameters

Option 3 illustrates the benefits of a plasma closure velocity that is twice as high as the closure velocity of option 2. In option 3, the core volume drops by a factor of 4 (a factor of 2 in the area and a factor of 2 in the mean diameter), and the leakage current also drops by a factor of 2.

Magnetic Core Requirements

Switch Stages	Saturation Time	Ferrite ΔB=0.65T, H=500A/m		Metglas <ΔB>=2T, H=2kA/m @ 1μs
1	1.3 μs	Volume (m^3)	6.1	0.64
		Diameter (m)	3.7	1.2
		Leakage (kA)	1.8	2.4
6	210 ns	Volume (m^3)	0.17	0.018
		Diameter (m)	0.62	0.2
		Leakage (kA)	0.3	0.5-1.0
6	100 ns	Volume (m^3)	0.04	
		Diameter (m)	0.3	
		Leakage (kA)	0.15	
Assuming	V = 250 kV	$\mu_s = \mu_o$		
	$\overline{V}$ = 2 cm/μs	L = 52 nH		[Total allowed for 11.4 Ω
	E = 100 kV/cm	Z = 5.7 Ω		Blumlein, 20 ns rise]

Table 8.2: Magnetic core requirements

8.2 Peak Current

Present switch designs carry 3 to 4 kA for about 300 ns. A straightforward way to increase the current carrying capability of the switch is to increase the number of trigger sites. By linear extrapolation, a 45 kA design would require, to first order, 15 trigger sites. This 3 to 4 kA current is at present a limit of the driver circuits available at the University of South Carolina. Currents in excess of 4 kA per site may be possible.

8.3 Jitter Control

The measured jitter of present switches [unpublished] is ± 4 ns. The source of the jitter in present switches appears to be a combination of:

- Erratic initial conditions of the core arising from a lack of external resets for the core
- Lack of external voltage regulation.

According to the discussion group, a switch configuration that incorporates reset and voltage regulation could achieve ± 1 ns jitter.

8.4 High Power Operation

The discussion group identified some possible high average power operation problems:

- Triggering at continuous repetition
- Electrode heating
- Pressure build-up due to impurity outgassing

Present switches drop less than 200 V in the forward direction. This is the resolution limit of present instrumentation.

8.5 Lifetime

The group discussed the design of a vacuum gap with a long lifetime. The group considers the composition of the conducting plasma in the gap critical to lifetime and to reproducible operation. Measurements will have to establish whether conduction takes place in residual/impurity gas plasma or metal vapor plasma (trigger or vacuum gap electrode).

With residual gas plasma conduction, a gradual change of operating characteristics throughout a burst of pulses could result from changes in gas composition during operation. Preliminary data indicates that switch characteristics are constant during the burst.

Conduction by metal vapor plasmas may not change the properties of the switch during the burst but may result in:

- Changes of electrode topography over many bursts of pulses. These changes may limit the peak voltage in the vacuum gap requiring larger gaps for longer lifetimes. Larger gaps, however, require larger magnetic core areas to handle the same voltage as discussed above.
- Deposition of electrode material on the vacuum envelope and on the trigger insulator. Vapor shields may reduce deposition on the envelope.
- Electrode material deposition on the trigger insulator. As long as the insulator properties are unchanged this material may be a beneficial source of conducting plasma in the gap.

In addition, the lifetime of the switch depends upon the trigger insulator material:

- Present material is $BaTiO_3$
- Macor insulators provide unreliable triggering

- On the basis of experience with insulator materials, M. Kristiansen suggested silicon carbide reinforced alumina
- Silicon nitride is unacceptable because it becomes conducting after 1 shot.

8.6 Present Capabilities and Future Requirements

Table 8.3 presents a comparison of the present capabilities of MDVS and the requirements for future linac switches. The table provides a brief outline of how to meet these requirements. Figure 8.1 displays possible switch configurations considered by the group.

	Present	Avenues	Requirements
Operating Volt.	40 kV	See options below*	250 kV
Switch Current	3 kA	Multiple trigger sites (15)	45 kA
Pulse Width	300 ns	Presently achievable	100 ns
Jitter	± 4 ns	Improve regulation & reset	± 1 ns
Repetition rate	10 kHz		300 - 1 kHz
Losses	5 J/pulse		30% (total system)
Lifetime	10^7	Limits: trigger and electrodes	10^9
Risetime	40-50 ns	Limited by L_{sat} & Z_{drive}	20 ns

*Options: 6 series gaps - 3 mm gaps @ 40 kV/gap - 100 ns Mag delay
1 gap - 25 mm gap @ 250 kV/gap - 800 ns Mag delay
or increase plasma velocity

Table 8.3: Avenues leading from present capabilities to requirements for MDVS

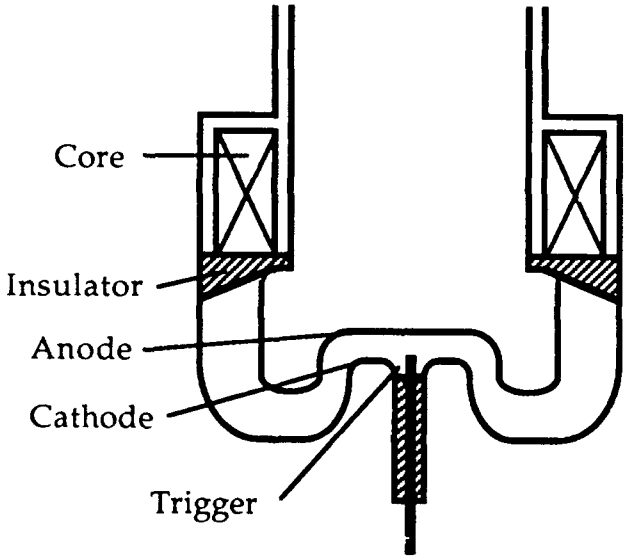

V_{oc} ~ 40 kV
gap = 3-4 mm
τ mag = 100 ns
L_{sat} = 600 nH
I_{Leak} = 20 A

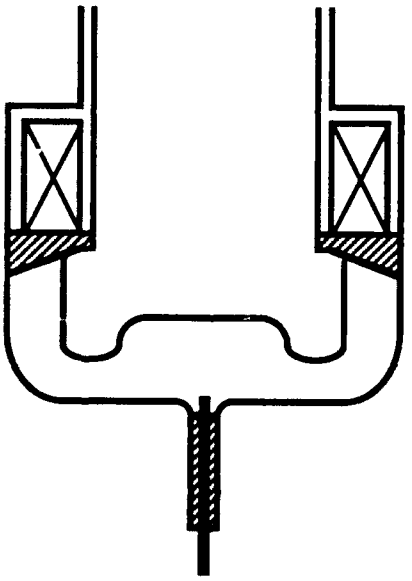

V_{oc} = 250 kV
gap = 25 mm
τ mag = 800 ns
L_{sat} < 60 nH
I_{Leak} < 500 A

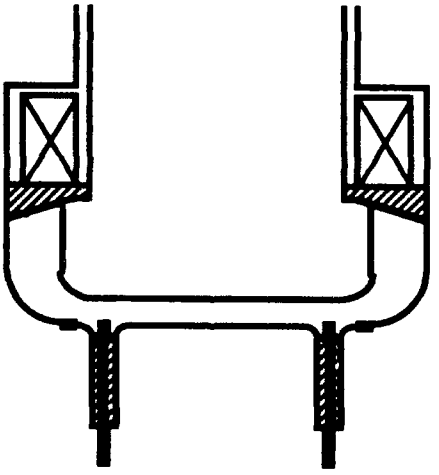

V_{oc} ~ 250 kV
gap ~ 25 mm
Multiple sites

Figure 8.1: Switch and Core Configurations

8.7 Research Directions

The research direction to meet the requirements are:

- Increase the plasma velocity. Group discussions suggested deliberate plasma acceleration may increase the velocity between factors of 3 and 10 (6 to 20 cm μs^{-1}).
- Create a number of conduction sites through multiple trigger sites
- Control jitter through input voltage control and core reset techniques.

8.8 Specific Research Requirements

- Triggering plasma injection
  - Increase plasma injection velocity
  - Improve trigger life
  - Investigate trigger insulator materials

- Conducting plasma
  - Verify composition through spectroscopy during burst operation

- Electrodes
  - Evaluate contribution of electrode material to switch operation
  - Investigate performance of low vapor pressure metal cathodes in burst operation
  - Investigate refractory (metal or graphite) anodes that vaporize with difficulty
  - Develop geometries that reduce erosion and vapor deposition on envelope
  - Establish conditioning effects
  - Measure erosion rates

- Magnetic cores
  - Establish optimum magnetic core material (ferrite vs. Metglas)
  - Ferrites for < 100 ns
  - Metglas for > 100 ns

9 Super Emissive Cathode Switch Working Group Report

The discussions of the super-emissive cathode switch working group revolved around:

- Progress on SEC switches
- The complementarity of technology between SEC switches and thyratrons
- The R&D path that will lead to a prototype switch.

9.1 SEC Progress and Technology Complementarity with Thyratrons

Special factors have accelerated SEC switch progress such that the technology has now reached the development stage. These factors, among others, are:

- Over a decade of independent research and development efforts in several countries
- Continuity of modest funding
- A balanced contribution of fundamental and applied research
- A development stimulus by user requirements
- Availability of thyratron switch technology that transfers, to some extent, to SEC devices.

Therefore, there was agreement within the working group that:

- A modest investment (2 or 3 million dollars total) and 2 or 3 years of R&D would provide a definite answer whether an SEC switch can meet the requirements outlined in Section 3
- A sufficiently broad based expertise exists to fabricate devices during the development program
- Mass production techniques apply to SEC construction
- The switch geometry allows low impedance/low inductance feeds to meet the risetime requirements.

9.2 SEC Switch Development Plan

The working group considered an SEC development plan that would lead to a 250 kV switch through an intermediate 125 kV design as a short term (1 year goal). The 1 year development program would follow the plan of Table 9.1 This program would attempt to:

- Demonstrate high current in a single gap at 25 kV
- Demonstrate higher voltage (50 kV) in a single gap

- Demonstrate 80 kV voltage hold-off in two gaps (80 kV)
- Reach 125 kV with two gaps.

The 125 kV design would be the basis for the 250 kV development program. This program would investigate

- A three-gap (80 kV per gap) design
- A series connection of single gap switches,

followed by a sequence of switches that would lead from 250 kV designs at a low repetition rate to 250 kV designs at a high repetition rate.

Switch	Month	Gap	I (kA)	V (kV)	Pulse Length (ns)	Jitter (+/- ns)	Frequency (kHz)	Risetime (ns)
1	2	1	10	25	100	3	0.3	45
2	4	1	10	25	100	1	1.0	40
3	6	1	20	50	100	1	<1.0	40
4	8	2	20	80	100	3	0.5	45
5	9	1	20	50	100	1	>1.0	<40
6	11	2	20	>100	100	1	<1.0	<45

Table 9.1 A one-year development program leading to a 125 kV switch.

Other discussions of the working group revolved around:

- The allowable inductance to meet the current risetime goals
- The gap configuration to meet the voltage requirements.

There was substantial concern in the working group about the compatibility of the 250 kV peak voltage and the 25 nH inductance constraints. A consensus developed that meeting these two constraints simultaneously poses a major challenge in the design of the switch housing and the electrode-discharge configuration.

10 Solid State Switch Working Group Report

10.1 Switching System Design Using Available Technology

Switch parameters - One of the first tasks undertaken by the PCSS working group was to determine the viability of a switching system designed on the basis of available performance parameters. Table 10.1 is a spreadsheet the working group used to define four alternate designs. Column 1 is a design for silicon devices. Column 2 is for GaAs devices with the contacts deposited on the face of the switch (lateral), optical triggering by a diode laser array, and lock-on operation. Column 3 is for GaAs devices with contacts deposited on the ends of the switch (longitudinal), optical triggering by Nd:YAG laser, and lock-on operation. Column 4 is a design based on the geometry presented in Section 6.2, controlled by an e-beam, and not dependent on lock-on.

Meanings of the spread sheet parameters - The spreadsheet parameters are self explanatory. V_{out}, Current, Pulse length, and PRF are load parameters. V_{sw} is the open-state voltage seen by the switch to account for losses. E is the average open-state field on the switch. J_l is the current per unit length on a thin current channel (short wavelength illumination) device. J_a is the current per unit area for a thick (long wavelength illumination) device. V_{on} and E_{on} are the closed-state voltage across the switch and electric field respectively. Driver parameters are for the control device (laser or e-beam source).

Design Conclusions - Several conclusions were drawn from the design exercise.

- The switching parameter space of interest is achievable with PCSS
- Prepulse and jitter will be less than for any other system
- The flexible geometry and scalability are an advantage when designing a system architecture
- The actual switches are cheap compared to other devices operating at this voltage
- When higher repetition rate lasers become available, the system should be capable of higher rep-rate operation with minimal modifications
- Device life is still largely unknown and likely to be a problem requiring further research, especially in lock-on
- Efficiency needs improvement
- The trigger and other auxiliary equipment could be expensive.

Material	Si	GaAs	GaAs	GaAs
Driver	YAG laser	Diode laser	Nd:YAG laser	e-beam
Mode	Linear	Lock-on	Lock-on	Linear
Switch Geometry		Lateral	Longitudinal	Longitudinal
V_{out} (kV)	250	250	250	250
Current (kA)	40	40	40	40
Pulse length (ns)	200	200	200	200
PRF (Hz)	1000	1000	1000	1000
V_{SW} (kV)	260	290	260	250
E (kV/cm)	50	30	100	100
J_l (kA/cm)	1	0.5	NA	NA
J_a (kA/cm^2)	NA	NA	4	0.5
E_{on} (kV/cm)	2.5	4	4	1.5
R_{on} (Ω)	0.3	N/A	N/A	N/A
E_{cont} (mJ)	300	6	0.6	3000
Height (cm)	5	10	3	2.5
Width (cm)	40	80	60	9
Thick (cm)	0.1	0.1	3	9
V_{on} (kV)	12.5	40	12	3.75
$E/_{pulse}$ (kJ)	2.1	2.3	2.1	2.0
P_{av} (MW)	2.1	2.3	2.1	2.0
$P_{av/diss}$ (MW)	0.11	0.31	0.08	0.03
P_{rem} (kW/cm^2)	0.5	0.4	0.5	0.4
Wavelength (μm)	0.532	0.532	1.06	-
Driver eff	0.01	0.01	0.01	0.15
Switch eff	0.91	0.74	0.91	0.97
P for driver (kW)	30	0.6	0.06	20
Life (shots)		Unknown		
Cost/unit				
Driver (k$)	1000	100	60	50
Switches (k$)	20	40	20	40
TOTAL (k$)	1020	140	80	90

NA - Not Applicable
N/A - Not Available

Table 10.1: Alternate designs for solid state switches that would meet requirements using present technology

10.2 Research Directions in PCSS

This section outlines research directions discussed at the workshop. It became clear early in the discussions that PCSS is still in the research stage. Funding will be required to develop the approach into an inexpensive alternative for accelerator applications. Several areas of research were identified.

10.2.1 Device Life

Device life is probably the most important issue regarding PCSS. To increase efficiency and optimize system size, the open-state field across the switch should be as high as possible. High-field, high-power operation degrades device life dramatically. Several avenues were discussed in regard to device life research. A discussion follows.

Lack of data is a definite handicap for accurate predictions of device life. Most of the on-going research has been directed at exploring the performance limits of devices with little regard for device life time. Careful gathering of life data is an essential first step to develop extended-life devices.

Filamentation, the formation of constricted conduction channels in GaAs, was presented as a potential life-limiting mechanism, especially in lock-on operation. There is indirect evidence both for and against filamentation. It was generally agreed that filamentation could be an important issue and should be resolved. The most definitive filamentation test would be time-and-space resolved current density measurements on an operating device. Post-mortem analysis, though less accurate, was also thought to be important in searching for tracks and changes in the material properties.

Material migration of defects in the semiconductor crystal and contact migration into the GaAs may affect device life. Post-mortem studies should be performed to detect material migration.

Several other **contact issues** were discussed as possible life limiting mechanisms in PCSS. GaAs is mildly piezoelectric. It is possible that shock waves generated in the material may be detrimental to contact life; post-mortem analysis will help establish whether contact shock damage exists.

Field shaping at the contacts is important to open-state voltage holdoff and could be important to prevent formation of filaments and other inhomogeneities in current distribution. Field shaping through design of the contact geometry will increase power density attainable with PCSS.

A **lattice matching** layer between the GaAs and the contacts may improve device life.

Other **contact materials** may yield less migration, better lattice match and better shock properties. This research is already being pursued at a low level.

Research on **alternate materials** (see Table 7.1.2) should be continued to improve understanding of the conduction mechanism in semiconductors and to search for a material that will switch higher energy densities with longer life.

Doping the PCSS material will change the band structure and may impact switching behavior and device life significantly.

Quality assurance is an area for vast potential improvement. Removing random factors through quality control of switch materials will ease research into PCSS significantly. At present, production and quality control of GaAs lags that of Si by 10-15 years.

10.2.2 Diagnostics

Diagnostic research of device materials and device operation can significantly increase the understanding of PCSS.

Material diagnostics to measure trap parameters (density, kind, etc.) is needed to provide models with appropriate initial and boundary conditions and compare new devices with used and failed devices. Trap and contact migration are thought to be potential mechanisms of device failure. Appropriate material diagnostics will help determine the validity of the theories by measuring the trap and metal densities. To be conclusive, these diagnostics will be required both before and after switching.

Direct diagnostics to measure current and voltage simultaneously with such parameters as optical absorption, electric field, recombination radiation, and temperature - all spatially resolved - will allow detection and study of such phenomena as filaments, avalanche, lock-on, etc. These measurements are far more difficult than the electrical measurements performed to date.

10.2.3 Modeling

Modeling of device physics based on first principles and semi-empirical formulations is necessary to understand the mechanism of lock-on switch operation. Modeling and experiment must be cultivated in parallel to provide understanding of switch behavior.

10.2.4 Efficiency and cost

Switching efficiency and cost are of concern in any system. The low efficiency and high cost of available lasers limit **linear switching** to applications where high cost and low efficiency are acceptable. **Lock-on operation** results in device gain which can be used to increase the overall switching system efficiency. Further research on device life is required to make lock-on operation viable. **Higher efficiency drivers**, high efficiency lasers or electron beams, for example, will also increase system efficiency. A combination of high-efficiency driver and lock-on should bring PCSS switching systems to an acceptable overall efficiency.

11 High-Repetition Rate Hydrogen Spark Gaps[9]

11.1 Introduction

To develop a compact, high power, high repetition rate switch, efforts have concentrated on spark gaps because of their ability to withstand high voltages and conduct high currents in single pulse applications. The Naval Surface Warfare Center (NAVSWC) is studying the voltage recovery of unblown pressurized spark gaps.

The NAVSWC work has focused on improving the repetition rates of spark gaps without resorting to gas flows at high rates. The research has focused on H_2 as the switching medium. A low molecular weight endows H_2 with a high molecular speed and high thermal diffusivity. These two properties are advantageous for repetitive switching applications in spark gaps because they allow for a recovery time (~ 1 ms) that is an order of magnitude shorter than for other gases (10 ms for air, N_2, 0_2, Ar, SF_6). A high pressure (up to 7 MPa) H_2 fill also allows a shorter gap that reduces resistance, inductance and enhances thermal contact between the gas and the electrodes. At the same time, the high pressure increases the thermal capacity of the gas, increases turbulence which is beneficial for heat transfer and reduces the statistical time lag for breakdown.

Recovery of the switch can be improved by operating the switch well below self-break, i.e. operating the switch at a voltage that is significantly less than the DC breakdown voltage when the switch is at ambient temperature. This allows the switch to hold voltage even before the gas and the electrodes have had a chance to cool down. Test have shown that undervolting the gap by 50% can reduce the recovery time by an order of magnitude.

11.2 The NAVSWC High Pressure Hydrogen Spark Gap

A section of the NAVSWC spark gap appears in Figure 11.1. For scaling purposes, the diameter of the stainless steel housing is 20 cm. The housing can withstand pressures of 7 Mpa (1000 psi). The insulators are MACOR ceramic, the electrodes and trigger pin are Elkonite copper tungsten. Silicon rubber O-rings seal the assembly. Trigger-gap and main-gap spacings are typically 3 mm. A Maxwell 100 kV generator (Model 40295) triggers the switch through isolation capacitors.

---

[9] S. Moran of Naval Surface Warfare Center (NAVSWC) contributed this section. Work supported by Naval Warfare Systems Command, PMW-145.

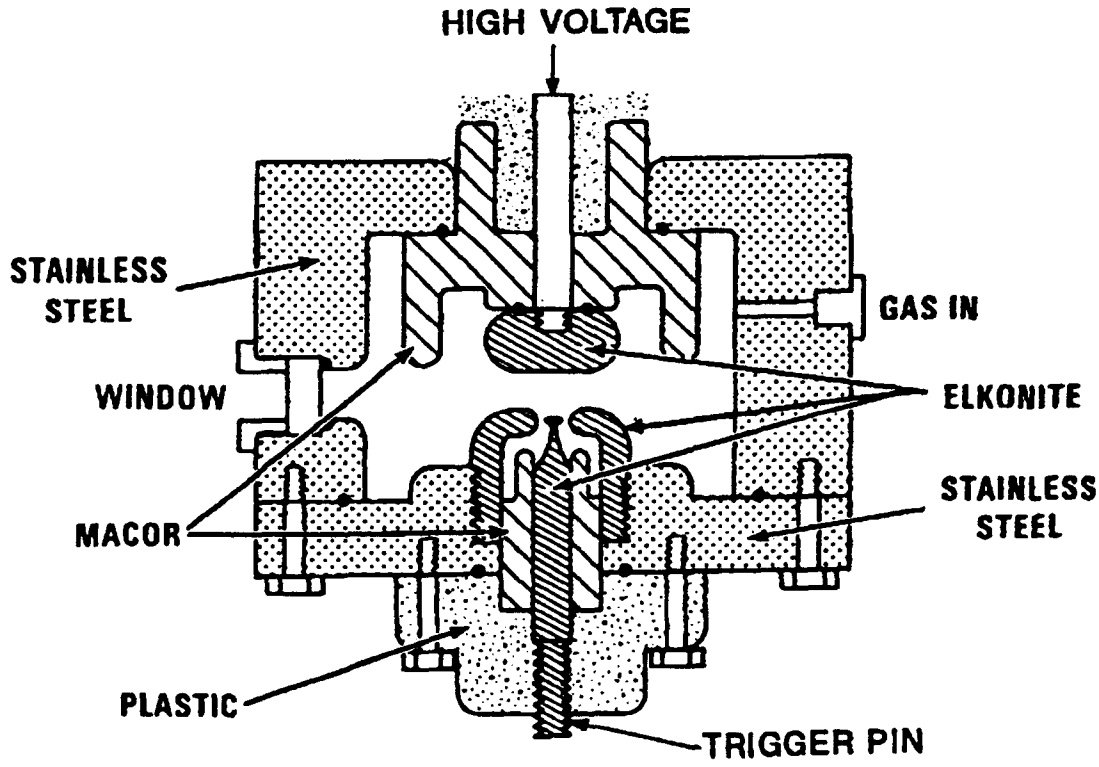

Figure 11.1. The NAVSWC High Pressure Hydrogen Switch

11.3 A Development Chronology

In 1987 tests demonstrated switching of 200 A at 120 kV (5 J) with fast rising pulses.

In 1988 recovery was demonstrated at 60 kV, 35 kA and 200 J with < 1 Ω impedance, a 200 ns water dielectric pulse forming line as a source and a resistive load. In these tests the voltage was reapplied, as a resonant charge waveform, during the recovery period. In some tests at 7 MPa, the gap self-fired near the peak of the second resonance charge and fully recovered suggesting that multiple pulsing would be possible with a repetitive trigger.

In 1989 two hydrogen switches that connect two 10 μF capacitors (12.5 kJ @ 50 kV) to a common resistive 0.1 Ω load demonstrated 100 μs recovery time. Separate single shot triggers fired each switch. The resistive load damped the oscillations after one cycle providing a 10 μs, 170 kA current pulse. These experiments demonstrated that the recovery of an undervolted high pressure H_2 switch is a surprisingly weak function of the energy discharged through the switch. Jitter, while not measured, was below 100 ns. This system also operated single shot without a resistive load with a 260 kA, 80 μs oscillating pulse.

Work began in 1990 on a system to deliver five high-voltage pulses through H_2 switches. A schematic of the circuit appears in Figure 11.2 Five primary 0.7 μF capacitors charge to 50 kV through high voltage relays. Each primary capacitor connects to one terminal of a H_2 switch. The other terminals connect to a common node that is the primary of a 1:12 step-up transformer. Therefore, the system will function only if the last triggered H_2 switch recovers before the next one fires. This system has demonstrated 200 ns recovery times with highly damped (4 μs period, ~3 μs exponential decay) pulses that reach a 40 kA peak with switch pressures of 1.2 MPa (Moran, 1990a; also 1990b).

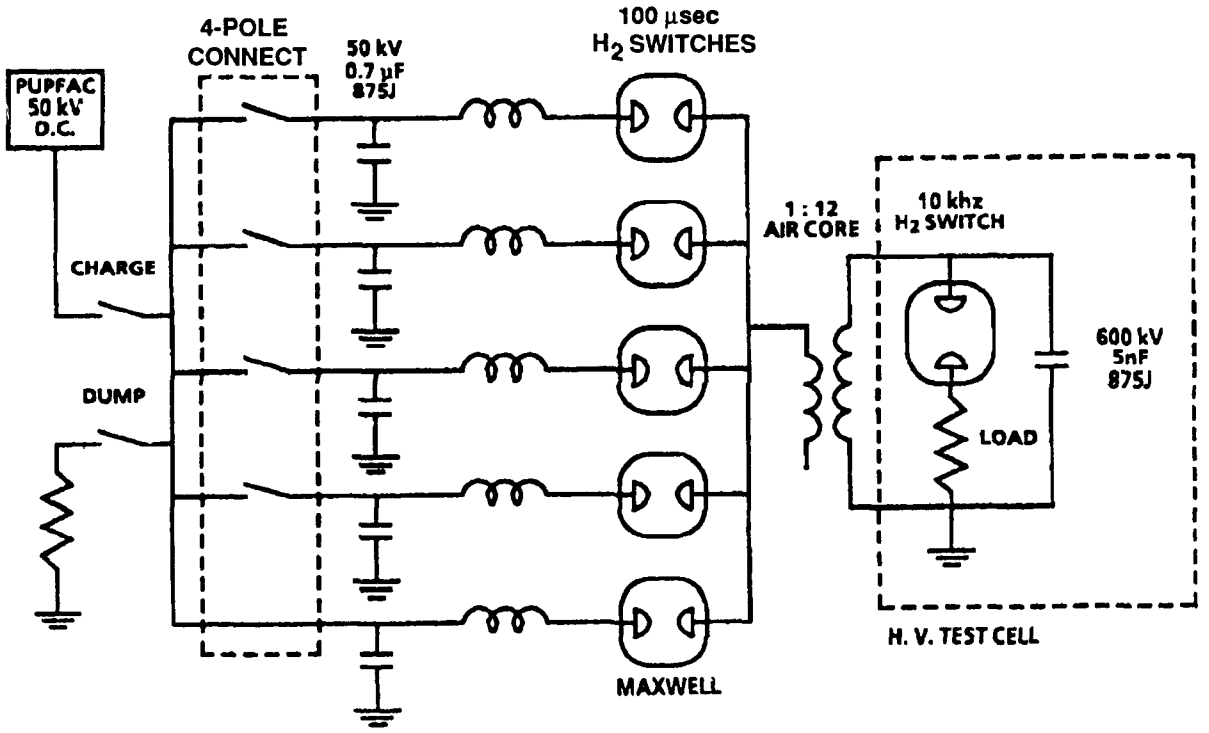

Figure 11.2: The 5 Pulse Test Circuit

The output of the transformer will resonantly charge a water dielectric capacitor to 600 kV in 10 μs. This capacitor will discharge into a resistive load through a hydrogen switch designed to hold 500 kV and conduct peak currents of 50 kA. A sketch of this switch appears in Figure 11.3. Testing of this switch, to begin in 1991, will reveal whether it is possible to operate a high pressure hydrogen switch that holds 500 kV, for short bursts at 10 kHz repetition rates.

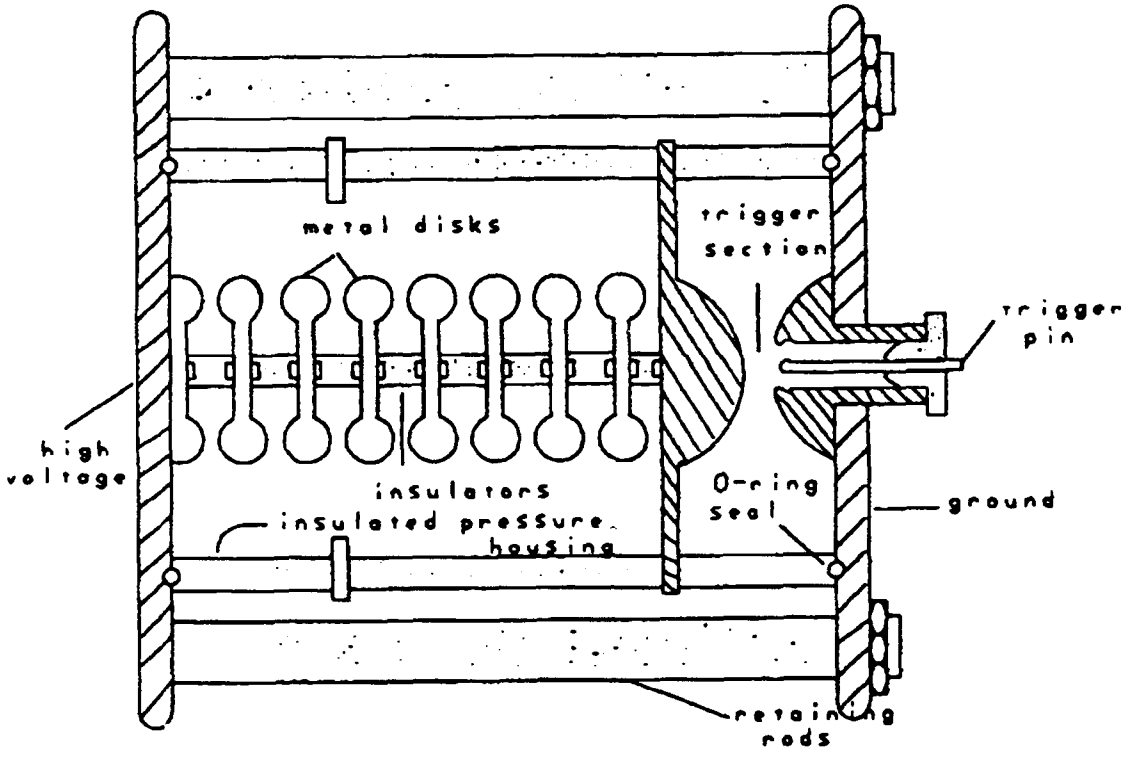

Figure 11.3: A Sketch of the 600 kV High Pressure Hydrogen Switch

References:

Moran, S. L., "Hydrogen Spark Gap for Rep-Rated Compact Accelerators," Proceedings of the Joint Services Charged Particle Beam Review Conference, San Diego, (1990a).

Moran, S. L., "High Repetition Rate Hydrogen Gap," Proc. 19th Mod. Symp., IEEE 90-CH2839-9 (1990b) 227-231; also: Special Issue: IEEE Transactions on Electron Devices (Modulator Symposium, in preparation).

Appendix 1

Working Groups:		
	SEC	Super Emissive Cathode Switches
	MDVS	Magnetically Delayed Vacuum Switches
	PCSS	Sold State Switches

MDVS Edmond Chu
Maxwell Laboratories, Inc.
8888 Balboa Avenue
San Diego, CA 92123

MDVS Roger Dougal
Department of Electrical & Computer Engineering
University of South Carolina
Columbia, SC 29208

PCSS Andris Faltens
Lawrence Berkeley Laboratory
MS-47-112
One Cyclotron Road
Berkeley, CA 94720

SEC Martin Gundersen
MG, SSC 420, MC 0484
Univ. of Southern California
Los Angeles, CA 90089-0484

SEC George Kirkman-Amemiya
Integrated Applied Physics
140 E. Santa Clara St., Suite 19
Arcadia, CA 91006

MDVS Magne Kristiansen
Texas Tech University
Department of EE
P.O. Box 4439
Lubbock, TX 79409

SEC Lawrence Luessen
Naval Surface Warfare Center
Code F-45
Dahlgren, VA 22448-5000

SEC Stuart Moran
Naval Surface Warfare Center
Code F12
Dahlgren, VA 22448

MDVS Eugene Nolting
White Oak Lab., Naval Surf.
Weapons Center, R401
10901 New Hampshire Ave.
Silver Spring, MD 20910

SEC William Nunnally
UTA Center of Energy, Conversion Research
P. O. Box 19380
Arlington, TX 76019

SEC Hans Riege
CERN, PS Division
CH1211 Geneve 23
Geneva, Switzerland

MDVS Leland Schlitt
2725 Briarwood Drive
Livermore, CA 94550

PCSS Karl Schoenbach
Old Dominion University
Dept. of Electrical Engineering
Norfolk, VA 23508

PCSS Ian Smith
Pulse Sciences, Inc.
600 McCormick Street
San Leandro, CA 94577

SEC Francisco Villa
Stanford Linear Accelerator Center
2575 Sandhill Rd.
Central Lab, Rm.262
Menlo Park, CA 94026

PCSS Fred Zutavern
Sandia National Laboratory
Division 1248
Albuquerque, NM 87185

Lawrence Livermore National Laboratory attendees:

	Don G. Ball, L-574
SEC	James Bardsley, L-296
	Edward Cook, L-574
SEC	Marco Di Capua, L-153
SEC	Gary R. Dreifuerst, L-574
PCSS	Robert Druce, L-153
	Victor George, L-465
PCSS	Wayne Hofer, L-153
	Thomas Innes, L-153
MDVS	Ronald Kihara, L-153
	Hugh C. Kirbie, L-627
SEC	Douglas Larson, L-492
	Donald J. Meeker, L-469
MDVS	Bernard T. Merritt, L-574
MDVS	Mark A. Newton, L-627
MDVS	Thaddeus J. Orzechowski, L-626
MDVS	Philip L. Pincosy, L-035
PCSS	Michael Pocha, L-156
SEC	Louis L. Reginato, L-627
MDVS	George E. Vogtlin, L-153
SEC	Bruce Warner, L-574
PCSS	Jick Yee, L-156

Pulsed Power Issues and Accomplishments

An Open Discussion at the 1991 ONR/SDIO Pulsed Power Meeting

Arthur H. Guenther, Chair

Pulsed power is a critical technology for the United States and a design limiting or enabling technology for SDIO in particular. Efficient, reliable operation and expanded applications of high voltage, high current modulators and generators are constrained by existing technology. Pulsed power, identified as a critical technology by the Department of Defense, is also a *dual-use* technology. Pulsed power systems include pulsed lasers, accelerators for high energy physics, directed energy weapons and microwave sources for defense. Pulsed power can be employed in other applications such as food processing, medicine and materials science–all requiring efficient, reliable, reproducible long life sources. Weight, size and other engineering characteristics are also current R&D issues–particularly for any space-based application.

The open discussion identified accomplishments within the SDIO/ONR program and key issues for future research.

Pulsed power source components include capacitors, switches, inductors, insulators, and related control systems. The principal limiting element for most applications are the switch issues and include, for example, short life or inadequate timing characteristics. As a result of this and limited budgets, switch development is the main focus of activity within the program. Program goals include improvement of switch performance characteristics such as life, jitter, peak current, stand-off voltage, and coulombs passed. Emphasis is given according to the specifics of an application.

Two principal achievements were identified by the majority of the participants. Super-emissive cathode (SEC) switch technology, as represented by the pseudospark and back-lighted thyratron (BLT), was identified as closest to implementation with regard to SDIO goals. This notable technological achievement is undergoing commercialization at the present time.

In addition, optically controlled solid state switches (OCSS) were identified as having many potentially significant advantages. The OCSS promises modular design flexibility, size and weight reduction, manufacturability (reliability, uniformity and volume capacity) together with superb on/off timing capabilities. Other adjunct OCSS areas included new materials (III-V and II-VI semiconductors, high temperature superconductors).

SEC switch R&D support by the SDIO includes experimental activities, modeling support, transition support to operational systems, and commercialization through the SBIR program. As a direct result of SDIO support the SEC BLT switch has demonstrated both size and weight reduction with improved pulsed power switching performance characteristics. Essential SEC research at this stage includes development of a collaborative life-testing program.

OCSS support has resulted in identification of certain physical processes that are distinct from low power semiconductor devices, and has resulted in the development of novel models for high current transport, together with required advanced diagnostic techniques. Research is addressing materials limitations. One recommendation is the involvement of the solid state laser community in the research activity–in particular that of laser array diodes and diode pumped solid state active elements.

Panel members recommended in their overview presentation:

1) Enhanced dissemination of SDIO and other DoD goals and applications of this technology.

2) Review of status of adjunct capacitor, other component, and prime power activity and requirements.

3) Enhanced communication was identified as a critical need by all members. Communication is especially necessary during these changing times when new opportunities can be identified and funding is limited.

Areas identified for funding include:

Gaseous spark gaps, and dissemination and consideration of recent advances made in the understanding of spark gap erosion,

Superconducting switches,

Silicon hybrid switches, including insulated gate switches and MOS-controlled thyristors.

A number of applications were identified and discussed. For example, within the DoD, the Navy identifies low-flying, low radar-cross-section anti-ship missiles as a critical problem for pulsed power R&D. Pulsed power will impact the development of tactical weapons, directed energy weapons, electronic countermeasures and phased array electronically steerable radars–all significant areas. SDIO requirements include 1kJ at 1kHz of HPM energy at 1-4 GHz, and the development of pulsed power for EML terminal and theater missile defense.

Non-defense applications include materials processing, cutting, food sterilization, waste treatment, pollution control, oil recovery and exploration, and electric space propulsion, sludge treatment, and medical accelerators.

Pulsed power activities are benefiting from both improved understanding in a physical and analytical sense as well as reduction to engineering practice and experience. Balance in this program is appropriate and the program appears well focussed and well managed involving the very best of participants. Their achievements need to be disseminated to a larger potential user community–particularly that relating to commercial opportunities.

PARTICIPANTS AT THE FOURTH SDIO/ONR PULSED POWER MEETING 1991

June 20-21, 1991

Dr. Norman Bardsley
Lawrence Livermore National Laboratory
7000 East Avenue, L-296
Livermore, CA 94550

Major Charles Beatty
HQ Defense Nuclear Agency
6801 Telegraph Road
Alexandria, VA 22310-3398

Dr. Edward E. Bowles
General Atomics
P.O. Box 85608
San Diego, CA 92186

Capt. Christopher G. Braun
ETDL - Attn: SLCET-ML
Ft. Monmouth, NJ 07703

Dr. Brian Ditchek
GTE Labs Inc.
40 Sylvan Road
Waltham, MA 02254

Dr. William Donaldson
Lab. for Laser Energetics
East River Road
Rochester, NY 14623-1229

Dr. Robert Druce
Pulsed Power Systems
Electronics Engineering
Lawerence Livermore National Lab.
Livermore, CA 94550

Dr. Klaus Frank
University of Erlangen
Tandemlabor
Erwin-Rommel-Str. 1
D-8520 Erlangen
W. Germany

Dr. David M. Giorgi
ECR Corporation
990 Highland Dr., #101
Solana Beach, CA 92075

Major Thomas E. Gist
WL/POOX-3
Wright Patterson AFB
Ohio 45433-6563

Dr. Arthur H. Guenther
Sandia National Labs.
Dept. 0450
Albuquerque, NM 87185-5800

Prof. M. Gundersen
Dept. of Electrical Engineering-Electrophysics
University of Southern California
Los Angeles, CA 90089-0484

Mr. Peyman Hadizad
Dept. of Electrical Engineering-Electrophysics
University of Southern California
Los Angeles, CA 90089-0484

Dr. Kevin Harris
Stanford Linear Accelerator Center
2575 Sand Hill Road
Menlo Park, CA 94025

Dr. Mark W. Heyse
Wright Laboratory
(WL/MNSH)
Eglin Air Force Base, FL 32542

Mr. Tseng-Yang Hsu
Dept. of Electrical Engineering-Electrophysics
University of Southern California
Los Angeles, CA 90089-0484

Mr. Jung H. Hur
Dept. of Electrical Engineering-Electrophysics
University of Southern California
Los Angeles, CA 90089-0484

Mr. Cal Johnson
Assistant Director
Space Power Institute
231 Leach Center
Auburn University
Auburn, AL 36849-5320

Dr. George Kirkman-Amemiya
Integrated Applied Physics
50 Thayer Road
Waltham, MA 02154

Dr. J. Kolawole
Science Applications Intl. Corp. (SAIC)
1247-B N. Elgin Parkway
Shalimar, FL 32579

Prof. Magne Kristiansen
Dept. of Electrical Engineering
Texas Tech University
P.O. Box 4439
Lubbock, TX 79409

Prof. Mark J. Kushner
Dept. of Electrical & Computer Engineering
University of Illinois
1406 W. Green Street
Urbana, IL 61801

Prof. Vishnu K. Lakdawala
Dept. of Electrical Engineering
Old Dominion University
Norfolk, VA 23508

Prof. Chi H. Lee
Dept. of Electrical Engineering
University of Maryland
College Park, MD 20742

Dr. Mark Levinson
GTE Labs., Inc.
40 Sylvan Road
Wlaltham, MA 02254

Mr. Rong Lin Liou
Dept. of Electrical Engineering-Electrophysics
University of Southern California
Los Angeles, CA 90089-0484

Mr. Lawrence H. Luessen
Naval Surface Warfare Center
Attn: Code F 45
Dahlgren, VA 22448-5000

Dr. Yitzhak Maron
Weizmann Institute of Science
Dept. of Physics
Rehovot 76100
Israel

Dr. Craig Maxwell
STD Resarch Corporation
P.O. Box C
Arcadia, CA 91066

Dr. Michael S. Mazzola
Naval Surface Weapons Center
Code F-45
Dahlgren, VA 22448-5000

Dr. Glen McDuff
99 Pinon Heights
Sandia Park, NM 87047

Dr. William Moeny
Tetra Corporation
3701 Hawkins St., NE
Albuquerque, NM 87109-4512

Dr. Tom Naff
Physics International Company
2700 Merced St.
San Leandro, CA 94577

Prof. William C. Nunnally
University of Texas-Arlington
Department of Electrical Engg.
Arlington, TX 76019

Dr. Bernie Penetrante
Lawrence Livermore Natl. Lab.
7000 E. Avenue, L-296
Livermore, CA 94550

Mr. N. Reinhardt
Integrated Applied Physics
50 Thayer Road
Waltham, MA 02154

Dr. Gabriel Roy
ONR - Code 1132P
800 N. Quincy Street
Arlington, VA 22217-5000

Lt. Col. P. Rustan
SDIO/T/IS
The Pentagon
Washington, DC 20301-7100

Prof. W. J. Sarjeant
Room 314A, Bonner Hall
SUNY Buffalo
4232 Ridge Lea Road
Amherst, NY 14226

Prof. Karl H. Schoenbach
Dept. of Electrical Engineering
Old Dominion University
Norfolk, VA 23508

Mr. Timothy J. Sommerer
Dept. of Electrical & Computer Engineering
University of Illinois
1406 W. Green Street
Champaign, IL 61801

Prof. Tangali S. Sudarshan
University of South Carolina
College of Engineering
Columbia, SC 29208

Dr. Edward Taconi, Jr.
Wright Laboratory
WL/MNSH
Eglin Air Force Base, FL 32542-5434

Mr. Larwence C. Walko
WL/POOX-3
Wright Patterson AFB
Ohio 45433-6563

Prof. Frazer Williams
Dept. of Electrical Engineering
University of Nebraska-Lincoln
Lincoln, NE 68588-0511

Mr. H. Zhao
Dept. of Electrical Engineering-Electrophysics
University of Southern California
Los Angeles, CA 90089-0484

Dr. F. J. Zutavern
Sandia National Labs
Division 1248
P.O. Box 5800
Albuquerque, NM 87185